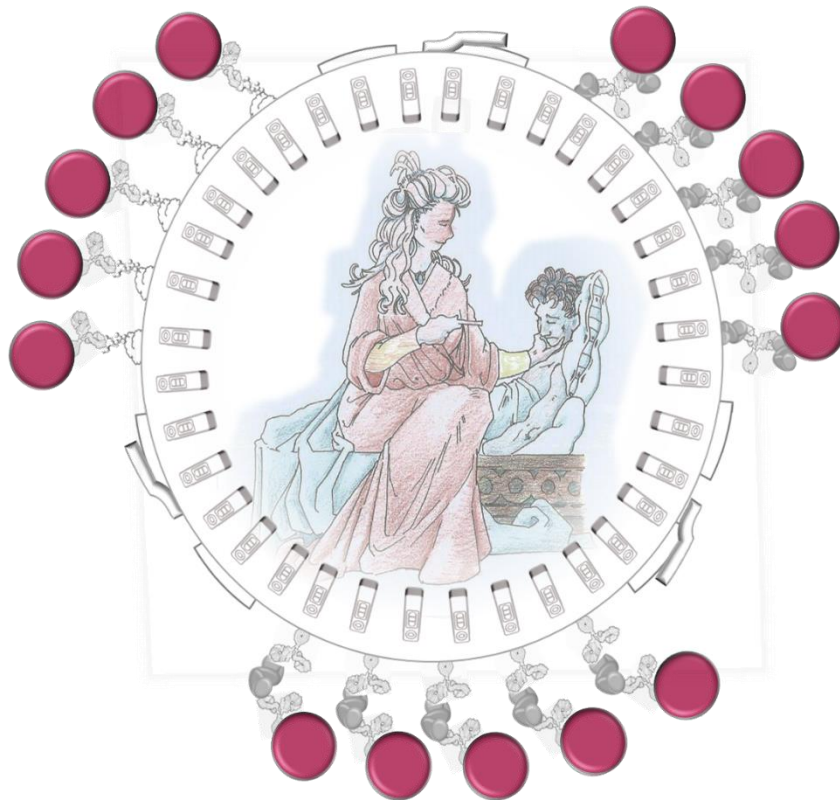


Università degli Studi di Torino



Doctoral School of Sciences and Innovative Technologies  
PhD program in Pharmaceutical and Biomolecular Sciences  
(XXXIII cycle)



**Lateral flow immunoassays for infectious diseases:  
strategic approach, design, and development for  
point-of-care testing**

Candidato: Simone Cavalera

Tutor: prof. Laura Anfossi

**Università degli Studi di Torino**



**PhD program in Pharmaceutical and Biomolecular Sciences**

**Thesis project carried out at  
Department of Chemistry**

**CYCLE: 33th**

**TITLE OF THE THESIS:**

**LATERAL FLOW IMMUNOASSAYS FOR INFECTIOUS DISEASES:  
STRATEGIC APPROACH, DESIGN, AND DEVELOPMENT FOR  
POINT-OF-CARE TESTING**

**THESIS' AUTHOR: Simone CAVALERA**

**SUPERVISOR: prof. Laura ANFOSSI**

**PhD PROGRAMME CO-ORDINATOR: prof. Roberta CAVALLI**

**ACADEMIC YEARS OF ENROLMENT: 2017-2020**

**CODE OF SCIENTIFIC DISCIPLINE: CHIM01**

# Index

<b>Chapter 1</b>	<b>Introduction</b>	<b>5</b>
	<b>The concept of diagnosis and the Point-Of-Care Tests</b>	<b>6</b>
<b>1.1</b>	The Lateral Flow Immunoassay	9
<b>1.2</b>	Components of the LFIA	11
<b>1.2.1</b>	The sample pad	11
<b>1.2.2</b>	The conjugate pad	11
<b>1.2.3</b>	The membrane	12
<b>1.2.4</b>	The adsorbent pad	12
<b>1.2.5</b>	Drawing of the Test and Control lines	13
<b>1.2.6</b>	Lamination and Cutting	14
<b>1.3</b>	Immunoreagents	16
<b>1.3.1</b>	Antibodies	16
<b>1.3.2</b>	Antigens	18
<b>1.3.3</b>	Labels and probes	18
<b>1.3.4</b>	Gold nanoparticles	19
<b>1.4</b>	LFIA: formats and application	21
<b>1.4.1</b>	Competitive LFIA	21
<b>1.4.2</b>	Non-competitive LFIA	23
<b>1.4.3</b>	Multiplexing	27
<b>1.4.4</b>	Increasing the sensitivity	28
<b>1.5</b>	Rapid Diagnosis of Infectious diseases	29
<b>1.5.1</b>	Validation of diagnostic tests for infectious diseases	32
	<b>References</b>	<b>34</b>
<b>Chapter 2</b>	<b>Aim of the Thesis</b>	<b>45</b>
<b>2.1</b>	Human Infectious diseases	48
<b>2.1.1</b>	Human Immunodeficiency virus	48
<b>2.1.2</b>	Severe Acute Respiratory Syndrome Coronavirus 2 (SARSCOV2)	52
<b>2.2</b>	Animal Infectious Diseases	56
<b>2.2.1</b>	Canine Visceral Leishmaniasis (CVL)	56
<b>2.2.2</b>	Foot-and-mouth Disease Virus (FMDV)	58
	<b>References</b>	<b>60</b>
<b>Chapter 3</b>	<b>The ‘total antibody’ LFIA</b>	<b>67</b>
<b>3.1</b>	SarS-Cov2 Total Antibody LFIA	69
<b>3.1.1</b>	Architecture of the test	70
<b>3.1.2</b>	Materials and methods	71
<b>3.1.3</b>	Results and Discussion	75
<b>3.1.4</b>	Conclusions	82
<b>3.2</b>	Visceral Leishmaniasis Total Antibody LFIA	83
<b>3.2.1</b>	Architecture of the test	84
<b>3.2.2</b>	Materials and methods	86
<b>3.2.3</b>	Results and Discussion	89
<b>3.2.4</b>	Conclusions	96
	<b>References</b>	<b>98</b>

<b>Chapter 4</b>	<b>The Class-specific antibody LFIA</b>	102
<b>4.1</b>	Multimodal x <sup>2</sup> LFIA	104
<b>4.1.1</b>	Design of the prototypes	105
<b>4.1.2</b>	Materials and methods	107
<b>4.1.3</b>	Results and Discussion	112
<b>4.1.4</b>	Conclusions	119
<b>4.2</b>	Dual approach detecting IgA to SARS CoV-2	120
<b>4.2.1</b>	Architecture of the test	121
<b>4.2.2</b>	Materials and methods	122
<b>4.2.3</b>	Results and Discussion	127
<b>4.2.4</b>	Conclusions	131
<b>References</b>		132
<b>Chapter 5</b>	<b>Direct Antigen LFIA</b>	136
<b>5.1</b>	Direct and Serotyping LFIA for FMDV	138
<b>5.1.1</b>	Architecture of the test	139
<b>5.1.2</b>	Materials and methods	141
<b>5.1.3</b>	Results and Discussion	146
<b>5.1.4</b>	Conclusions	157
<b>References</b>		159
<b>Chapter 6</b>	<b>Therapeutic Drug Monitoring LFIA</b>	161
<b>6.1</b>	Compliance monitoring LFIA for Tenofovir	163
<b>6.1.1</b>	From the cradle to the architecture of the test	164
<b>6.1.2</b>	Materials and methods	167
<b>6.1.3</b>	Results and discussion	178
<b>6.1.4</b>	Conclusions	192
<b>References</b>		193
<b>Chapter 7</b>	<b>Conclusions</b>	196
<b>Acknowledgements</b>		199
<b>Dedications</b>		200
<b>Appendix</b>		201



# Chapter 1



---

## Introduction

---

## The concept of *diagnosis* and the Point-Of-Care Tests

The word ‘diagnosis’ gathers a wide array of flexible meanings [1]. The root dates back to the ancient Greek διάγνωσις (diagnōsis), from διαγιγνώσκω (diagignōskō, “to discern”), which in turn derived from διά (diá, “through”) + γινώσκω (gignōskō, “to know”) [2]. This evolving concept is recognized as a “fundamental abstract reasoning concept in healthcare”, as reported by M.E. Maitland in 2010 [3]. In a broad sense, it refers to the rationalization of a symptom into a problem requiring an intervention, as a crucial part of any kind of problem-solving process. Majorly, this word is applied to medicine, meaning the combination of the observation of clinical signs and detection, or quantification, of biomarkers for assessing a pathological condition (infection, inflammation, chronic disease, etc.). Diagnoses are the “classification tools” of medicine and are pivotal in the ways medicine exerts its role in society, as assumed by A. Jutel in “*Sociology of diagnosis: a preliminary review*” [4]. As described by P. Cappelletti in 2020 [5], the process that ends with a diagnosis and that includes the generation of the clinical information has been represented by the brain-to-brain loop proposed by George Lundberg in the 80s [6]. The model has been revisited over the years yielding to the concept of the Total Testing Process (TTP), which includes the *pre*-preanalytical and *post*-postanalytical phases, involving a network of brains on both clinical and laboratory side, and highlights the patients’ role in the decision process.

The three phases of the classical tripartition (pre-analytical, analytical, and post-analytical) have been extended by the Nexus vision proposed by H.M.J. Goldschmidt, who introduced two additional phases: the *pre*-preanalytical (i.e the evaluation of the context of the patient and the comparison between laboratory-based and other ways to obtain information regarding the individual) and the *post*-postanalytical (i.e the evaluation of the new context following the initial diagnosis and the possible consequences for the patient) [7]. In addition, the concept of *outcome* enters in this scheme as the long term follow up of the condition of the patient after the whole analytical phase, focussing the attention on the patient as the real end-user of the process, upon which all the quality of the process falls back. The new concept of clinical laboratory interface, with the *pre-pre* and *post-post* phases, must be fused with a vision involving a multidisciplinary team to be effectively patient-centred. Evolving this concept, the brain-to-brain loop also admits the *extra-laboratory testing* and, furtherly, *the point-of-care testing*, as an extension of the clinical-laboratory interface.

To resume, the diagnostic process is a complex, patient-centred, and collaborative activity that involves information gathering and clinical reasoning with the goal of understanding a patient's health problem [1]. Generally, consists in connecting clinical signs (symptoms or altered levels of bioactive or biomarking compounds) to a “clinical decision”. This last is made by a physician on the base of the combination of several factors. The observation of the visible clinical signs and generic bioactive molecules is often not sufficient. More specific tests and analyses must be carried targeting specific biomarkers, to exclude illnesses with same symptomatic signs. The physician, as a detective, gather all the information, weights the relative significance of the clues, and formulates his hypothesis, the clinical decision, as an official diagnosis.

Focussing on detecting and quantifying clinical targets and biomarkers, many different optimized and validated instrumental methods are used, exploiting the most diverse techniques. Hereafter the word ‘diagnosis’ will be used as the aim of such methods and techniques. The high variability that characterizes the field of the clinical conditions leads to an unavoidable variability in the diagnostic approaches. Nevertheless, most of the *figures-of-merit* persist between the different strategies used to diagnose pathologies. The clinical sensitivity and specificity are the capacity of a diagnostic test to correctly classify positive and negative individuals to a clinical condition, and they have

always to be as the highest as possible, as still recently remarked and discussed by J. Shreffler and M.R. Huecker in *Diagnostic Testing Accuracy: Sensitivity, Specificity, Predictive Values and Likelihood Ratios* [8].

Nowadays, the concept of clinical diagnosis is split in complementary approaches: the screening tests and the confirmation analysis as underlined by C.S. Kosack, A.L. Page and P.R. Klatser in the *Bulletin of the World Health Organization* in 2017 [9].

The confirmation consists of instrumental methods for the quantitative detection of biomarkers or direct imaging of pathological conditions. The response must be extremely specific to avoid the risk of misclassification and subsequent wrong choice of the treatment. The result of a clinically validated confirmatory test represents an official clinical response, with all the implications that this entails. Though being necessary, confirmatory tests are also typically expensive and time consuming, require qualified personnel for the execution and interpretation of the results and can be led only in laboratory settings. To avoid the saturation of the Public Health system, the workload of the confirmatory tests must be lightened by recurring to preliminary screening tests. On respect to confirmatory tests these have complementary characteristics: generally, a greater coverage, high sensitivity, and sufficient specificity (depending on the target).

In 2012 the World Health Organization included these aspects into a set of figures of merits resumed under the acronym "ASSURED", which means Affordable, Sensitive, Specific, User-friendly, Rapid and robust, Equipment-free, and Deliverable to the end-user. These descriptors depict the class of the so called "point of care tests (POCT)", analytical tools that are generally used as screening techniques, and/or where laboratory methods are unsustainable [10]. The perfect fit between the needs of WHO regarding infectious diseases and the POCTs was immediately widely highlighted by the scientific panorama, as described by N.P. Pai et al. in *Point-of-Care Testing for Infectious Diseases: Diversity, Complexity, and Barriers in Low- And Middle-Income Countries* in the same year (2012) [11]. In their review, the authors underlined the limits of the laboratory-based techniques, overcome by the POCT "promises".

Among the possible analytical methods exploitable for setting POCTs, the ones based on immunochemistry, also called immunoassays, are remarkable. An immunoassay is an analytical method based on the specific and high affinity recognition of an antigen by a specific antibody, and the measurement of the antigen-antibody complex formation by means of a label that provides a detectable signal (gold nanoparticles, horseradish peroxidase, fluorescein, latex nanoparticles, etc... depending on the application). The reaction between the two immunoreagents forms a complex that can be directly or indirectly revealed. The main requirement is that the efficiency of the complex formation is sufficient for the revelation. As reported in the chapter 1.3 of the *Handbook of Immunoassay Technologies* by S.K. Vashist and J.H.T. Luong, (2018) [12] immunoassays are trans disciplinarily used, with fields of application ranging from industrial to food safety, from clinical to forensics and veterinary sciences. The enzyme-linked immunosorbent assay (ELISA) is far the most famous in the series of dozens of possible configurations of immunoassays [13]–[16]. These methods are typically performed in centralized laboratories by manual intervention of trained technicians taking generally around 2 hours because of their multiple-step processes. In the clinical practice, chemiluminescence based immunoassays (CLIA) are widely used bioanalytical methods for determining various biomarkers and are generally automatized and rapid, but they need of instrumental readers and laboratory settings [17]–[21]. The Point-of-Care translation of the laboratory-based immunoanalytical methods is the Immuno-Chromatographic Strip Test (ICST), also known as Lateral Flow Immunoassay (LFIA). The LFIA technique is undoubtedly the most successful screening diagnostic tool as it furthermore fulfils all the ASSURED criteria [22]–[28].

The immunochemical principles applied in microarray formats have been widely studied in the last decades, as well [30]–[47]. Nevertheless, they are still unable to break through into the market and for this reason are scarcely applied on-field.

On the contrary, LFIA currently represent the most important systems for on-field diagnostic worldwide. Their invention dates back to 1956 [47], and LFIA have been extensively used in diagnostics for decades and produced by dozens of companies for many kinds of application. Their versatility is one of the very crucial point of their fortune because of their extremely high customizability [25], [26], [48]–[53]. Though many efforts have been dedicated to increase sensitivity, diversify the detection panorama, and decrease the cost of immunoreagents, this technique still holds strongly on its golden standards regarding materials (nitrocellulose membranes), labels (colloidal gold and visual inspection of the result), and recognition elements (antibodies) used. In this thesis the importance of the strategic design of LFIA will be exhaustively explored and discussed in connection with the increase of the sensitivity and the improvement of its inherent multiplexing capability.

# 1.1



## The Lateral Flow Immunoassay

In the exhaustive review by M. Sajid et al. *Designs, formats and applications of lateral flow assay*, the authors have explained the key points of the LFIA technique [54]. In addition, another review focussing on the main steps and features of the production of the LFIA strip was recently published on Nature Protocols by A. Parolo et al. [53].

The general structure of the LFIA is reported in Figure 1.1 and consists in an ensemble of components providing chemical, physical, and mechanical features. Basically, it appears as a multilayer array strip. On a backing plastic support (Figure 1.1 a) a thin layer of porous nitrocellulose membrane (Figure 1.1 b) adheres. The backing support acts as a platform for the assembling of the different components of the test and confers physical rigidity to the device. At the ends two cellulose or glass fibre pads are pasted, the sample pad, and the adsorbent pad (Figure 1.1 c-d). The sample pad absorbs gradually the liquid sample, acts a physical pre-treatment reducing the matrix effects. The absorbent pad works as the driving force for the capillary flow and a sink for the liquid processed through the strip. Between one of these pads and the beginning of the nitrocellulose membrane is stuck another pad, generally made of polyester or glass fibre, called conjugate pad (Figure 1.1 e).

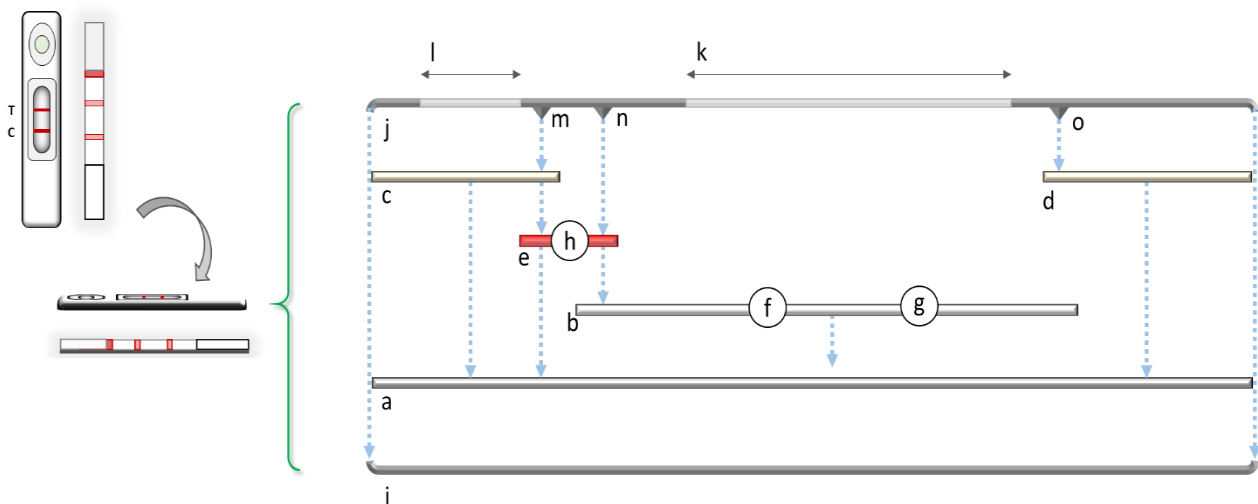


**Figure 1.1** The structure of the typical ICST. a) backing support, b) nitrocellulose porous membrane c) sample pad, d) adsorbent pad, e) conjugate pad, f-g) immunoreagents areas, h) labelled immunoreagent, i-j) cassette, k) reading window, l) sample well, m-o) pressure teeth.

On defined regions (generally lines or spots) of the nitrocellulose, solutions containing immunoreagents are dispensed (Figure 1.1 f-g). These can be one or more specific areas called Test lines and one Control line. The role of the test lines will be to give evidence of the interaction with the target molecule and, consequently, the required information. The Control Line ensures the correct functioning of the test by binding with the probe independently on the presence of the target. The conjugate pad is impregnated with a suitable labelled immunoreagent solution and dried (Figure 1.1 h). The assembled strip is enclosed and stored into a plastic cassette (Figure 1.1 i-j) providing a window in the area, which includes the reactive regions on the nitrocellulose (reading

window, Figure 1.1 k). Another hole is present in correspondence of the sample pad, upon which the sample will be introduced (sample well, Figure 1.1 l). The cassette provides some pressure points assuring the correct flow of the sample/labelled conjugate mix solution along the components array (Figure 1.1 m-o). The LFIA starts by applying the liquid sample on the sample pad (Figure 1.2).

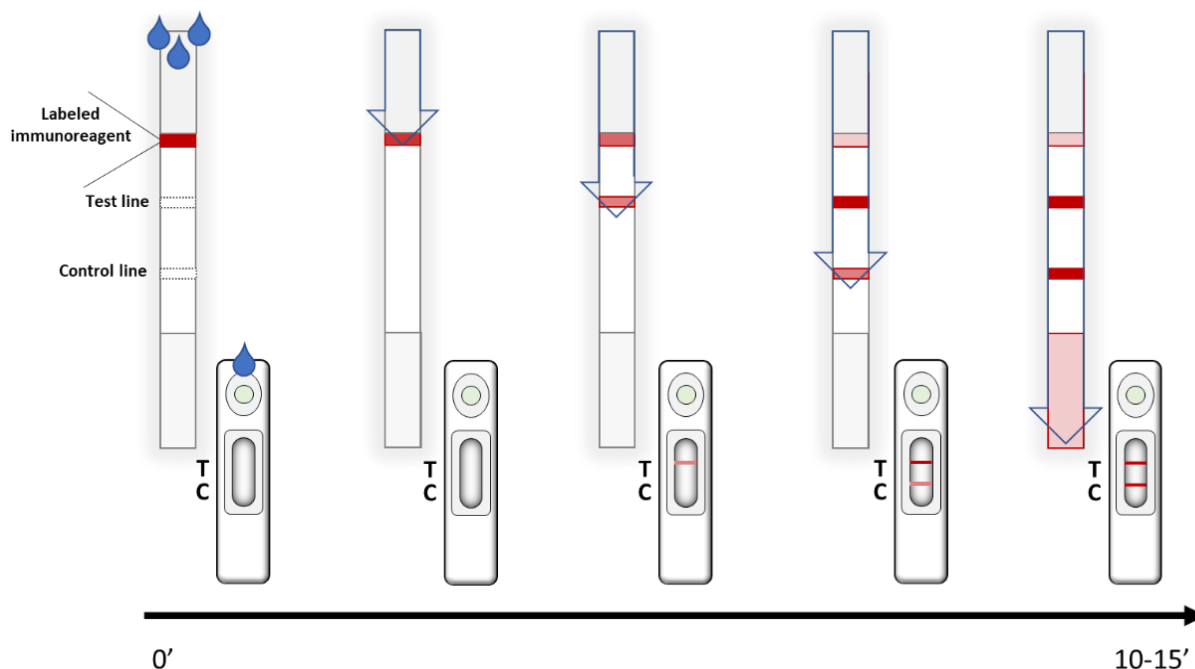


**Figure 1.2** Run of the assay: execution of the test and progression in time. Visually the appearance after the addition of the sample in the sample well changes in intensity until the complete appearance of the reacting bands.

The solution resuspends the labelled immunoreagents from the conjugate pad and the analytes and the labelled probe flow by capillary forces along the membrane and through the lines, where immunoreactions take place. Usually, they do not require external reagents for completing the assay besides the liquid sample. Results are quick and easy to interpret, usually without the help of equipment for qualitative assays. Deriving from the latex agglutination assay (Plotz and Singer, 1956) [55], the LFIA was later patented, improved, evolved multiple times by several companies and producers. Its establishment between 1980 and 1990 did not mean the lack of further improvements [56]–[59]. In 1988 the appearance of the Clearblue Pregnancy Test™, developed and patented by Unipath, signed the beginning of the commercial success of LFIAs thanks, upon the many advantages, to their simplicity and user-friendly format [60]. The technique has been furtherly improved in the years, searching for even more performing materials and immunoreagents to face the needs of the diagnostic challenges [61]–[87]. The application of the technology has expanded well beyond clinical diagnostics to food and feed [88]–[96], veterinary [97]–[101], environmental health and safety [102]–[108], drug testing and therapeutic drug monitoring [109]–[113], agriculture and biowarfare [114]–[118].

## 1.2



### Components of the LFIA

Basing on the key references in literature, such as the reviews from M. Sajid (2016) and A. Parolo (2020), but also R. Wong (2009), K. Koczula (2016) and A. van Amerongen (2018), the main LFIA components and their description is reported in the following sections [26], [29], [53], [54], [119].

#### 1.2.1 The sample pad

Ideally, the whole amount of the liquid sample must flow homogeneously, then an appropriate material to collect and distribute the sample is needed. This is the function of the sample pad, which, in addition, filter insoluble interference of the matrix. This aspect is particularly remarkable considering that the lack of manual pre-treatment and extraction processes is one of the main features representing an advantage of LFIA on respect to instrumental analysis. There are several materials used to manufacture sample pads, but the mainly used are cellulose fibre and treated glass fibre. They can be used unmodified or, if required, these materials can be impregnated with buffers containing proteins, salts, surfactants, and/or other additives. Some reasons to pre-treat the sample pad are discrepancy between the optimal pH for the assay and the natural pH of the sample; presence of insoluble matter and viscous substances, such as mucins or large-size proteins; inclusion of stabilizing agents for long term conservation; and so on. The pad is typically pre-treated by dipping it in the suitable solution and drying. On the other hand, this step can accidentally introduce sources of variability, including baking phenomena, buffer concentration gradients and edge effects upon drying.

#### 1.2.2 The conjugate pad

Independently on the kind of probe used in the test, the labelled immunoreagent providing the analytical signal must be efficiently inserted in the test and stably stored. The shelf life of a LFIA test can range between 6 month and 2 years and the stability of the entire strip usually corresponds to the stability of the labelled immunoreagent. The function of the conjugate pad is holding the detector probe in a dry state, maintaining it stable and releasing it efficiently and reproducibly when the assay is run. The resuspension upon sample application must be rapid and quantitative. The materials can be glass fibre or polyester. Hydrophilicity, low protein binding, rapid soaking and an overall chemical inertness are the main requirements. As for the stability, the conjugate pad is the main contributor to the coefficient of variation of the LFIA. As the sample pad, it is often pre-treated to avoid loss of robustness and reproducibility. The pre-treatment involves the immersion of the pad in a suitable solution of proteins, polymers, and surfactants, followed by drying paying attention to the same criticalities cited for the sample pad (chapter 1.2.1).

### 1.2.3 The membrane

The membrane is the analytical medium of the test onto which the reagents are immobilised or flow through and into which they interact. The two main functions of the membrane are to irreversibly bind immunoreagents in well-defined areas and to allow for the correct flowing of the assayed solution. Concerning the reactive areas, called test and control lines, the main requirements are: i) strong binding with proteins or peptide antigens, ii) limited diffusion of liquids, iii) appropriate porosity (determining the flow rate), iv) maintenance of the stability of the immobilized immunoreagents. It accepts the labelled immunoreagent and the sample, flow them consistently to the reaction areas, allow the reactions at the test and control lines to happen, and dispose the unbound fluids, label, and reactants. Often made of nitrocellulose as a layer, the membrane is thin and fragile, so it is attached to a plastic or nylon base layer to simplify cutting and handling. Other material types available from the market, including nylon, polyether sulfone and polyvinylidene fluoride have had limited success, apparently due to factors including cost, limited utility, the need for education regarding new chemistry and processing requirements, and resistance to change due to the large bank of existing experience in the use of nitrocellulose. The commercial nitrocellulose is made by reacting cellulose from plant origin with nitric acid to obtain nitrate ester in place of the former hydroxyls. Optimal substitution rates for better filming properties range between 1.8 and 2.3. The porosity and pore size of the membrane are controlled by different parameters like the solvents used, evaporation speed, temperature, humidity and obviously the polymer properties (e.g., molecular weight, size distribution and solubility). The membranes used in LFIA need hydrophilicity and consistent flow characteristics. Nitrocellulose is naturally hydrophobic, and surfactants are used to increase wettability to the resulting material. The protein binding capacity is given by a combination between hydrostatic, hydrogen and hydrophobic interactions and is estimated around 100 µg of IgG per cm<sup>2</sup>. Proteins bind to nitrocellulose because of the attraction between the dipoles of the amidic peptide bonds and of the nitrate esters. Subsequently, the hydrophobic interaction between the carbon containing nitrocellulose and the hydrophobic portion of the protein completes the adsorption. Salt, surfactant, and sugar free media are recommended to maximize protein absorption. The use of nitrocellulose to immobilize proteins was introduced in 1970s and improved in the following years to match the requirements of LFIA.

Nitrocellulose membranes are classified based on the capillary flow rates. Manufacturers most often specify the capillary flow time as the time required for water to travel up and completely fill a 4-cm long strip of membrane. In fact, the driving force of the LFIA is the capillarity. Exploiting the surface tension of high surface-to-volume ratio media the liquid moves toward its narrow path despite the gravity force. The competition between the forces favours the adhesive forces towards the walls of the capillary on respect to the cohesive forces of the molecules of the liquid itself. The pore size, viscosity and surface tension of the fluid and their mutual interaction affect the capillary flow rate. In addition, as labelled immunoreagents are particles, an important aspect to consider is the ability of a particle to migrate through the membrane related to the pores size. The pores in the membrane must be sufficiently large to allow the passage of the particle probes.

### 1.2.4 The absorbent pad

To promote the flowing of a large volume of sample and the decrease of the background signal an adsorbent pad is typically used. The absorbent pad is specifically designed to pull all the liquid that is processed through the strip and to hold it for the duration of the assay. Enhancing the capillary driving force, it absorbs all the unreacted substances and avoids back diffusion phenomena. The



higher is the bed volume of the adsorbent pad the better will be the quality of the run. Allowing higher volumes of samples increases the sensitivity and permits a better washing of the background signal given by unbound labelled immunoreagents. The most employed material to make this pad is high-density cellulose.

### 1.2.5 Drawing of the Test and Control lines

Some of the basic requirements of LFIAs are reproducibility and robustness of the system. The single strip derives from the slicing of a membrane upon which the reacting lines are dispensed. Thus, the deposition of these lines must be effective, efficient, controlled, and homogeneous along the whole length of the membrane as for the dispensation of several membranes. Dispensing microvolumes of solutions containing proteins and additives in a controlled and reproducible way to the porous membrane is technically challenging and cannot efficiently be performed manually. The deposition of the test and control line reagents on the membrane is performed using automatic contact or non-contact dispensing instruments. The contact dispensing can cause the damage of the nitrocellulose membrane; therefore, the non-contact dispensing method provides the best solution for quantitatively dispensing proteins onto nitrocellulose. In our Bioanalytical laboratory, we use a XYZ3050 platform equipped with several BioJet Quanti™ from BioDot (Irvine, CA, USA) that are a non-contact, pump-driven solenoid dispenser (Figure 1.3).



**Figure 1.3.** BioDot XYZ3050 platform equipped with five BioJet Quanti™.

The dispenser uses a drop actuator such as a solenoid hydraulically pumped with a syringe pump. The drop volume can be regulated so that the dispensation mode between separate drops or multiple drops formed lines. The drop-to-drop and line coefficients of variation ( $\pm 5\%$  and  $1-2\%$ , respectively), allows for reproducible and effective deposition of immunoreagents on the membranes. Ideally, protein solutions are instantly adsorbed by the nitrocellulose membranes. For this reason, the line width will present the size of an 'half drop' hemisphere. Setting  $15-20\text{nL}$  drops the size of the typical LFIA test and control lines range between  $0.5$  and  $1.0$  mm.

## 1.2.6 Lamination and cutting

The different components and pads above described are properly assembled and overlapped in the lamination process. In correspondence of the overlapping, a pressure promotes the right direction for the run (Figure 1.1) and efficient mixing and prompt resuspension of the label; favour the transfer of the mixture to the membrane and to the adsorption pad (Figure 1.4).

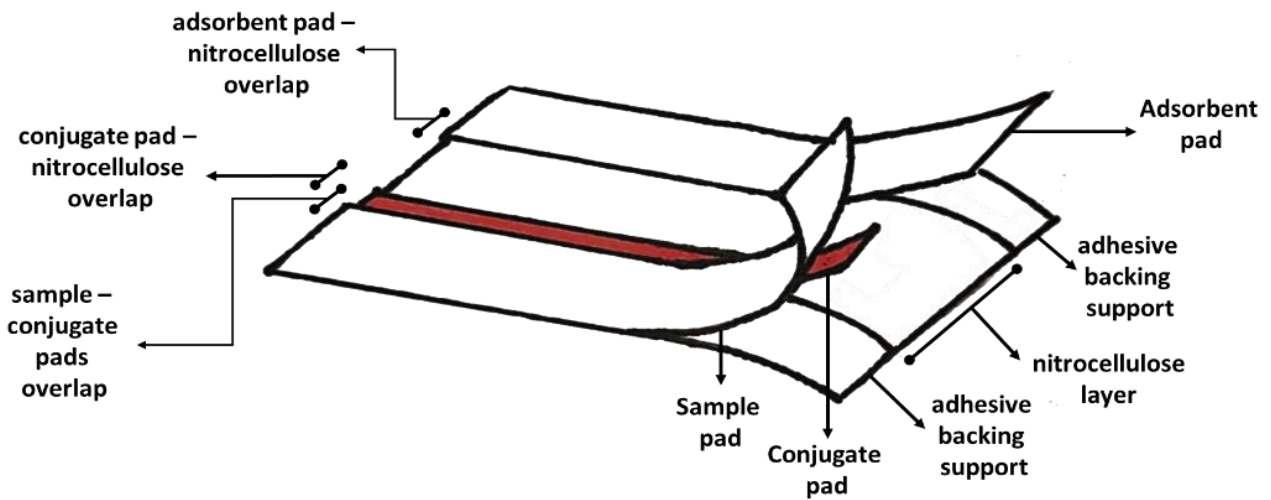


**Figure 1.4.** The alignment and overlapping array of an assembled LFIA membrane before cutting.

The format of the LFIA is the strip test, obtained by cutting the laminate. There are many types of suitable cutters for producing reproducible in width strips avoiding the disassembly of the laminate (guillotine, single rotary blades, and rotary card cutter. In this work we used a CM4000 guillotine from BioDot (Irvine, CA, USA) (Figure 1.5)

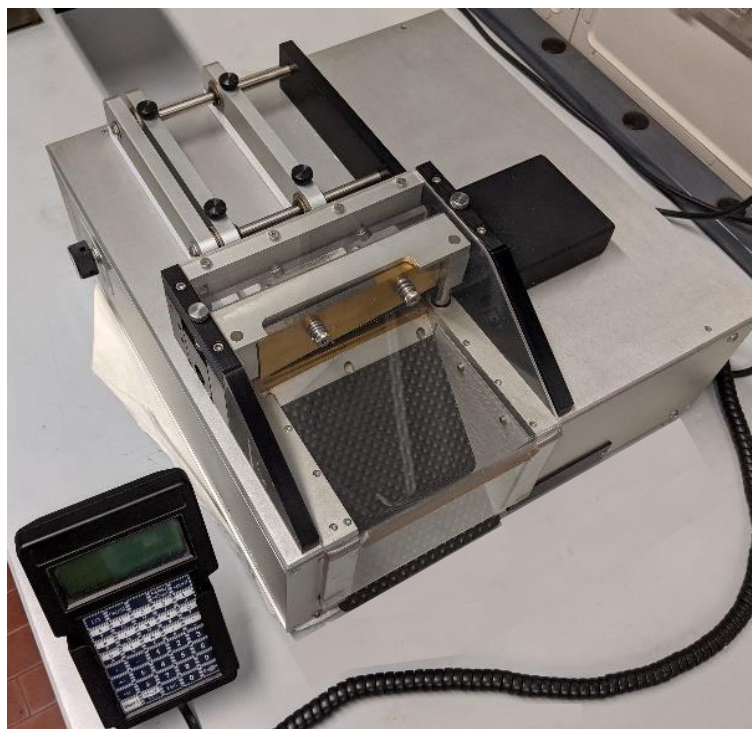


**Figure 1.5.** Guillotine BioDot CM4000 Cutter

The width of the strip depends on a compromise between the economic sight, according to which thinner strip are preferable and the easy interpretation of the result. Also, delamination can occur if the dimensions are too narrow. In addition, the reproducibility can be affected since decreasing the width the strip-to-strip CV will unavoidably increase. Typical LFIA strip width range is 3-8 mm.

## 1.3



# Immunoreagents

The use of the antibody-antigen pairs to exploit immunocomplex formation persists as a golden standard of the wide array of analytical approaches. Though the many efforts made to find alternatives to the use of antibodies (DNA probes, DNA-zymes [120], aptamers [121], [122] and molecularly imprinted polymers (MIPs) [123] they still hold as the most efficient and reliable among the recognition elements. On the other side a larger variability is admitted for the antigenic counterpart. Especially for those formats that include the use of antigens for recognition of small molecules the design of an appropriate antigen from the target molecule can be challenging. The proper use of an antigen can add unexpected and useful opportunities to increase specificity, sensitivity and multiplexing capability as will be reported in the following chapters.

### 1.3.1 Antibodies

Antibodies, also known as immunoglobulins, is a class of bioactive compounds interacting with exogenous matters and compounds. Their structure, characteristics and classification are well known in the literature, as summarized by H.W. Schroeder and L. Cavacini in their article *Structure and function of immunoglobulins* [124].

Different classes of immunoglobulins exist, among which those used as bioligands belong to the G class. Immunoglobulins G (IgG) are 150kDa proteins produced by the immune system of vertebrate animals to face pathogenic or viral infections. They are characterized by the ability to bind to a specific antigen. The IgG is composed by 4 aminoacidic chains: 2 heavy chains (50kDa) and 2 light chains (25kDa) linked covalently by disulphide bridges (Figure 1.6). They present several domains, including a hinge region, a glycosylation site, 2 domains in each of the light chains and 3 in each of the heavy chains. Almost the whole protein sequence is constant, except for the variable region, including amino acids both from the light and from the heavy chains.

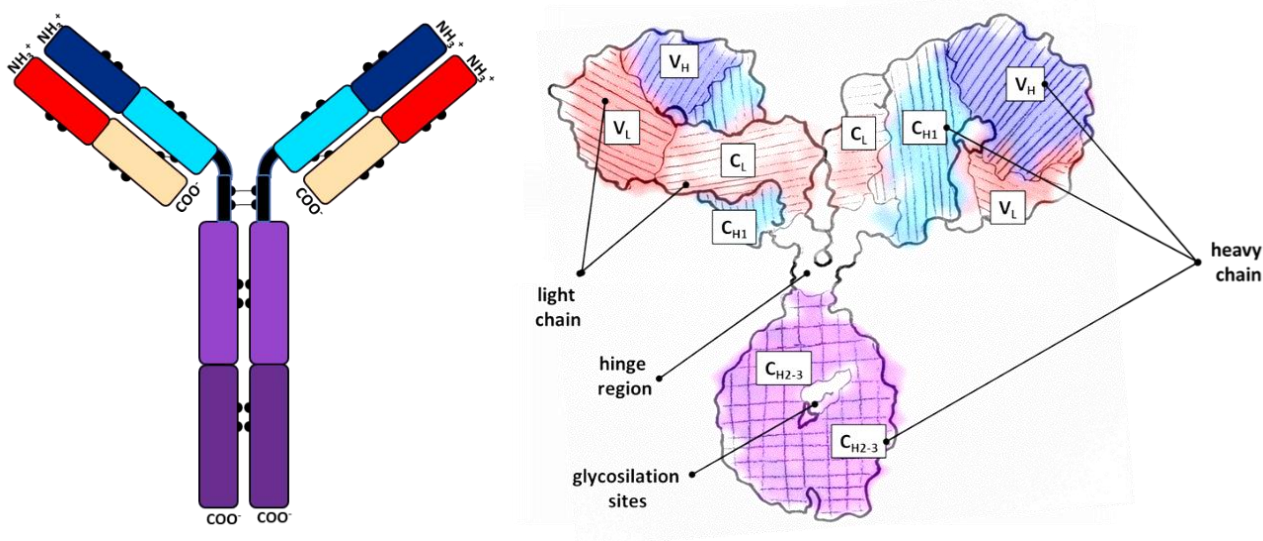


**Figure 1.6.** Schematic (left) and spatial (right) representation of an IgG antibody.

This aspect conceptually separates the antibody structure in a variable region (V) and a constant region (C). The V region contains the binding site for the antigen and for this reason is called Fraction antigen binding (Fab), whereas the C is called Fraction crystallizable (Fc). The C region can be called constant because varies very little. Nevertheless, these minimal variations are sufficient to define different classes of antibodies (IgA, IgM, IgG, IgE, IgD and IgY), having different characteristics and functions. The IgG class is the most abundant in the serum and IgG are responsible of the so-called “immune memory”. IgG generally appear after some time from the first exposure to the pathogen. This time-lapse is called “seroconversion” and is variable in time depending on the nature of the pathogen and, slightly, on the individual. The IgA class protects mucous membranes from pathogens and these immunoglobulins are generally highly concentrated in mucous and saliva where they are present in a dimeric form. They are present also in the serum but less concentrated (higher than IgM but lower than IgG) and are found in the monomeric form. The IgM are pentameric and are, in most cases, the first class of antibodies produced facing up to an infection. After the seroconversion period they lower and leave the place to the IgG class.

Chemical and structural interactions concur toward the formation of the complex between the antibody and the antigen. The strength of this interaction is exploited by the immunoanalytical methods. Every antigen-antibody pair presents different binding performance, estimated by the affinity constants  $K$ . The weak and strong forces (H bonds, electrostatic and Van der Waal forces) concur differently to the overall strength of the interaction depending exclusively by the interaction with the ligand. The affinity constant  $K$  ( $M^{-1}$ ) is empirically estimated as the equilibrium between the dissociation and association events and ranges from  $10^{14}$  (high affinity) to  $10^6$  (low affinity). The affinity constant strongly influences the performance of the immunoanalytical method.



Antibodies are naturally produced by the immune system to face situation the body interpret as dangerous. as analytical tools, they are elicited by introducing into immunocompetent host a high-molecular weight compound. Modern antibody production techniques allow producing two kinds of antibodies: monoclonal and polyclonal antibodies [125]. Polyclonal means that the whole antibody population derives from different antibody producing cells and will present a heterogeneous affinity. On the contrary, monoclonal antibodies are originated from clones of many copies of the same antibody producing cell and the binding characteristics of the whole amount of the antibodies correspond to the characteristic of the single antibody. The first step of the production of both the types is the immunization of a competent animal (mouse, rabbit, goat, sheep, horse): a series of administration of an immunogenic derivative of the target molecule (a recombinant antigen, a vaccine or a small molecule derivative linked to a protein). This event provokes the immune reaction with the appearance of a polyclonal response. Collecting and purifying the serum of an immunized animal (antiserum) a polyclonal antibody (pAb) is obtained. In a typical polyclonal antibody preparation, only 0.2 - 2% of the total antibodies are directed against the antigen of interest [126]. If the spleen cells of the sacrificed animal are isolated and immortalized by fusion with myeloma cells, antibodies can be produced continuously. Then, these cells are split and assayed serially until the isolation of clones containing copies of the same antibody. These antibodies are called monoclonal antibodies (mAb). They are generally very specific but, usually, their employment in immunoanalytical tests brings to lower sensitivity. Nowadays mAbs are also used for immunotherapy and treatment of many diseases from cancer to drug refractive migraine [127]. All protocols for antibody production should be reviewed by animal welfare committees to

ensure they comply with the guidelines for humane treatment of the animals. A good quality LFIA requires high specific antibodies with high affinity for the target antigen.

### 1.3.2 Antigens

The antigen is a target of the binding site of an antibody and, in general, a molecule able to bind an antibody. Some large antigens, such as viral or bacterial proteins or macromolecules, present many epitopes (molecule moieties involved in the antibody recognition). On the contrary, many other target molecules, such as drugs or toxins, are too small (<3kDa) to elicit the generation of the immune response, even if they are able to bind an antibody and are called haptens. The haptens are covalently linked to a carrier protein to increase their dimension and elicit the immune response [128]. Consequently, the hapten-carrier conjugate elicits the production of a panel of antibodies, among which some are directed toward the carrier protein, others to the linking group, and some toward the hapten. To obtain hapten-specific antibodies from polyclonal antisera, a separation step is required, more likely by affinity chromatography. The ideal hapten-carrier structure must not modify the structure of the target, to avoid production of antibodies toward something too different from the target, leading to a scarce affinity.

### 1.3.3 Labels and probes

Labels are of utmost importance for the LFIA being it the only way to directly, or indirectly, detect the formation of the immunocomplexes in the test and control lines. Undoubtedly, labels and the corresponding detection method influences the LFIA performances. But is also true that after 30 years of continuous research some labels still hold firmly as the golden standards of the technique. Among the requirements of a suitable label there are cost-effective production, simple and conservative conjugation to immunoreagents avoiding non-specific binding, high stability under various chemical conditions and temperatures, wide signal dynamic range, high signal-to-noise ratio and, most important, ability of flowing uniformly through the porous membrane. In the last decades, many kinds of labels have been employed both in the literature and in industrial production: nanomaterials (e.g., carbon, silver, gold and selenium nanoparticles and dye-containing liposomes), fluorescent (e. g. quantum dots) and chemiluminescent (e.g., horseradish peroxidase). In his review, “*A review of fluorescent signal-based lateral flow immunochromatographic strips*” (2017) [129], Gong et al. gather and describe diverse fluorescent reporters, such as fluorescent dyes, quantum dots (QDs), an up-converting phosphor (UCP), lanthanide labels, and other fluorescence nanoparticles. Concerning liposomes many attempts of their inclusion in LFIA were made, including the one K. Edwards and A. Baeumner proposed in 2009[130] for detecting myoglobin, or the ones from J.A.A. Ho for aflatoxin B1 [131] and *Salmonella* [132] detection. Chemiluminescence catalysed by luciferase and horseradish peroxidase has widely been exploited to enhance sensitivity. Some recent examples are the works from G.R. Han and M.G. Kim for the detection of troponin (2020) [133], the self-contained proof-of-concept approach by J. Deng et al. (2018) [134] and the work by J.M. Park et al. using platinum nanoparticle as substrate (2015) [135], but also from the recent past such as the one from Y. Wang et al. for the detection of nucleic acids (2012) [136]. Notwithstanding, nanomaterials are still the most used signal reporters for LFIA [137]. Especially, they are largely employed for the infectious disease diagnostics, as emerges from the review from R. Banerjee and

A. Aishwal, *Recent advances in nanoparticle-based lateral flow immunoassay as a point-of-care diagnostic tool for infectious agents and diseases* (2018) [138].

Nanomaterials have several advantages over fluorescent and chemiluminescent probes, which did not resound the expected success because of several issues concerning their performance, cost, and toxicity (quantum dots), complicated conjugation protocols, and lower than expected signal to noise ratio (horseradish peroxidase), need of addition of steps (disruption of liposome vesicles). Among the nanomaterials, carbon nanoparticles have been proposed by A. van Amerongen in 1993 [139] but are debated and their utility controversial, as they allow increasing of the signal-to-noise contrast given by their black colour but their conjugation to antibody is challenging. Silver nanoparticles present, often, instability but show an array of different possible colour obtainable by simply changing synthesis parameters [140]. Selenium nanoparticles (e.g. HIV ABBOTT test [141]) and latex particles (pregnancy test) are widely used on the market. Since gold nanoparticles represent the label employed in all the LFIAs developed in this work they will be furtherly described.

### 1.3.4 Gold nanoparticles

Gold nanoparticles (GNPs) have been used as a pigment since the 17<sup>th</sup> century and studied as a colloidal sol from the second half of the 19<sup>th</sup> century [142]. Being made of a transition metal in the presence of suitable conditions, they can exhibit an intense visible colour. This is due to the surface plasmon resonance (SPR) phenomenon affecting some transition metal nanoparticles. The light can be adsorbed if the diameter of the nanoparticle is in the order of magnitude of 1/10 of its wavelength, simply by resonating with its electronic density [143], [144]. The collective coherent oscillation of the free d electrons of gold (conduction band electrons) causes a dipole formation due to the charge separation that oscillates along the electromagnetic field of the incident light.

This absorption is typically between 516-540 nm for 13-40 nm diameter GNPs (figure 1.6). This manifests itself in a red colour whose intensity, photometrically measured as optical density (OD), depends on the number of nanoparticles in the solution. Also, the wavelength of the maximum OD is related to the shape and dimension of the nanoparticles. The gold nanoparticles can be obtained in other dimensions. For a 20 nm GNP, the total extinction is nearly all contributed by absorption. When the size increases to 40 nm, the scattering contribution is no longer negligible and when increases to 80 nm, the extinction is contributed by both absorption and scattering in a similar degree [145]. For relatively coarse GNPs dispersions the scattering and the absorption occurs within the orange range of the spectrum. This results in blue or violet colour of such sols in the transmitted light. Moreover, nanoparticle optical properties are also sensitive to the proximity of other plasmonic materials. When two or more plasmonic nanoparticles are near each other their surface plasmons couple as the conduction electrons on each particle surface collectively oscillate. This coupling effect is responsible for the dramatic changes in the visible colour of plasmonic nanoparticle sol when nanoparticles aggregate [146].



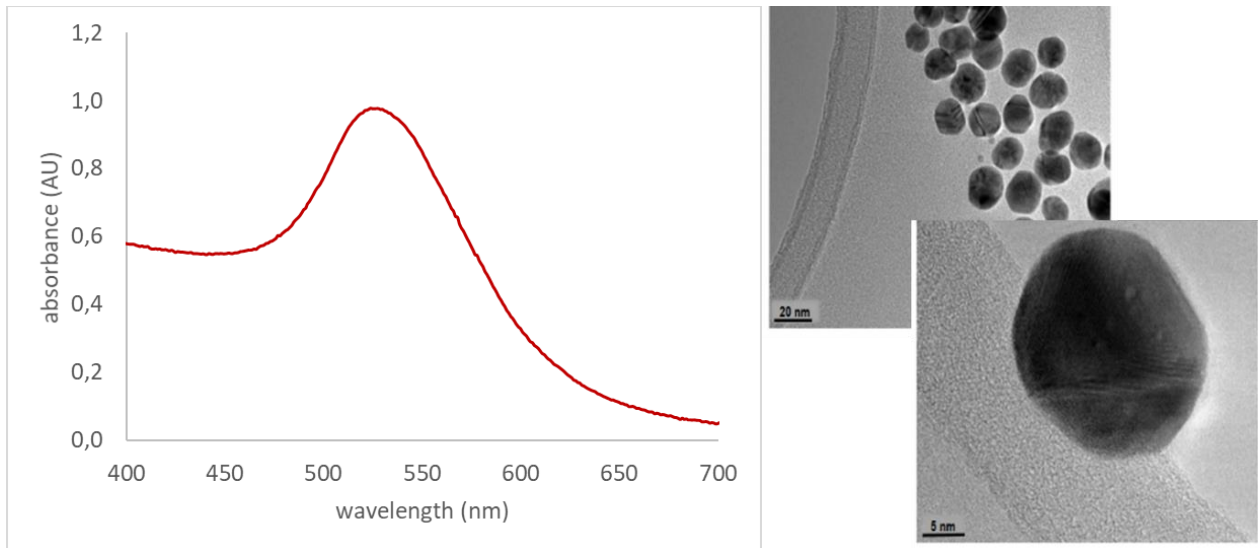


**Figure 1.6.** A typical example of a colloidal gold solution synthesized in laboratory and used in the works described in following chapters. On the left the visible spectrum of a solution of gold nanoparticles with optical density 1. On the right Imagen taken by means of transmission electron spectroscopy

One of the first examples of the use of GNPs as labels in LFIA was reported by J.K. Horton et al. [147] for the detection of mouse immunoglobulins. Since then, GNPs labels have been widely used in the development of antibody-based LFIA for food analysis [148], [149] and point-of-care diagnostics, including environmental chemical contaminants and infectious agent monitoring [150]. GNPs of various sizes are available on the market. In addition, there are various synthetic protocols to produce colloidal gold in the laboratory depending on the particle size desired. Basically, all methods use a reducing agent to convert ionic gold into metallic gold in a controlled manner. The most common approach to synthesize GNPs in aqueous solution relies on the tetrachloroauric acid ( $\text{HAuCl}_4$ ) reduction by means of sodium citrate and was reported for the first time by E.A. Hauser and J.E. Lynn [151] and subsequently improved by J. Turkevich et al. [152] and G. Frens [153]. In this method, citrate serves as both the reducing agent and as the anionic stabilizer of GNPs [154]. All the GNP solutions used in this work was made following the Turkevich method:

- 100 ml of 0.01% (w/v) solution of  $\text{HAuCl}_4$  in milliQ water must be heated to  $100^\circ\text{C}$  under vigorous stirring avoiding concentration by means of a six-bulb condenser.
- 1.2 ml of a freshly prepared and filtered 1% w/v solution of sodium citrate must be added quickly to the boiling solution.
- Once the desired colour appears wait for 2-3 minutes, cool down the GNPs and store at  $4^\circ\text{C}$ .

Besides the facile production, the stability over time in colloidal form and the intense absorption in the visible region of the spectrum, another important property that explains the popularity of GNPs as labels in immunoassay is their affinity towards most proteins and especially immunoglobulins. Thanks to this feature, stable labelled immunoreagents can be produced by passive adsorption [155].



## 1.4



### LFIA: formats and application

The LFIA is a versatile platform to realize immunoassays. Even considering the transition from the multi-step protocol of the traditional ELISA to a single step with all the reactions concentrated in 10 minutes, the principle and the opportunities are almost the same of any immunoassay platform. The several formats of LFIA can be subdivided in two major categories that derive from the immunoassay basic principles: competitive assays and non-competitive assays. The following brief description of LFIA formats summarizes concepts reported in the review by M. Sajid et al. [54] *Designs, formats and applications of lateral flow assay: A literature review*, by S. Kasetsirikul et al. (*Challenges and perspectives in the development of paper-based lateral flow assays*, (2019), [156] and by A. E. Urusov et al. who listed and discussed the steps required for the development of LFIA (*Towards Lateral Flow Quantitative Assays: Detection Approaches*) [157]. Hints on recent improvement of the assay, especially as concerns the applications to the topic of the thesis are based on the *Six decades of lateral flow immunoassay: from determining metabolic markers to diagnosing COVID-19* by B.G. Andryukov (2020) [27].

#### 1.4.1 Competitive LFIA

This format is the only chance when the target is a small molecule, unable to bind simultaneously to more than one antibody. It is based on the competition between the target molecule and its derivative (antigen) immobilized on the test line for binding to a specific labelled antibody. The scheme is depicted in Figures 1.7-8. In the format with direct labelling, (Figure 1.7) when the target is present, it binds to the labelled antibody subtracting it from binding to the antigen immobilized on the test line. When the target is absent (or below the detection limit), the labelled antibody binds to the antigen on the test line. So, the presence of the analyte causes the disappearance of the test line signal. An increased sensitivity has been associated to using indirect labelling of the specific antibody (Figure 1.8) [158]. In this strategy, the revelation is made by means of a labelled secondary antibody.

## 1) Competitive LFIA

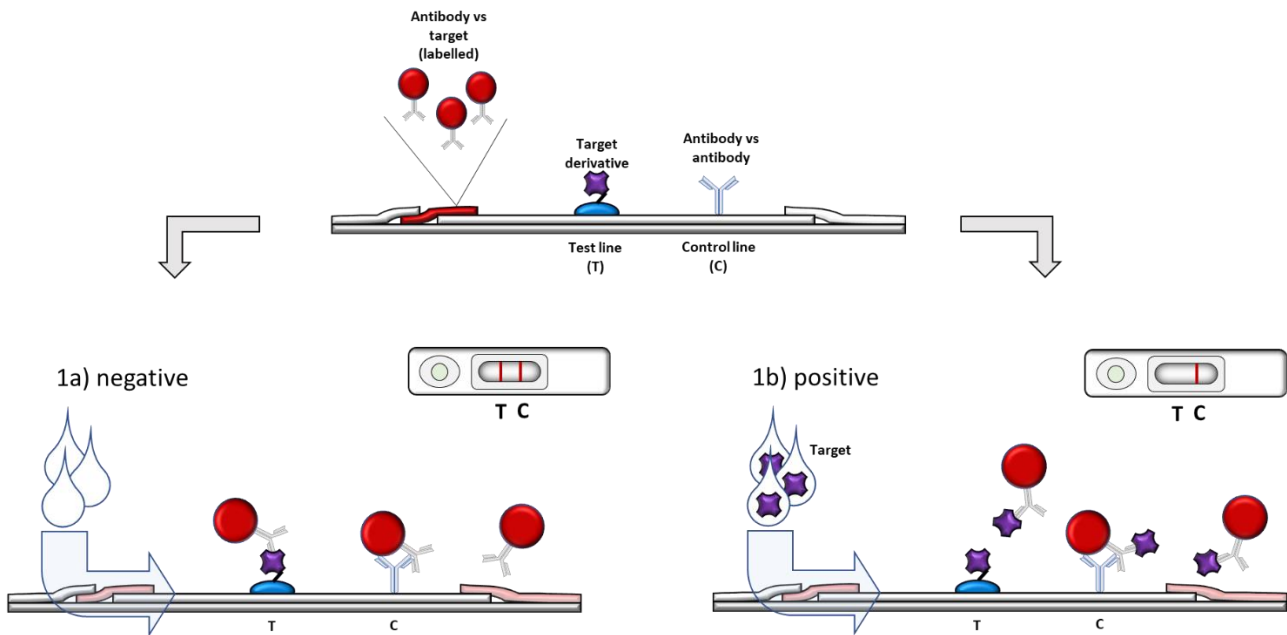


**Figure 1.7.** Scheme of the typical competitive LFIA: the antigen and a secondary antibody form the test and the control line, respectively (1). The specific antibody is labelled with gold nanoparticles as the probe. In the case of a negative sample (1a) the probe binds to the antigen at the test line and the colour appears for the accumulation of the probe. In the case of a positive sample (1b) the target inhibits the binding of the probe toward the antigen and the colour does not appear on the test line.

## 2) Competitive LFIA with indirect labelling of the antibody

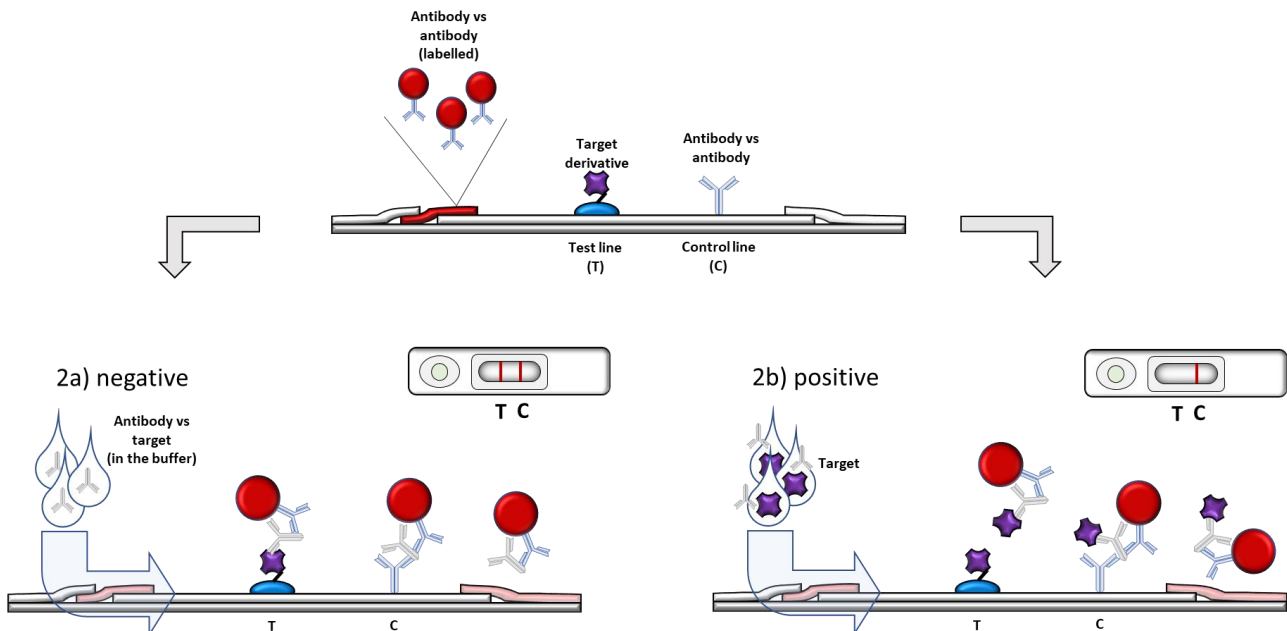


**Figure 1.8.** Scheme of the typical competitive LFIA with indirect labelling of the antibody. The strip composition and the assay principle are as described above, except for the fact that the specific antibody is present in the running buffer and the secondary antibody is labelled with gold nanoparticles as the probe. In the case of a negative sample (1a) the probe binds to the antibody, and the complex is captured by the test line so that the colour appears for the accumulation of the probe. In the case of a positive sample (1b) the target occupies the binding sites of the specific antibody and the complex is unable to be captured by the test line thus the colour does not appear.

The competitive approach can be used also for analytes of higher dimension. Being a less sensitive format on respect to the non-competitive counterpart it is not generally applied unless the non-competitive format is unavailable for steric hindrance issues or lack of sufficient binding epitopes. As the control line, typically a secondary antibody or a generic antibody-binding reagent is used to bind the excess of the labelled immunoreagent. In the development of a competitive test is important to balance the quantities of immunoreagents to maximize the response to minimum change of the target concentration; neither the labelled antibody nor the target antigen should be in excess compared to the target.

### 1.4.2 Non-competitive LFIA

This format can be used for molecules that have at least two epitopes. It is based on the mechanism of capture-revelation. In the case the target is an antigen, it is captured by an antibody immobilized in correspondence of the test line and revealed by another labelled antibody and that is the reason for which it also known as *sandwich* direct assay. Their development requires the production of two antibodies with complementary binding ability. To reach this goal, whenever possible, recombinant antigens, showing one specific epitope are prepared. Alternatively, antigens are extracted and purified from the pathogens.

The typical sandwich-type LFIA (Figure 1.9) can be designed in two different ways depending on the nature of the target antigen. If the antigen shows repeated equivalent epitopes, just one antibody can be used to act as the capturing and the detector reagent (*homologous sandwich*). If multiple equivalent epitopes do not exist, the use of two different antibodies is necessary (*heterologous sandwich*). Typically, large protein complexes, virus particles and cells present several repeated epitopes while peptides and proteins have different epitopes and require the production of two specific antibodies directed towards different portions of the molecule.

If the target is an antibody, as for serological assays, the antigen is used for capturing and/or for detection. Contrarily to the competitive format, in this case the presence of the target causes the appearance of the signal at the test line. The scheme is depicted in Figures 1.9-12. The non-competitive LFIA are affected by a great number of variables, such as: the number and nature of antigen epitopes, the sensitivity and specificity of the d antibodies, the ratios and balances between the target and similar molecules in the sample, etc...

### 1) Direct non-competitive LFIA

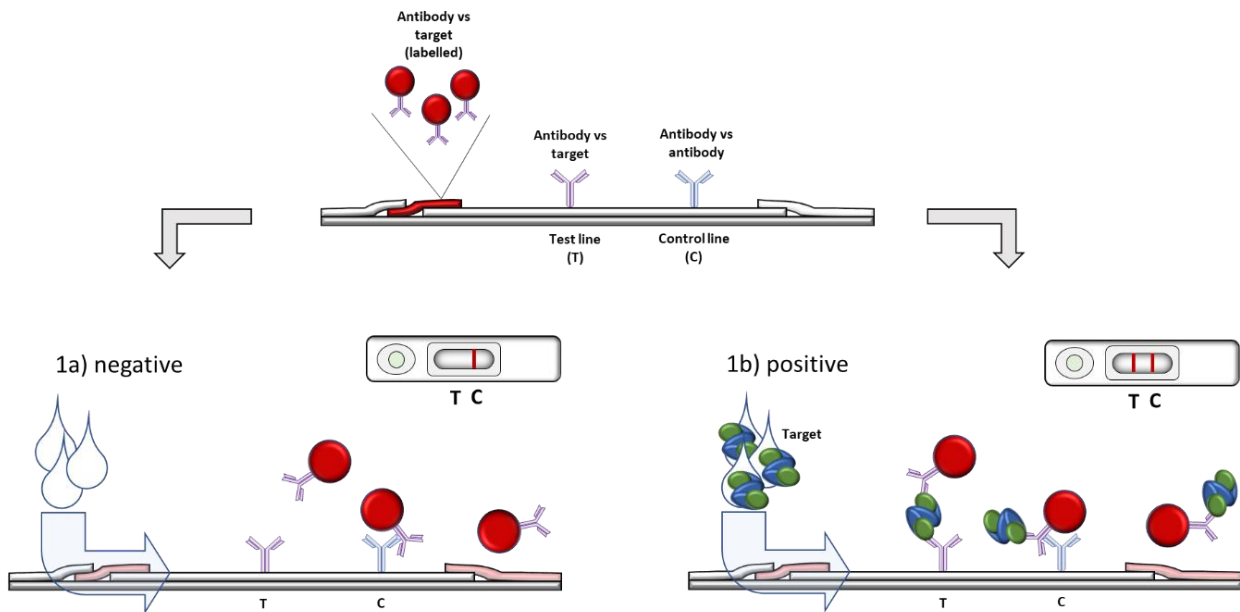


**Figure 1.9.** Scheme of the typical sandwich-type (or two sites immunometric) LFIA. The test line is formed by a specific antibody and the control line by a secondary antibody (1). A secondary specific antibody is labelled with gold nanoparticles and used for signal reporting. In the case of a negative sample (1a) the labelled antibody binds only to the control line. In the case of a positive sample (1b) the antigen is stapled by the two antibodies, giving colour by accumulation of the probe also on the test line.

As the control line, any kind of secondary antibody (anti-antibodies) or antibody-binding proteins (Staphylococcal protein A or Streptococcal protein G) can be used to bind the excess of probe flowing towards the adsorbent pad. Where the target is an antibody, the selection of a specific class of immunoglobulin to be targeted is accomplished by using suitable secondary reagents.

Concerning the use of LFIA for diagnosing infectious diseases, the antigen from the pathogen is exploited to characterize the antibody and the antigen is the only reagent on which relies the specificity. Depending on the class of antibodies, the abundance into the matrix, the affinity for the antigen, the characteristics of the antigen (stability to time, pH and temperature, solubility, similarity to the native form, compatibility with labels and/or nitrocellulose membranes), different formats can be applied.

## 2) Antibody non-competitive LFIA – Capture by antigen

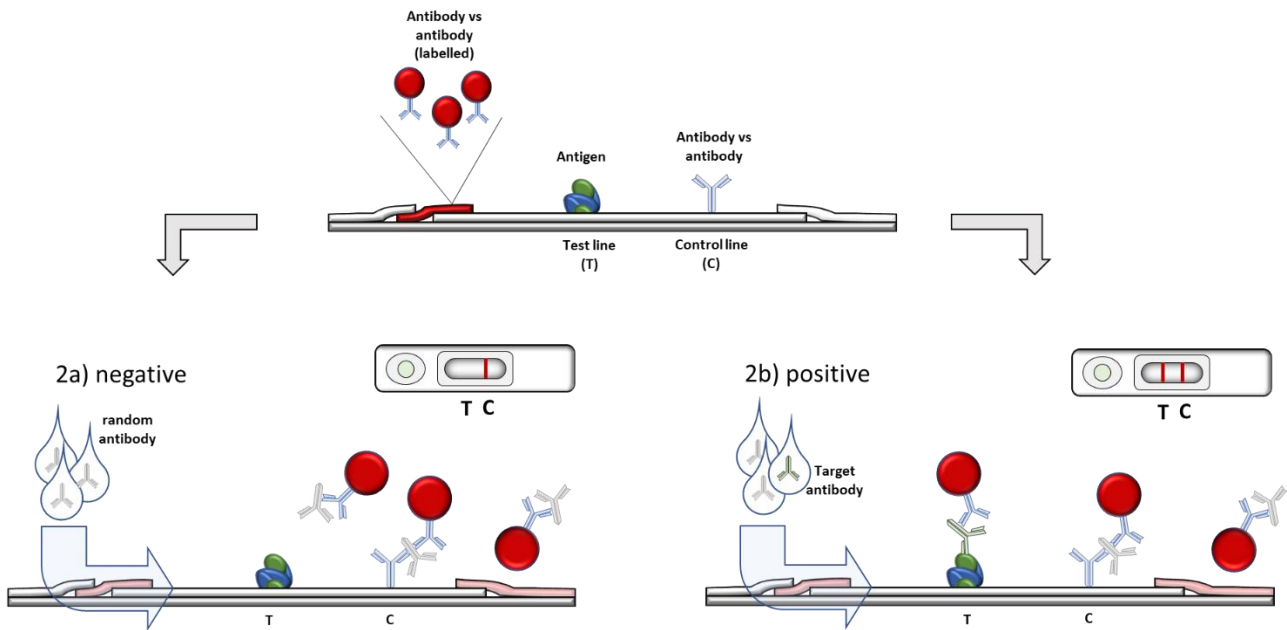


**Figure 1.10.** Scheme of the indirect antibody LFIA with immobilized antigen. The antigen is the capture reagent on the test line, while the control is given by a secondary antibody (2). The secondary antibody is labelled with gold nanoparticles for signal reporting. In the case of a negative sample (2a) the probe binds to generic antibodies without interactions with the test line. In the case of a positive sample (2b) the probe-target antibody complex binds to the antigen, giving colour by accumulation of the probe on the test line.

## 3) Antibody non-competitive LFIA – Capture by secondary antibody

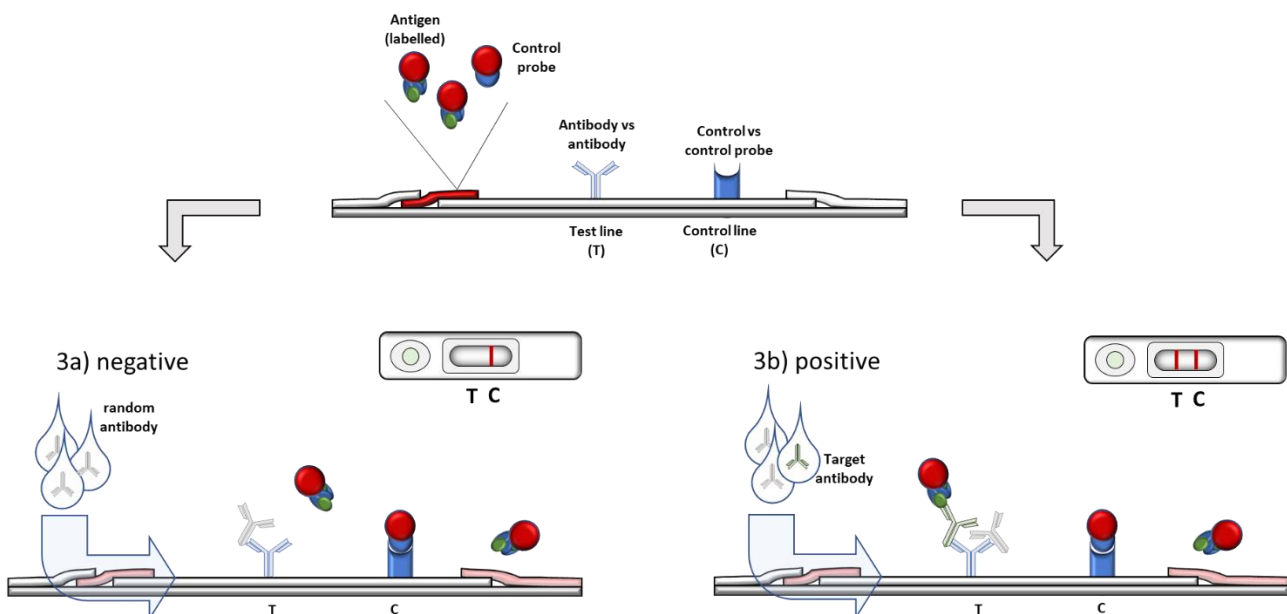


**Figure 1.11.** Scheme of the antigen-probe indirect antibody LFIA. The secondary antibody is the capture reagent on the test line, while the control is given by an ad-hoc reagent for the control probe. On the test line the secondary antibody and on the control line (3). The antigen is labelled with gold nanoparticles and mixed with the control probe for signal reporting. In the case of a negative sample (3a) the generic antibodies are captured by the test line, but the probe does not interact with them. The control line binds the control robe without any other influence. In the case of a positive sample (3b) the antigen probe binds the target antibody and then the secondary antibody when reaches the test line.

#### 4) Antibody non-competitive LFIA – Double antigen sandwich

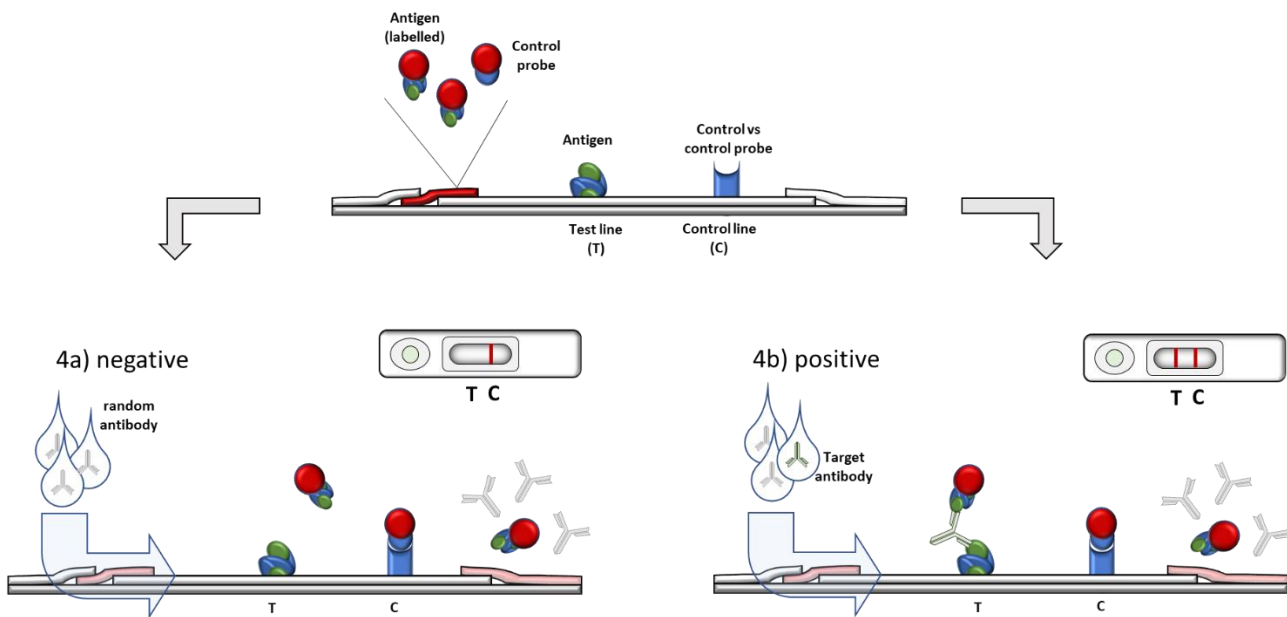


**Figure 1.12.** Scheme of the double-antigen indirect antibody LFIA. The antigen is present on the test line and as the antigen-probe. the control line is made by an ad-hoc pair (4). The antigen-probe is mixed with the control probe for signal reporting. In the case of a negative sample (4a) there is no binding except for the one at the control line. In the case of a positive sample (2b) the antigen-probe binds the target antibody, and the adduct is captured by the antigen on the test line.

The affinity required for the capture should be generally higher than the one required for detection. The time-lapse spent on the test line, during the flow, is very short (milliseconds), while from the resuspension of the probe to the reach of the test line passes many seconds during which the labelled reagents and the target are free to interact in solution. The antigen can be used for the capture (Figure 1.10) to specifically interact with the target antibodies, which are then revealed by a secondary antibody. This approach is expected to be more effective for high affinity antibodies or when many non-specific antibodies are present in the sample. This format can be reversed (Figure 1.11) exploiting the high binding capacity of the secondary antibodies and antibody-binding proteins, leaving to the probe the selection of the specific antibodies. This approach can be used when the affinity for the antigen is low or when the target antibodies are few in the sample. This strategy implies the labelling of the antigen. This last is needed, also, for the third format, the *double-antigen* (Figure 1.12). In this case the antigen is used both for capturing and for signal reporting. In this format, the generic antibodies, present in the matrix, do not interfere in the test. In principle, if the affinity of the target antibody for the antigen is high enough, this format should reach the maximal sensitivity through the maximal specificity. However, the use of labelled antigens introduces the problem of the control line, that cannot work as a standard control line. Generally, when a labelled antigen is used, an ad-hoc probe-capture pair (e.g., labelled biotin-avidin) is added to the system, assuming the control probe and test probes behave equivalently during the flow. This is, especially for poorly stable antigenic probes, a quite rough approximation and the risk is to increase the number of false positive and/or false negative results.

When the target is present in very large amount the so-called *Hook-effect* occurs: the saturation of the labelled and capture immunoreagents by the excess of the target provokes a loss in the analytical signal, rising the risk of false negatives. High-dose hook effect can be avoided by increasing the quantity of the antibodies and by reducing the amount of the sample by dilution [159]. During

the development of LFIA in the sandwich format, this phenomenon must be considered, especially for systems with wide analyte concentration ranges.

### 1.4.3 Multiplexing

To be univocal, the clinical decision often needs more than a single clue. For this reason, complementary information items are given by biomarkers involved in the diagnostic framework. The LFIA is such a versatile technique that the multitarget upgrade of the assay is almost always possible. Another advantage of multiplexing a LFIA strip on respect to other immunoassays is that it is possible to obtain information about all the involved targets within the single 10 minutes run from the single sample. All the formats mentioned above can be multiplexed through several strategies [160]. The different strategies are reported by exhaustive reviews such as “*Design of Multiplex Lateral Flow Tests: A Case Study for Simultaneous Detection of Three Antibiotics*” by A. Bartosh et al. (2020) [161], “*Multiplexed detection of biomarkers in lateral-flow immunoassays*” by L. Huang et al. (2020) [162] and “*Multiplex Lateral Flow Immunoassay: An Overview of Strategies towards High-throughput Point-of-Need Testing*” by L. Anfossi et al (2018) [163]. The use of multiple test lines drawn along the same strip by using different immunoreagents on different test lines allow for discrimination through spatial resolution (Figure 1.13a). Spatial multiplexing can also be realized by using microfluidic to produce microarrays as discussed by A. van Amerongen et al. in the chapter 7.2 of the *Handbook of Immunoassay Technologies* (2018) [160] (Figure 1.13b-d). Despite the high number of publications present in literature, array-like systems seem not to find a proportional fortune on the market. The reason can be the need of special reading devices, though they are often developed to be incorporated into portable devices or smartphone applications.

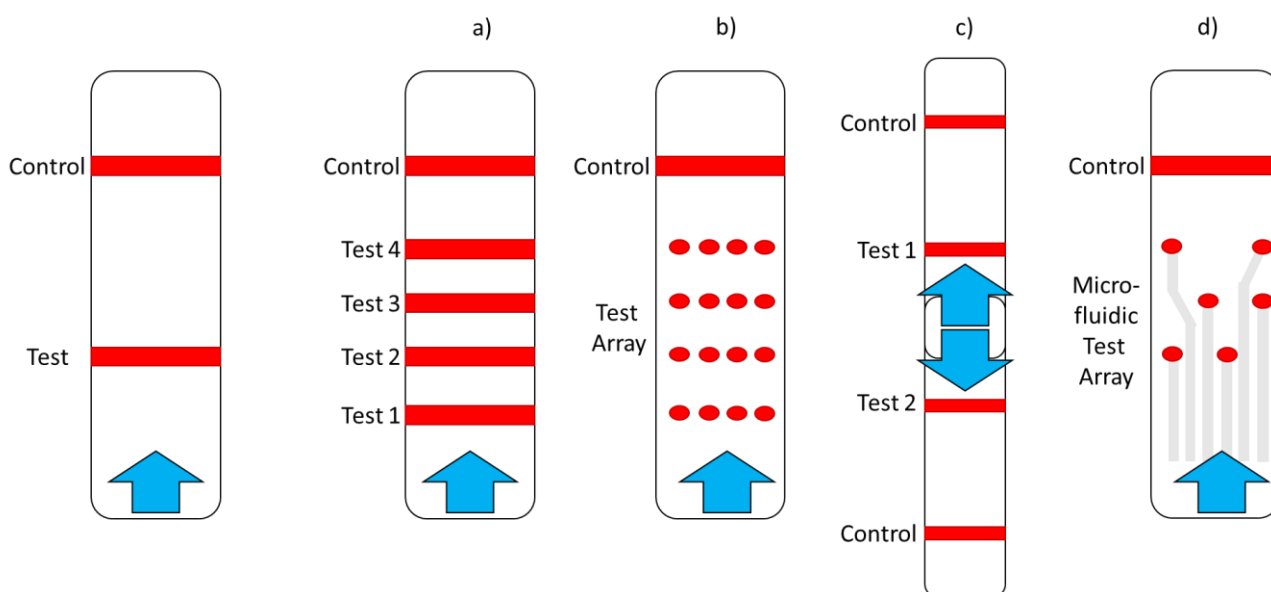


**Figure 1.13.** Currently used multiplexing strategies for LFIA: multiple lines (a), microarray of reactive spots (b), multi-flow (c) and microfluidic systems(d).

The same problem is affecting the use of alternative probes (differently coloured probes or mixing colorimetric, chemiluminescent, fluorescent, magnetic labels and so on) to differentiate by the detection [140], [164], [165] . Another feasible route for increasing the number of information

obtained by a single analysis relies in including more than a strip in the same device [166]. All these strategies present pros and cons and the optimal approach strongly depends on the specific application.

#### **1.4.4 Increasing the sensitivity**

Depending on the application, the sensitivity requirements of the LFIA device can be different. The great challenge of the LFIAs is the lowering of the limit of detection when the analyte is at very low concentration. Concerning infectious diseases this often is directly connected to the possibility to achieve early detection of a suspect case. For this reason, the quest of even more sensitive and effective devices is endless. Researchers are following this path as a holy grail, trying many approaches especially by using enhancing approaches (e.g. as described in the *Improvement in Detection Limit for Lateral Flow Assay of Biomacromolecules by Test-Zone Pre-enrichment* by Y. Zhang et al. in 2020 [167]), by using novel probes exploiting theoretically more sensitive physical phenomena (fluorescence or chemiluminescence) or by using new and complicated technologies (e.g. using laser excitation as proposed by H. Ye et al. in 2020 [168]).

In the chapter *Ways to Reach Lower Detection Limits of Lateral Flow Immunoassays* by A.V. Zherdev and B.B. Dzantiev (2018) in the book *Rapid Test - Advances in Design, Format and Diagnostic Applications* [169], the authors individuated the 'big five rules' for developing effective and sensitive LFIA including proper: sample, receptor, interaction, response, and output. They underlined the "role to antibodies affinity and specificity" and the "locations of the immunoreagents on the test strip" as "factors determining assay parameters".

Basing on these principles and combining with the diagnostic issues encountered in the thesis project, remarkable importance was given to the strategic design of the LFIA devices.



## 1.5



### Rapid diagnosis of infectious diseases

Infectious diseases are clinical issues provoked by an infection from a foreign organism (virus, bacterium, fungus, etc..) acting as a pathogen. After the infection, generally the immune system elicits an immune response and this a common aspect between infections from different pathogens [170]. On the contrary, symptoms can differ significantly, and, in many cases, the first stages of the infection are asymptomatic. The nature of infectious diseases is to spread from a host to another exploiting it as an incubator for replication, transforming it into a reservoir. Many pathogens cannot survive without a host, so they are naturally 'designed' to infect the largest possible number of individuals. This aspect renders the infection not only a problem for the individual, but for all the community. Quarantines and isolation, as seen in the last year, can cause not only health but also economic, social, behavioural, and political issues all around the world [171]–[173]. The transmission can occur, in many cases, in stages where the symptoms are still not present, and this is the main reason for which rapid screening tests are crucial to control the largest number of individuals in the lowest time [9], [174]. The importance of a prompt diagnosis to rapidly manage isolation and quarantines is self-evident. Higher screening capability allows for monitoring the susceptible population, at-risk communities and numerous groups previously exposed to infected individuals.

Infectious disease tests are generally based on the yes/no response to the presence or absence of direct or indirect biomarker [175].

For instance, the presence of antibodies specific to HIV antigens in the serum of an individual indirectly assesses the positivity to HIV. As explained in chapter 1.3.1, the classes of antibodies can be differently present depending on the stage of the infection. Targeting IgM or IgG enables discriminating between an early stage or an advanced stage, helping to understand the period of infection and the possible spread of transmission. On the other hand, the presence of the HIV antigens assesses directly (and earlier than antibodies) the exposure to the pathogen.

Regarding application to medical sciences, it is important to consider the implications of the strategy involving a first screening diagnosis. Usually, a less specific approach in favour of a more sensitive test is preferred; however how much of the specificity can be sacrificed is questionable. Sometimes is important to widening the number of biomarkers to be detected, sometimes it is useless or counterproductive. Clinical specificity and sensitivity are defined according to a binary classification of subjects and an ideal test is expected to correctly discriminate patients with the disease from patients who are disease free [176].

The diagnostic sensitivity and specificity are used to define the performances of any kind of clinical screening test used for binary decisions. Their mathematical expression is:

- *sensitivity* (Se) or *true positive rate* (TPR),  $\frac{TP}{TP+FN}$  is the probability that a sick/infected individual is correctly classified.
- *specificity* (Sp) or *true negative rate* (TNR),  $\frac{TN}{TN+FP}$  is the probability that a healthy individual is correctly classified.

where symbol meaning is the following:

- *positive* (P), sick/infected individual taking part to the study.
- *negative* (N), healthy individual taking part to the study.
- *true positive* (TP), are the ones correctly classified as sick/infected.
- *true negative* (TN), are the ones correctly classified as healthy.
- *false positive* (FP), are the healthy misclassified as sick/infected.
- *false negative* (FN), are the sick misclassified as healthy.

Besides  $Se$  and  $Sp$ , other parameters are often used to evaluate the clinical performance of a test:

- *positive predictive value* (PPV) or *precision*.  $\frac{TP}{TP+FP}$  is the probability that a positive result corresponds to a sick individual.
- *negative predictive value* (NPV).  $\frac{TN}{TN+FN}$  is the probability that a negative result corresponds to a healthy individual.
- *false negative rate* (FNR) or *miss-rate*.  $\frac{FN}{FN+TP}$  is the probability that a positive subject is misclassified as negative.
- *false positive rate* (FPR) or *fall-out*.  $\frac{FP}{FP+TN}$  is the probability that a negative subject is misclassified as positive.
- *false omission rate* (FOR).  $\frac{FN}{FN+TN}$  is the probability that a negative result is false.

Concerning infectious diseases, generally, the screening should be as much sensitive as possible, whereas the confirmation should be very specific, to un-mask false positive results. In the case of infectious diseases, the risk of false positives is world-widely accepted because justified by the importance of a prompt and quick intervention. In addition, the intervention in a suspect case is, generally, less invasive on respect to other kind of pathologies requiring biopsies, scintigraphy, or other invasive sampling necessary for the confirmation analysis.

As advanced before, the role of the LFIA in the diagnosis of infectious diseases was widely underlined in these years, as can be found in the WHO Bulletin in 2012, the N.P. Pai et al. review "*Point-of-Care Testing for Infectious Diseases: Diversity, Complexity, and Barriers in Low- And Middle-Income Countries*" (2012) [11], the "*Development of Multiplexed Infectious Disease Lateral Flow Assays: Challenges and Opportunities*" by K.M. Hanafiah et al. (2017) [177] and several other reviews. Among the many mentioned ones, an important aspect considering the importance of LFIA for diagnosing of infectious diseases is the fact that they can be executed, by the end user,

without the need to expose sanitary personnel to the risk of infection. This aspect directly affects also on the number of tests that can be executed and the subsequent amount of information collectable from the crisis units and reference epidemiological labs. The negative counterpart is the influence of the subjective interpretation of the results that can be minimized by clear instructions and by extremely performant devices giving the most straightforward outcomes. Many POCTs, especially in the format of LFIA devices, have been developed and used for decades for diagnosing infectious diseases in human and animal healthcare. Table 1 reports, as an example, the routine tests used for returning travellers at the Centre of Diagnostic Control and Prevention by E. Rabold and J. Waggoner [178].

**Table 1.** Centre of Diagnostic Control and Prevention suggested available tests for returning travellers, chapter 11, 2020 Yellow Book, Traveller’s Health

SYNDROME	PATHOGEN	SPECIMEN	ADDITIONAL INFORMATION
<b>Lateral flow immunochromatographic tests and small panels</b>			
<b>Systemic febrile illness</b>	Ebola virus <sup>1</sup>	Whole blood	Received emergency use authorization by FDA and WHO. May not be appropriate for excluding illness in early infection.
	Dengue virus <sup>1</sup>	Serum	Not FDA-cleared. Highly variable diagnostic performance. Antibodies may cross-react with other flaviviruses.
	Malaria <sup>1</sup>	Whole blood	Best performance characteristics for <i>Plasmodium falciparum</i> infections. Many versions may be available in endemic areas.
<b>Gastrointestinal infections</b>	Norovirus, rotavirus, adenovirus <sup>1</sup>	Stool sample	Available in the United States individually or in combination. Adenovirus rapid tests are approved for ocular specimens.
<b>Respiratory infections</b>	Group A <i>Streptococcus</i>	Throat swab	Rapid antigen and molecular tests <sup>2</sup> available. both are specific but molecular tests have improved sensitivity.
	Influenza	NP or throat swab	Rapid test sensitivity 50%–70%; negative testing should not direct treatment.
	<i>Legionella pneumophila</i> <sup>1</sup>	Urine	Only detects serogroup 1. Recommended by IDSA for patients with more severe disease.
	Respiratory syncytial virus	NP or throat swab	Accurate antigen assays, recommended if results will affect management.
	<i>Streptococcus pneumoniae</i>	Urine	Recommended by IDSA for use in certain patient populations.

<b>Sexually transmitted infections</b>	<i>Chlamydia trachomatis</i> and <i>Neisseria gonorrhoea</i> <sup>1</sup>	Urine, vaginal swab	Molecular tests remain gold standard; a sample-to-answer molecular assay is available. <sup>1,2</sup>
	HIV	Whole blood, oral fluids	Antibody and antibody/antigen kits available. Molecular testing preferred for acute infection.
	<i>Treponema pallidum</i>	Whole blood	Antibody detection, may not be appropriate for acute infections.
	<i>Trichomonas vaginalis</i>	Vaginal swab	Rapid antigen testing is specific with sensitivity approximately 90%.
	BV pathogens	Vaginal swab	Identifies increased sialidase activity, an enzyme associated with BV pathogens.

Abbreviations: BV, bacterial vaginosis; FDA, US Food and Drug Administration; IDSA, Infectious Disease Society of America; NP, nasopharyngeal; WHO, World Health Organization.

<sup>1</sup> Not waived by Clinical Laboratory Improvement Amendments.

<sup>2</sup> Not immunochromatographic assay

The screening diagnostics of infectious diseases can follow many different approaches using different formats. Majorly, considering the high molecular weight targets, they use non-competitive formats. The targets are typically viral or bacterial antigens (proteins, glycoproteins, lipoproteins) or antibodies (typically IgG) directed towards these antigens. Relevant to the field of chronic infectious diseases is also the follow up of the patient by monitoring the therapy. As an example, the management of HIV-infected subjects requires to assess in real time the compliance to the treatment to quickly discriminate if the therapeutic failure is due to drug resistance or to non-adherence, for assuring the best treatment for the subject and, also, for avoiding the development of drug resistant viral strains. This discipline is called therapeutic drug monitoring (TDM), and the targets are generally drugs, pro-drugs, or their metabolites, which are measured in biological fluids. As therapeutic drugs are small molecules, the only immunoassay format available for their detection is the competitive one.

### 1.5.1. Validation of diagnostic tests for infectious diseases

The field of In Vitro Diagnostic (IVD) is regulated by the Directive 98/79/EC. The minimal requirements for rapid in vitro IVD tests are reported in the 2009/886/EC: Commission Decision of 27<sup>th</sup> November 2009 [179].

Briefly, considering devices to be used with serum and blood specimens (e.g., HIV test) all the positives must be correctly classified (diagnostic sensitivity =100%) by the CE labelled device and the specificity must be at least 99.5%. For validation purposes, the negative samples must represent the target population to whom the device is addressed. the number of samples to be tested for the validation of the diagnostic depends on its application but is comprises between 300 and 400 for positive and from 5000 for negative samples. For other biological fluids (e.g., saliva or urine) the common technical specifications (CTS) must be the same so they must be evaluated in parallel with a serum (or plasma) test on the same subjects. Considering the tests for the home-diagnostics, they must satisfy the same specificity and sensitivity requirements in the CTS of the professional user

ones and the crucial parts of the evaluation must be carried out by end-users to validate the protocol and user instruction. In general, any new device must be validated with an already validated, certified, and updated one.

Starting from 26 May 2022, the Directive will be replaced by Regulation (EU) 2017/746 on in vitro diagnostic medical devices entailing some modifications including the mandatory delegation to third party of the validation process [180].

## References

- [1] E. P. Balogh, B. T. Miller, and J. R. Ball, *Improving diagnosis in health care*. National Academies Press, 2016.
- [2] “diagnosis - Wiktionary.” <https://en.wiktionary.org/wiki/diagnosis> (accessed Sep. 25, 2020).
- [3] M. E. Maitland, “A transdisciplinary definition of diagnosis,” *Journal of Allied Health*, vol. 39, no. 4. J Allied Health, pp. 306–313, Dec. 2010, Accessed: Feb. 02, 2021. [Online]. Available: <https://pubmed.ncbi.nlm.nih.gov/21184028/>.
- [4] A. Jutel, “Sociology of diagnosis: A preliminary review,” *Sociology of Health and Illness*, vol. 31, no. 2. Sociol Health Illn, pp. 278–299, Mar. 2009, doi: 10.1111/j.1467-9566.2008.01152.x.
- [5] P. Cappelletti, “Brain-to-brain loop 2020: è ancora utile il ciclo di Lundberg?,” *Rivista Italiana della Medicina di Laboratorio*, vol. 13, no. 3–4. Springer-Verlag Italia s.r.l., pp. 127–133, Dec. 01, 2017, doi: 10.1007/s13631-017-0160-z.
- [6] G. D. Lundberg, “Acting on Significant Laboratory Results,” *JAMA J. Am. Med. Assoc.*, vol. 245, no. 17, pp. 1762–1763, May 1981, doi: 10.1001/jama.1981.03310420052033.
- [7] H. M. J. Goldschmidt, “The NEXUS vision: An alternative to the reference value concept,” *Clin. Chem. Lab. Med.*, vol. 42, no. 7, pp. 868–873, 2004, doi: 10.1515/CCLM.2004.142.1.
- [8] J. Shreffler and M. R. Huecker, *Diagnostic Testing Accuracy: Sensitivity, Specificity, Predictive Values and Likelihood Ratios*. StatPearls Publishing, 2020.
- [9] C. S. Kosack, A. L. Page, and P. R. Klatser, “A guide to aid the selection of diagnostic tests,” *Bull. World Health Organ.*, vol. 95, no. 9, pp. 639–645, Sep. 2017, doi: 10.2471/BLT.16.187468.
- [10] G. Wu, M. H. Zaman, G. Wu, and M. H. Zaman, “Low-cost tools for diagnosing and monitoring HIV infection in low-resource settings,” no. July, pp. 914–920, 2012, doi: 10.2471/BLT.12.102780.
- [11] N. P. Pai, C. Vadnais, C. Denkinger, N. Engel, and M. Pai, “Point-of-Care Testing for Infectious Diseases: Diversity, Complexity, and Barriers in Low- And Middle-Income Countries,” *PLoS Med.*, vol. 9, no. 9, p. e1001306, Sep. 2012, doi: 10.1371/journal.pmed.1001306.
- [12] S. K. Vashist and J. H. T. Luong, “Immunoassays: An overview,” in *Handbook of Immunoassay Technologies: Approaches, Performances, and Applications*, Elsevier, 2018, pp. 1–18.
- [13] S. Avrameas, “Historical Background of the Invention of EIA and ELISA,” *Clin. Chem.*, vol. 52, no. 7, pp. 1430a – 1431, Jul. 2006, doi: 10.1373/clinchem.2006.069724.
- [14] R. M. Lequin, “Enzyme immunoassay (EIA)/enzyme-linked immunosorbent assay (ELISA),” *Clin. Chem.*, vol. 51, no. 12, pp. 2415–2418, Dec. 2005, doi: 10.1373/clinchem.2005.051532.
- [15] E. Engvall, “Perspective on the historical note on EIA/ELISA by Dr. R.M. Lequin,” *Clinical Chemistry*, vol. 51, no. 12. p. 2225, Dec. 2005, doi: 10.1373/clinchem.2005.059618.
- [16] S. Aydin, “A short history, principles, and types of ELISA, and our laboratory experience with peptide/protein analyses using ELISA,” *Peptides*, vol. 72, pp. 4–15, Mar. 2015, doi: 10.1016/j.peptides.2015.04.012.
- [17] R. Soleimani *et al.*, “Clinical usefulness of fully automated chemiluminescent immunoassay for quantitative antibody measurements in COVID-19 patients,” *J. Med. Virol.*, vol. 93, no. 3, pp. 1465–1477, Mar. 2021, doi: 10.1002/jmv.26430.
- [18] C. Wang, J. Wu, C. Zong, J. Xu, and H. X. Ju, “Chemiluminescent immunoassay and its applications,” *Fenxi Huaxue/ Chinese Journal of Analytical Chemistry*, vol. 40, no. 1. Chinese Academy of Sciences, pp. 3–10, 2012, doi: 10.1016/S1872-2040(11)60518-5.
- [19] M. Infantino *et al.*, “Diagnostic accuracy of an automated chemiluminescent immunoassay

- for anti-SARS-CoV-2 IgM and IgG antibodies: an Italian experience," *J. Med. Virol.*, vol. 92, no. 9, pp. 1671–1675, Sep. 2020, doi: 10.1002/jmv.25932.
- [20] L. Cinquanta, D. E. Fontana, and N. Bizzaro, "Chemiluminescent immunoassay technology: what does it change in autoantibody detection?," *Autoimmun. Highlights*, vol. 8, no. 1, Dec. 2017, doi: 10.1007/s13317-017-0097-2.
- [21] J. Liu, H. Qiao, and Z. Deng, "Chemiluminescence immunoassay," *Chem. Bull. / Huaxue Tongbao*, vol. 63, no. 7, pp. 49–53, Jan. 2000, doi: 10.1016/b978-012214730-2/50016-9.
- [22] A. Romeo, T. S. Leung, and S. Sánchez, "Smart biosensors for multiplexed and fully integrated point-of-care diagnostics," *Lab Chip*, vol. 16, no. 11, pp. 1957–1961, 2016, doi: 10.1039/c6lc90046a.
- [23] H. Kim, D. R. Chung, and M. Kang, "A new point-of-care test for the diagnosis of infectious diseases based on multiplex lateral flow immunoassays," *Analyst*, vol. 144, no. 8. Royal Society of Chemistry, pp. 2460–2466, Apr. 21, 2019, doi: 10.1039/c8an02295j.
- [24] W. C. Mak, V. Beni, and A. P. F. Turner, "Lateral-flow technology: From visual to instrumental," *TrAC - Trends in Analytical Chemistry*, vol. 79. Elsevier B.V., pp. 297–305, May 01, 2016, doi: 10.1016/j.trac.2015.10.017.
- [25] L. Anfossi, F. Di Nardo, S. Cavalera, C. Giovannoli, and C. Baggiani, "Multiplex lateral flow immunoassay: An overview of strategies towards high-throughput point-of-need testing," *Biosensors*, vol. 9, no. 1, 2018, doi: 10.3390/bios9010002.
- [26] K. M. M. Koczula and A. Gallotta, "Lateral flow assays," *Essays Biochem.*, vol. 60, no. 1, pp. 111–120, Jun. 2016, doi: 10.1042/EBC20150012.
- [27] B. G. Andryukov, "Six decades of lateral flow immunoassay: From determining metabolic markers to diagnosing covid-19," *AIMS Microbiology*, vol. 6, no. 3. AIMS Press, pp. 280–304, 2020, doi: 10.3934/microbiol.2020018.
- [28] A. E. Urusov, A. V. Zherdev, and B. B. Dzantiev, "Towards lateral flow quantitative assays: Detection approaches," *Biosensors*, vol. 9, no. 3. MDPI AG, Sep. 01, 2019, doi: 10.3390/bios9030089.
- [29] G. A. Posthuma-Trumpie, J. Korf, and A. Van Amerongen, "Lateral flow (immuno)assay: Its strengths, weaknesses, opportunities and threats. A literature survey," *Anal. Bioanal. Chem.*, vol. 393, no. 2, pp. 569–582, Jan. 2009, doi: 10.1007/s00216-008-2287-2.
- [30] A. W. Martinez, S. T. Phillips, G. M. Whitesides, and E. Carrilho, "Diagnostics for the developing world: Microfluidic paper-based analytical devices," *Anal. Chem.*, vol. 82, no. 1, pp. 3–10, 2010, doi: 10.1021/ac9013989.
- [31] R. Ota, K. Yamada, K. Suzuki, and D. Citterio, "Quantitative evaluation of analyte transport on microfluidic paper-based analytical devices ( $\mu$ PADs)," *Analyst*, vol. 143, no. 3, pp. 643–653, Feb. 2018, doi: 10.1039/c7an01702b.
- [32] Y. Fuchiwaki, K. Goya, and M. Tanaka, "Practical high-performance lateral flow assay based on autonomous microfluidic replacement on a film," *Anal. Sci.*, vol. 34, no. 1, pp. 57–63, 2018, doi: 10.2116/analsci.34.57.
- [33] B. K. Yap, S. N. M. Soair, N. A. Talik, W. F. Lim, and I. Lai Mei, "Potential point-of-care microfluidic devices to diagnose iron deficiency anemia," *Sensors (Switzerland)*, vol. 18, no. 8. MDPI AG, Aug. 10, 2018, doi: 10.3390/s18082625.
- [34] A. Yakoh, S. Chaiyo, W. Siangproh, and O. Chailapakul, "3D Capillary-Driven Paper-Based Sequential Microfluidic Device for Electrochemical Sensing Applications," *ACS Sensors*, vol. 4, no. 5, pp. 1211–1221, May 2019, doi: 10.1021/acssensors.8b01574.
- [35] E. Fu, "Paper Microfluidics for POC Testing in Low-Resource Settings," 2019, pp. 325–352.
- [36] L. Wentland, R. Polaski, and E. Fu, "Characterization methods in porous materials for the rational design of multi-step processing in the context of a paper microfluidic phenylalanine test," *Anal. Methods*, vol. 12, no. 6, pp. 768–780, Feb. 2020, doi: 10.1039/c9ay02500f.

- [37] G. Ruiz-Vega *et al.*, "Electrochemical POC device for fast malaria quantitative diagnosis in whole blood by using magnetic beads, Poly-HRP and microfluidic paper electrodes," *Biosens. Bioelectron.*, vol. 150, Feb. 2020, doi: 10.1016/j.bios.2019.111925.
- [38] S. G. Jeong, D.-H. Kim, J. Kim, J.-H. Kim, S. Song, and C.-S. Lee, "Programmable microfluidic flow for automatic multistep digital assay in a single-sheet 3-dimensional paper-based microfluidic device," *Chem. Eng. J.*, vol. 411, p. 128429, May 2021, doi: 10.1016/j.cej.2021.128429.
- [39] G. E. Fridley, H. Le, and P. Yager, "Highly sensitive immunoassay based on controlled rehydration of patterned reagents in a 2-dimensional paper network," *Anal. Chem.*, vol. 86, no. 13, pp. 6447–6453, Jul. 2014, doi: 10.1021/ac500872j.
- [40] D. M. Cate, J. A. Adkins, J. Mettakoonpitak, and C. S. Henry, "Recent developments in paper-based microfluidic devices," *Analytical Chemistry*, vol. 87, no. 1. American Chemical Society, pp. 19–41, Jan. 06, 2015, doi: 10.1021/ac503968p.
- [41] S. G. Jeong, J. Kim, S. H. Jin, K. S. Park, and C. S. Lee, "Flow control in paper-based microfluidic device for automatic multistep assays: A focused minireview," *Korean Journal of Chemical Engineering*, vol. 33, no. 10. Springer New York LLC, pp. 2761–2770, Oct. 01, 2016, doi: 10.1007/s11814-016-0161-z.
- [42] C. Castro, C. Rosillo, and H. Tsutsui, "Characterizing effects of humidity and channel size on imbibition in paper-based microfluidic channels," *Microfluid. Nanofluidics*, vol. 21, no. 2, Feb. 2017, doi: 10.1007/s10404-017-1860-4.
- [43] M. M. Gong and D. Sinton, "Turning the Page: Advancing Paper-Based Microfluidics for Broad Diagnostic Application," *Chemical Reviews*, vol. 117, no. 12. American Chemical Society, pp. 8447–8480, Jun. 28, 2017, doi: 10.1021/acs.chemrev.7b00024.
- [44] K. Yamada, H. Shibata, K. Suzuki, and D. Citterio, "Toward practical application of paper-based microfluidics for medical diagnostics: state-of-the-art and challenges," *Lab on a Chip*, vol. 17, no. 7. Royal Society of Chemistry, pp. 1206–1249, Apr. 07, 2017, doi: 10.1039/c6lc01577h.
- [45] T. H. Kim, Y. K. Hahn, J. Lee, D. Van Noort, and M. S. Kim, "Solenoid Driven Pressure Valve System: Toward Versatile Fluidic Control in Paper Microfluidics," *Anal. Chem.*, vol. 90, no. 4, pp. 2534–2541, Feb. 2018, doi: 10.1021/acs.analchem.7b03791.
- [46] R. B. Channon *et al.*, "Rapid flow in multilayer microfluidic paper-based analytical devices," *Lab Chip*, vol. 18, no. 5, pp. 793–802, Mar. 2018, doi: 10.1039/c7lc01300k.
- [47] J. M. Singer, "Citation Classic Commentaries: The latex fixation test.," *Curr. Contents*, vol. 51, no. 21, p. 110, 1977, doi: 10.1210/en.2011-1316.
- [48] F. Nardo *et al.*, "Direct vs mediated coupling of antibodies to gold nanoparticles: the case of salivary cortisol detection by lateral flow immunoassay," *ACS Appl. Mater. Interfaces*, vol. 11, pp. 32758–32768, 2019.
- [49] H.-M. C. J. Y. JH Soh, "Strategies for developing sensitive and specific nanoparticle-based lateral flow assays as point-of-care diagnostic device," *Nano Today*, vol. 30, p. 100831, 2020.
- [50] V-T. Nguyen *et al.*, "Recent advances in high-sensitivity detection methods for paper-based lateral-flow assay," *Biosens. Bioelectron.*, vol. 152, p. 112015, 2020.
- [51] M. S. EB Bahadır, "Lateral flow assays: principles, designs and labels," *Trends Anal. Chem.*, vol. 82, pp. 286–306, 2016.
- [52] A. M. C Parolo, "Paper-based nanobiosensors for diagnostics," *Chem. Soc. Rev.*, vol. 42, pp. 450–457, 2013.
- [53] C. Parolo *et al.*, "Tutorial: design and fabrication of nanoparticle-based lateral-flow immunoassays," *Nature Protocols*, vol. 15, no. 12. Nature Research, pp. 3788–3816, Dec. 01, 2020, doi: 10.1038/s41596-020-0357-x.



- [54] M. Sajid and M. Daud, "Designs , formats and applications of lateral flow assay : A literature review," *J. Saudi Chem. Soc.*, vol. 19, no. 6, pp. 689–705, 2015, doi: 10.1016/j.jscs.2014.09.001.
- [55] C. M. Plotz and J. M. Singer, "The latex fixation test. I. Application to the serologic diagnosis of rheumatoid arthritis.," *Am. J. Med.*, vol. 21, no. 6, pp. 888–892, Dec. 1956.
- [56] J. L. Vaitukaitis, G. D. Braunstein, and G. T. Ross, "A radioimmunoassay which specifically measures human chorionic gonadotropin in the presence of human luteinizing hormone," *Am. J. Obstet. Gynecol.*, vol. 113, no. 6, pp. 751–758, Jul. 1972, doi: 10.1016/0002-9378(72)90553-4.
- [57] "US4703017A - Solid phase assay with visual readout - Google Patents." <https://patents.google.com/patent/US4703017A/en> (accessed Feb. 02, 2021).
- [58] "Capillary immunoassay and device therefor comprising mobilizable particulate labelled reagents," Jul. 1993.
- [59] "US4855240A - Solid phase assay employing capillary flow - Google Patents." <https://patents.google.com/patent/US4855240A/en> (accessed Feb. 02, 2021).
- [60] "(16) (PDF) Global Business Strategy Case Study: Clearblue Profile." [https://www.researchgate.net/publication/315085182\\_Global\\_Business\\_Strategy\\_Case\\_Study\\_Clearblue\\_Profile](https://www.researchgate.net/publication/315085182_Global_Business_Strategy_Case_Study_Clearblue_Profile) (accessed Feb. 02, 2021).
- [61] Y. Huang, "Development of up-converting phosphor technology-based lateral flow assay for quantitative detection of serum PIVKA-II: inception of a near-patient PIVKA-II detection tool," *Clin. Chim. Acta*, vol. 488, pp. 202–208, 2019.
- [62] H. Yang, "A novel quantum dots-based point of care test for syphilis," *Nanoscale Res. Lett.*, vol. 5, pp. 875–881, 2010.
- [63] A. S. S Dalirirad, "Lateral flow assay using aptamer-based sensing for on-site detection of dopamine in urine," *Anal. Biochem.*, vol. 596, p. 113637, 2020.
- [64] G. Mosley, "Improved lateral-flow immunoassays for chlamydia and immunoglobulin M by sequential rehydration of two-phase system components within a paper-based diagnostic," *Microchim. Acta*, vol. 184, pp. 4055–4064, 2017.
- [65] A. H. A. Hassan et al., "Validity of a single antibody-based lateral flow immunoassay depending on graphene oxide for highly sensitive determination of E. coli O157:H7 in minced beef and river water," *Food Chem.*, vol. 297, p. 124965, 2019.
- [66] D. Boulware, "Multisite validation of cryptococcal antigen lateral flow assay and quantification by laser thermal contrast," *Emerg. Infect. Dis.*, vol. 20, pp. 45–53, 2014.
- [67] S. Fukushi, "Characterization of novel monoclonal antibodies against the MERS-coronavirus spike protein and their application in species-independent antibody detection by competitive ELISA," *J. Virol. Methods*, vol. 251, pp. 22–29, 2018.
- [68] J. Hu, "Advances in paper-based point-of-care diagnostics," *Biosens. Bioelectron.*, vol. 54, pp. 585–597, 2014.
- [69] M. Zarei, "Infectious pathogens meet point-of-care diagnostics," *Biosensors and Bioelectronics*, vol. 106. Elsevier Ltd, pp. 193–203, May 30, 2018, doi: 10.1016/j.bios.2018.02.007.
- [70] J. Si et al., "A signal amplification system on a lateral flow immunoassay detecting for hepatitis e-antigen in human blood samples," *J. Med. Virol.*, vol. 91, no. 7, pp. 1301–1306, Jul. 2019, doi: 10.1002/jmv.25452.
- [71] I. V. Safenkova, V. G. Panferov, N. A. Panferova, Y. A. Varitsev, A. V. Zherdev, and B. B. Dzantiev, "Alarm lateral flow immunoassay for detection of the total infection caused by the five viruses," *Talanta*, vol. 195, pp. 739–744, Apr. 2019, doi: 10.1016/j.talanta.2018.12.004.
- [72] Z. Rong et al., "Smartphone-based fluorescent lateral flow immunoassay platform for highly sensitive point-of-care detection of Zika virus nonstructural protein 1," *Anal. Chim. Acta*,

vol. 1055, pp. 140–147, May 2019, doi: 10.1016/j.aca.2018.12.043.

- [73] L. Ou, “Development of a lateral flow immunochromatographic assay for rapid detection of *Mycoplasma pneumoniae*-specific IgM in human serum specimens,” *J. Microbiol. Methods*, vol. 124, pp. 35–40, 2016.
- [74] M. El-Tholoth, M. Branavan, A. Naveenathayalan, and W. Balachandran, “Recombinase polymerase amplification–nucleic acid lateral flow immunoassays for Newcastle disease virus and infectious bronchitis virus detection,” *Mol. Biol. Rep.*, vol. 46, no. 6, pp. 6391–6397, Dec. 2019, doi: 10.1007/s11033-019-05085-y.
- [75] S. Kumar, P. Bhushan, V. Krishna, and S. Bhattacharya, “Tapered lateral flow immunoassay based point-of-care diagnostic device for ultrasensitive colorimetric detection of dengue NS1,” *Biomicrofluidics*, vol. 12, no. 3, May 2018, doi: 10.1063/1.5035113.
- [76] J. Hwang, S. Lee, and J. Choo, “Application of a SERS-based lateral flow immunoassay strip for the rapid and sensitive detection of staphylococcal enterotoxin B,” *Nanoscale*, vol. 8, no. 22, pp. 11418–11425, Jun. 2016, doi: 10.1039/c5nr07243c.
- [77] Y. H. Huang *et al.*, “Development of a nucleic acid lateral flow immunoassay for the detection of human polyomavirus BK,” *Diagnostics*, vol. 10, no. 6, Jun. 2020, doi: 10.3390/diagnostics10060403.
- [78] J. Wang *et al.*, “Rapid detection of *Escherichia coli* O157 and shiga toxins by lateral flow immunoassays,” *Toxins (Basel)*, vol. 8, no. 4, Mar. 2016, doi: 10.3390/toxins8040092.
- [79] C. S. Jørgensen, S. A. Uldum, J. F. Sørensen, I. C. Skovsted, S. Otte, and P. L. Elverdal, “Evaluation of a new lateral flow test for detection of *Streptococcus pneumoniae* and *Legionella pneumophila* urinary antigen,” *J. Microbiol. Methods*, vol. 116, pp. 33–36, Sep. 2015, doi: 10.1016/j.mimet.2015.06.014.
- [80] K. Nielsen *et al.*, “Development of a lateral flow assay for rapid detection of bovine antibody to *Anaplasma marginale*,” *J. Immunoass. Immunochem.*, vol. 29, no. 1, pp. 10–18, Jan. 2008, doi: 10.1080/15321810701734693.
- [81] H. K. Oh *et al.*, “High sensitive and broad-range detection of cortisol in human saliva using a trap lateral flow immunoassay (trapLFI) sensor,” *Analyst*, vol. 143, pp. 3883–3889, 2018.
- [82] A. Golden, “Extended result reading window in lateral flow tests detecting exposure to *Onchocerca volvulus*: a new technology to improve epidemiological surveillance tools,” *PLoS One*, vol. 8, p. e69231, 2013.
- [83] A. Chamorro-Garcia, “Detection of parathyroid hormone-like hormone in cancer cell cultures by gold nanoparticle-based lateral flow immunoassays,” *Nanomedicine*, vol. 12, pp. 53–61, 2016.
- [84] B. Dieplinger *et al.*, “Analytical and clinical evaluation of a rapid quantitative lateral flow immunoassay for measurement of soluble ST2 in human plasma,” *Clin. Chim. Acta*, vol. 451, pp. 310–315, 2015.
- [85] X. Yan, “CdSe/ZnS quantum dot-labeled lateral flow strips for rapid and quantitative detection of gastric cancer carbohydrate antigen 72-4,” *Nanoscale Res. Lett.*, vol. 11, 2016.
- [86] Z. Lin, “Development of an immunochromatographic lateral flow device for rapid detection of *Helicobacter pylori* stool antigen,” *Clin. Biochem.*, vol. 48, pp. 1298–1303, 2015.
- [87] A. Sakurai, “Multi-colored immunochromatography using nanobeads for rapid and sensitive typing of seasonal influenza viruses,” *J. Virol. Methods*, vol. 209, pp. 62–68, 2014.
- [88] C. Wang, “Lateral flow immunoassay integrated with competitive and sandwich models for the detection of aflatoxin M1 and *Escherichia coli* O157:H7 in milk,” *J. Dairy Sci.*, vol. 101, pp. 8767–8777, 2018.
- [89] D. Kong, “Ultrasensitive and eco-friendly immunoassays based monoclonal antibody for detection of deoxynivalenol in cereal and feed samples,” *Food Chem.*, vol. 270, pp. 130–137, 2019.

- [90] R. Verheijen et al., "Development of a one step strip test for the detection of (dihydro)streptomycin residues in raw milk," *Food Agric. Immunol.*, vol. 12, pp. 31–40, 2000.
- [91] M. Principato, "Detection of target staphylococcal enterotoxin B antigen in orange juice and popular carbonated beverages using antibody-dependent antigen-capture assays," *J. Food Sci.*, vol. 75, pp. T141–T147, 2010.
- [92] M. Magiati et al., "Lateral flow test for meat authentication with visual detection," *Food Chem.*, vol. 274, pp. 803–807, 2019.
- [93] X. Yang, "A lateral flow immunochromatographic strip test for rapid detection of oseltamivir phosphate in egg and chicken meat," *Sci. Rep.*, vol. 8, 2018.
- [94] K. K Luo et al., "Paper-based lateral flow strip assay for the detection of foodborne pathogens: principles, applications, technological challenges and opportunities," *Crit. Rev. Food Sci. Nutr.*, vol. 60, pp. 157–170, 2020.
- [95] B. Ngom et al., "Development and application of lateral flow test strip technology for detection of infectious agents and chemical contaminants: a review," *Anal. Bioanal. Chem.*, vol. 397, pp. 1113–1135, 2010.
- [96] N. A. Byzova, S. V. Vinogradova, E. V. Porotikova, U. D. Terekhova, A. V. Zherdev, and B. B. Dzantiev, "Lateral flow immunoassay for rapid detection of grapevine leafroll-associated virus," *Biosensors*, vol. 8, no. 4, Nov. 2018, doi: 10.3390/bios8040111.
- [97] K. Morioka et al., "Development and Evaluation of a Rapid Antigen Detection and Serotyping Lateral Flow Antigen Detection System for Foot-and-Mouth Disease Virus," *PLoS One*, vol. 10, no. 8, pp. 1–10, Aug. 2015, doi: 10.1371/journal.pone.0134931.
- [98] R. Greenwald, "Improved serodetection of *Mycobacterium bovis* infection in badgers (*Meles meles*) using multiantigen test formats," *Diagn. Microbiol. Infect. Dis.*, vol. 46, pp. 197–203, 2003.
- [99] M.-Z. Zhang et al., "Development of a colloidal gold-based lateral-flow immunoassay for the rapid simultaneous detection of clenbuterol and ractopamine in swine urine," *Anal. Bioanal. Chem.*, vol. 395, no. 8, p. 2591, 2009, doi: 10.1007/s00216-009-3181-2.
- [100] Q. Wang, Y. Liu, M. Wang, Y. Chen, and W. Jiang, "A multiplex immunochromatographic test using gold nanoparticles for the rapid and simultaneous detection of four nitrofurantol metabolites in fish samples," *Anal. Bioanal. Chem.*, vol. 410, no. 1, pp. 223–233, 2018, doi: 10.1007/s00216-017-0714-y.
- [101] P. Sastre et al., "Development of a novel lateral flow assay for detection of African swine fever in blood," vol. 12, no. 1, p. 206, Sep. 2016, doi: 10.1186/s12917-016-0831-4.
- [102] J. Choi, "Sensitive biomolecule detection in lateral flow assay with a portable temperature–humidity control device," *Biosens. Bioelectron.*, vol. 79, pp. 98–107, 2016.
- [103] M. Blazková et al., "Immunochromatographic colloidal carbon-based assay for detection of methiocarb in surface water," *Biosens. Bioelectron.*, vol. 25, pp. 753–758, 2009.
- [104] L. Yao, "MWCNTs based high sensitive lateral flow strip biosensor for rapid determination of aqueous mercury ions," *Biosens. Bioelectron.*, vol. 85, pp. 331–336, 2016.
- [105] Z. Wu, "Aptamer-based fluorescence-quenching lateral flow strip for rapid detection of mercury (II) ion in water samples," *Anal. Bioanal. Chem.*, vol. 409, pp. 5209–5216, 2017.
- [106] D. Quesada-González et al., "Uranium (VI) detection in groundwater using a gold nanoparticle/paper-based lateral flow device," *Sci. Rep.*, vol. 8, 2018.
- [107] J. Ramage, "Comprehensive laboratory evaluation of a specific lateral flow assay for the presumptive identification of abrin in suspicious white powders and environmental samples," *Biosecur. Bioterror.*, vol. 12, pp. 49–62, 2014.
- [108] Y. Liu, "Detection of 3-phenoxybenzoic acid in river water with a colloidal gold-based lateral flow immunoassay," *Anal. Biochem.*, vol. 483, pp. 7–11, 2015.
- [109] M. Hudson, "Drug screening using the sweat of a fingerprint: lateral flow detection of  $\Delta 9$ -

- tetrahydrocannabinol, cocaine, opiates and amphetamine," *J. Anal. Toxicol.*, vol. 43, pp. 88–95, 2019.
- [110] G. Tan, "Ultrasensitive quantitation of imidacloprid in vegetables by colloidal gold and time-resolved fluorescent nanobead traced lateral flow immunoassays," *Food Chem.*, vol. 311, p. 126055, 2020.
- [111] Z. Li et al., "Development and clinical validation of a sensitive lateral flow assay for rapid urine fentanyl screening in the emergency department," *Clin. Chem.*, vol. 66, pp. 324–332, 2020.
- [112] M. Blažková et al., "Strip-based immunoassay for rapid detection of thiabendazole," *Biosens. Bioelectron.*, vol. 25, pp. 2122–2128, 2010.
- [113] Q. Hu, "An up-converting phosphor technology-based lateral flow assay for point-of-collection detection of morphine and methamphetamine in saliva," *Analyst*, vol. 143, pp. 4646–4654, 2018.
- [114] F. Di Nardo *et al.*, "Colour-encoded lateral flow immunoassay for the simultaneous detection of aflatoxin B1 and type-B fumonisins in a single Test line," *Talanta*, vol. 192, no. July 2018, pp. 288–294, 2019, doi: 10.1016/j.talanta.2018.09.037.
- [115] H. Jiang, "Silver nanoparticle-based fluorescence-quenching lateral flow immunoassay for sensitive detection of ochratoxin A in grape juice and wine," *Toxins (Basel)*, vol. 9, p. 83, 2017.
- [116] L Anfossi, G. D'Arco, G. Giraudi, C. Giovannoli, C. Baggiani, "Lateral-flow immunoassays for mycotoxins and phycotoxins: a review," *Anal. Bioanal. Chem.*, vol. 405, pp. 467–480, 2013.
- [117] S. Song *et al.*, "Multiplex Lateral Flow Immunoassay for Mycotoxin Determination," *Anal. Chem.*, vol. 86, no. 10, pp. 4995–5001, May 2014, doi: 10.1021/ac500540z.
- [118] A. Foubert, "Development of a rainbow lateral flow immunoassay for the simultaneous detection of four mycotoxins," *J. Agric. Food Chem.*, vol. 65, pp. 7121–7130, 2017.
- [119] "Lateral flow immunoassay," *Japanese Journal of Medical Mycology*, vol. 57, no. 3. Japanese Society for Medical Mycology, p. J 125, 2016, doi: 10.1007/978-1-59745-240-3.
- [120] Y. Xiang, P. Wu, L. H. Tan, and Y. Lu, "DNzyme-functionalized gold nanoparticles for biosensing," *Adv. Biochem. Eng. Biotechnol.*, vol. 140, pp. 93–120, 2014, doi: 10.1007/10\_2013\_242.
- [121] M. Mousivand, L. Anfossi, K. Bagherzadeh, N. Barbero, A. Mirzadi-Gohari, and M. Javan-Nikkhah, "In silico maturation of affinity and selectivity of DNA aptamers against aflatoxin B1 for biosensor development," *Anal. Chim. Acta*, vol. 1105, pp. 178–186, Apr. 2020, doi: 10.1016/j.aca.2020.01.045.
- [122] L. Anfossi, G. D'Arco, M. Calderara, C. Baggiani, C. Giovannoli, and G. Giraudi, "Development of a quantitative lateral flow immunoassay for the detection of aflatoxins in maize," *Food Addit. Contam. - Part A Chem. Anal. Control. Expo. Risk Assess.*, vol. 28, no. 2, pp. 226–234, Feb. 2011, doi: 10.1080/19440049.2010.540763.
- [123] G. Spano, S. Cavalera, F. Di Nardo, C. Giovannoli, L. Anfossi, and C. Baggiani, "Development of a biomimetic enzyme-linked immunosorbent assay based on a molecularly imprinted polymer for the detection of cortisol in human saliva," *Anal. Methods*, vol. 11, no. 17, pp. 2320–2326, 2019, doi: 10.1039/c9ay00317g.
- [124] H. W. Schroeder and L. Cavacini, "Structure and function of immunoglobulins," *J. Allergy Clin. Immunol.*, vol. 125, no. 2 SUPPL. 2, p. S41, Feb. 2010, doi: 10.1016/j.jaci.2009.09.046.
- [125] N. S. Lipman, L. R. Jackson, L. J. Trudel, and F. Weis-Garcia, "Monoclonal Versus Polyclonal Antibodies: Distinguishing Characteristics, Applications, and Information Resources," *ILAR J.*, vol. 46, no. 3, pp. 258–268, Jan. 2005, doi: 10.1093/ilar.46.3.258.
- [126] M. C. Brown, "Antibodies: Key to a Robust Lateral Flow Immunoassay," in *Lateral Flow Immunoassay*, Humana Press, 2009, pp. 1–16.

- [127] A. Ibekwe, C. Perras, and M. Mierzwinski-Urban, *Monoclonal Antibodies to Prevent Migraine Headaches*. Canadian Agency for Drugs and Technologies in Health, 2016.
- [128] J. Song, R. M. Wang, Y. Q. Wang, Y. R. Tang, and A. P. Deng, "Hapten design, modification and preparation of artificial antigens," *Fenxi Huaxue/ Chinese J. Anal. Chem.*, vol. 38, no. 8, pp. 1211–1218, 2010, doi: 10.1016/S1872-2040(09)60063-3.
- [129] X. Gong *et al.*, "A review of fluorescent signal-based lateral flow immunochromatographic strips," *Journal of Materials Chemistry B*, vol. 5, no. 26. Royal Society of Chemistry, pp. 5079–5091, Jul. 04, 2017, doi: 10.1039/c7tb01049d.
- [130] K. A. Edwards and A. J. Baeumner, "Liposome-enhanced lateral-flow assays for the sandwich-hybridization detection of RNA," *Methods Mol. Biol.*, vol. 504, pp. 185–215, 2009, doi: 10.1007/978-1-60327-569-9\_13.
- [131] J. A. A. Ho and R. D. Wauchope, "A strip liposome immunoassay for aflatoxin B1," *Anal. Chem.*, vol. 74, no. 7, pp. 1493–1496, Apr. 2002, doi: 10.1021/ac010903q.
- [132] J. A. A. Ho, S. C. Zeng, W. H. Tseng, Y. J. Lin, and C. H. Chen, "Liposome-based immunostrip for the rapid detection of Salmonella," *Anal. Bioanal. Chem.*, vol. 391, no. 2, pp. 479–485, May 2008, doi: 10.1007/s00216-008-1875-5.
- [133] G. R. Han and M. G. Kim, "Highly sensitive chemiluminescence-based lateral flow immunoassay for cardiac troponin I detection in human serum," *Sensors (Switzerland)*, vol. 20, no. 9, May 2020, doi: 10.3390/s20092593.
- [134] J. Deng, M. Yang, J. Wu, W. Zhang, and X. Jiang, "A Self-Contained Chemiluminescent Lateral Flow Assay for Point-of-Care Testing," *Anal. Chem.*, vol. 90, no. 15, pp. 9132–9137, Aug. 2018, doi: 10.1021/acs.analchem.8b01543.
- [135] J. M. Park, H. W. Jung, Y. W. Chang, H. S. Kim, M. J. Kang, and J. C. Pyun, "Chemiluminescence lateral flow immunoassay based on Pt nanoparticle with peroxidase activity," *Anal. Chim. Acta*, vol. 853, no. 1, pp. 360–367, 2015, doi: 10.1016/j.aca.2014.10.011.
- [136] Y. Wang, C. Fill, and S. R. Nugen, "Development of chemiluminescent lateral flow assay for the detection of nucleic acids," *Biosensors*, vol. 2, no. 1, pp. 32–42, 2012, doi: 10.3390/bios2010032.
- [137] J. Guo, S. Chen, J. Guo, and X. Ma, "Nanomaterial Labels in Lateral Flow Immunoassays for Point-of-Care-Testing," *J. Mater. Sci. Technol.*, vol. 60, pp. 90–104, Jan. 2021, doi: 10.1016/j.jmst.2020.06.003.
- [138] R. Banerjee and A. Jaiswal, "Recent advances in nanoparticle-based lateral flow immunoassay as a point-of-care diagnostic tool for infectious agents and diseases," *Analyst*, vol. 143, no. 9. Royal Society of Chemistry, pp. 1970–1996, May 07, 2018, doi: 10.1039/c8an00307f.
- [139] A. van Amerongen *et al.*, "Colloidal carbon particles as a new label for rapid immunochemical test methods: Quantitative computer image analysis of results," *J. Biotechnol.*, vol. 30, no. 2, pp. 185–195, Aug. 1993, doi: 10.1016/0168-1656(93)90112-Z.
- [140] C. W. Yen *et al.*, "Multicolored silver nanoparticles for multiplexed disease diagnostics: Distinguishing dengue, yellow fever, and Ebola viruses," *Lab Chip*, vol. 15, no. 7, pp. 1638–1641, Apr. 2015, doi: 10.1039/c5lc00055f.
- [141] "<https://www.fda.gov/media/86959/download>."  
<https://www.fda.gov/media/86959/download> (accessed Feb. 02, 2021).
- [142] "X. The Bakerian Lecture. —Experimental relations of gold (and other metals) to light," *Philos. Trans. R. Soc. London*, vol. 147, pp. 145–181, Dec. 1857, doi: 10.1098/rstl.1857.0011.
- [143] M. E. K. Richard M. Pashley, "Applied Colloid and Surface Chemistry | Wiley," 2004.  
<https://www.wiley.com/en-us/Applied+Colloid+and+Surface+Chemistry-p-9780470868829> (accessed Feb. 03, 2021).

- [144] X. Huang and M. A. El-Sayed, "Gold nanoparticles: Optical properties and implementations in cancer diagnosis and photothermal therapy," *Journal of Advanced Research*, vol. 1, no. 1. Elsevier, pp. 13–28, Jan. 01, 2010, doi: 10.1016/j.jare.2010.02.002.
- [145] P. K. Jain, K. S. Lee, I. H. El-Sayed, and M. A. El-Sayed, "Calculated absorption and scattering properties of gold nanoparticles of different size, shape, and composition: Applications in biological imaging and biomedicine," *J. Phys. Chem. B*, vol. 110, no. 14, pp. 7238–7248, Apr. 2006, doi: 10.1021/jp057170o.
- [146] U. Kreibig and M. Vollmer, *Optical Properties of Metal Clusters*, vol. 25. Berlin, Heidelberg: Springer Berlin Heidelberg, 1995.
- [147] J. K. Horton, S. Swinburne, and M. J. O'Sullivan, "A novel, rapid, single-step immunochromatographic procedure for the detection of mouse immunoglobulin," *Journal of Immunological Methods*, vol. 140, no. 1. J Immunol Methods, pp. 131–134, Jun. 24, 1991, doi: 10.1016/0022-1759(91)90135-3.
- [148] J. Singh, S. Sharma, and S. Nara, "Evaluation of gold nanoparticle based lateral flow assays for diagnosis of enterobacteriaceae members in food and water," *Food Chemistry*, vol. 170. Elsevier Ltd, pp. 470–483, Mar. 01, 2015, doi: 10.1016/j.foodchem.2014.08.092.
- [149] G. Kim, J. Lim, and C. Mo, "A Review on Lateral Flow Test Strip for Food Safety," *J. Biosyst. Eng.*, vol. 40, no. 3, pp. 277–283, Sep. 2015, doi: 10.5307/jbe.2015.40.3.277.
- [150] N. A. Byzova, A. V. Zherdev, B. N. Khlebtsov, A. M. Burov, N. G. Khlebtsov, and B. B. Dzantiev, "Advantages of highly spherical gold nanoparticles as labels for lateral flow immunoassay," *Sensors (Switzerland)*, vol. 20, no. 12, pp. 1–15, 2020, doi: 10.3390/s20123608.
- [151] H. N. Holmes, "Experiments in Colloid Chemistry (Hauser, E. A.; Lynn, J. E.)," *J. Chem. Educ.*, vol. 18, no. 7, p. 349, Jul. 1941, doi: 10.1021/ed018p349.4.
- [152] J. Turkevich, P. C. Stevenson, and J. Hillier, "A study of the nucleation and growth processes in the synthesis of colloidal gold," *Discuss. Faraday Soc.*, vol. 11, no. c, pp. 55–75, 1951, doi: 10.1039/DF9511100055.
- [153] G. Frens, "Controlled Nucleation for the Regulation of the Particle Size in Monodisperse Gold Suspensions," *Nat. Phys. Sci.*, vol. 241, no. 105, pp. 20–22, Jan. 1973, doi: 10.1038/physci241020a0.
- [154] M. Hu *et al.*, "Gold nanostructures: Engineering their plasmonic properties for biomedical applications," *Chem. Soc. Rev.*, vol. 35, no. 11, pp. 1084–1094, Oct. 2006, doi: 10.1039/b517615h.
- [155] P. Chun, "Colloidal Gold and Other Labels for Lateral Flow Immunoassays," in *Lateral Flow Immunoassay*, Humana Press, 2009, pp. 1–19.
- [156] S. Kasetsirikul, · Muhammad, J. A. Shiddiky, and N.-T. Nguyen, "Challenges and perspectives in the development of paper-based lateral flow assays," vol. 24, p. 17, 2020, doi: 10.1007/s10404-020-2321-z.
- [157] A. E. Urusov, A. V. Zherdev, and B. B. Dzantiev, "Towards lateral flow quantitative assays: Detection approaches," *Biosensors*, vol. 9, no. 3. MDPI AG, Sep. 01, 2019, doi: 10.3390/bios9030089.
- [158] A. V. Bartosh, A. E. Urusov, A. V. Petrakova, H. Kuang, A. V. Zherdev, and B. B. Dzantiev, "Highly sensitive lateral flow test with indirect labelling for zearalenone in baby food," *Food Agric. Immunol.*, vol. 31, no. 1, pp. 653–666, Jan. 2020, doi: 10.1080/09540105.2020.1750570.
- [159] J. Schiettecatte, E. Anckaert, and J. Smits, "Interferences in Immunoassays," in *Advances in Immunoassay Technology*, InTech, 2012.
- [160] A. Van Amerongen, J. Veen, H. A. Arends, and M. Koets, "Lateral flow immunoassays," in *Handbook of Immunoassay Technologies: Approaches, Performances, and Applications*,

Elsevier, 2018, pp. 157–182.

- [161] A. V. Bartosh, D. V. Sotnikov, O. D. Hendrickson, A. V. Zherdev, and B. B. Dzantiev, “Design of Multiplex Lateral Flow Tests: A Case Study for Simultaneous Detection of Three Antibiotics,” *Biosensors*, vol. 10, no. 3, p. 17, Feb. 2020, doi: 10.3390/bios10030017.
- [162] L. Huang, S. Tian, W. Zhao, K. Liu, X. Ma, and J. Guo, “Multiplexed detection of biomarkers in lateral-flow immunoassays,” *Analyst*, vol. 145, no. 8. Royal Society of Chemistry, pp. 2828–2840, Apr. 21, 2020, doi: 10.1039/c9an02485a.
- [163] L. Anfossi, F. Di Nardo, S. Cavalera, C. Giovannoli, and C. Baggiani, “Multiplex lateral flow immunoassay: An overview of strategies towards high-throughput point-of-need testing,” *Biosensors*, vol. 9, no. 1, 2018, doi: 10.3390/bios9010002.
- [164] F. Di Nardo, C. Baggiani, C. Giovannoli, G. Spano, and L. Anfossi, “Multicolor immunochromatographic strip test based on gold nanoparticles for the determination of aflatoxin B1 and fumonisins,” *Microchim. Acta*, vol. 184, no. 5, pp. 1295–1304, 2017, doi: 10.1007/s00604-017-2121-7.
- [165] C. Wang, F. Hou, and Y. Ma, “Simultaneous quantitative detection of multiple tumor markers with a rapid and sensitive multicolor quantum dots based immunochromatographic test strip,” *Biosens. Bioelectron.*, vol. 68, pp. 156–162, 2015, doi: <https://doi.org/10.1016/j.bios.2014.12.051>.
- [166] X. Huang, Z. P. Aguilar, H. Xu, W. Lai, and Y. Xiong, “Membrane-based lateral flow immunochromatographic strip with nanoparticles as reporters for detection: A review,” *Biosensors and Bioelectronics*, vol. 75. Elsevier Ltd, pp. 166–180, Nov. 01, 2015, doi: 10.1016/j.bios.2015.08.032.
- [167] Y. Zhang *et al.*, “Improvement in Detection Limit for Lateral Flow Assay of Biomacromolecules by Test-Zone Pre-enrichment,” *Sci. Rep.*, vol. 10, no. 1, p. 9604, Jun. 2020, doi: 10.1038/s41598-020-66456-1.
- [168] H. Ye, Y. Liu, L. Zhan, Y. Liu, and Z. Qin, “Signal amplification and quantification on lateral flow assays by laser excitation of plasmonic nanomaterials,” *Theranostics*, vol. 10, no. 10. Ivyspring International Publisher, pp. 4359–4373, 2020, doi: 10.7155/thno.44298.
- [169] A. V. Zherdev and B. B. Dzantiev, “Ways to Reach Lower Detection Limits of Lateral Flow Immunoassays,” in *Rapid Test - Advances in Design, Format and Diagnostic Applications*, InTech, 2018.
- [170] N. R. C. (US) C. on R. O. in Biology, “The Immune System and Infectious Diseases,” 1989, Accessed: Feb. 03, 2021. [Online]. Available: <https://www.ncbi.nlm.nih.gov/books/NBK217803/>.
- [171] J. M. Diamond, *Guns, germs, and steel : the fates of human societies*. New York : Norton, [2005] ©2005.
- [172] Kimberly Chriscaden, “Impact of COVID-19 on people’s livelihoods, their health and our food systems.” <https://www.who.int/news/item/13-10-2020-impact-of-covid-19-on-people’s-livelihoods-their-health-and-our-food-systems> (accessed Feb. 03, 2021).
- [173] Reimund Schwarze, “Opinion: The known and the unknown economic and social consequences of pandemics | PreventionWeb.net.” <https://www.preventionweb.net/news/view/72070> (accessed Feb. 03, 2021).
- [174] J. M. G. Wilson and G. Jungner, “PRINCIPLES AND PRACTICE OF SCREENING FOR DISEASE.”
- [175] H. Hwang, B. Y. Hwang, and J. Bueno, “Biomarkers in infectious diseases,” *Disease Markers*, vol. 2018. Hindawi Limited, 2018, doi: 10.1155/2018/8509127.
- [176] A. Ghaaliq, L. Mb, C. Frca, A. McCluskey, and B. Mb, “Clinical tests: sensitivity and specificity,” doi: 10.1093/bjaceaccp/mkn041.
- [177] K. Mohd Hanafiah, N. Arifin, Y. Bustami, R. Noordin, M. Garcia, and D. Anderson, “Development of Multiplexed Infectious Disease Lateral Flow Assays: Challenges and

Opportunities,” *Diagnostics*, vol. 7, no. 3, p. 51, Sep. 2017, doi: 10.3390/diagnostics7030051.

- [178] “Rapid Diagnostic Tests for Infectious Diseases - Chapter 11 - 2020 Yellow Book | Travelers’ Health | CDC.” <https://wwwnc.cdc.gov/travel/yellowbook/2020/posttravel-evaluation/rapid-diagnostic-tests-for-infectious-diseases> (accessed Feb. 03, 2021).
- [179] European Commission, “COMMISSION DECISION of 27 November 2009 amending Decision 2002/364/EC on common technical specifications for in vitro diagnostic medical devices,” *Off. J. Eur. Union*, no. 3, 2009.
- [180] European Commission, “Regulation (EU) 2017/746 of the European parliament and of the council on in vitro diagnostic medical devices,” *Off. J. Eur. Union*, vol. 5, no. 5, pp. 117–176, 2017.



# Chapter 2



---

## Aim of the Thesis

---

This thesis is based on the idea, suggested by the research group expertise, and confirmed by the words of A.V. Zherdev and B.B. Dzantiev, that an intelligent strategical design applied to LFIA's golden standard materials and formats can increase the performance and widen the versatility of the technique to solve many diagnostic issues.

To demonstrate this belief, reactive lines positioning, versatile reagents, and studies of saturation phenomena were carried to investigate and improve the performance in six cases of infectious diseases diagnosis and patients' management. In each of the following chapters, describing specific projects, a strategical approach or element was included, involved, and exploited.

Following the strong demand for rapid screening diagnosis of SARS CoV-2 to face the ongoing pandemic, a "total antibody" LFIA test was developed and the results are reported in **Chapter 3.1**. The total antibody is a serological test aiming at detecting immunoglobulins independently on the class to which they belong. The strategic approach was the inclusion of two non-competitive formats for targeting the total antibody response in the same strip in the form of two spatially separated test lines. The first test line was made by the Staphylococcal protein A (SpA) as the capture reagent, exploiting its multi-binding capacity and affinity to different classes of antibodies (format described in chapter 1.4.2, figure 1.11, Antibody non-competitive LFIA – Capture by secondary antibody). The second test line had a viral antigen (nucleocapsid protein, N) as the capture reagent and was based on the double-antigen approach (format described in chapter 1.4.2, figure 1.12, Antibody non-competitive LFIA – Double antigen sandwich). Using the GNP-labelled nucleocapsid protein as the signal reporter, the two strategies aimed at reaching the highest sensitivity, considering that the different classes of antibodies could show a different affinity in the two approaches.

The total antibody approach was used also for an animal healthcare application, described in the **Chapter 3.2**, i.e., the diagnosis of the canine visceral leishmaniasis. In this work a single total antibody strategy was used exploiting a specific chimeric recombinant antigen as the capture and the SpA as the signal reporter (format described in chapter 1.4.2, figure 1.10, Antibody non-competitive LFIA – Capture by antigen). Considering the reactivity of SpA towards immunoglobulins of several animal species, the intention was to demonstrate the flexibility given by using an interspecies antibody-binding protein to expand the applicability of the test also with sera from cats and foxes.

Antibody testing can include applications requiring high specificity or optimal discrimination between antibody classes or target-serotype. The work reported in **Chapter 4.1** aimed to demonstrate the importance of the strategical design to face up to a diagnostic issue by using different approaches. The HIV infection was used as an ideal case of study because it involves well time/stage-defined classes of antibodies and well distinguished serotypes. In such a situation, the roles of the immunoreagents used to target the antibodies can be switched following several formats. In addition, by adding a different label such as gold nanostars (GNSs) to include a versatility element, the spectrum of possible ways through which the discrimination is realized was widened further. Three different upgrades of the standard spatial multiplexing approach were used to distinguish early or advanced infection from HIV1 or HIV2 serotypes. To do this, a second label to produce differently coloured probes (GNPs and GNSs) was included. Three strategies basing on the inclusion of the two labels in the three non-competitive formats described in 1.4.2, figures 1.10, 11 and 12, were studied and ended in the production of three prototypes. The multimodal LFIA ( $x^2$ LFIA) prototypes were studied by means of well-characterized serum samples from panels including 1 negative, 1 fully seroconverted HIV2 positive, 1 fully seroconverted HIV1 positive and 3 seroconverting HIV1 positive sera.

Sometimes, the diagnostic interest focusses on monitoring a specific class of antibodies, as described in the work reported in **Chapter 4.2**. In this case, the format described in chapter 1.4.2, figure 1.10, Antibody non-competitive LFIA – Capture by antigen, aimed at targeting a single antibody class (IgA) to SARS CoV-2 in saliva samples. In that work, two different labels with different

result readouts were compared. The nucleocapsid protein from SARS CoV-2 (N) was used for the specific capture of the anti SARS CoV-2 antibodies. A dual strategy for signal reporting and detection was applied. For the colorimetric reading, an anti-human IgA antibody was labelled with GNPs and the quantitative measurement of the colour produced by GNP accumulation was obtained by a smartphone reader. A chemiluminescence system made by labelling the same antibody with horseradish peroxidase was included to achieve higher sensitivity. The preliminary results of this proof-of-concept study demonstrated the potential of the device to follow efficiently the production of IgA to SARS CoV-2, that will be helpful to accumulate data on their role on the antibody response to the infection. The novelty of this project was to target the sole IgA class of antibodies to SARS CoV-2 that are suggested to be more informative of an early infection on respect to other classes of immunoglobulins.

For many infectious diseases, a general good correlation of the viral load of an infection with the antibody response is observed. Nevertheless, directly targeting the presence of the viral, or bacterial, antigens provide an earlier diagnosis on respect to any kind of serological test. The bottleneck for the development of antigen LFIA is the availability of specific antibodies targeting the appropriate antigen of the pathogen. In **Chapter 5.1** a multiplex LFIA for the diagnosis and differentiation of infection from (at least) five FMDV serotypes was developed. In that work, the typical approach for antigen detection (format described in chapter 1.4.2, figure 1.9, Direct non-competitive LFIA) was used. A library of monoclonal antibodies (1 pan-reactive and 7 serotype specific) was employed for capturing and/or signal reporting. Two distinct devices have been developed for the two geographically distributed groups of FMDV strains: Eurasian and African. While the “Africa” device included homologous sandwiches, using the same antibodies both for the capture and for signal reporting, the “Eurasia” provides a general positivity output and a serotyping output by homologous and heterologous sandwich-immunoassay, respectively. In a multiplex strip, involving homologous and heterologous sandwiches, the challenge of the development is the understanding of the mutual interference of the antibodies and of the reactive lines, considering cross-reactivity, relative affinity, and distance from the sample pad. A new type of Hook effect was disguised, which happens specifically in the LFIA platform due to peculiar order in which the immunocomplexes form. The information achieved from such a study would be helpful in any kind of LFIA involving multiplexing.

Considering diagnostics in a broader sense, it is possible to diagnose a correct therapeutic administration simply by targeting the drug in a sample from a patient. Translating this assumption into an immunoassay, we carried the study described in **Chapter 6.1** on the development of a rapid test for the detection of an antiretroviral drug used for the treatment of HIV, Tenofovir (TFV), in non-conventional matrices, for the rapid assessment of the compliance to the therapy. The TFV is a small molecule and this forced us to develop a direct competitive assay (format described in Chapter 1.4.1, figure 1.7, direct competitive LFIA). TFV in saliva is very low concentrated, especially when deriving from the more recent drug formulations. A TFV-based antigen and a specific antibody for TFV were needed to develop an extremely sensitive test, considering that there are not commercially available immunoreagents for this target. The synthesis of the antigen was made by means of the insertion of a 5-carbon spacer arm (TFVh) and subsequent linkage to a carrier protein (TFVh-BSA). The immunogenic antigen was inoculated into six mice for the generation of monoclonal antibodies.

In this case, the improvement was given by the strategy applied for monoclonal antibodies selection. Considering the final purpose of the test, the selection was based on a competitive format, including the free TFV as the competitor.

In the following paragraph, the four infectious diseases faced in this thesis will be briefly introduced, and the importance of the use of LFIA in their diagnosis will be highlighted.

## 2.1



# Human Infectious Diseases

The contribution of the POCTs to the human global healthcare is resounding. In this work two pandemic outbreaks affecting humans that have been particularly shocking worldwide will be considered. The support and contribution of the rapid test has been, and could be even more, decisive for the management of pandemics and for reducing the spread of the infection. Different approaches for the rapid diagnosis of Human Immunodeficiency Virus (HIV) infection and of the Severe Acute Respiratory Syndrome Coronavirus 2 (SARS CoV-2) infection will be discussed in the following chapters.

### 2.1.1 Human Immunodeficiency Virus (HIV)

The Human Immunodeficiency Virus (HIV) infection causes the death by Acquired Immuno-Deficiency Syndrome (AIDS) condition of hundreds of thousand people worldwide [1]. The last report from UNAIDS reveals 1.7 million of newly infected people in 2018 added to the over 35 million HIV positive individuals and the AIDS-related deaths are 770 thousands [2]. The World Health Organization (WHO) aims to halve this number before 2030, considering a partial target to reach less than 500 thousand deaths before the end of 2020.

The disease can manifest in several stages. In the Primary infection (Acute HIV) some people infected by HIV develop a flu-like illness within two to four weeks after the virus enters the body. This illness may last for a few weeks. Possible signs and symptoms include nonspecific symptoms (fever, headache, muscle aches and joint pain, rash, sore throat and painful mouth sores, swollen lymph glands, mainly on the neck, diarrhoea, weight loss, cough, night sweats). Then a Clinical latent infection (Chronic HIV), where HIV is still present in the body and in white blood cells appears. However, many people may not have any symptoms or infections during this time.

As the virus continues to multiply and destroy the immune cells mild infections or chronic signs and symptoms can appear (fever, fatigue, swollen lymph nodes, diarrhoea, weight loss, thrush, shingles by herpes zoster, pneumonia). Untreated, HIV typically turns into AIDS in about 8 to 10 years.

When AIDS occurs, the immune system has been severely damaged, more likely to develop opportunistic infections or opportunistic cancers. The signs and symptoms of some of these infections may include sweats, chills, recurring fever, chronic diarrhoea, swollen lymph glands, persistent white spots, or unusual lesions on your tongue or in your mouth, persistent, unexplained fatigue, weakness, weight loss, skin rashes or bumps.

The following list reports the WHO recommendations for HIV testing and diagnosis, from the *Consolidated guidelines on HIV testing services*. (Geneva: World Health Organization; 2015) [3]

#### *High-prevalence settings*

In settings with greater than 5% HIV prevalence in the population tested, a diagnosis of HIV positive should be provided to people with two sequential reactive tests.

For individuals with discrepant test results where Assay 1 is reactive, Assay 2 is non-reactive and Assay 3 is reactive, the results should be considered inconclusive and

the client should be asked to return in 14 days for retesting.

For individuals with discrepant test results where Assay 1 is reactive, Assay 2 is non-reactive and Assay 3 is non-reactive, the final result should be considered HIV negative.

*Low-prevalence settings*

In settings with less than 5% HIV prevalence in the population tested, a diagnosis of HIV positive should be provided to people with three sequential reactive tests.

For individuals where the Assay 1 result is reactive and Assay 2 result is non-reactive, the final result should be considered HIV negative. However, in the case of such results and where Assay 1 is a fourth-generation assay (antibody/antigen [Ab/Ag]) and Assay 2 is an Ab-only assay, the result should be considered inconclusive and the person should be retested after 14 days.

For individuals with results in which Assay 1 is reactive, Assay 2 is reactive, and Assay 3 is non-reactive, the result should be considered inconclusive and the client should be asked to return in 14 days for retesting.

*All settings*

HIV testing services may use combinations of rapid diagnostic tests (RDTs) or combinations of RDTs/ enzyme immunoassays (EIAs)/supplemental assays rather than EIA/Western blot combinations.

The fight to HIV pandemic is made by the dual approach of treatment and prophylaxis. The rapid screening diagnostic is one of the main prevention measures. Therefore, HIV is one of the main field of application for the POCTs [1]. HIV antibody-screening tests, also known as third generation HIV tests, are playing an important role in the management of HIV infection worldwide, allowing for self-diagnosis and providing rapid response, which facilities prompt intervention also in limited resource settings. In particular for infant infection diagnosis (EID). It is also confirmed by the recommendations by WHO reported in Table 2.1.

Table 2.1: Imprinted from The Guidelines from WHO for serological rapid testing of HIV.

Age group	Known HIV exposed	Unknown HIV exposure status and breastfeeding	Unknown HIV exposure status and not breastfeeding*
0–4 months	Not useful, as exposure is known and RDT cannot determine infection status	<b>Test mother</b> If mother is not available, RDT in the child can reliably assess exposure.	<b>Test mother</b> If mother is not available, RDT in the child reliably determines exposure.
5–8 months	Not useful, as exposure is known and RDT cannot determine infection status at this age	<b>Test mother</b> If mother is not available, a positive RDT establishes exposure, but a negative RDT does not fully rule it out. Infants with positive RDT will still need NAT to confirm infection. Infants with negative RDT who are still breastfeeding will need NAT at the end of breastfeeding. If sick and mother is not available, perform NAT directly to assess HIV infection status.	<b>Test mother</b> If mother is not available, RDT for the child does not fully rule out exposure. If sick and mother is not available, perform NAT directly to assess HIV infection status.

<b>9–18 months</b>	RDT useful to rule out established HIV infection Infants with <i>positive</i> RDT will still need NAT to confirm infection. Infants with <i>negative</i> RDT who are still breastfeeding will need NAT at the end of breastfeeding.	<b>Test mother</b> If mother is not available, a positive RDT establishes exposure, but a negative RDT does not fully rule it out. Infants with positive RDT will still need NAT to confirm infection. RDT useful to rule out established HIV infection. Infants with positive RDT will still need NAT to confirm infection. Infants with negative RDT who are still breastfeeding will need NAT at the end of breastfeeding. If sick and mother is not available, perform NAT directly to assess HIV infection status. <sup>b</sup>	<b>Test mother</b> If mother is not available, RDT in the child does not fully rule out exposure. RDT is useful to rule out established HIV infection. <ul style="list-style-type: none"> <li>• Infants with positive RDT will still need NAT to confirm infection.</li> <li>• Infants with negative RDT who are not breastfeeding can be considered uninfected.</li> </ul> If sick and mother is not available, perform NAT directly to assess HIV infection status.
<b>&gt;18 months</b>	Serological testing (including RDT) is recommended to assess HIV infection status unless still breastfed. If still breastfed, serological testing (including RDT) should be provided 3 months after cessation of breastfeeding.		

### Rapid test for serological diagnosis of HIV

The first HIV LFIA appeared in the early 2000s and evolved to achieve early diagnostic and serotyping capacity to discriminate between HIV1 and HIV2 infection [4]. Both viral strains are present worldwide. HIV1 is strongly prevalent, while HIV2 is endemic in Western-African region and characterized by lower morbidity and mortality [5], [6]. Discriminating between the two serotypes is important for several reasons, such as the epidemiologic registration, the monitoring of the infection on the territory and, especially, for the individuation of the appropriate treatment. In fact, the two infections show differences in their management [7]. Current anti-retroviral therapy (ARV) bases on drugs from seven classes, combined in bi- or trivalent multiclass fixed-dose administrations. ARV is designed to reach the major effectiveness in inhibiting the activity and proliferation of HIV1 as the majoritarian strain [8]–[10]. HIV2 is intrinsically resistant to some ARV classes (e.g. Non-Nucleoside Reverse Transcriptase Inhibitors, NNRTI) and, for this reason, serotyping is crucial for the treatment [11]–[13]. The available HIV antibody-screening LFIAs discriminate between HIV1 and HIV2 by exploiting the specificity of the recognition between the type-dependent viral proteins and the human anti-HIV antibodies [14]. Recombinant envelope glycoproteins named gp41 and gp36 are generally used as the antigens to specifically recognize HIV1 and HIV2 antibodies, respectively [5], [15]. Spatial resolution is the most common strategy to multitargeting by the single assay [16]–[22]. For instance, in a typical HIV serotyping test, the discrimination is made by coating the specific antigens in two spatially confined bands (test lines). Anti-human antibodies, or highly specific proteins (such as staphylococcal protein A or streptococcal protein G) are used to reveal the specific antibodies bound to HIV-antigens [23], [24]. In colorimetric assays these biospecific agents are labelled with coloured materials, such as gold or selenium nanoparticles. Briefly, human anti-HIV antibodies bind to one of the separately coated HIV antigens depending on the serotype and the formation of the complex is measured by the further reaction with the signal reporter. In case of infection, a coloured line forms in correspondence of the specific HIV-antigen and the serotype is identified by the position of the coloured test line. Alternatively, the double antigen format

can be adopted, in which the same antigen is used for capturing and as the detection probe [23]. As for any kind of infectious disease, it is useful to discriminate also between early and advanced stage of infection [25]. Usually, the infection stage is discriminated by agents specifically targeting the class of antibodies, IgM and IgG, as markers of early and long-term immune response, respectively. In a typical multi-target LFIA the number of information items corresponds to the number of test lines drawn on the strip. However, reacting bands cannot be increased endless and thus the number of information that can be obtain in a single test is limited to few [23], [24]. Multiplexing approaches exploiting probes with tuneable signals have been reported, based on fluorescence and chemiluminescence encoding [26]–[28]. Nevertheless, these approaches need instrumentation that limits on-field applications.

### Control of compliance – Tenofovir monitoring

From the beginning of the epidemic, the number of infection and AIDS-related deaths increased until the appearance of the multi-drug combinatory therapy, called High Activity Anti-Retroviral Treatment (HAART), in 1996. Since then, the progressive application of the HAART has increased the life expectancy up to a non-infected profile [29]–[31]. Unfortunately, the efficacy of HAART is weakened by the low adherence to drug regimens, due to several causes, such as the misunderstanding of complicated regimens, the refusal of the therapy because of psychological and physical side effects, carelessness/inattention, etc [32]–[35]. The noncompliance to the therapy bears to intoxications by overdose intake, or to limited efficacy of the therapy itself, and to the development of drug-resistance caused by sub-effective administrations [36]. Thus, efficient and rapid diagnostic tools to control the compliance to the HAART are strongly demanded.

Tenofovir (TFV) is a long-established drug used in in the prophylaxis and the treatment of the infections of HIV and Hepatitis C Virus (HCV) [37], [38]. It belongs to the class of the nucleotide reverse transcriptase inhibitors (NRTI) and carries out its pharmacological activity by blocking the functionality of the reverse transcriptase, thus inhibiting the production of viral proteins [39]. It is included, together with other antiretroviral (ARV) drugs, in several commercial coformulations (e.g., with emtricitabine and rilpivirine in Atripla, Descovy, Odefsey, or Eviplera; with elvitegravir in Genvoya; and with bictegravir in Biktevy), TFV is administered as a prodrug, in particular either as the diisoproxil fumarate (TDF) or the alafenamide (TAF) salts. After absorption, the prodrug is hydrolysed to release TFV by the plasmatic esterases, and then phosphorylated into the active form tenofovir diphosphate (TDP) in the cell [40]. The free unphosphorylated fraction of TFV present in the bloodstream is the cause of its toxicity, which is considerably reduced for TAF administered regimens [41], [42]. The drug shows an average 17-h plasmatic half-life, and 70-80% is excreted in urine as unmodified TFV. The plasmatic and urinary concentrations of TFV have been recently investigated and correlated to the adherence to the HAART by the TARGET study [43]–[45]. The salivary levels of TFV in TDF-treated (perfectly adherent) patients was established by V. De Lastours et al. (2011) [46] as ranging between 0.4 and 25 ng/ml with a mean value of 2.75 ng/ml. Considering TAF recommended doses, an around 10-fold lower level is expected for TAF administration. A large fraction of the HIV-positive patients under HAART treatment are currently administered with a coformulation including one of the two TFV prodrugs [47]. Hence, detecting TFV represents a versatile tool to monitor the adherence to several combined fixed-dose administrations. Among methods to measure TFV in biological specimens most are based on liquid chromatography coupled to tandem mass spectrometry



(HPLC-MS/MS), which are accurate, precise, and sensitive [48]. Nevertheless, they require expensive equipment and qualified technicians for operating. In addition, HPLC-MS/MS equipment is usually available only in centralized laboratories. Point-of-care devices able to discriminate among TFV levels above or below the one expected for therapy adherence will enable physicians to routinely control the patients and timely intervening in case of therapeutic failure, with saving time and cost compared to recurring to instrumental analysis.

### **2.1.2 Severe acute respiratory Syndrome Coronavirus 2 (SARS CoV-2)**

The global diffusion of the new Betacoronavirus SARS CoV-2 (Severe acute respiratory syndrome coronavirus 2) since January 2020 has posed an unexpected and terrifying global threat. The virus causes a severe respiratory illness characterized by fever, headache, body aches, a dry cough, hypoxia, and to a lesser extent pneumonia. Transmission occurs by contact with infectious material, such as respiratory droplets or body fluids. The mortality and morbidity of the pandemic SARS CoV-2 are still uncertain and apparently variable according to age and sex; as an example, fatality rates have been estimated between 1.7% and 2.8% for females and males, respectively, in China and Republic of Korea [49]. However, the rate of infection and mortality seems variable around the world and certain regions have been much more adversely impacted than others [50]. A possible co-cause for the inefficacy of containment actions is the failing or delayed identification of infected people. In a few countries, the use of diagnostic testing on a massive scale has been a cornerstone of successful containment strategies. In contrast, several countries have encountered the rapid spreading of the infection due to the limited testing capacity and the insufficient provision of reagents for executing the test on the global scale. The pandemic has highlighted the importance of rapid, specific, and accurate diagnostic tests in limiting the spread of infection and monitoring patients' viral load and therapy. The current standard method for the diagnosis of SARS infection is based on the detection of the viral RNA in nasopharyngeal swabs. Viral RNA is detected by means of the reverse-transcriptase real-time polymerase chain reaction (rRT-PCR) [51], [52]. Around 200 diagnostic tests have been developed to detect the RNA of SARS CoV-2. Laboratory-based serological methods, such as ELISA (Enzyme-linked Immunosorbent Assay) and CLIA (Chemiluminescence immunoassay), are emerging as complementary diagnostic tools in the attempt of widening access to diagnosis, screening asymptomatic persons, and providing information on immunity state for recovered persons to end isolation [51]. Although accurate, laboratory-based assays cannot guarantee the massive case finding so helping curb the epidemic. They suffer from many limitations, such as long turnaround times (they generally take on average over 2 to 3 hours to generate results). Furthermore, rRT-PCR tests require certified laboratories, expensive equipment, and trained technicians to operate, thus limit the outbreak containment effort. These challenges may be even greater in low-resource settings.



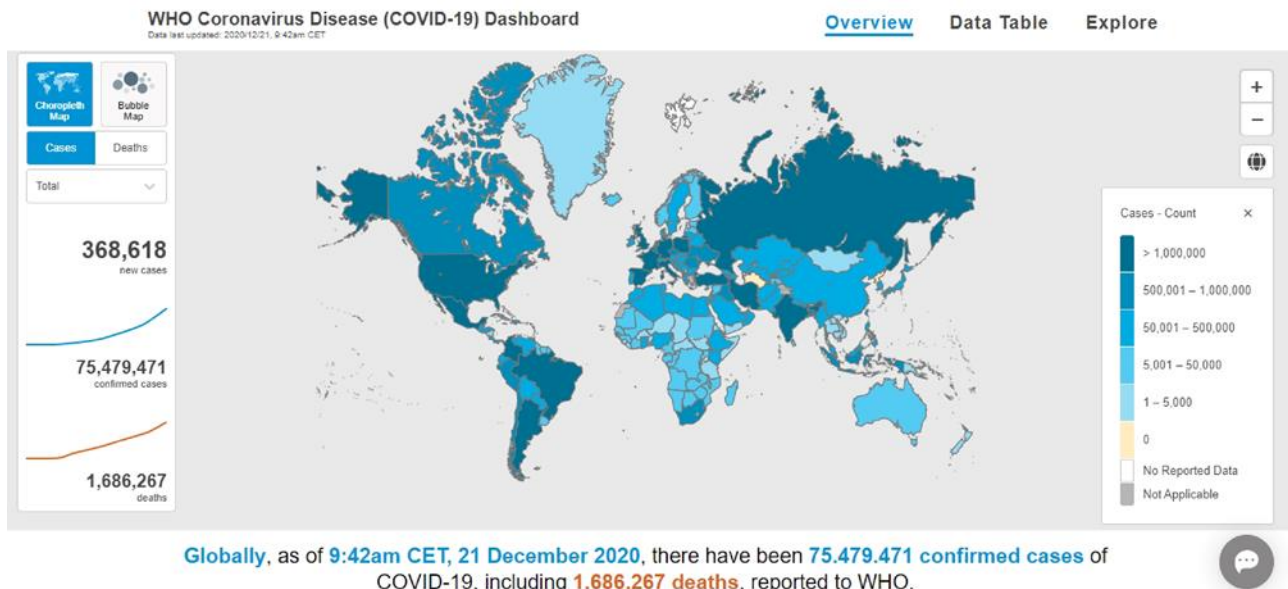


**Figure 2.1.** The SARS CoV-2 spread as reported from WHO website <https://covid19.who.int> (last access 21 December 2020)

## LFIA for antibody response to SARS CoV-2

Urgent clinical and public health needs are driving an unprecedented global effort to increase testing capacity for SARS CoV-2 infection. A common format for point-of-care detection of the immune response to a virus is to measure virus specific antibodies (IgM and IgG, or in combination) in serum using the LFIA, where gold nanoparticles are used to label biospecific reagents such as secondary antibodies. Point-of-care devices based on the LFIA principle have been made available by several manufacturers. These devices aimed at detecting the serologic response to the infection by specifically and separately targeting immunoglobulins belonging to the M and G classes in the serum of the subject. The idea underneath the assay design is that the contact with the virus elicits first the production of IgM that initially raise and rapidly decrease, while IgG are produced in a second time and persist in the blood after recovery [53]. A typical antibody response to exposure to antigen involves the primary humoral immune responses typified by the appearance of IgM within the first three to five days following the exposure, followed by IgG production within the first week [54]. IgG persist after the virus is no longer detectable, indicating previous infection, while IgM are transient, so their presence is associated to a recent infection. Therefore, the ability of recognizing the class of anti-SARS CoV-2 immunoglobulins has been regarded as a viable way to identify infected patients and to discriminate those who surpassed the illness and can safely end isolation. However, this approach has resorted in poor specificity and sensitivity and has led to a wide disbelief on the usefulness and informative capability of rapid tests and sometimes of serological tests in general for the management of the pandemic. The point-of-care tests developed in the early phase of the outbreak considered that the infection will elicit the production of IgM first, followed by the production of IgG. Consequently, the positivity to the sole IgM or IgG were linked to diagnosis of early infection and past infection (i.e., recovered subject), respectively. The contemporary presence of both classes of immunoglobulins was regarded as the indication of seroconversion. Unfortunately, as reported for previous SARS and MERS virus, the sequential production of IgM and IgG is questionable when the immune system encounter SARS CoV-2 [53], [55].

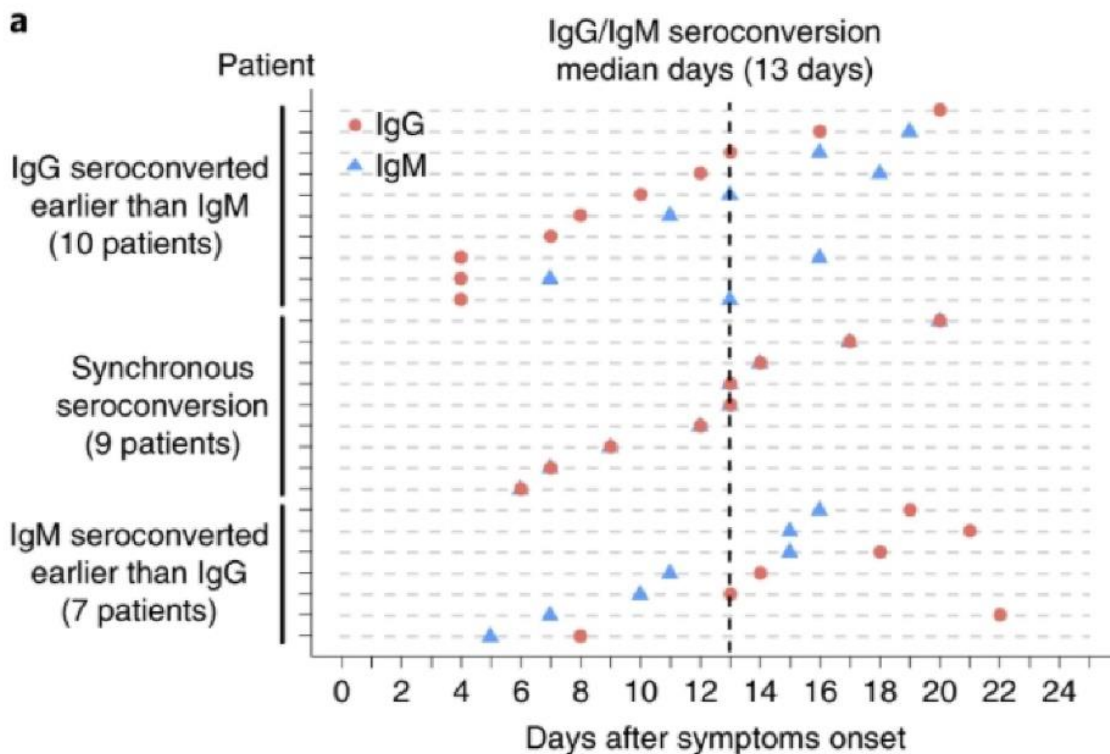


**Figure 2.2.** The seroconversion for SARS CoV-2 positive sera, directly printed from the work by Q.X. Long et al. [57].

In fact, convincing evidence of the simultaneous, sequential, or inverted production of IgM and IgG during seroconversion have been reported [55]. In some cases, IgM were completely absent [56]. Therefore, the strategy based on the separate identification of IgM and IgG and the quantification of the IgM/IgG ratio lacks sensitivity and is not useful in defining the phase of a SARS-CoV-2 infection [57], [58] (figure 2.2). Accordingly, C. Li et al. developed a rapid test combining the IgM and IgG detection as a rapid diagnostic tool for SARS CoV-2 infection [53]. The architecture of the LFIA device was the traditional one, with two test lines comprising anti-human IgM and anti-human IgG as the capturing reagents and a recombinant SARS CoV-2 antigen labelled with gold nanoparticle (GNP) as the probe to generate visible signals. Independently on the immunoglobulin detected, the test was assigned as positive. The diagnostic sensitivity improved; however, at the expenses of the specificity, which resulted from the sum of matrix effects on each line. Alternative approaches targeting the “total antibody response” to the SARS CoV-2 infection are needed to provide adequate sensitivity while preserving specificity.

On the other hand, physiologically, the response to a viral infection begins with the production of specific immunoglobulins secreted at the site of infection. As other virus affecting the respiratory traits, also SARS CoV-2 elicits the production of another class of specific immunoglobulins, the A class (IgA), in respiratory specimens and the presence of specific anti-SARS CoV-2 IgA in the blood has also been reported [55], [57], [59], [60]. These secretory IgA play an important role in the protection and homeostatic regulation of the respiratory mucosal epithelium, which separates the outside environment from the inside of the body. This primary function of IgA is referred to as “immune exclusion”, a process limiting the access of microorganisms and antigens to vulnerable mucosal barriers. Conventional ELISA methods based on microtiter plates on bench-top format have accurately measured serum IgA, defining their behaviour during COVID-19 infection. These studies show that serum IgA are produced with time-dependent kinetics and in larger amounts than IgM [60], [61], suggesting that IgA may be useful in the serological characterization of COVID-19-infected individuals and as an alternative and more reliable biomarker of early COVID-19 infection compared

to IgM. In details, the production of SARS-CoV-2-specific IgA has been reported in the serum of seroconverting individuals in the first week after symptoms onset [61], [62], IgA appeared first [63] and were found in higher amount than IgG in the early stage of the infection [64]. Furthermore, IgA levels were correlated to severity of the disease [63]. The IgA are transported in the mucus via transepithelial transport and could be present in saliva or oral fluid, where they are the main antibody isotype present [65], [66]. As a complement to IgG detection, one significant advantage of targeting IgA is the possibility of using saliva instead of blood for the analysis. Salivary anti-SARS-CoV-2 IgA have been shown to correlate with serum amounts [67]. Saliva collection has several advantages over blood withdrawal, especially for point-of-care testing [68]. Saliva can be collected easily by the patient, reducing the risk associated with contact between operator and patient. Furthermore, saliva collection is particularly suitable for babies and elderly people, and for cheap population screening in low-resource settings. However, at present, there are no rapid tests for detecting SARS-CoV-2-specific IgA in saliva. The rapid and specific detection of serum and salivary IgA could deliver early and hopefully time-dependent information about the infection. Due to inconsistent findings about the evolution of IgM levels during infection, a serological marker of recovery is needed to reduce the number of rRT-PCR analyses and support decision-making about ending quarantine. Moreover, a portable easy-to-use test for serum and salivary IgA could help evaluate the individual response to therapy in large populations. LFIA for detecting IgA towards any infectious agents in oral fluids or serum have not been reported to date.

## 2.2



### Animal Infectious Diseases

The application of LFIA in infectious diseases diagnostics includes, also, the field of animal healthcare, as introduced in the chapter 1. It is important to monitor and prevent diffusion of animal infectious diseases for several reasons. The first is the ethical concerns involved in animal healthcare, including pet care and livestock health surveillance [69], [70]. The second is the economic side, for breeders and food and feed supply chain control [71], [72]. The third important reason to efficiently prevent the spreading of animal infectious diseases is the perpetual risk of the jump of a viral strain from animal to humans, the so-called *spillover* [73]. The spillover is, but not only, a matter of probability. The virus lifecycle include replication by transcription and translation of the genetic material. The process is far to be immune from errors, and these can lead to dead or mutated virus. If the mutation of the new virus is suitable to the infection of other species the jump is successful and the new virus can be spread through the new population. One of the most famous case of spillover is the HIV deriving from *Simian Immunodeficiency Virus* (SIV) and, probably also the SARS CoV-2 deriving from a previous virus affecting bats [74], [75]. As a matter of fact, the less is the spread of the infection, the less is the number of replications and subsequently the risk of spillover. Apart from spillover, animals may represent the reservoir for human pathogens. In this case, the animal may show no or mild symptoms, but it is able to transmit the infection to humans. Companion animals, which live in close contact with humans, are particularly dangerous as reservoirs for infection [76], [77]. For these reasons protecting animals by limiting the transmission of infectious diseases indirectly means to protect humans, as well.

#### 2.2.1 Canine Visceral Leishmaniasis (CVL)

Visceral leishmaniasis (VL) is a zoonotic disease, caused by the protozoan parasite *Leishmania infantum* that is transmitted to vertebrate hosts through the bites of infected female phlebotomine sand flies, endemic in many countries throughout Latin America and Asia [78]. It ranked second in mortality and fourth in morbidity among tropical diseases and is considered as one of the world's most neglected diseases by the WHO (World Health Organization) [79]. In European countries, the incidence risk of VL is still relatively low, although the disease is spreading to regions previously referred as non-endemic, probably because of climate change and population movements [80], [81]. However VL impact on human health is severe (HVL) and is characterized by fever, weight loss, splenomegaly, hepatomegaly, and anaemia [78]. It is estimated that more than 700,000 new cases and about 20,000-30,000 deaths occur annually worldwide due to HVL [79]. Although *Leishmania amastigotes* parasites more than 70 vertebrate hosts; domestic dogs are considered the main reservoir for human infection [78], [80], [82]. Infected dogs have very variable clinical manifestations that range from apparently healthy to severely diseased. Many infected dogs may never exhibit clinical signs, thus making difficult to early detect canine visceral leishmaniasis (CVL) [83]. Nevertheless, both symptomatic and asymptomatic dogs can transmit the parasite to other dogs and humans (Figure 2.3) [80]. Therefore, early detection and prompt treatment of infected animals

help to reduce spreading of transmission and represent a relevant part of the prevention and control of the burden of disease in humans.

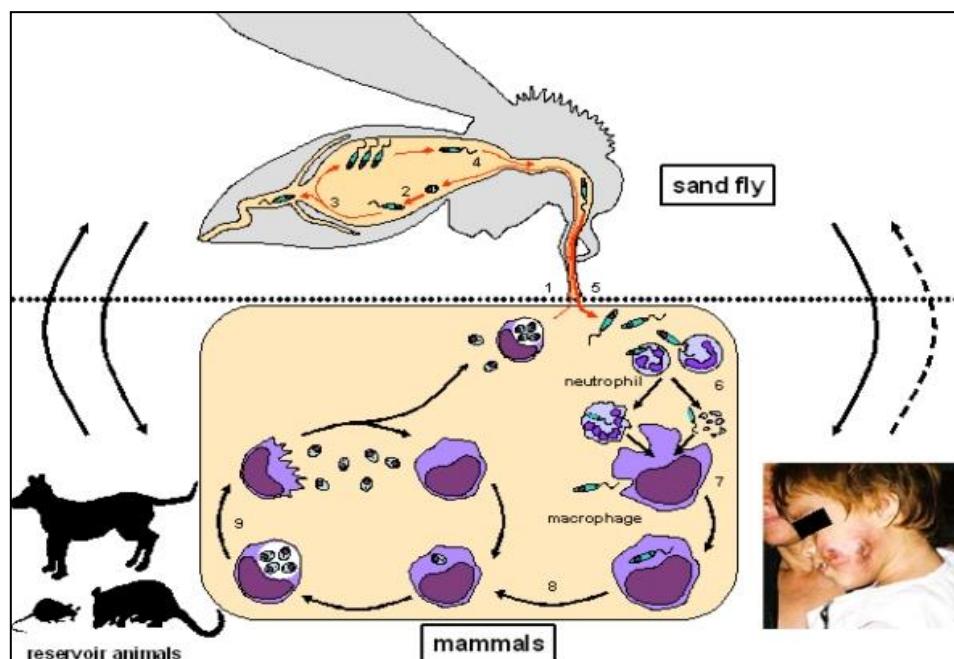


**Figure 2.3.** Visceral leishmaniasis (VL) is a zoonotic infectious disease caused by the parasite *Leishmania infantum*. Infection is transmitted by phlebotomine sand-flies. Several domestic and wild mammals act as reservoirs for the infection, among which domestic dogs are considered the main reservoir for human infection. Infected dogs have very variable clinical manifestations; nevertheless, both symptomatic and asymptomatic dogs are able to transmit the parasite to other dogs and humans.

### LFIA for antibody response to CVL

CVL can be diagnosed by combining clinical and epidemiological parameters with parasitological, serological, or molecular methods [78]. According to the World Organisation for Animal Health, serology is the preferred diagnostic method for CVL. Detection of anti-leishmanial antibodies is commonly realized by three techniques: the immunofluorescent antibody test (IFAT), the ELISA, and the LFIA. The IFAT is considered as the reference method for anti-leishmanial serology in dogs and is used as the reference test for the validation of new diagnostic methods, though data on its diagnostic sensitivity and specificity are controversial [80]. Furthermore, IFAT suffers from operator-dependent variability. The ELISA is also very sensitive and specific, with the advantage of easier standardization [84]. Both IFAT and ELISA provide quantitative results, defined as the antibody titre (the last 2-fold serial dilution of sample providing a positive result). However, the rapid and cost-effective detection of infected dogs is a key point in the control of infection and infection transmission. Several commercial LFIA devices are available [85] that varies for simplicity of use, rapidity, and sensitivity [83]. The specificity of these tests is generally high, while the diagnostic sensitivity is usually low (30–70%) and largely dependent on leishmaniasis stage [79], [83], [84]. A limited sensitivity strongly reduces the effectiveness of control of infection transmission, also frustrating attempts of preventing the spread of the disease in humans.

In addition to inadequate sensitivity, existing LFIA kits for diagnosing leishmaniasis are designed for detecting specifically CVL and HVL. Although dogs are considered the most important domestic reservoirs of *L. infantum*, several species of wild mammals have been recognized as hosts and potential reservoirs of *Leishmania* parasites [86]. In addition, domestic mammals (sheep, goats,



cattle, and donkey) have been suggested as the reservoir hosts responsible of a HVL outbreak occurred in 2008-2009 in China [87]. Therefore, versatile diagnostic tools that can be adapted for VL diagnosis in other mammals beside dogs are also demanded.

## 2.2.2 Foot-and-Mouth Disease Virus (FMDV)

Foot-and-mouth disease (FMD) virus, a member of the *Picornaviridae* family, *Aphthovirus* genus, is a viral disease of livestock [88]. The earliest descriptions of the FMD date back to 16<sup>th</sup> century, and still, more than a century after the virus identification [89], it causes annual costs due to production losses and vaccination estimated at €5.3–€17 billion (US\$6.5–US\$21 billion) in FMDV-endemic areas [90], [91]. The FMDV is extremely contagious and affects cattle, swine, sheep, goat, and other cloven-hoofed ruminants. Symptoms are generally severe in cattle and swine, including lesions on the tongue, muzzle, oral cavity, coronary bands, and teats, and, frequently fever, loss of appetite, weight loss, hypersalivation, depression, growth retardation, and severe decrease in milk production, which could persist after recovery [88], [92]. Two recent outbreaks of foot-and-mouth disease (FMD) in countries previously classified as FMD-free (Taiwan in 1997 and the United Kingdom in 2001) increased public awareness of the risk associated to this dangerous infectious disease (Figure 2.4).



Figure 2.4: Impact of FMDV outbreaks on animal and human life

Therefore, a global strategy for the control of FMD was endorsed in 2012 [93]. Currently, there is no treatment for FMD and the main strategies to limit spreading of the infection base on containment and vaccination [90]. Seven serologically distinct types of the virus have been isolated

(named O, A, C, SAT 1, SAT 2, SAT 3 and Asia 1) which are endemic in different countries worldwide and wide spread throughout the world, particularly in Asia, Africa and the Middle East [90], [94]. Though some multivalent vaccines are available, the increasing occurrence of antigenically dissimilar sub-strains suggest the importance of the production of vaccines from locally isolated virus. For this reason, serotyping and monitoring the strains have become strategic to control FMDV on a global scale. FMD diagnosis bases on clinical signs and is confirmed by virus detection on several kind of samples (serum, vesicular epithelium and fluid, buccal samples, mammary secretions, nasal and upper respiratory tract secretions, aerosols and so forth) [95]. Many techniques had been employed for the purpose, including direct complement fixation test (CFT), and reverse transcription-polymerase chain reaction (RT-PCR) [95]–[97]. Molecular diagnostic techniques have been widely explored in the past [97] while currently, the use of immunological methods is suggested for the detection of FMDV antibodies and antigens by international organization as FAO/WRL [96], [98]–[104]. Antigen-based assays can directly detect the presence of the virus, while serological approaches aimed at detecting the immune response to the pathogen are considered as indirect confirmation of the infection. Direct enzyme immunoassays are typically applied for the detection, typing, and strain differentiation of FMDV isolates with high sensitivity [94], [104]. Despite their reliability and accuracy these diagnostic tests are labour intensive and need to be operated in laboratory setting by trained personnel. Thus, alternatives approaches enabling the on-field and cost-effective FMDV detection are sought to allow the effective monitoring and timely implementation of control measures, especially in developing countries [95].

### LFIA for FMDV antigens

LFIA for the detection of FMDV serotypes based on the sandwich-type assay with pair of specific antibodies have been described [105]–[109]. Some authors used broad-specific antibodies (usually indicated as “PAN-FMDV”) for setting up devices capable of diagnosing the FMD, without differentiating on the virus serotype [105], [110]. Multiplexing LFIAs, including several test lines with different specificity, have been also reported [106], [111]. In particular, M. Yang et al. developed a single device including three test lines formed by O-, Asia 1-, and A specific antibodies to capture selectively the virus serotype and a broad-specific labelled antibody to stain captured antigens [106]. The multiplexing capability was further increased in the work of Morioka et al., who added a C-type specific and a PAN-FMDV test line enabling the detection of seven FMD virus by the PAN-FMDV line and the simultaneous differentiating of up to four serotypes (O, A, Asia 1, and C) [111]. More recently, the LFA technology has been exploited for revealing the product of the recombinase polymerase amplification (RPA-LFD) as diagnostic tools for FMD diagnosis [112], [113]. The developed devices were able to detect separately the viral RNA of O, A, and Asia 1 FMDV types with sensitivity comparable to the one of bench-top PCR. However, none of the available tools enables the prompt and accurate identification of all circulating FMDVs, with sufficient diagnostic sensitivity and specificity.

## References

- [1] “UNAIDS data 2018.”
- [2] F. Sheet, G. A. Update, N. Hiv, and N. Hiv, “2018 GLOBAL HIV STATISTICS,” pp. 1–6, 2019.
- [3] Kimberly Chricaden, “Impact of COVID-19 on people’s livelihoods, their health and our food systems.” <https://www.who.int/news/item/13-10-2020-impact-of-covid-19-on-people’s-livelihoods-their-health-and-our-food-systems> (accessed Feb. 03, 2021).
- [4] World Health Organization, “HIV ASSAYS: operational characteristics (Phase 1), Report 14: Simple/Rapid Tests,” no. Report 15, p. 64, 2004.
- [5] B. Bottiger *et al.*, “Envelope Cross-Reactivity between Human Immunodeficiency Virus Types 1 and 2 Detected by Different Serological Methods : Correlation between Cross-Neutralization and Reactivity against the Main Neutralizing Site,” vol. 64, no. 7, pp. 3492–3499, 1990.
- [6] D. J. Jamieson, C. C. King, and A. P. Kourtis, “Human immunodeficiency virus infection,” *Clin. Gynecol. Second Ed.*, pp. 360–370, 2015, doi: 10.1017/CBO9781139628938.026.
- [7] W. Daniel, F. Venter, N. Ford, and M. Vitoria, “Diagnosis and monitoring of HIV programmes to support treatment initiation and follow up and improve programme quality,” pp. 117–122, 2017, doi: 10.1097/COH.0000000000000354.
- [8] B. K. Titanji, D. Pillay, and C. Jolly, “Combination antiretroviral therapy and cell–cell spread of wild-type and drug-resistant human immunodeficiency virus-1,” *J. Gen. Virol.*, vol. 98, no. 4, pp. 821–834, 2017, doi: 10.1099/jgv.0.000728.
- [9] R. D. Moore and R. E. Chaisson, “Natural history of HIV infection in the era of combination antiretroviral therapy,” no. June, 1999.
- [10] H. F. Günthard *et al.*, “Antiretroviral drugs for treatment and prevention of HIV infection in Adults: 2016 recommendations of the international antiviral society-USA Panel,” *JAMA - J. Am. Med. Assoc.*, vol. 316, no. 2, pp. 191–210, 2016, doi: 10.1001/jama.2016.8900.
- [11] D. K. Ekouevi *et al.*, “Characteristics of HIV-2 and HIV-1/HIV-2 Dually Seropositive Adults in West Africa Presenting for Care and Antiretroviral Therapy: The IeDEA-West Africa HIV-2 Cohort Study,” *PLoS One*, vol. 8, no. 6, pp. 2–9, 2013, doi: 10.1371/journal.pone.0066135.
- [12] J. Drylewicz *et al.*, “First-year lymphocyte T CD4+ response to antiretroviral therapy according to the HIV type in the IeDEA West Africa collaboration,” *AIDS*, vol. 24, no. 7, p. 1043–1050, Apr. 2010, doi: 10.1097/qad.0b013e3283377a06.
- [13] J. L. Diane E. Handy, Rita Castro, “基因的改变NIH Public Access,” *Bone*, vol. 23, no. 1, pp. 1–7, 2011, doi: 10.1161/CIRCULATIONAHA.110.956839.
- [14] T. C. Granade, S. Workman, S. K. Wells, A. N. Holder, S. M. Owen, and C.-P. Pau, “Rapid Detection and Differentiation of Antibodies to HIV-1 and HIV-2 Using Multivalent Antigens and Magnetic Immunochromatography Testing,” *Clin. Vaccine Immunol.*, vol. 17, no. 6, pp. 1034 LP – 1039, Jun. 2010, doi: 10.1128/CVI.00029-10.
- [15] N. Meda *et al.*, “Serological diagnosis of human immunodeficiency virus in Burkina Faso: Reliable, practical strategies using less expensive commercial test kits,” *Bull. World Health Organ.*, vol. 77, no. 9, pp. 731–739, 1999.
- [16] M.-Z. Zhang *et al.*, “Development of a colloidal gold-based lateral-flow immunoassay for the rapid simultaneous detection of clenbuterol and ractopamine in swine urine,” *Anal. Bioanal. Chem.*, vol. 395, no. 8, p. 2591, 2009, doi: 10.1007/s00216-009-3181-2.
- [17] Q. Wang, Y. Liu, M. Wang, Y. Chen, and W. Jiang, “A multiplex immunochromatographic test using gold nanoparticles for the rapid and simultaneous detection of four nitrofurantoin metabolites in fish samples,” *Anal. Bioanal. Chem.*, vol. 410, no. 1, pp. 223–233, 2018, doi: 10.1007/s00216-017-0714-y.



- [18] S. Song *et al.*, “Multiplex Lateral Flow Immunoassay for Mycotoxin Determination,” *Anal. Chem.*, vol. 86, no. 10, pp. 4995–5001, May 2014, doi: 10.1021/ac500540z.
- [19] J. Peng, Y. Wang, L. Liu, H. Kuang, A. Li, and C. Xu, “Multiplex lateral flow immunoassay for five antibiotics detection based on gold nanoparticle aggregations,” *RSC Adv.*, vol. 6, no. 10, pp. 7798–7805, 2016, doi: 10.1039/C5RA22583C.
- [20] Y. Sun *et al.*, “Development of an immunochromatographic lateral flow strip for the simultaneous detection of aminoglycoside residues in milk,” *RSC Adv.*, vol. 8, no. 17, pp. 9580–9586, 2018, doi: 10.1039/C8RA01116H.
- [21] B. Liu *et al.*, “A gold immunochromatographic assay for simultaneous detection of parathion and triazophos in agricultural products,” *Anal. Methods*, vol. 10, no. 4, pp. 422–428, 2018, doi: 10.1039/C7AY02481A.
- [22] N. A. Taranova, A. N. Berlina, A. V Zherdev, and B. B. Dzantiev, “‘Traffic light’ immunochromatographic test based on multicolor quantum dots for the simultaneous detection of several antibiotics in milk,” *Biosens. Bioelectron.*, vol. 63, pp. 255–261, 2015, doi: <https://doi.org/10.1016/j.bios.2014.07.049>.
- [23] D. Daskalakis, “HIV diagnostic testing: Evolving technology and testing strategies,” *Top. Antivir. Med.*, vol. 19, no. 1, pp. 18–22, 2011.
- [24] M. D. P. Boyle, “Bacterial Immunoglobulin-Binding Proteins,” P. J. B. T.-E. of I. (Second E. Delves, Ed. Oxford: Elsevier, 1998, pp. 323–327.
- [25] N. Moshgabadi *et al.*, “Sensitivity of a rapid point of care assay for early HIV antibody detection is enhanced by its ability to detect HIV gp41 IgM antibodies,” *J. Clin. Virol.*, vol. 71, pp. 67–72, 2015, doi: 10.1016/j.jcv.2015.08.005.
- [26] C. Wang, F. Hou, and Y. Ma, “Simultaneous quantitative detection of multiple tumor markers with a rapid and sensitive multicolor quantum dots based immunochromatographic test strip,” *Biosens. Bioelectron.*, vol. 68, pp. 156–162, 2015, doi: <https://doi.org/10.1016/j.bios.2014.12.051>.
- [27] W. Wang, X. Su, H. Ouyang, L. Wang, and Z. Fu, “A novel immunochromatographic assay based on a time-resolved chemiluminescence strategy for the multiplexed detection of ractopamine and clenbuterol,” *Anal. Chim. Acta*, vol. 917, pp. 79–84, 2016, doi: <https://doi.org/10.1016/j.aca.2016.03.001>.
- [28] C.-W. Yen *et al.*, “Multicolored silver nanoparticles for multiplexed disease diagnostics: distinguishing dengue, yellow fever, and Ebola viruses,” *Lab Chip*, vol. 15, no. 7, pp. 1638–1641, 2015, doi: 10.1039/C5LC00055F.
- [29] C. C. K. and A. P. K. D. J. Jamieson, “Human immunodeficiency virus infection,” in *Clinical Gynecology*, 2nd ed., M. I. S. Eric J. Bieber, Joseph S. Sanfilippo, R. Horowitz, Ed. 2015, pp. 360–370.
- [30] A. Trickey *et al.*, “Survival of HIV-positive patients starting antiretroviral therapy between 1996 and 2013: a collaborative analysis of cohort studies,” *Lancet HIV*, vol. 4, no. 8, pp. e349–e356, Aug. 2017, doi: 10.1016/S2352-3018(17)30066-8.
- [31] F. Diamond, “HIV/AIDS treatment drastically reduces mortality and helps limit transmission,” *Manag. Care*, vol. 27, no. 11, pp. 16–17, Nov. 2018, Accessed: Feb. 03, 2021. [Online]. Available: <https://pubmed.ncbi.nlm.nih.gov/30620299/>.
- [32] W. M. Bezabhe, L. Chalmers, L. R. Bereznicki, and G. M. Peterson, “Adherence to Antiretroviral Therapy and Virologic Failure,” *Med. (United States)*, vol. 95, no. 15, Apr. 2016, doi: 10.1097/MD.0000000000003361.
- [33] J. Kim, E. Lee, B. J. Park, J. H. Bang, and J. Y. Lee, “Adherence to antiretroviral therapy and factors affecting low medication adherence among incident HIV-infected individuals during 2009-2016: A nationwide study,” *Sci. Rep.*, vol. 8, no. 1, Dec. 2018, doi: 10.1038/s41598-018-21081-x.

- [34] S. A. Iacob, D. G. Iacob, and G. Jugulete, "Improving the adherence to antiretroviral therapy, a difficult but essential task for a successful HIV treatment-clinical points of view and practical considerations," *Frontiers in Pharmacology*, vol. 8, no. NOV. Frontiers Media S.A., Nov. 23, 2017, doi: 10.3389/fphar.2017.00831.
- [35] T. N. Gengiah, A. Moosa, A. Naidoo, and L. E. Mansoor, "Adherence challenges with drugs for pre-exposure prophylaxis to prevent HIV infection," *International Journal of Clinical Pharmacy*, vol. 36, no. 1. Kluwer Academic Publishers, pp. 70–85, 2014, doi: 10.1007/s11096-013-9861-1.
- [36] N. A. Bokulich, M. Ziemski, M. S. Robeson, and B. D. Kaehler, "Measuring the microbiome: Best practices for developing and benchmarking microbiomics methods," *Computational and Structural Biotechnology Journal*, vol. 18. Elsevier B.V., pp. 4048–4062, Jan. 01, 2020, doi: 10.1016/j.csbj.2020.11.049.
- [37] J. S. Orman and C. M. Perry, "Tipranavir: A review of its use in the management of HIV infection," *Drugs*, vol. 68, no. 10. pp. 1435–1463, 2008, doi: 10.2165/00003495-200868100-00006.
- [38] R. Byrne, I. Carey, and K. Agarwal, "Tenofovir alafenamide in the treatment of chronic hepatitis B virus infection: rationale and clinical trial evidence," *Therapeutic Advances in Gastroenterology*, vol. 11. SAGE Publications Ltd, Jan. 01, 2018, doi: 10.1177/1756284818786108.
- [39] H. B. Fung, E. A. Stone, and F. J. Piacenti, "Tenofovir disoproxil fumarate: A nucleotide reverse transcriptase inhibitor for the treatment of HIV infection," *Clin. Ther.*, vol. 24, no. 10, pp. 1515–1548, Oct. 2002, doi: 10.1016/S0149-2918(02)80058-3.
- [40] G. E. Chittick *et al.*, "Pharmacokinetics of tenofovir disoproxil fumarate and ritonavir-boosted saquinavir mesylate administered alone or in combination at steady state," *Antimicrob. Agents Chemother.*, vol. 50, no. 4, pp. 1304–1310, Apr. 2006, doi: 10.1128/AAC.50.4.1304-1310.2006.
- [41] H. H. Ng *et al.*, "Tenofovir disoproxil fumarate: Toxicity, toxicokinetics, and toxicogenomics analysis after 13 weeks of oral administration in Mice," *Int. J. Toxicol.*, vol. 34, no. 1, pp. 4–10, Jan. 2015, doi: 10.1177/1091581814565669.
- [42] B. Fernandez-Fernandez *et al.*, "Tenofovir nephrotoxicity: 2011 update," *AIDS Research and Treatment*, vol. 2011. 2011, doi: 10.1155/2011/354908.
- [43] T. R. Cressey *et al.*, "A randomized clinical pharmacokinetic trial of Tenofovir in blood, plasma and urine in adults with perfect, moderate and low PrEP adherence: The TARGET study," *BMC Infect. Dis.*, vol. 17, no. 1, Jul. 2017, doi: 10.1186/s12879-017-2593-4.
- [44] M. Simiele *et al.*, "A LC-MS method to quantify tenofovir urinary concentrations in treated patients," *J. Pharm. Biomed. Anal.*, vol. 114, pp. 8–11, Oct. 2015, doi: 10.1016/j.jpba.2015.05.001.
- [45] P. L. Anderson, "What Can Urine Tell Us About Medication Adherence?," *EclinicalMedicine*, vol. 2–3. Lancet Publishing Group, pp. 5–6, Aug. 01, 2018, doi: 10.1016/j.eclinm.2018.09.003.
- [46] V. De Lastours, J. Fonsart, R. Burlacu, B. Gourmel, and J. Molina, "Concentrations of Tenofovir and Emtricitabine in Saliva : Implications for Preexposure Prophylaxis of Oral HIV Acquisition ☐," vol. 55, no. 10, pp. 4905–4907, 2011, doi: 10.1128/AAC.00120-11.
- [47] H. F. Günthard *et al.*, "Antiretroviral drugs for treatment and prevention of HIV infection in Adults: 2016 recommendations of the international antiviral society-USA Panel," *JAMA - J. Am. Med. Assoc.*, vol. 316, no. 2, pp. 191–210, Jul. 2016, doi: 10.1001/jama.2016.8900.
- [48] A. Calcagno *et al.*, "Tenofovir plasma concentrations according to companion drugs: A cross-sectional study of HIV-positive patients with normal renal function," *Antimicrob. Agents Chemother.*, vol. 57, no. 4, pp. 1840–1843, Apr. 2013, doi: 10.1128/AAC.02434-12.

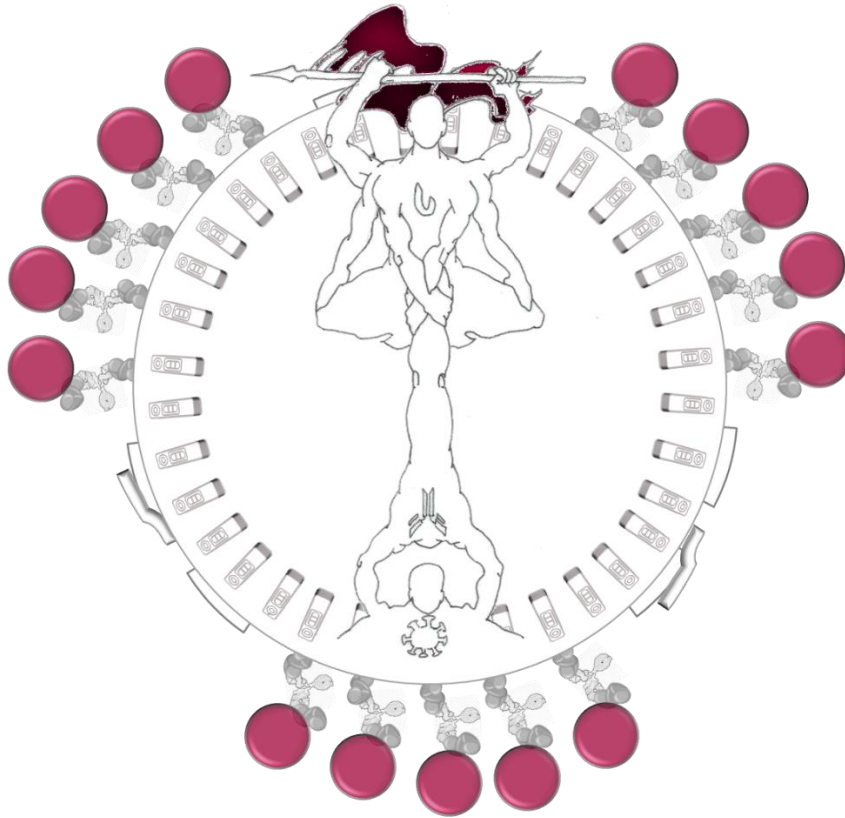
- [49] R. Pansini and D. Fornacca, "COVID-19 higher induced mortality in Chinese regions with lower air quality," 2020, doi: 10.1101/2020.04.04.20053595.
- [50] W. Wang *et al.*, "Detection of SARS-CoV-2 in Different Types of Clinical Specimens," *JAMA - Journal of the American Medical Association*, vol. 323, no. 18. American Medical Association, pp. 1843–1844, May 12, 2020, doi: 10.1001/jama.2020.3786.
- [51] M. P. Cheng *et al.*, "Diagnostic Testing for Severe Acute Respiratory Syndrome-Related Coronavirus 2: A Narrative Review," *Annals of internal medicine*, vol. 172, no. 11. NLM (Medline), pp. 726–734, Jun. 02, 2020, doi: 10.7326/M20-1301.
- [52] C. Y. P. Lee, R. T. P. Lin, L. Renia, and L. F. P. Ng, "Serological Approaches for COVID-19: Epidemiologic Perspective on Surveillance and Control," *Frontiers in Immunology*, vol. 11. Frontiers Media S.A., p. 879, Apr. 24, 2020, doi: 10.3389/fimmu.2020.00879.
- [53] C. Li and L. Ren, "Recent progress on the diagnosis of 2019 Novel Coronavirus," *Transboundary and Emerging Diseases*, vol. 67, no. 4. Blackwell Publishing Ltd, pp. 1485–1491, Jul. 01, 2020, doi: 10.1111/tbed.13620.
- [54] A. M. Morris, G.P.; and Gronowski, "Laboratory approaches to serology testing," in *Clinical Chemistry Theory Analysis Correlation*, 5th ed., Kaplan L.A. Pesce A.J, Ed. Eds, Mosby, Inc, (USA), 2010.
- [55] F. Pérez-García, R. Pérez-Tanoira, J. Romanyk, T. Arroyo, P. Gómez-Herruz, and J. Cuadros-González, "Alltest rapid lateral flow immunoassays is reliable in diagnosing SARS-CoV-2 infection from 14 days after symptom onset: A prospective single-center study," *J. Clin. Virol.*, vol. 129, Aug. 2020, doi: 10.1016/j.jcv.2020.104473.
- [56] G. Bauer, "The variability of the serological response to SARS-corona virus-2: Potential resolution of ambiguity through determination of avidity (functional affinity)," *Journal of Medical Virology*, vol. 93, no. 1. John Wiley and Sons Inc, pp. 311–322, Jan. 01, 2021, doi: 10.1002/jmv.26262.
- [57] Q. X. Long *et al.*, "Antibody responses to SARS-CoV-2 in patients with COVID-19," *Nat. Med.*, vol. 26, no. 6, pp. 845–848, Jun. 2020, doi: 10.1038/s41591-020-0897-1.
- [58] K. K. W. To *et al.*, "Temporal profiles of viral load in posterior oropharyngeal saliva samples and serum antibody responses during infection by SARS-CoV-2: an observational cohort study," *Lancet Infect. Dis.*, vol. 20, no. 5, pp. 565–574, May 2020, doi: 10.1016/S1473-3099(20)30196-1.
- [59] Z. Li *et al.*, "No Title," vol. 92, no. 9, Sep. 2020, doi: 10.1002/jmv.25727.
- [60] H. Q. Yu *et al.*, "Distinct features of SARS-CoV-2-specific IgA response in COVID-19 patients," *European Respiratory Journal*, vol. 56, no. 2. European Respiratory Society, Aug. 01, 2020, doi: 10.1183/13993003.01526-2020.
- [61] C. Dahlke *et al.*, "Distinct early IgA profile may determine severity of COVID-19 symptoms: An immunological case series," *medRxiv*. medRxiv, p. 2020.04.14.20059733, Apr. 17, 2020, doi: 10.1101/2020.04.14.20059733.
- [62] A. Padoan *et al.*, "IgA-Ab response to spike glycoprotein of SARS-CoV-2 in patients with COVID-19: A longitudinal study," *Clin. Chim. Acta*, vol. 507, pp. 164–166, Aug. 2020, doi: 10.1016/j.cca.2020.04.026.
- [63] Z. Huang *et al.*, "Characteristics and roles of severe acute respiratory syndrome coronavirus 2-specific antibodies in patients with different severities of coronavirus 19," *Clin. Exp. Immunol.*, vol. 202, no. 2, pp. 210–219, Nov. 2020, doi: 10.1111/cei.13500.
- [64] M. Infantino *et al.*, "Closing the serological gap in the diagnostic testing for COVID-19: The value of anti-SARS-CoV-2 IgA antibodies," *J. Med. Virol.*, Mar. 2020, doi: 10.1002/jmv.26422.
- [65] L. Guo *et al.*, "Profiling early humoral response to diagnose novel coronavirus disease (COVID-19)," *Clin. Infect. Dis.*, vol. 71, no. 15, pp. 778–785, Aug. 2020, doi: 10.1093/cid/cia310.

- [66] J. Ceron *et al.*, "Use of Saliva for Diagnosis and Monitoring the SARS-CoV-2: A General Perspective," *J. Clin. Med.*, vol. 9, no. 5, p. 1491, May 2020, doi: 10.3390/jcm9051491.
- [67] N. Pisanic *et al.*, "COVID-19 serology at population scale: SARS-CoV-2-specific antibody responses in saliva," *J. Clin. Microbiol.*, vol. 59, no. 1, Jan. 2021, doi: 10.1128/JCM.02204-20.
- [68] D. S. Y. Ong, S. J. de Man, F. A. Lindeboom, and J. G. M. Koeleman, "Comparison of diagnostic accuracies of rapid serological tests and ELISA to molecular diagnostics in patients with suspected coronavirus disease 2019 presenting to the hospital," *Clin. Microbiol. Infect.*, vol. 26, no. 8, pp. 1094.e7-1094.e10, Aug. 2020, doi: 10.1016/j.cmi.2020.05.028.
- [69] R. H. Jacobson, "Validation of serological assays for diagnosis of infectious diseases," *OIE Rev. Sci. Tech.*, vol. 17, no. 2, pp. 469–486, 1998, doi: 10.20506/rst.17.2.1119.
- [70] S. Momčilović, C. Cantacessi, V. Arsić-Arsenijević, D. Otranto, and S. Tasić-Otašević, "Rapid diagnosis of parasitic diseases: current scenario and future needs," *Clinical Microbiology and Infection*, vol. 25, no. 3. Elsevier B.V., pp. 290–309, Mar. 01, 2019, doi: 10.1016/j.cmi.2018.04.028.
- [71] F. M. Tomley and M. W. Shirley, "Livestock infectious diseases and zoonoses," *Philosophical Transactions of the Royal Society B: Biological Sciences*, vol. 364, no. 1530. Royal Society, pp. 2637–2642, Sep. 27, 2009, doi: 10.1098/rstb.2009.0133.
- [72] L. O. Fresco, "Challenges for food system adaptation today and tomorrow," *Environ. Sci. Policy*, vol. 12, no. 4, pp. 378–385, Jun. 2009, doi: 10.1016/j.envsci.2008.11.001.
- [73] R. K. Plowright *et al.*, "Pathways to zoonotic spillover," *Nature Reviews Microbiology*, vol. 15, no. 8. Nature Publishing Group, pp. 502–510, Aug. 01, 2017, doi: 10.1038/nrmicro.2017.45.
- [74] M. Letko, S. N. Seifert, K. J. Olival, R. K. Plowright, and V. J. Munster, "Bat-borne virus diversity, spillover and emergence," *Nature Reviews Microbiology*, vol. 18, no. 8. Nature Research, pp. 461–471, Aug. 01, 2020, doi: 10.1038/s41579-020-0394-z.
- [75] P. M. Sharp and B. H. Hahn, "Origins of HIV and the AIDS pandemic," *Cold Spring Harb. Perspect. Med.*, vol. 1, no. 1, Sep. 2011, doi: 10.1101/cshperspect.a006841.
- [76] K. J. Esch and C. A. Petersen, "Transmission and epidemiology of zoonotic protozoal diseases of companion animals," *Clin. Microbiol. Rev.*, vol. 26, no. 1, pp. 58–85, Jan. 2013, doi: 10.1128/CMR.00067-12.
- [77] M. J. Day *et al.*, "Surveillance of zoonotic infectious disease transmitted by small companion animals," *Emerg. Infect. Dis.*, vol. 18, no. 12, p. e1, Dec. 2012, doi: 10.3201/eid1812.120664.
- [78] M. da S. Solcà *et al.*, "Evaluating the Accuracy of Molecular Diagnostic Testing for Canine Visceral Leishmaniasis Using Latent Class Analysis," *PLoS One*, vol. 9, no. 7, p. e103635, Jul. 2014, doi: 10.1371/journal.pone.0103635.
- [79] "Leishmaniasis." Accessed: Feb. 03, 2021. [Online]. Available: <https://www.who.int/en/news-room/fact-sheets/detail/leishmaniasis>.
- [80] A. Adel, D. Berkvens, E. Abatih, A. Soukhehal, J. Bianchini, and C. Saegerman, "Evaluation of Immunofluorescence Antibody Test Used for the Diagnosis of Canine Leishmaniasis in the Mediterranean Basin: A Systematic Review and Meta-Analysis," *PLoS One*, vol. 11, no. 8, p. e0161051, Aug. 2016, doi: 10.1371/journal.pone.0161051.
- [81] E. Ferroglio, M. Maroli, S. Gastaldo, W. Mignone, and L. Rossi, "Canine leishmaniasis, Italy," *Emerg. Infect. Dis.*, vol. 11, no. 10, pp. 1618–1620, 2005, doi: 10.3201/eid1110.040966.
- [82] C. Adams E, Hasker E, "Diagnostics evaluation series No. 4: Visceral Leishmaniasis Rapid Diagnostic Test Performance," no. 4, 2011.
- [83] W. Pinto, A. J. Ribeiro, and V. M. Tafuri, "The Immunochromatography Use in Canine Visceral Leishmaniasis in Brazil: A 'Quick Solution' of a Complex Diagnostic? Rapid Test in Dogs with Leishmaniasis," 2016.

- [84] S. Paltrinieri, L. Gradoni, X. Roura, A. Zatelli, and E. Zini, "Laboratory tests for diagnosing and monitoring canine leishmaniasis," *Veterinary Clinical Pathology*, vol. 45, no. 4. American Society for Veterinary Clinical Pathology, pp. 552–578, Dec. 01, 2016, doi: 10.1111/vcp.12413.
- [85] "SNAP Leishmania - IDEXX UK." <https://www.idexx.co.uk/en-gb/veterinary/snap-tests/snap-leishmania/> (accessed Feb. 03, 2021).
- [86] R. M. Cardoso *et al.*, "Expanding the knowledge about Leishmania species in wild mammals and dogs in the Brazilian savannah," *Parasites and Vectors*, vol. 8, no. 1, Mar. 2015, doi: 10.1186/s13071-015-0780-y.
- [87] C. H. Gao, J. Y. Wang, S. Zhang, Y. T. Yang, and Y. Wang, "Survey of wild and domestic mammals for infection with leishmania infantum following an outbreak of desert zoonotic visceral leishmaniasis in Jiashi, People's Republic of China," *PLoS One*, vol. 10, no. 7, Jul. 2015, doi: 10.1371/journal.pone.0132493.
- [88] "OIE. Foot & Mouth Disease (FMD) [Online] (2018)." <https://www.oie.int/en/animal-health-in-the-world/animal-diseases/foot-and-mouth-disease/> (accessed Sep. 22, 2020).
- [89] B. W. J. Mahy, "Introduction and history of foot-and-mouth disease virus.," *Curr. Top. Microbiol. Immunol.*, vol. 288, pp. 1–8, 2005, doi: 10.1007/3-540-27109-0\_1.
- [90] S. M. Jamal and G. J. Belsham, "Foot-and-mouth disease: past, present and future," *Vet. Res.*, vol. 44, no. 1, p. 116, 2013, doi: 10.1186/1297-9716-44-116.
- [91] K. Poonsuk, L. Giménez-Lirola, and J. J. Zimmerman, "A review of foot-and-mouth disease virus (fmdv) testing in livestock with an emphasis on the use of alternative diagnostic specimens," *Anim. Heal. Res. Rev.*, vol. 19, no. 2, pp. 100–112, 2018, doi: 10.1017/S1466252318000063.
- [92] R. P. Kitching and S. Alexandersen, "Clinical variation in foot and mouth disease: Pigs," *Rev. Sci. Tech.*, vol. 21, pp. 513–518, Jan. 2003, doi: 10.20506/rst.21.3.1367.
- [93] M. J. Grubman and B. Baxt, "Foot-and-Mouth Disease," *Clin. Microbiol. Rev.*, vol. 17, no. 2, pp. 465 LP – 493, Apr. 2004, doi: 10.1128/CMR.17.2.465-493.2004.
- [94] B. Admassu, K. Getnet, A. Shite, and S. Mohammed, "Review on Foot and Mouth Disease: Distribution and Economic Significance," *Acad. J. Anim. Dis.*, vol. 4, no. 3, pp. 160–169, 2015, doi: 10.5829/idosi.ajad.2015.4.3.95165.
- [95] C. L. Wong, C. Y. Yong, H. K. Ong, K. L. Ho, and W. S. Tan, "Advances in the Diagnosis of Foot-and-Mouth Disease," *Front. Vet. Sci.*, vol. 7, p. 477, 2020, doi: 10.3389/fvets.2020.00477.
- [96] L. Ma, J. Zhang, H. Chen, J. Zhou, Y. Ding, and Y. Liu, "An overview on ELISA techniques for FMD," *Virology*, vol. 8, p. 419, Sep. 2011, doi: 10.1186/1743-422X-8-419.
- [97] N. Longjam, R. Deb, A. K. Sarmah, T. Tayo, V. B. Awachat, and V. K. Saxena, "A Brief Review on Diagnosis of Foot-and-Mouth Disease of Livestock: Conventional to Molecular Tools," *Vet. Med. Int.*, vol. 2011, p. 905768, 2011, doi: 10.4061/2011/905768.
- [98] E. M. Abu Elzein and J. R. Crowther, "Enzyme-labelled immunosorbent assay techniques in foot-and-mouth disease virus research.," *J. Hyg. (Lond)*, vol. 80, no. 3, pp. 391–399, Jun. 1978, doi: 10.1017/s0022172400024840.
- [99] J. R. Crowther and E. M. Abu-el Zein, "Detection and quantification of foot and mouth disease virus by enzyme labelled immunosorbent assay techniques.," *J. Gen. Virol.*, vol. 42, no. 3, pp. 597–602, Mar. 1979, doi: 10.1099/0022-1317-42-3-597.
- [100] E. M. Elzein and J. R. Crowther, "The specific detection of foot-and-mouth disease virus whole particle antigen (140S) by enzyme labelled immunosorbent assay.," *J. Hyg. (Lond)*, vol. 83, no. 1, pp. 127–134, Aug. 1979, doi: 10.1017/s0022172400025894.
- [101] P. L. Roeder and P. M. Le Blanc Smith, "Detection and typing of foot-and-mouth disease virus by enzyme-linked immunosorbent assay: a sensitive, rapid and reliable technique for primary diagnosis.," *Res. Vet. Sci.*, vol. 43, no. 2, pp. 225–232, Sep. 1987.

- [102] C. Hamblin, I. T. Barnett, and R. S. Hedger, "A new enzyme-linked immunosorbent assay (ELISA) for the detection of antibodies against foot-and-mouth disease virus. I. Development and method of ELISA," *J. Immunol. Methods*, vol. 93, no. 1, pp. 115–121, Oct. 1986, doi: 10.1016/0022-1759(86)90441-2.
- [103] N. P. Ferris and M. Dawson, "Routine application of enzyme-linked immunosorbent assay in comparison with complement fixation for the diagnosis of foot-and-mouth and swine vesicular diseases," *Vet. Microbiol.*, vol. 16, no. 3, pp. 201–209, 1988, doi: [https://doi.org/10.1016/0378-1135\(88\)90024-7](https://doi.org/10.1016/0378-1135(88)90024-7).
- [104] G. Paiba *et al.*, "Validation of a Foot-and-mouth disease antibody screening Solid-phase competition ELISA (SPCE)," *J. Virol. Methods*, vol. 115, pp. 145–158, 2004, doi: 10.1016/j.jviromet.2003.09.016.
- [105] J. K. Oem, N. P. Ferris, K.-N. Lee, Y.-S. Joo, B.-H. Hyun, and J.-H. Park, "Simple and Rapid Lateral-Flow Assay for the Detection of Foot-and-Mouth Disease Virus," *Clin. Vaccine Immunol.*, vol. 16, no. 11, pp. 1660 LP – 1664, Nov. 2009, doi: 10.1128/CVI.00213-09.
- [106] M. Yang, N. R. Caterer, W. Xu, and M. Goolia, "Development of a multiplex lateral flow strip test for foot-and-mouth disease virus detection using monoclonal antibodies.," *J. Virol. Methods*, vol. 221, pp. 119–126, Sep. 2015, doi: 10.1016/j.jviromet.2015.05.001.
- [107] T. Jiang *et al.*, "A simple and rapid colloidal gold-based immunochromatographic strip test for detection of FMDV serotype A," *Virol. Sin.*, vol. 26, no. 1, pp. 30–39, 2011, doi: 10.1007/s12250-011-3166-5.
- [108] M. Yang, M. Goolia, W. Xu, H. Bittner, and A. Clavijo, "Development of a quick and simple detection methodology for foot-and-mouth disease virus serotypes O, A and Asia 1 using a generic RapidAssay Device," *Virol. J.*, vol. 10, no. 1, p. 125, 2013, doi: 10.1186/1743-422X-10-125.
- [109] M. Yang, B. Mudabuka, K. Quizon, and C. Nfon, "Generation of monoclonal antibodies against foot-and-mouth disease virus SAT 2 and the development of a lateral flow strip test for virus detection," *Transbound. Emerg. Dis.*, vol. 66, no. 3, pp. 1158–1166, May 2019, doi: 10.1111/tbed.13076.
- [110] N. P. Ferris *et al.*, "Development and laboratory validation of a lateral flow device for the detection of foot-and-mouth disease virus in clinical samples," *J. Virol. Methods*, vol. 155, no. 1, pp. 10–17, 2009, doi: <https://doi.org/10.1016/j.jviromet.2008.09.009>.
- [111] K. Morioka *et al.*, "Development and Evaluation of a Rapid Antigen Detection and Serotyping Lateral Flow Antigen Detection System for Foot-and-Mouth Disease Virus," *PLoS One*, vol. 10, no. 8, pp. 1–10, Aug. 2015, doi: 10.1371/journal.pone.0134931.
- [112] H. Wang, P. Hou, G. Zhao, L. Yu, Y. Gao, and H. He, "Development and evaluation of serotype-specific recombinase polymerase amplification combined with lateral flow dipstick assays for the diagnosis of foot-and-mouth disease virus serotype A, O and Asia1," *BMC Vet. Res.*, vol. 14, no. 1, p. 359, 2018, doi: 10.1186/s12917-018-1644-4.
- [113] L. Liu *et al.*, "Visual and equipment-free reverse transcription recombinase polymerase amplification method for rapid detection of foot-and-mouth disease virus," *BMC Vet. Res.*, vol. 14, no. 1, p. 263, 2018, doi: 10.1186/s12917-018-1594-x.

# Chapter 3



---

## The total antibody LFIA

---

## Introduction

The antibody detection by LFIA generally addresses the IgG class as the most abundant and persistent in the serum. Sometimes, other classes of antibodies can be addressed. The IgM are targeted when the question is the presence of biomarkers of an early infection. In this case distinguishing between IgM and IgG can give additional information on the stage of the disease to correlate with early infection, infectivity or acquired immunity[1]–[4]. However, the optimal discrimination capacity requires the maximal specificity, which usually is achieved at the expense of the sensitivity. In addition, many tests do not discriminate between classes but target only one class, supposed to be the majoritarian one. This approach is preferable for diseases causing immunosuppression or when the test is dedicated to non-conventional matrices, such as saliva, where the excess of non-specific antibodies is less prominent than in the blood or serum. Nevertheless, the use of antibody binding reagents, such as the Staphylococcal protein A (SpA) from *Staphylococcus Aureus* or protein G from *Streptococcus*, allow for targeting the sum of the various class of antibodies elicited as a response to the pathogen[5]. SpA can bind up to five immunoglobulins and is able to bind to different classes of antibodies, though with different affinities. The use of the SpA as the capture or detection bioligand allows to widen the range of types of antibodies detected and enhances the overall sensitivity thanks to the high binding capacity[6]. Another way to target different classes of antibodies is the double-antigen approach, introduced in the chapter 1.4.2, These two strategies are good candidates to increase the sensitivity of the assay through targeting the sum of several classes of antibodies, following the hereafter mentioned “*total antibody*” approach. In this chapter the total antibody approaches are introduced, consisting in the wise use of “non-specific” or “broadly specific” bioligands to increase the sensitivity and the versatility of the resulting devices.

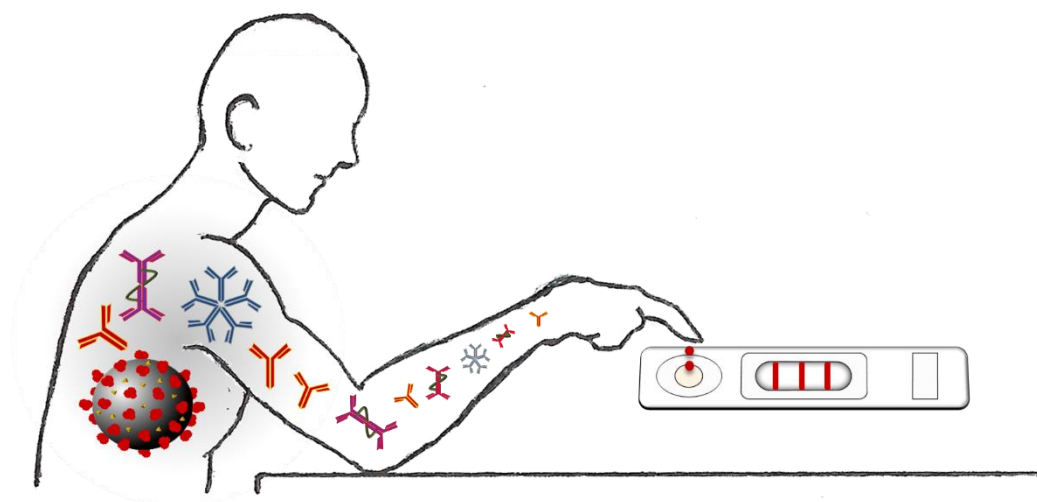
In the following sections, two total antibody tests are reported for human and animal healthcare, demonstrating to be the most convenient serological detection strategy in the presence of SarS-CoV2 infection in humans, in terms of sensitivity, and Visceral Leishmaniasis in dog (and other mammals) in terms of versatility.



## 3.1



### SARS CoV-2 Total Antibody LFIA



Based on

S. Cavallera, B. Colitti, S. Rosati, G. Ferrara, L. Bertolotti, C. Nogarol, C. Guiotto, C. Cagnazzo, M. Denina, F. Fagioli, F. Di Nardo, M. Chiarello, C. Baggiani, L. Anfossi, **A multi-target lateral flow immunoassay enabling the specific and sensitive detection of total antibodies to SARS CoV-2**, *Talanta*, Volume 223, Part 1, 2021, 121737, ISSN 0039-9140, <https://doi.org/10.1016/j.talanta.2020.121737>.

#### Abstract

*A rapid test for detecting total immunoglobulins directed towards the nucleocapsid protein (N) of severe acute syndrome coronavirus 2 (SARS CoV-2) was developed, based on a multi-target lateral flow immunoassay comprising two test lines. Both test lines bound to several classes of immunoglobulins (G, M, and A). Specific anti-SARS immunoglobulins were revealed by a colorimetric probe formed by N and gold nanoparticles. Targeting the total antibodies response to infection enabled achieving 100% diagnostic specificity (95.75–100, C.I. 95%, n = 85 healthy and with other infections individuals) and 94.6% sensitivity (84.9–98.9, C.I. 95%, n = 62 SARS CoV-2 infected subjects) as early as 7 days post confirmation of positivity. Agreeing results with a reference serological ELISA were achieved, except for the earlier detection capability of the rapid test. Follow up of the three seroconverting patients endorsed the hypothesis of the random rise of the different immunoglobulins and strengthened the ‘total antibodies’ approach for the trustworthy detection of serological response to SARS CoV-2 infection.*

### 3.1.1 Architecture of the test

We designed a double line LFIA, in which both lines were able to detect the three Ig classes, while with different selectivity. The combination of the information provided by the two lines enabled ensuring as high as possible diagnostic specificity. The specific detection of anti- SARS CoV-2 antibodies was guaranteed by the probe, which comprised a recombinant SARS CoV-2 nucleocapsid protein (N) and gold nanoparticles as colorimetric signal reporters. Staphylococcal protein A (SpA) is known to bind to Fc domain of human IgG; moreover, has been shown to bind to Fab domains of some IgM and IgA[7], [8]. The use of the antigen as capturing and detection reagent in sandwich ELISA has also been reported as a convenient strategy to increase sensitivity and reduce matrix interference in serological assays[9], [10]. The higher sensitivity and ability to detect seroconversion earlier than conventional direct/indirect ELISA of double-antigen ELISAs rely on the response to total antibodies present in the sample, regardless to the class of Ig revealed. A double-antigen sandwich ELISA based on the nucleocapsid antigen has been indicated as an effective screening method for the serodiagnosis of SARS-associated coronavirus[11]. In fact, the nucleocapsid protein of SARS-related virus has high immunogenic activity and is abundantly overexpressed during infection. In fact, several serological assays for detecting SARS CoV-2 antibodies employ the N protein as the antigen[12]–[14]. In addition, antibodies towards N have been shown to be able to neutralize the virus, with an excellent correlation between the existence of anti-N antibodies and the neutralizing ability of the serum[15]. Hence, we created a recombinant N antigen and expressed it in *E. coli*. The full open reading frame encoding the N protein of SARS CoV-2 was amplified and cloned in prokaryotic expression vector in N-terminal fusion of 6xhis tail and purified by Immobilized metal affinity chromatography (IMAC). Test lines were formed by SpA and the recombinant N antigen.

The clinical performance of the ‘total antibody’ LFIA was tested on eighty-five sera collected in 2018 (before SARS CoV-2 outbreak) and on sixty-two infected subjects (confirmed as SARS CoV-2 positive by the reference rRT-PCT) enrolled from three different centres. Finally, the LFIA was applied to follow seroconversion of three hospitalized patients. The same sera used for the two LFIAs were also analysed by validated ELISA targeting anti-SARS CoV-2 IgG in the view of rationalize results from the LFIA.

### 3.1.2 Materials and Methods

#### Immunoreagents, chemicals and materials

Gold (III) chloride trihydrate (ACS reagent), mouse antihuman immunoglobulin A monoclonal antibody A ( $\alpha$ -chain specific), staphylococcal protein A (SpA), casein sodium salt from milk, avidin, sucrose, polyethylene glycol 10000 (PEG), and bovine serum albumin (BSA) were obtained from Sigma–Aldrich (St. Louis, MO, USA). Tween20 and other chemicals were purchased from VWR International (Milan, Italy). Nitrocellulose membranes with cellulose adsorbent pad and blood separator sample pads were purchased by MDI membrane technologies (Ambala, India) and glass fibre conjugate pads were obtained from Merck Millipore (Billerica, MA, USA). The ELISA kit was an indirect ELISA for the detection of anti SARS-CoV2 antibodies (ERADIKIT™ COVID19-IgG from In3diagnostic srl, Turin, Italy)[16]. The commercial ELISA kit was registered as IVD-CE according to European Directive 98/79/CE for the detection of IgG in serum samples. The performances declared by the manufacturer are i) sensitivity of 96% if the ELISA test is performed on samples collected after 20 days after the first positive swab; ii) analytical and diagnostic specificity of 100%; iii) repeatability and reproducibility: Coefficient of Variation <5%. Statistical calculations were carried out with SigmaPlot 11.0 software.

#### SARS CoV-2 nucleocapsid recombinant protein (N)

The full open reading frame encoding the N protein was RT-PCR amplified from a nasal swab of SARS CoV-2 infected donor and cloned into pSER prokaryotic expression vector in frame with 6xhis tail as described[17]. Plasmid preparation from at least two PCR positive culture were extracted and sequenced to confirm presence and correct in frame orientation of N gene. The protein of interest was induced in early log phase positive culture by IPTG 1mM for 2 hours. Bacteria were collected by centrifugation and lysed by physical-chemical methods. The recombinant N protein was recovered in the 1M urea extraction fraction and purified by immobilized metal affinity chromatography under denaturing condition. Fractions of eluted proteins were analysed by SDS-PAGE and concentrations were estimated by DC protein assay (BioRad, Hercules, CA, USA). For GNP conjugation, pooled eluted fractions were dialyzed against 100 volumes of carbonate/bicarbonate buffer.

#### Preparation of GNPs and conjugation of SARS CoV-2 nucleocapsid to GNPs (GNP-N)

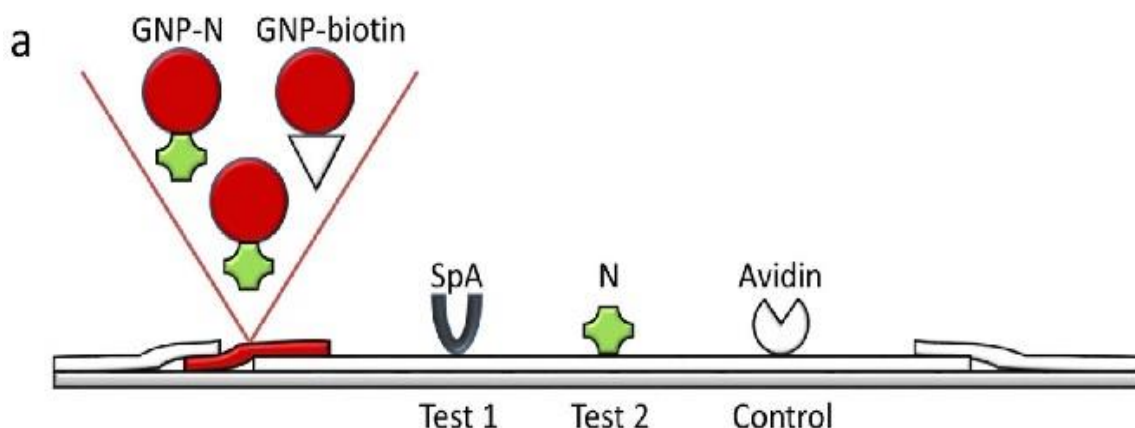
GNPs with a SPR band at 525 nm and mean diameter of ca. 30 nm were prepared by tetrachloroauric acid reduction with sodium citrate[18]. Briefly, 1 mL of 1% w/v sodium citrate was added to 0.01% of boiling tetrachloroauric acid under vigorous stirring. The colour of the solution changed gradually from light yellow to red thus confirming the successful formation of gold nanoparticles. Signal reporters used in the LFIA were prepared by adsorbing SARS CoV-2 nucleocapsid (N) protein onto GNPs. In details, 100  $\mu$ g of N were added dropwise to 10 ml of GNPs under gentle stirring for 40 min at room temperature. Then, 1 ml of casein (5% in borate buffer) was added and reacted for 10 min to saturate free GNP surface. GNP-N conjugates were recovered by centrifugation (10000 rpm, 15

min) and washed twice with borate buffer supplemented with 0.5% casein. Finally, GNP-N were re-suspended in GNP storage buffer (borate buffer with 0.5% casein, 0.25% Tween 20, 2% sucrose, and 0.02% sodium azide) and stored at 4°C until use. Bovine beta casein was linked with Sulfo-NHS-LC-Biotin (Thermo Scientific, Waltham, MA, USA) following protocol recommended by manufacturer. The probe GNP-biotin was then prepared by passive adsorption of the casein-biotin onto GNP by using the same protocol as above. For the GNP-anti IgA conjugate the anti-IgA was added to a pH-adjusted GNP solution (pH 8,5), in the proportion 10 µg per ml of GNP (optical density, OD 1). The uncovered GNP surface was saturated with BSA and the GNP-anti IgA were concentrated and recovered by centrifugation as previously described.

## Design and Development of the LFIA device

Conventional strategies to design rapid tests for infectious disease diagnosis involve dropping a specific antigen (either native or recombinant) to form the test line and labelling high affinity anti-human immunoglobulins for the detection of the binding event occurred between the antigen (capturing reagent) and the patient' serological response. Typically, anti-human immunoglobulins G (anti-IgG) are used for the purpose[19]. The reverse option (i.e., the capturing reagent comprises anti-IgG while the specific recognition event is linked to the binding to the labelled antigen from the pathogen) has the advantage that several lines can be arranged on a single strip test and the serological response to the infection can be discriminated, thus providing information on the stage of the seroconversion. Eventually, the capability of detecting IgM besides IgG helps earlier diagnosis. Devices based on the reverse approach have been speedily made available for the rapid and point-of-care diagnosis of SARS CoV-2 infection[20]–[25]. However, as observed for SARS and MERS virus[15], [26], also the new coronavirus elicits the random production of either IgM or IgG in the acute phase of the infection. In addition, secretory IgA have been found in the blood of infected individuals and have been shown to correlate with the neutralizing effect of the immune response[27]. All considered, we designed a novel 'total antibodies' approach for revealing all classes of immunoglobulins with the aim of increasing the diagnostic sensitivity and enabling the as early as possible identification of infected individuals. Accordingly, we used a recombinant N antigen as the capturing agent and as the detection probe. In this double-antigen approach SARS CoV-2 specific immunoglobulins interacted with the N protein that formed the test line and were revealed by the same N protein labelled with a colorimetric reporter (Figure 3.1.1, test line 2), independently on the Ig class.

Although the prompt identification of infected individuals is a relevant concern to circumvent the spread of the infection, equally important is the trustworthiness with which positivity is ascertained.



Indeed, a false positive assignment is detrimental for the subject (who may become confident in a false immunity) and for the society because is still susceptible of being infected and of spreading the infection.

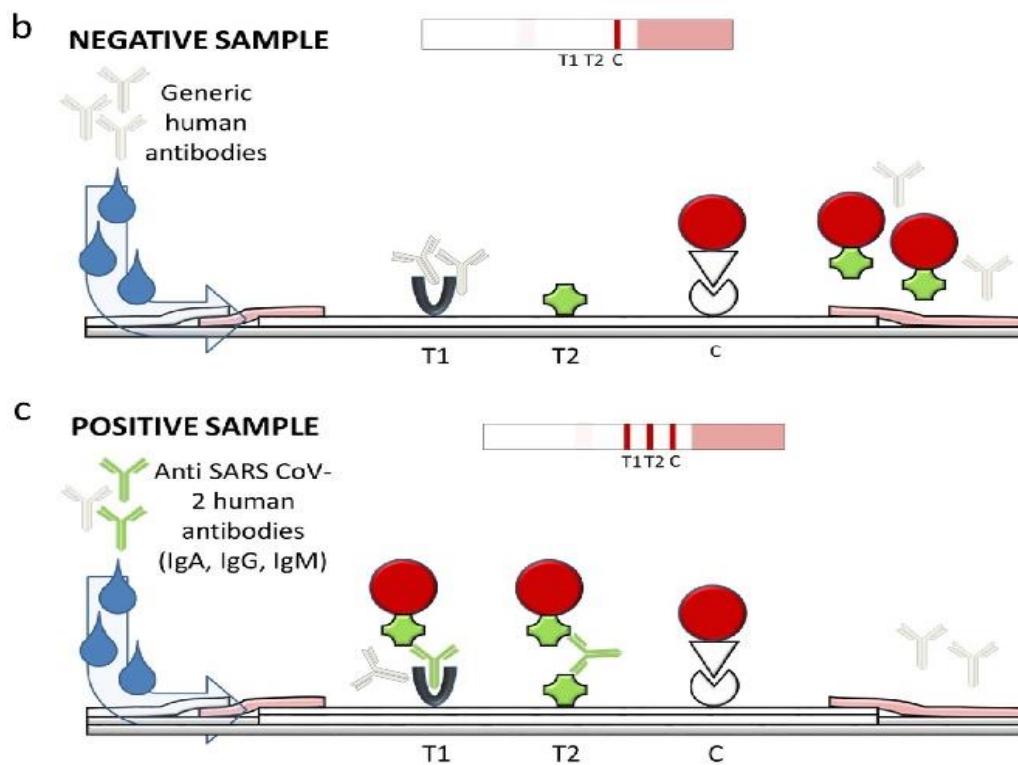


**Figure 3.1.1:** Scheme of the LFIA device for the rapid serological diagnosis of SARS CoV-2. (a) The strip is composed of the analytical membrane onto which the protein A (SpA), the SARS CoV-2 nucleocapsid protein (N) and avidin are coated to form the two test (T1 and T2) and the control (C) lines, respectively. The signal reporter is made of a mix of GNP-labelled N and biotin. (b) A single visible line (C) is expected for a human serum that does not contain any anti-N antibodies (negative sample, b). (c) The presence of specific anti-N antibodies (IgG, IgM and IgA) is revealed because of the simultaneous binding to the labelled N and to SpA (T1) and/or to N (T2).

Therefore, the as high as possible diagnostic specificity is an imperative demand for serological tests, as well as sensitivity. In this view, we inserted a second test line comprising staphylococcal protein A as the capturing reagent. SpA can bind to human immunoglobulins. In details, it specifically and strongly interacts with the Fc of human IgG and with Fab of some human IgM and IgA. Ideally, both test lines were able to reveal the presence of the complete serological response to SARS CoV-2 while we expected that non-specific interactions differently affected the two lines.

### Fabrication of the LFIA device

For the ‘total antibody’ LFIA the protein A was applied to the nitrocellulose (NC) membrane to form the first test line (0.5 mg/ml) and the protein N was applied to form a second test line (1.0 mg/ml). Avidin (1.0 mg/ml) was used as the capturing reagent for the GNP-biotin conjugate at the Control line. Reagents were dotted at 1  $\mu\text{L cm}^{-1}$  by means of a XYZ3050 platform (Biodot, Irvine, CA, USA), equipped with BioJetQuanti™ 3000 Line Dispenser for non-contact dispensing, keeping 3 mm between the lines. The signal reporters (GNP-N and GNP-biotin conjugates mix) were absorbed onto the glass fibre conjugate pad previously saturated with GNP dilution buffer (borate buffer with 0.25% Tween 20, 2% sucrose and 0.02% sodium azide). The conjugates were mixed with a ratio of 4/1 (GNP-N/GNP-biotin) and diluted with GNP dilution buffer to optical density 2.5. The conjugate pads of the

two devices were dipped into the respective GNP conjugate solutions and dried for 4 hours at room temperature. NC membranes were dried at 37°C for 60 minutes under vacuum, layered with sample, conjugate and absorbent pads, cut into strips (4.2 mm width) by means of a CM4000 guillotine (Biodot, Irvine, CA, USA) and inserted into plastic cassettes (Kinbio, China) to fabricate the ready-to-use LFIA device. Cassettes were stored in the dark in plastic bags containing silica at room temperature until use.

### The Lateral Flow Immunoassay for SARS CoV-2 serological diagnosis

For the analysis, samples were thawed at room temperature, carefully mixed, and diluted by 1:10 using the running buffer (Tris 34 mM/Glycine 80 mM buffer pH 8, 0.2% casein, 1% Tween 20, 0.05% sodium azide). Assays to detect SARS CoV-2 antibodies were carried out at room temperature, by applying 80 µl of diluted serum to the sample well. Qualitative results were judged by the naked eye after 20 minutes from sample application. Samples were analysed in duplicate and results were observed by three operators. Images of LFIA devices were also acquired by a portable scanner (OpticSlim 550 scanner, Plustek Technology GmbH, Norderstedt, Germany) and the areas of the coloured lines were quantified by means of the ImageJ software (NIH, USA). Values below 100 arbitrary units (a.u.) corresponded to no signal detected by the naked eye and were then set at zero.

### Serum Samples

The double-test line LFIA was tested on a total of 85 negative human sera kindly provided by the S. Luigi Gonzaga Hospital (Orbassano, Torino, Italy) and collected in 2018. Among them, 25 samples were known to pertain to individuals with other infections (hum immunodeficiency virus n=2, hepatitis C virus n=6, Epstein Barr virus n=3, cytomegalovirus n=4) or monoclonal gammopathy (n=10) (Table 3.1.1). No false positive results (0/85) were observed at the T1 line, while 2 false positives were found at the T2 line (false positive rate, FPR = 2.4%). Based on the combined interpretation of the two lines, 100% (95.75-100%, C.I. 95%) diagnostic specificity was achieved. It should be noticed that we were not able to test pre-covid sera belonging to patients infected by other respiratory virus, and by other human coronaviruses. However, with a notable exception of SARS-Cov/2003 and MERS-CoV (the former not circulating since 2004 and the latter restricted to middle east area), the N antigen employed in this work showed less than 28% amino acid homology with other human alpha or beta-coronaviruses. Moreover, cross-reactivity was not observed in a previous study using the same antigen by ELISA or western blot, when human plasma with positive antibodies against NL63, 229E, OC43 and HKU1 (prototype human coronavirus strains) were probed.[28]

**Table 3.1.1.** Description of the population of SARS CoV-2 infected individuals enrolled for the study

<i>Total rRT-PCR+</i>	<i>sex</i>		<i>age</i>	
	M	F	median	range
62	43	19	53	7 - 89

### 3.1.3 Results and Discussion

#### Recombinant nucleocapsid production

The N recombinant antigen was successfully expressed as partially soluble protein. Purification was achieved under mild denaturing condition (1M urea fraction) and evaluated by SDS-PAGE, showing a single protein band of molecular weight corresponding to the expected size. Sequence analysis of each of two bacterial clones confirmed the identity and correct orientation of the insert.

#### Study on the stabilization of GNP-N conjugates

Concerning the 'total antibody' LFIA, particularly challenging was the aspect of N protein labelling with GNPs. Studies aimed at reaching stable and functional GNP-N conjugates were conducted by varying the pH and amount of the N protein during adsorption onto GNP surface and the additive used to saturate the free GNP surface (Table 3.1.2). Optimal conditions were established on a pass-no pass approach based upon i) avoiding GNP agglomeration during and after the conjugation process, ii) providing no signal for negative samples, and iii) showing intense colouring with positive samples.

**Table 3.1.2.** Experimental conditions tested for the adsorption of the recombinant antigen onto GNPs. Selected conditions for the preparation of GNP-N conjugate are shown in bold. The saturation agents were dissolved in borate buffer. The same buffer was used in the saturation, washing and resuspension steps of the conjugation.

<i>pH of GNP sol</i>	<i>N amount (<math>\mu\text{g ml}^{-1} \text{OD}^{-1}</math>)</i>	<i>Saturation</i>		<i>Agglomeration tendency</i>	<i>Signal</i>	
		<i>agent</i>	<i>concentration (% w/v)</i>		<i>negative sample</i>	<i>positive sample</i>
8	10	BSA	1	weak	++	
8	10	Casein	0.5	no	-	-
10	10	BSA	1	weak	++	
10	30	BSA	1	moderate		
10	10	Casein	0.5	no	+	+
10	30	Casein	0.5	no	+	+
10	10	yeast extract	1	strong		
10	10	PEG-BSA	1-1	weak	+	+
10	30	PEG-BSA	1-1	strong		
<b>9</b>	<b>10</b>	<b>Casein</b>	<b>0.5</b>	<b>no</b>	<b>-/+</b>	<b>++</b>
9	30	Casein	0.5	no	-/+	++

For the experiments, 3 negative and 3 positive serum samples, as classified by the reference ELISA, were tested. The evaluation was made by naked eye observation between 5 and 30 minutes from sample application. Symbols represent: (-) absent, (-/+) weak, (+) moderate, and (++) strong red-colour developed at the test lines. The performance of the GNP-N was considered acceptable if the agglomeration tendency was negligible or weak (pass), the signal for negative sample was absent/weak or moderate (pass) and the signal of positive samples from moderate to strong (pass). GNP-N adsorption was carried at room temperature under gentle stirring. Stable GNP-N conjugates were obtained by using 10 µg/ml\*OD of N to GNPs at pH 9 with casein in the overcoating, washing and storage buffers. The effect of proteins and polymers usually added to limit non-specific binding of the probe to capturing reagents and to limit matrix effect were evaluated by checking their impact on the LFIA performance. Also, adding the modifier to the running buffer or pre-adsorbing it on the conjugate pad were considered. Optimal resuspension and flow of the GNP-N conjugate was realized when no proteins or polymers were pre-adsorbed (Table 3.1.3). The Tris-Glycine buffer supplemented with 0.2% w/v of casein was selected as the one enabling the complete removal of the residual colour at the test lines for negative samples while assuring strong signals for positive samples (Table 3.1.4). Finally, the concentrations of capturing reagents to draw test lines were defined according to achieving high sensitivity (Table 3.1.5).

**Table 3.1.3.** Study of the pre-adsorption of additives onto the conjugate pad. Conditions providing moderate to strong signals for negative samples were no further considered.

<i>Pre-absorbed protein</i>	<i>Signal</i>	
	<i>negative sample</i>	<i>positive sample</i>
<b>none</b>	-/+	++
BSA	++	
casein	-	-
PEG-BSA	++	
yeast extract	-	-

**Table 3.1.4.** Study on the composition of the running buffers. All buffers were supplemented with 1% v/v Tween20 and 0.05% w/v sodium azide. Conditions providing moderate to strong signals for the negative sample were no further considered.

<i>Buffer</i>	<i>pH</i>	<i>molarity (mM)</i>	<i>additives</i>	<i>negative samples</i>	<i>positive samples</i>
Phosphate	7.4	100	0.5% Glycerol	+	
Phosphate	7.4	100	0.5% Glycerol 0.13M NaCl	-	-
Tris-HCl	8.2	34	20% sucrose 2% BSA	++	



Carbonate	8.5	50	-	++	
Tris-Glycine	8	114	-	+	
Tris-Glycine	8	114	0.1% casein	+/-	++
<b>Tris-Glycine</b>	<b>8</b>	<b>114</b>	<b>0.2% casein</b>	-	<b>+</b>
Tris-Glycine	8	114	0.5% casein	-	-/+

**Table 3.1.5.** Identification of the optimal concentrations for test line reagents

		<i>SpA</i>		<i>N</i>	
<i>SpA</i> (mg/ml)	<i>N</i> (mg/ml)	<i>negative</i> <i>samples</i>	<i>positive</i> <i>samples</i>	<i>negative</i> <i>samples</i>	<i>positive</i> <i>samples</i>
0.2	1.5	-	+	-/+	++
0.5	1.5	-	++	-/+	++
<b>0.5</b>	<b>1.0</b>	-	++	-	++
0.5	0.5	-	++	-	-/+

### Testing the human sera with the LFIA device

Accordingly, the colouring of one test line can be regarded as a (maybe false) positive outcome, while two coloured test lines represented a strong evidence of positivity. On the other hand, no signal present in correspondence of both test lines was considered as a robust indication of negativity. The overall architecture and the principle of functioning of the multi-target LFIA are depicted in Figure 3.1. Several parameters affect LFIA performance, such as the quality and amount of bioreagents used. Especially, the colloidal stability of the GNP conjugates largely impacts on the outcome of the test, both in terms of sensitivity and specificity. Well-dispersed and stable probes were obtained by optimizing all the phases in which GNP-N were involved from their preparation to the environment in which they were store dried in the device to the resuspension buffer. The amounts of SpA, N and avidin to from the two test and one control lines, respectively, and of GNP-N probe were defined according to reaching clearly visible red colouring of the lines for a known positive sample (as tested by the reference ELISA kit) and no signal for a pre-covid negative sample (Table 3.1.2).

The ability of the multi-target LFIA of detecting anti-SARS CoV-2 antibodies was investigated on 62 human sera belonging to individuals with confirmed infection. The diagnosis was made according to the reference rRT-PCR on oral nasal swab. Serum was obtained from individuals included in the study at different times from the diagnosis and, in some cases, after their recovery (defined as subjects who were tested negative by two rRT-PCR on subsequent swabs). A description of the population included in the study is shown in Table 3.1.1. Parallel to the LFIA analysis, sera were submitted also to a serological ELISA kit targeting anti-SARS CoV-2 IgG. The ELISA kit was a semi-quantitative assay, which provided results as “percentage optical density” (pOD). The relative amounts of the IgG were

calculated according to manufacturer's instruction as  $(OD \text{ unknown} - OD \text{ negative control}) / (OD \text{ positive control} - OD \text{ negative control}) \times 100$ . Therefore, we were able to correlate LFIA outcomes to the clinical classification of the samples and, in addition, to the presence, and partially to the amount, of IgG in them. According to manufacturer's instruction, 47 sera out of the 62 provided pOD values exceeding the cut-off level of 40% and were classified as positive. Negativity to the serological assay for known infected individuals was attributed to either the closeness in time from infection of blood collection or to showing an IgG level close to the cut-off level. Notwithstanding, two individuals apparently did not develop a strong immune response to the infection even after weeks from the confirmation of infection.

The "total antibodies" LFIA tested as positive 54 individuals based on the colouring of the T1 line and 45 based on colouring of both test lines. No samples provided colouring of the T2 line in the absence of any T1 line signal. Possibly, when limited amounts of antibodies were present in the sample, they were captured by the first test line and were unable to significantly accumulate at the second one. Alternatively, the different response of the two lines represented the different ability of the two capturing reagents to interact with immunoglobulins. In such a case, SpA showed higher affinity than the antigen towards antibodies. Based on these results and on the specificity study, we opted for judging the positivity according to the colour of the T1 line. With this definition, almost perfect agreement between the LFIA and the ELISA kit was estimated by the Cohen's  $k$  (0.89) and by the accuracy values (95.2%, 90.4-98.1%). Moreover, disagreeing results were observed for six samples that were close to the cut-off level for the ELISA kit and which were scored as positive by the LFIA, and for one sample collected after 12 days post-infection, which was negative according to the ELISA kit while judged positive by the LFIA. In this respect, the 'total antibodies' LFIA confirmed to be highly sensitive.

To rationalize the binding events occurring at the two lines, semi-quantitative information from the LFIA devices was calculated as the colour intensity by digital processing of images. Interestingly, signals from both test lines were correlated to ELISA with positive Spearman correlation coefficients and P values below 0,050 (Figure 3.1.3). Significant relationships were observed also between SpA and N variables in the correlation table, though data from the double antigen T2 line were more scattered.

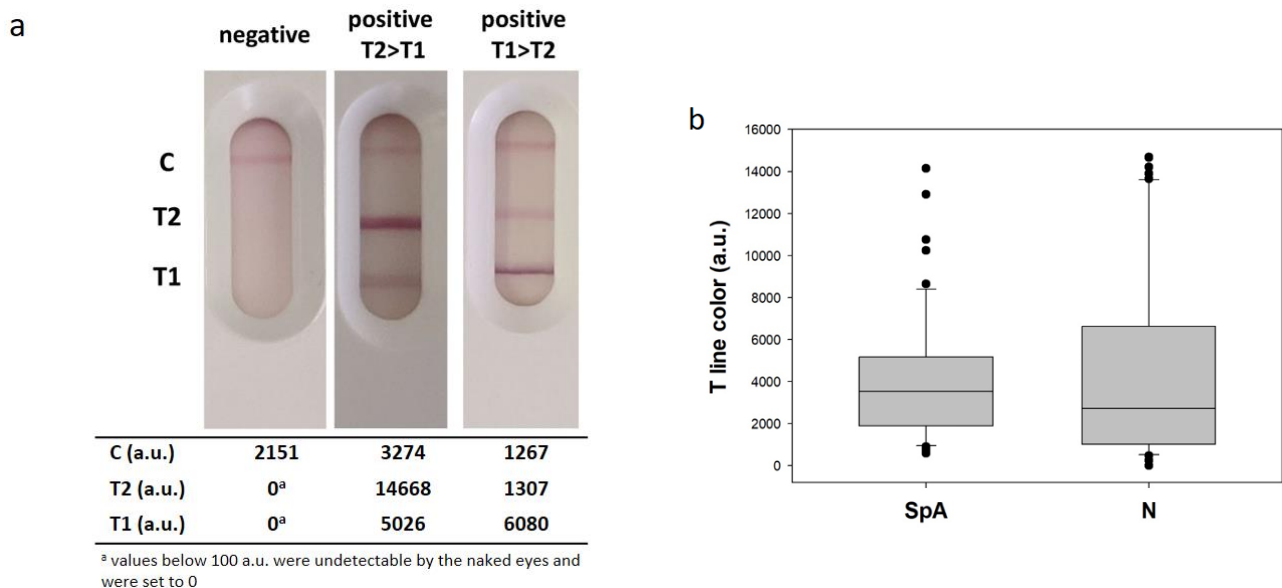


**Figure 3.1.3.** Comparison of the response provided by the two test lines. Images of the LFIA for detecting anti N antibodies for a negative and two positive samples (a) and distribution of signals provided by the two test lines for the 62 rRT-PCR+ samples (b).

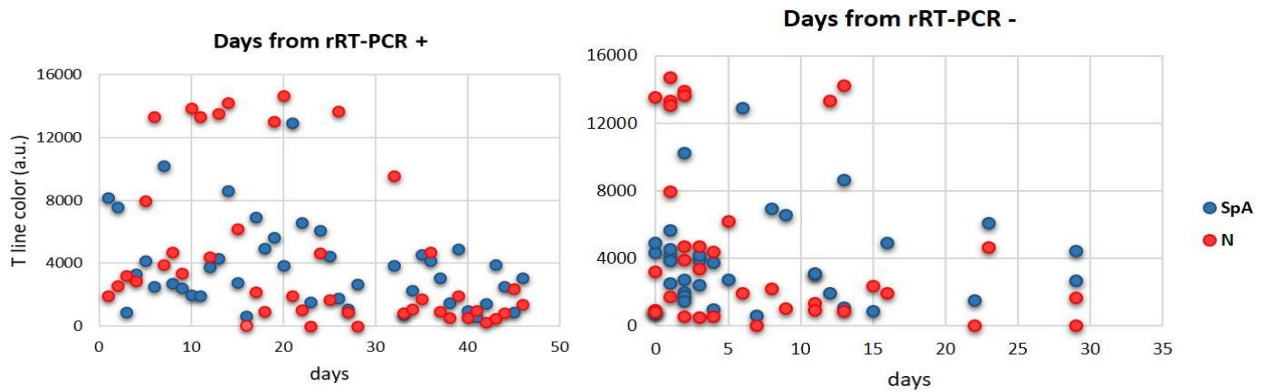


**Figure 3.1.4.** Signals from the Staphylococcal protein A (T1) and the antigen N (T2) were quantified and plotted towards time delay from the confirmation of infection (rRT-PCR+) and recovery (rRT-PCR-), respectively, as ascertained by the reference molecular diagnosis.

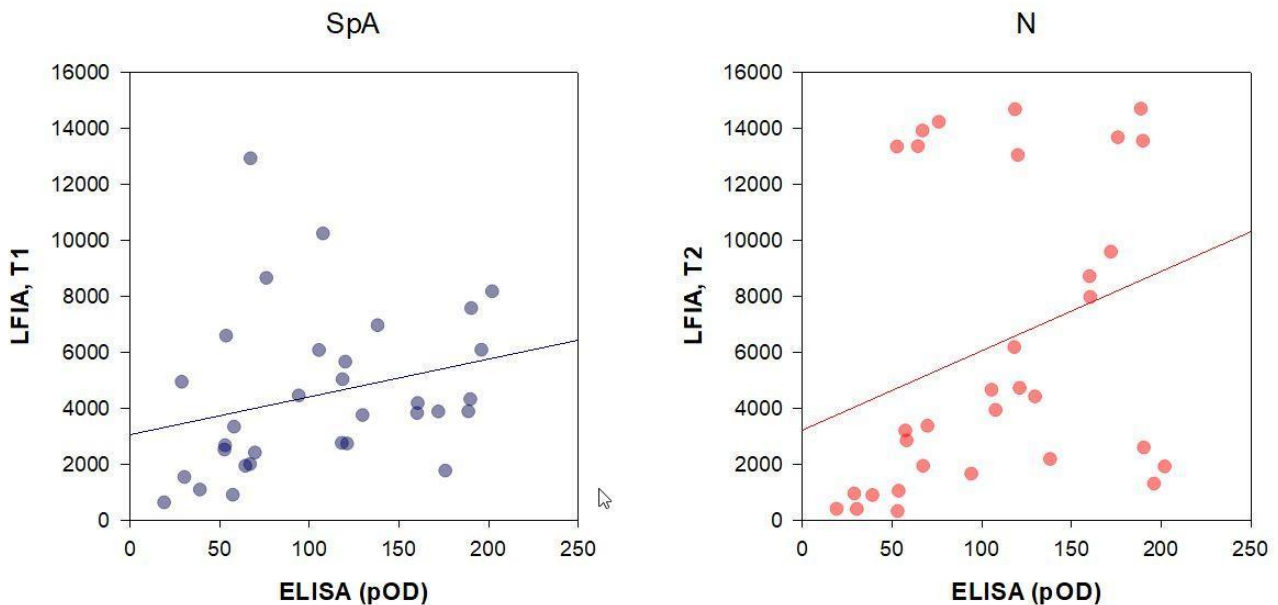


**Figure 3.1.5.** Correlation of signals measured at each test lines for the total antibody LFIA and the ELISA semi-quantitative determination of anti-SARS CoV-2 IgG.

compared to those from the T1 line (Figure 3.1.5). Furthermore, some samples showed more intense colour at the T1, others at the T2 line (Figure 3.1.3a) without apparent relationship with the ELISA score or other relevant factor, such as the seroconversion period. We interpret that both test lines were able to detect IgG in the human serum; however, they also revealed other immunoglobulins and the kind and/or the proportion in which they were detected varied among the lines. Comparing signals from the two test lines by the Mann-Whitney test, there was not a statistically difference among the data ( $P=0,264$ , Figure 3.1.3b). To further confirm that the LFIA was able to reveal immunoglobulins A and M and that these class of antibodies contributed to the overall observed signal, we labelled an anti-human IgA and an anti-human IgM antibody with gold nanoparticles. The probes were separately incorporated into a LFIA device including the N antigen as the test line (T2) and the usual control line. Two representative samples, chosen within positive ones, were analysed by the “single antibody” LFIA (i.e., the two positives shown in Figure 3.1.6). Interestingly, we observed a strong signal at the test line for one sample when staining with the anti-IgA, while the other one did not provide any colour. In particular, the sample containing IgA was the one with the stronger colouring at the T2 line (compared to the T1). Staining with anti-IgM also displayed some

relevant information. The signal at the test line was clearly visible for both samples, but the intensity was inversely correlated to the one measured in the “total antibody” mode (Figure 3.1.3 and 3.1.6).

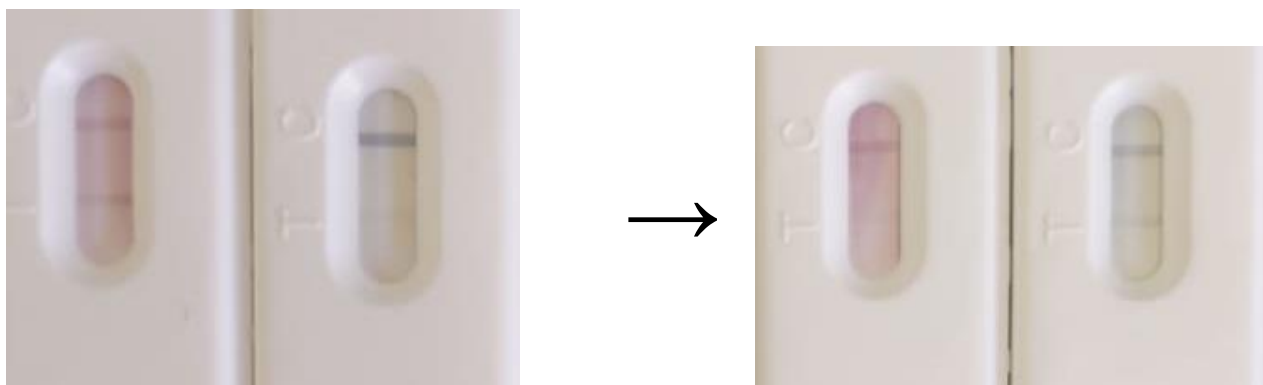


**Figure 3.1.6.** Results on LFIA devices with red GNP labelled anti human IgA antibodies and blue GNS (gold nanostars) labelled anti human IgM antibodies. On the left the sample #329 of the study at the beginning of the seroconversion. In the presence of the anti SARS Cov2 IgA are captured by the N protein on the test line and the signal is provided by the binding with labelled anti IgA antibodies. For the same sample, the presence of the IgM fraction is slightly revealed by the blue GNS labelled anti IgM antibody. On the right, the fully seroconverted serum showing the opposite result, the IgA are lower in intensity on respect to the IgM that increase with seroconversion. Details on the preparation of GNS are reported in Chapter 4.1.

### Diagnostic performances of the ‘total antibody’ LFIA device

The diagnostic performance of the “total antibodies” LFIA are summarize in Table 3.1.6. The signal generated at the test line formed by SpA provided diagnostic sensitivity above 94%, considering samples collected after one week from infection confirmation and 88.7% (78.2- 95.3%) including samples collected during the first week after rRT-PCR diagnosis. The combination of the two lines slightly decreased the sensitivity as the second test line provided three additional false negative results. According to discussion above, the SpA seemed to be able to capture very efficiently the antibodies. However, some samples showed a very faint colour at the T1 line while the T2 line was intensely coloured, which can help the visual interpretation of the result. the T line was more sensitive to this class of antibodies. The T1 line, constituted of SpA as the capturing reagent, showed limited variability as a function of time from molecular diagnosis and persisted after the viral load become undetectable. We hypothesized that the SpA test line was principally associated to the IgG presence. The signal produced at SpA line indicated that the serological response to SARS CoV-2 rises in the second week from infection confirmation and persists, at least for some weeks after recovery. The ability of promptly detecting the serological response to SARS CoV-2 infection was further ascertained by following the seroconversion of three donors (Figure 3.1.7). Identification of specific antibodies was achieved as early as five days post diagnosis. Although with different intensities, both test lines revealed the presence of immunoglobulins in the patients’ sera, with qualitatively no distinction while with a large inter-individual variability in terms of the signal intensities.

**Table 3.1.6.** Diagnostic performance of the ‘total antibodies’ LFIA

<sup>1</sup> Positive sample belonged to individuals with the infection as confirmed by rRT-PCR. Only samples collected from seven days post confirmation were included in the Table.

<sup>2</sup> Negative samples were sera collected pre-SARS outbreak.

	T1 line (C.I.95%)	T1+T2 lines (C.I. 95%)
<b>Sensitivity<sup>1</sup> (95% C.I)</b>	94,55% (84,88-98,86)	89,00% (77,75 – 95,89)
<b>Specificity<sup>2</sup> (95% C.I)</b>	100%	100%
<b>Positive predictive value</b>	100%	100%
<b>Negative predictive value</b>	96,59% (93,27–99,56)	93,41% (86,95 – 96,79)
<b>Accuracy</b>	97,86% (93,21–99,56)	95,71 (90,91 – 98,41)

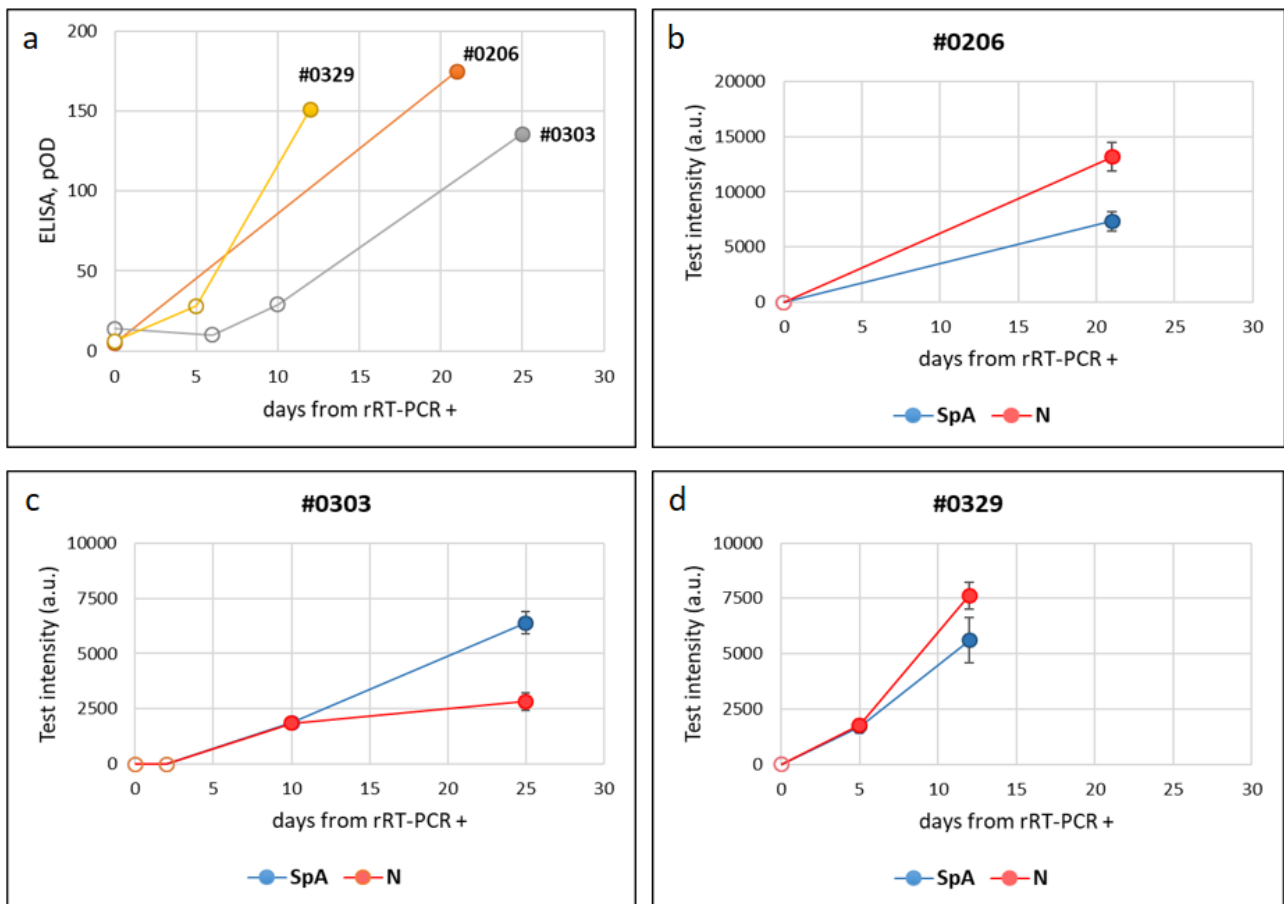


**Figure 3.1.7.** Time evolution of the serological response to SARS CoV-2 infection as detected by the ELISA kit (a) and by the total antibodies LFIA (b-d) for three individuals. Empty and full symbols represent negative and positive classification, respectively. Bars represent standard deviations of duplicate experiments.

### 3.1.4 Conclusions

The role that serological tests can play in the management of the pandemic has been limited because the diagnosis was largely delayed compared to rRT-PCR and, therefore, insufficient for a prompt intervention. Here, the authors propose a point-of-care tool for the early and sensitive detection of the serological response to SARS CoV-2 infection. The LFIA device candidates itself as a useful tool for monitoring the spread of the infection and to confirm recovery, and perhaps moving in the future, as a tool for population serosurvey to determine immune populations.

The novel strategy aimed at non-selectively detect the total serological response to infection combined to the production of an efficient probe including the SARS CoV-2 nucleocapsid protein enabled the rapid and effective detection of seroconversion in human serum at as early as 7 days post diagnosis of infection. We showed that the staphylococcal protein A could play the role of a broad-specific capturing reagent towards human immunoglobulins. Compared to the double-antigen approach showed similar or even superior diagnostic validity and contemporary early and long-term ability to detect the antibodies elicited by the SARS CoV-2 virus. Although the test line comprising the N antigen as the capturing reagent was apparently useless, its presence can help increasing the robustness of the result, especially when the test is judged by untrained operators and, in this sense, can be regarded as an internal double-check of positivity. As an alternative, we illustrated that a LFIA device including SpA enabled achieving the 100%-specificity goal and, contemporary high sensitivity when associated with the detection by the labelled N antigen.

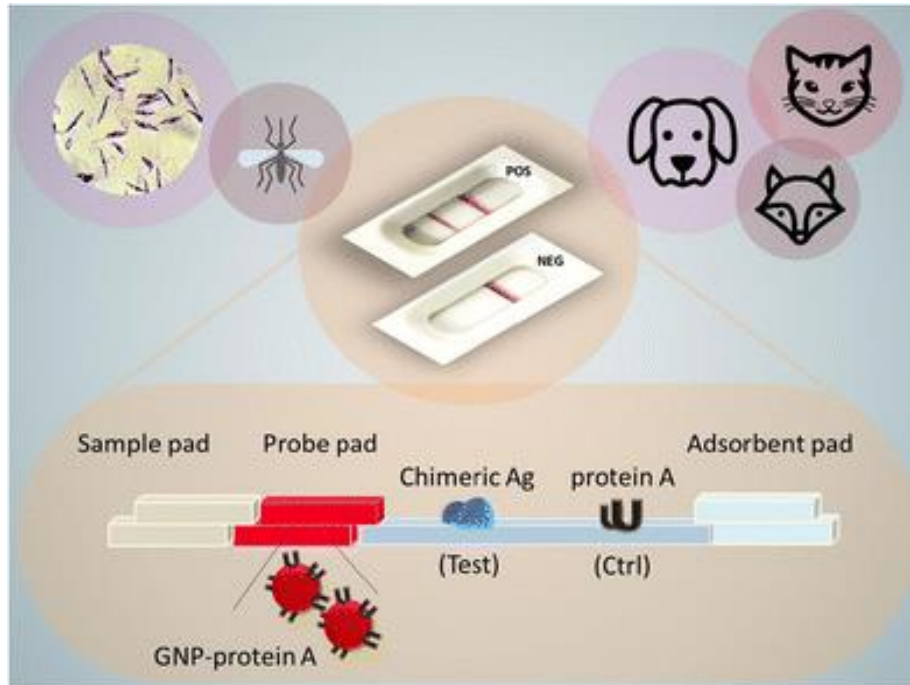
#### Ethic statements

This study is a part of the SIRIT project, which has been approved by the Committee on Bioethics of the University of Torino (31 March 2020), Ethics coordinator committee (AOU City of health and science of Turin; Prot. N ° 0035599 of 07/04/2020) and satellite ethics committees. Enrolled patients have signed regular Consent to the participation and processing of their personal data in accordance with Regulation (EU) 2016/679 (GDPR)

## 3.2



### Visceral Leishmaniosis Total Antibody LFIA



Based on

L. Anfossi, F. Di Nardo, M. Profiti, C. Nogarol, S. Cavalera, C. Baggiani, C. Giovannoli, G. Spano, E. Ferroglio, W. Mignone, S. Rosati, **A versatile and sensitive lateral flow immunoassay for the rapid diagnosis of visceral leishmaniasis**, *Analytical Bioanalytical Chemistry*, 410, 4123–4134, 2018, <https://doi.org/10.1007/s00216-018-1067-x>.

#### Abstract

*A rapid and portable tool for Visceral leishmaniasis (VL) diagnosis based on the lateral flow immunoassay (LFIA) technology is described herein. The device exploits a highly specific chimeric recombinant antigen as the recognition element for capturing anti-leishmanial antibodies, and protein A labelled with gold nanoparticles as the signal reporter. The LFIA shows excellent diagnostic sensitivity (98.4%), specificity (98.9%), and agreement with serological reference methods for diagnosing canine VL. The long-term stability of the LFIA device was confirmed based on six months of storage at room temperature or 4 °C, and the qualitative response of the device was not affected by limited thermal stress. The use of the broadly specific protein A means that the LFIA can be readily adapted to diagnose VL in dogs (the main reservoir for human infection) and other mammals, thus further assisting efforts to control the spread of VL.*

### 3.2.1 Architecture of the test

In this work, we describe the design of a rapid diagnostic tool for detecting anti-leishmanial antibodies that shows high diagnostic sensitivity and versatility, as it can be adapted for use with other mammals besides dogs and humans. This rapid test for diagnosing VL is a lateral flow immunoassay based on the one-site immunometric assay format. The specific recognition element is a recombinant chimeric antigen (rCAG) comprising three Leishmania antigens, which has been shown to be highly specific for VL [29], [30]. The signal reporter is staphylococcal protein A (SpA) labelled with gold nanoparticles (GNPs), which are used as coloured probes that permit visual interpretation of the qualitative result. Antileishmanial antibodies present in the sample bind to the chimeric antigen forming the so-called test line, and the rate of formation of the complex is measured by reaction with the labelled protein A. The protein A, which is also used for the control line, captures any excess immunoglobulins, regardless of their specificity for the leishmanial antigen. Again, the captured immunoglobulins are revealed by protein A labelled with GNPs. Therefore, two coloured lines form if anti-leishmanial antibodies are present in the sample, due to the accumulation of GNP-SpA at both the test and control zones. Only the control line is visible if the sample does not contain any anti-leishmanial antibodies (Fig. 3.2.1).

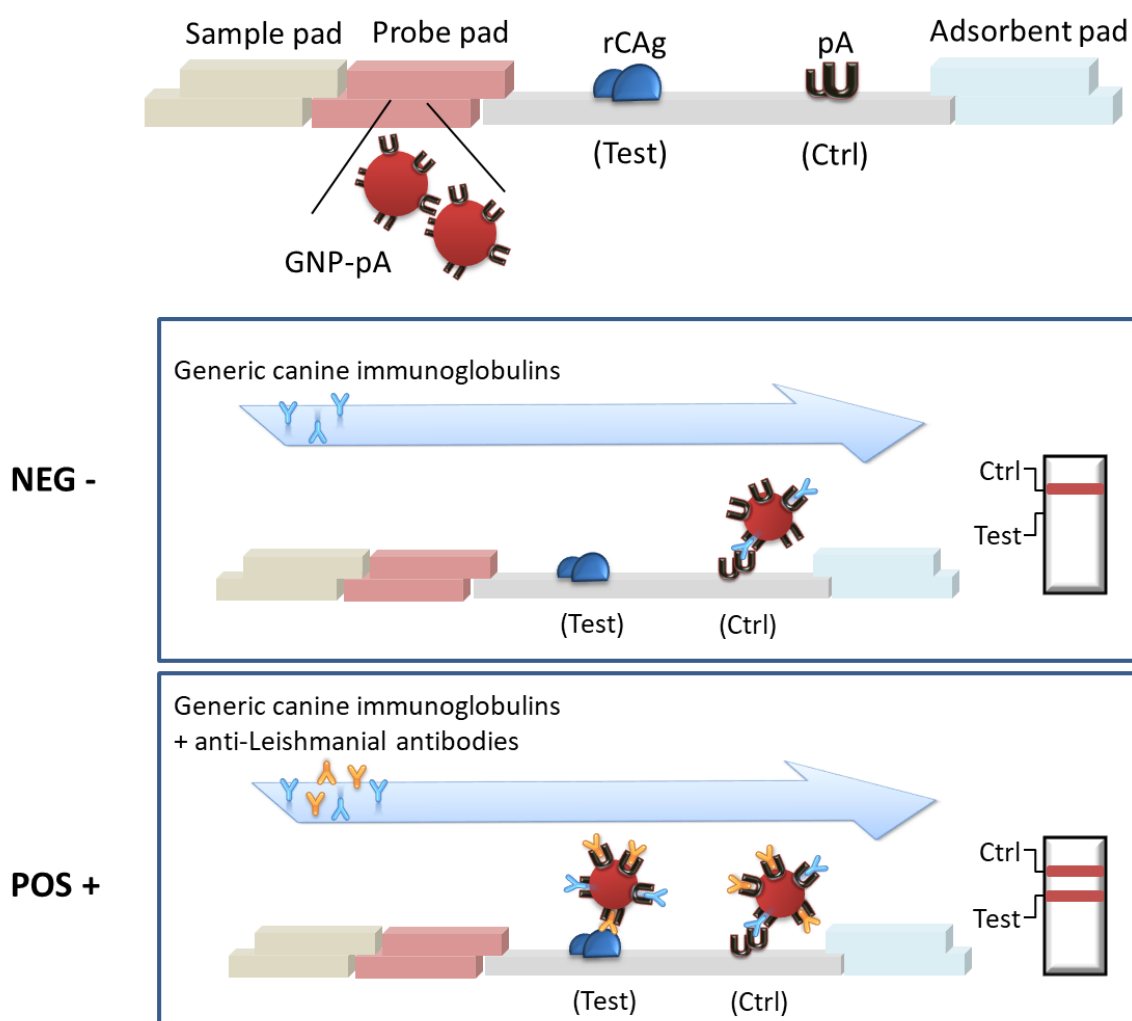


**Figure 3.2.1.** Scheme of the LFI device used for the rapid diagnosis of VL. The strip is composed of an analytical membrane onto which a recombinant chimeric antigen (*rCAG*) and protein A (*SpA*) are coated to form the test and control lines, respectively. The signal reporter consists of *SpA* labelled with gold nanoparticles that are coloured red due



to a surface resonance band at 525 nm. GNP-SpA is included in the device in dried form by pre-impregnating the probe pad. The device also includes a sample pad that adsorbs the sample and distributes it homogeneously to the membrane, and an adsorbent pad that decreases the background colour by increasing the volume of the flowing sample. A single visible line (*Ctrl*) is expected for a canine serum that does not contain any anti-leishmanial antibodies (negative sample) due to the interaction of generic immunoglobulins with the labelled SpA and with the SpA immobilised on the membrane. The presence of specific anti-leishmanial antibodies is revealed by the specific binding of these antibodies to the rCAG, which generates a second red line (*Test*)

The use of protein A as a generic recognition element that confers versatility to the assay, due to the ability of SpA to bind immunoglobulins from various animal species, has been reported for ELISA methods [31]–[33]. Some LFIA have also employed protein A/G as the labelled probe in combination with immunoglobulins as the capture reagent at the control line[34]. However, VL is commonly associated with hypergammaglobulinemia[35], and high levels of gamma globulins can saturate the binding capacity of the GNP-SpA probe, thus preventing it from reacting with the immunoglobulins forming the control line. The effect of this is an unacceptably high probability of an invalid result (control line not visible, Figure 3.2.1). To overcome this limitation, we also used SpA as the capture reagent on the control line. This allows the LFIA for diagnosing VL to be modified to detect antileishmanial antibodies belonging to different mammalian species while also assuring the validity of the test, even for subjects showing abnormal levels of immunoglobulins.

## 3.2.2 Materials and Methods

### Immunoreagents, chemicals and materials

Gold (III) chloride trihydrate (ACS reagent), protein A (pA), bovine serum albumin (BSA), rabbit immunoglobulins, swine immunoglobulins and polyvinyl alcohol (PVA) were obtained from Sigma–Aldrich (St. Louis, MO, USA). Triton X-100 and other chemicals were purchased from VWR International (Milan, Italy). Anti-dog IgG were purchased from Sigma Aldrich. Nitrocellulose membranes (HF180 plus card), cellulose absorbent pad and glass fibre conjugate pad were obtained from Merck Millipore (Billerica, MA, USA). Standard 14 glass fibre pads from Whatman (Maidstone, UK) were used as sample pads. K9-K39-K26 recombinant chimeric antigen (rCAg) was prepared as described in [30]. Statistical calculations were carried out with SigmaPlot 11.0 software.

### Preparation of GNPs and GNP-protein A conjugates (GNP-SpA)

GNPs with a SPR band at 525 nm and mean diameter of ca. 30 nm were prepared as reported in Chapter 3.1.2. Signal reporters used in the LFIA were prepared by adsorbing protein A onto GNPs. In details, 8 µg of SpA and 1 ml of borate buffer (pH 7.4) were mixed with 10 ml of GNPs and incubated for 30 min at 37°C. Then, 1 ml of BSA (1% in borate buffer) was added and reacted for 10 min at 37°C to saturate free GNP surface. GNP-SpA conjugates were recovered by centrifugation (14000 rpm, 15 min) and washed twice with borate buffer supplemented with 0.1% BSA. Finally, GNP-SpA were re-suspended in GNP storage buffer (borate buffer with 1% BSA, 0.25% Tween 20, 2% sucrose, and 0.02% sodium azide) and stored at 4°C until use.

### Fabrication of the LFIA device

The recombinant chimeric antigen[30] was applied to the nitrocellulose (NC) membrane to form the Test line (0.5 mg/ml). Protein A (0.2 mg/ml) was used as the capturing reagent at the Control line. Reagents were dotted at 1 µL cm<sup>-1</sup> by means of a XYZ3050 platform (Biodot, Irvine, CA, USA), equipped with BioJet Quanti™ 3000 Line Dispenser for non-contact dispensing, keeping a distance of 4 mm between the lines. The signal reporters (GNP-SpA conjugates) were absorbed onto the glass fibre conjugate pad previously saturated with GNP storage buffer. The pad was dipped into GNP-SpA solution (optical density 1) and dried for 3 hours at room temperature. NC membranes were dried at 37°C for 60 minutes under vacuum, layered with sample, conjugate and absorbent pads, cut into strips (4.2 mm width) by means of a CM4000 guillotine (Biodot, Irvine, CA, USA) and inserted into plastic cassettes (Kinbio, China) to fabricate the ready-to-use LFIA device. Cassettes were stored in the dark in plastic bags containing silica at room temperature until use.

## The Lateral Flow ImmunoAssay for canine leishmaniasis diagnosis

Assays to detect anti-leishmanial antibodies were carried out at room temperature, by applying 70 µl of diluted serum to the sample well. For the analysis, samples were thawed at room temperature, carefully mixed and diluted by 1:20 using the running buffer (phosphate buffer 20 mM, pH 7.4, 50mM NaCl, 1% BSA, 0.5% PVA, 0.1% Triton X-100). Qualitative results were judged by the naked eye after 15 minutes (Figure 3.2.2). Samples were analysed in duplicate and results were observed by three operators. Images of LFIA devices were also acquired by a portable scanner (OpticSlim 550 scanner, Plustek Technology GmbH, Norderstedt, Germany) and the area of the coloured lines was quantified by means of the QuantiScan 3.0 software (Biosoft, Cambridge, UK).

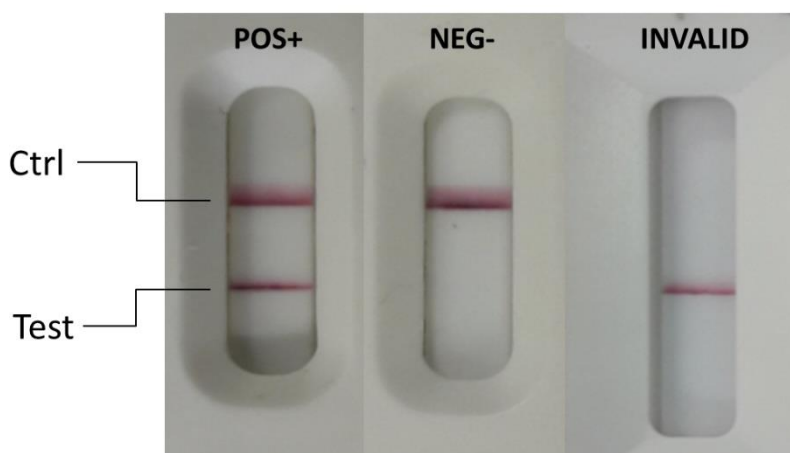


**Figure 3.2.2:** Typical results provided by the LFIA for detecting anti-leishmanial antibodies for a positive and a negative canine serum. Negativity is represented by the presence of single red line (the Control line), while positivity is observed as the presence of two red lines (Test and Control lines) after sample running. The strip is included into a plastic cassette providing a sample well and a reading window. When only the Test line is visibly coloured, the test is invalid.

### Serum samples

A total of 167 canine sera were used in the study; 37 serum samples were collected from an endemic region (West Liguria, Italy), while 130 samples belonged on non-endemic regions (Piemonte and Valle d'Aosta, Italy). Most canine sera were characterized by analysing them through more than one reference method: IFAT titration was carried out on 157 samples, PCR and western blot (WB) were carried out on 120 samples and 141 canine sera were analysed by a previously validated ELISA that was based on the same recombinant chimeric antigen employed for fabricating the LFIA [33]. Samples belonging to the non-endemic area were characterized by IFAT, PCR and WB. In order to classify canine sera, IFAT cut-off was set at 1/80 [33], [36]–[38], while PCR and WB were carried out according to the protocols described in E. Ferroglio et al.[39].

In details, 70 samples showed IFAT titre < 1/40 and were negative also according with PCR and WB methods; 40 samples showed IFAT titre > 1/80 and were positive also according with PCR and WB methods; 10 samples were analysed through WB and PCR and resulted as positive. These samples were also analysed by the ELISA that classified 5 samples as positive and 5 as negative.

Samples belonging to the non-endemic area were classified according with either the IFAT titre or the ELISA score; in particular, 7 with inconclusive classification (IFAT = 1/80) were analysed by the ELISA method. Further 102 samples were randomly chosen among those already characterized by other reference methods and submitted to ELISA qualification, as well. To evaluate the potential application of the assay to different animal species, 2 red fox sera (1 IFAT positive and 1 negative) and 9 cat sera were also analysed. Cat sera were characterized by PCR and WB; however, results were ambiguous and were considered inconclusive. Fox and cat samples were analysed by the versatile LFIA and by the reference ELISA (which also employed protein A as the probe, although conjugated to horseradish peroxidase).

### Validation of the LFIA device for detecting leishmaniasis in canine serum

The impact of serum matrix on the assay was studied by variably diluting a pool of positive and a pool of negative canine sera with phosphate buffer supplemented with various additives. In order to limit matrix interference, the following chemicals were considered: proteins (BSA, casein), surfactants (Tween 20, Triton X-100), polymers (polyvinyl alcohol), and salts (NaCl). Each additive was added to phosphate buffer at three different levels and used to dilute pooled sera 1:10 before LFIA analysis. In addition, the same compounds were also used for impregnating the sample pad, as an alternative to sample dilution. Accuracy of the assay was calculated as the rate of results agreeing with those provided by the reference methods (IFAT and ELISA) on canine sera. The Cohen's K parameter was calculated to evaluate concordance of the new LFIA with serological reference methods. The imprecision of the LFIA was considered to be due to the sum of 3 components: the within- and between-day variations due to the assay, and the biological variability. Accordingly, overall imprecision was estimated by an experimental design approach firstly proposed by V. Lattanzio et al. [40], [41], with minor modifications due to availability of biological samples [42]. The study was conducted by analysing 11 sets of canine serum, of which 7 were positive and 4 negatives. The samples were analysed on two days. On each day, samples were analysed in triplicate. Negative samples and positive samples were used to calculate the rate of false positivity (n=24) and false negativity (n=42), respectively. Robustness, in terms of the reliability of the assay response over time, was also studied: for that purpose, 10 serum samples (5 positive and 5 negative) were analysed in duplicate and the result was observed after 10, 20 and 60 minutes from sample application. The rate of false positive (n=10) and false negative (n=10) was calculated at each observation time.

### Stability of the LFIA device

With the aim of evaluating the shelf-life of the LFIA device, real-time stability and accelerated ageing experiments were carried out as follows [42], [43]. For the accelerated ageing experiment, LFIA cassettes were kept at 37°C for 7 days and tested on day 0, 1, 3 and 7. For the real-time stability experiment, LFIA cassettes were stored at room temperature and at 4°C for 6 months, and tested on week 0, 1, 2, 4, 8, 12, and 24. For each experiment, a pool of positive samples and a pool of negative samples were analysed in duplicate. For all experiments, LFIA devices were stored in the dark and with desiccant added.

### 3.2.3 Results and discussion

#### Optimization of the LFIA device

The LFIA device was designed as a versatile tool for diagnosing Leishmaniasis in various animal species. Hence, protein A was used as a broad selective recognition element and labelled with gold nanoparticles to fabricate the signal reporter (Figure 3.2.1). The same protein A was used also as the capturing reagent forming the Control line. Attempts were made using immunoglobulins from other animal species known to bind SpA (rabbit and swine) as the C-line capturing reagent, according to the strategy proposed by Intaramat et al. [34]. However, the rate of invalid test (i.e.: test in which the Control line is not visible) was unacceptably high, due to the unavailability of the GNP-SpA probe for binding to the immunoglobulins immobilized at the C-line. In fact, subjects infected by VL also show hypergammaglobulinemia [35] that saturated the binding capacity of the labelled SpA. The use of an anti-canine antibody partially solved the problem, however at the expenses of assay versatility. Therefore, we opted to use the same SpA as the C-line reagent. In such a way, the LFIA is putatively able to reveal immunoglobulins of all animal species that are bound by SpA.

The specificity of the LFIA is connected to the recognition element deposited at the Test zone, which is a recombinant chimeric antigen (rCAG) from the amastigote form of Leishmania parasite [30]. In details, the rCAG comprises three antigenic domains (K9, K39, and K26) from *L. Infantum* [44] and has proved to allow the highly sensitive and specific detection of anti-leishmanial antibodies by ELISA [33]. Most importantly, the rCAG is representative of the form of the Leishmanial amastigote antigens that are expressed in vertebrates, enabling to discriminate infected subjects from those who just underwent into contact with the phlebotomine vector. This is particularly relevant for correctly identifying infected subjects in endemic areas, where the probability of accidental contact with the vector is high, although not necessarily connected to the actual development of the infection [45].

The setting up and tuning of LFIA parameters to produce a rapid, sensitive and easy-to-handle LFIA device followed a checkerboard strategy, in which concentrations of the signal reporter (GNP-SpA), the recognition element for the Test line (rCAG) and the capturing reagent (SpA) for the Control line were variously combined. Pooled positive and negative canine sera were used during the optimization work to mitigate the influence of biological variability. Preliminary, the experimental conditions for optimal conjugation of SpA with gold nanoparticles were defined. In details, pH and amounts of the SpA were defined based on a compromise providing stable GNP-SpA conjugates [46] and high detectability in the LFIA device [47].

The protocol for executing the assay includes serum dilution with a running buffer. This additional step limits simplicity of use of the LFIA device for non-trained personnel and in low-resource settings. However, it was required for two main reasons. On one hand, serum is a viscous liquid that hardly flows across the LFIA membrane. As a consequence, the application of undiluted samples resulted in the lengthening of analysis time and increasing of rate of irreproducible results. Most importantly, the rate of false negative samples was unacceptably high due to the hook effect, associated to the hypergammaglobulinemia of subjects infected by VL [35]. The minimal sample dilution required for obtaining a clearly visible signal at the Test lines for most positive samples and in a reasonable time (15 minutes) was established as 1:20. Lower dilution factors (e.g.: 1:10) allowed for acceptable diagnostic sensitivity to be reached, however at the expenses of rapidity (accurate

results were observed after 60 minutes from sample applications). Commercial LFIA kits also involve some dilution of the serum, typically realized by applying a limited volume of the sample immediately followed by the addition of a larger volume of a diluent. The composition of the running buffer was defined with the aim of guarantee rapidity, high detectability, and reduced sample-to-sample result variation. At the purpose, several modifiers were added to the phosphate buffer, such as BSA, PVA, NaCl and Triton X-100. PVA was especially helpful for the rapid and complete re-dissolution of the dried GNP-SpA; while NaCl efficiently abated non-specific binding of GNP-SpA to the rCAg at the Test line, thus contributed to dramatically reducing false positive results.

### Analytical parameters of the LFIA for the qualitative detection of anti-Leishmanial antibodies in canine serum

The precision of the LFIA device was investigated following the approach firstly proposed by V. Lattanzio et al.[41] and widely applied for assessing performances of qualitative LFIAs [40], [42]. The strategy is based on designing a set of experiments to include three factors that contribute potentially to the overall precision of the assay, namely: the within-day, the between-day, and the biological variability. Therefore, seven positive and four negative serum samples were tested in replicate on the same day and on two distinct days. Positive samples included serum with high and low IFAT titres. No false positive (n=42) nor false negative (n=24) results were registered during the assessment, as a confirmation that the LFIA is precise enough for enabling reproducible detection of anti-leishmanial antibodies in canine serum. The mean coefficients of variation were calculated for positive canine sera by digitalizing images of the cassettes and converting them into quantitative data [48]. The area under the Test line (AreaT) was measured and used as the quantitative parameter for verifying repeatability and reproducibility. Mean coefficient of variations were calculated as 14.6% (n=12) and 15.5% (n=6) for the within- and between-day experiments, respectively (Figure 3.2.3a). The mean values of AreaT for the two days were compared by a one-way analysis of variance (ANOVA). The observed difference among the days was not statistically significant (P=0.145), although the power of the performed test was below the desired value (power of performed test with alpha=0.050: 0.199).

A larger variability was observed among the various canine samples; however, this was expected since samples were expressly chosen for having variable IFAT titres. Indeed, even if the LFIA is not able to provide quantitative results, obviously, the variable content of anti-leishmanial antibodies of samples reflected into differently coloured Test lines, where the higher the content of antibodies, the more coloured the Test line and vice versa.

A frequent issue of LFIAs for serological application is represented by the modification of the visual result over time. In particular, negative results (i.e.: assay in which only the Control line is visibly coloured) have the tendency to become positive (the Test line becomes coloured, as well). In order to define the minimum time required for observing a reliable response by the LFIA, and to verify the robustness of the response over time, the LFIA was used to detect anti-leishmanial antibodies in ten canine sera and the observation of the results was repeated after 10, 20 and 60 minutes from sample application. Four negative and six positive samples were analysed. Among positive samples, three were characterized by high IFAT titres (equal or above 1/640) and three by low IFAT titres (below 1/640). Each sample was tested in duplicate and results were observed by the naked eye. The colour at the Test line indicating positivity was detectable after ten minutes for all positive

samples, increased in the following 10 minutes, and then stabilized (Figure 3.2.3b). Precautionary, we set 15 minutes as the time for achieving a reliable response for low positive samples. Most interestingly, no colour at the Test line was visible for negative samples even after 60 minutes from sample application and this observation was confirmed for all negative samples analysed during LFIA validation. Therefore, the LFIA demonstrated to provide responses very stable over time.

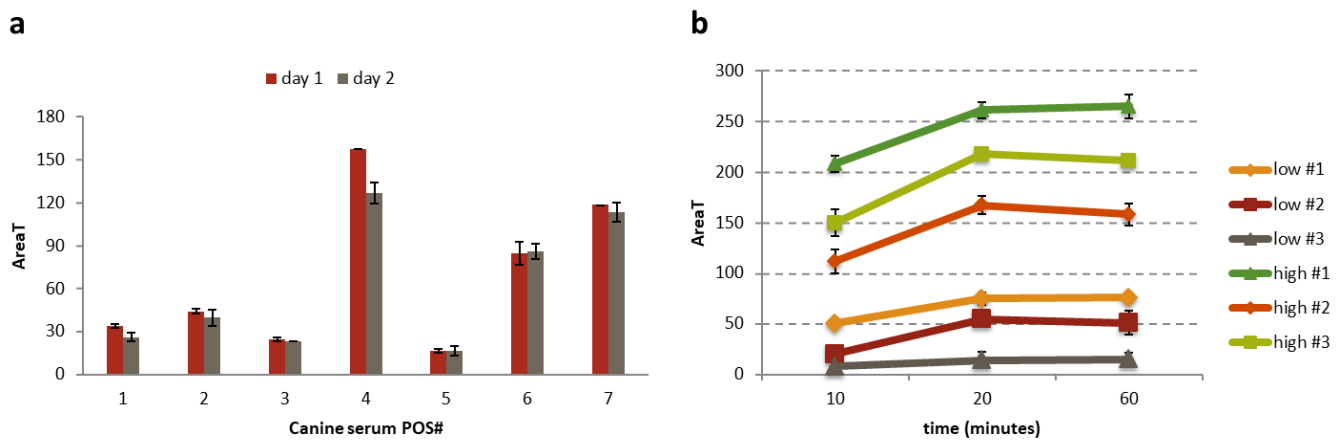


**Figure 3.2.3.** In-house validation of the LFIA for detecting anti-leishmanial antibodies: **(a)** within- and between- day variability of the LFIA response, bar represent standard deviations of the three replicates obtained on each day for the between-day experiment; **(b)** stability of the LFIA response over time for six positive samples

### Validation of the LFIA as a rapid tool for serological diagnosis of canine Leishmaniasis

The capability of the LFIA to correctly identify subjects infected by CVL was studied by analysing sera from a total of 167 dogs, belonging to both endemic (37 subjects) and non-endemic (130 subjects) areas. Considering that a gold standard reference method for diagnosing VL is still missing and that each of the analytical method usually employed show some limitations [36], [37], [49]–[53], we opted to classify canine serum based on IFAT and ELISA responses. Actually, IFAT method is commonly regarded as the reference for validation of new diagnostic tools [36], [49], [54]. On the other hand, the ELISA used in the study was based on the same capturing antigen exploited for fabricating the LFIA device. Thus, we considered that any discordance between the two methods should be attributed to the functioning of the LFIA itself and not to the specificity of the capturing reagent. For the same reason, we considered just the qualitative interpretation of the LFIA result (i.e.: colour present at the Test line) and we did not attempt to correlate quantitatively the LFIA output with IFAT titre. Most samples were characterized by the serological reference method and their classification as positive/negative was based on the general assumption that IFAT titres above 1/160 and below 1/40 are considered unequivocally positive and negative, respectively. IFAT titres comprise between 1/40 and 1/80 are considered as controversial [38], [50] and, commonly, the 1/80 level is considered as the decision cut-off [36]–[38]. The sensitive and specific ELISA was used to confirm classification of samples with an ambiguous titre and to assign samples without IFAT titre. Further 102 sera were also analysed by the ELISA. Most results obtained by the ELISA method agreed with those provided by the IFAT method. However, 11 samples gave conflicting results among the two reference methods. These samples belonged to a non-endemic area and were classified as positive based on the IFAT method, while negative according to the ELISA. The difference can be explained considering the different antigen used by the two reference techniques.

In particular, the ELISA employed the same chimeric antigen as the LFIA and therefore is more specifically directed to detect antibodies against the amastigote form of Leishmanial parasite, while the IFAT method employs an antigen from the promastigote form of the parasite. In conclusion, samples were classified as truly negative if having the IFAT titre below the cut-off titre (1/80) and a negative ELISA score [33]. Positivity was assigned to samples having the IFAT titre above the cut-off titre (>1/80) and a positive ELISA score. Sera with IFAT titre at the cut-off level (1/80) and without IFAT titre were classified based on the ELISA score only. Accordingly, 93 truly negative samples, 63 truly positive samples, and 11 ambiguous samples (positive according to IFAT, negative according to ELISA) were analysed by the LFIA during the study. Samples were blindly analysed through the LFIA in duplicate and were judged positive based on the presence of two visible lines. The visual result was assessed by three different operators, who observed the LFIA devices by the naked eye after 15 min from the application of the sample. Agreeing results were obtained within replicate measurements and between observations of the three operators for all canine sera. From these results, we obtained the figures of merits for the validation of the qualitative LFIA (Table 3.2.1).

**Table 3.2.1.** Classification of canine sera by the LFIA

	<b>N of positive result LFIA / reference method</b>	<b>Se (%)</b>	<b>False negative rate (%)</b>	<b>N of negative result LFIA / reference method</b>	<b>Sp (%)</b>	<b>False positive rate (%)</b>
Endemic	23 / 24	95.8	4.2	13 / 13	100	0
Non- endemic	39 / 39	100	0	79 / 80	98.8	1.2
	<b>62 / 63</b>	<b>98.4</b>	<b>1.6</b>	<b>92 / 93</b>	<b>98.9</b>	<b>1.1</b>

In particular, we calculated: the diagnostic sensitivity (Se) of the test, defined as the rate of truly positive results and the diagnostic specificity (Sp) of the test, defined as the rate of truly negative results [55]. The LFIA furnished one false negative result for a canine serum belonging to the endemic region. This sample had an IFAT titre equal to 1/80, which is considered as controversial and, especially for animals living in endemic area, can be related to an initial phase of the infection. A false positive result was observed for a sample belonging to the non-endemic area and, furthermore, classified as negative by both reference methods. Nevertheless, the LFIA demonstrated very high diagnostic sensitivity (98.4%, 95% confidence interval 91.47-99.96%) and specificity (98.9%, 95% confidence interval 94.15-99.97%), thus confirmed its applicability for accurately diagnosing CVL. Achieved sensitivity is higher than those of other rapid test kits, especially considering that the LFIA was able to correctly also discriminate samples with very low IFAT titres (1/40 and 1/80) while previously reported assays failed in classifying such kind of samples. Low IFAT titres can be associated to the early stage of the infection; so, the LFIA candidate as an effective tool for the prevention and control of CVL infection transmission by enabling early diagnosis. Canine sera with conflicting attribution based on the reference methods were not considered for calculation of diagnostic sensibility and specificity of the LFIA. Conversely, they were included in the comparison of LFIA with reference methods (Table 3.2.2) to calculate the accuracy.



**Table 3.2.2.** LFIA compared to the reference IFAT and ELISA methods

	<b>vs IFAT</b>	<b>vs ELISA</b>
<b>N samples</b>	140	140
<b>(pos / neg)</b>	(61 / 79)	(62 / 78)
<b>Accuracy (%)</b>	97.1	92.9
<b>K</b>	0.94	0.86

For this purpose, samples were classified differently, in accordance with the response of each individual reference method considered. The LFIA judgement provided 8 positive and 3 negative results on these ambiguous samples, thus the agreement was higher with the IFAT reference compared to the ELISA, even though the ELISA method used the same antigen specific for the amastigote VL parasite as the LFIA. In details, the accuracy of the test, defined as the fraction of tests correctly classified, was ca 93% and 97% assuming the IFAT or the ELISA method as the reference, respectively. The concordance with the two reference methods was estimated by the Cohen's k [55]. Excellent concordance was calculated with both reference methods. Moreover, by comparing the LFIA to the IFAT method, which is generally considered as the gold standard reference for Leishmaniasis diagnosis, the k value exceeded 0.9.

### Shelf-life study

Long-term and thermal stability are crucial factors for LFIA devices because they are designed for working on field. However, most materials and bio-reagents included in the device are intrinsically sensitive to environmental conditions.

The long-term stability of the LFIA device stored at 4 °C and at room temperature was investigated within six months. LFIA cassettes were individually packed, with light protection and in the presence of a desiccant. In details, a positive and a negative control were correctly attributed, based on the visual observation of the colour at the Test lines. Also, the quantification of coloured areas confirmed the visual observation (Figure 3.2.4a). Although we observed a slight decrease of Test line colour starting from day 7 compared to that measured at day 0 for both temperatures, we concluded that the LFIA is acceptably stable for six months and does not require a specific storage temperature.

In addition, accelerated ageing of the LFIA was carried out by keeping the LFIA device at 37°C for one week. The experiment allowed us to conclude that the LFIA device is insensitive to limited increase of the temperature (Figure 3.2.4b) that can occur due to ambient conditions (i.e.: use during summer season, storage in non-conditioned environment for short periods) and, therefore, is robust enough for the on-field usage.

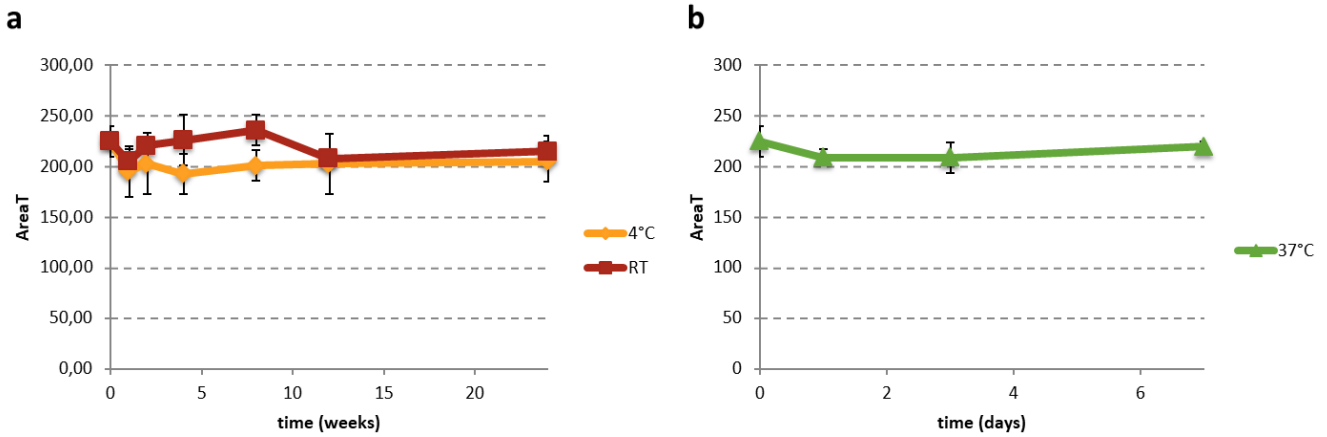


**Figure 3.2.4 (a)** shelf-life of the LFIA device as measured at 4 °C (circle) and room temperature (square) **(b)** thermal stability of the LFIA device at 37 °C. Bars in (b), (c), and (d) represent standard deviations of replicates experiments (n=2)

### Application of the LFIA for the diagnosis of VL in other animal species

Although dogs are considered the main reservoir for VL, other mammalian reservoirs have been reported and incriminated for transmission of the infection to humans [56], [57]. Companion animals like cats can be infected by *L. infantum* and transmit infection to sand flies [58] and several species of wild animals have been found infected in Europe [38]. In the past, wild species were considered as secondary reservoirs or occasional hosts; however the recent focus in Madrid with more than 600 human cases highlights the risk of VL spreading from wildlife to humans [59]. One major limitation for better understanding the dynamic of interaction between VL hosts and reservoirs is represented by the availability of diagnostic methods applicable for animals other than dogs. Indeed, most serological methods use probes that are specific for revealing canine immunoglobulins and necessitate modifying protocols for enabling detection of anti-leishmanial antibodies from other mammals. An example of a broad-specific serological assay for VL diagnosis in dogs and humans has been previously developed by the group in the ELISA format [33], based on a similar strategy. Protein A labelled with an enzyme was exploited as a versatile probe capable of revealing both human and canine anti-leishmanial antibodies. To demonstrate the versatility of the LFIA and its adaptability to detect anti-leishmanial antibodies produced by diverse animal species, two sera from red fox and nine from cat were analysed by the protocol optimized for CVL diagnosis. Red fox sera were characterized by IFAT titration and were known as one being positive and one negative. PCR and WB analyses provided controversial classification of feline sera, which were thus analysed by the reference ELISA. The ELISA provided a positive response for the red fox sample classified as positive by IFAT method and for three feline samples. The observed disagreement between molecular and serological techniques is frequent when cats are tested by both methods [58], due to the immune response of cats that differ from dogs as the low number of clinical cases demonstrates.

LFIA analysis was conducted in two replicates; no invalid tests were observed, which means that the GNP-SpA probe is suitable for adapting the LFIA for diagnosing VL in cat and red fox sera. Furthermore, LFIA judgement on red fox sera matched those obtained by both reference methods (ELISA and IFAT). Regarding feline sera, three samples were classified as positive and six as negative

(Figure 3.2.5), thus providing an excellent concordance with the reference ELISA. The observed discordance with respect to PCR was attributed to the variability of results among molecular and serological diagnostic methods, often underlined in the few available literature [58]. More interestingly, the strategy used to develop the LFIA based on the broad-specific GNP-SpA probe enabled the detection of immunoglobulins from different mammals (dogs, cats, and red fox) and the recombinant chimeric antigen was able to capture anti-leishmanial antibodies from other carnivores.

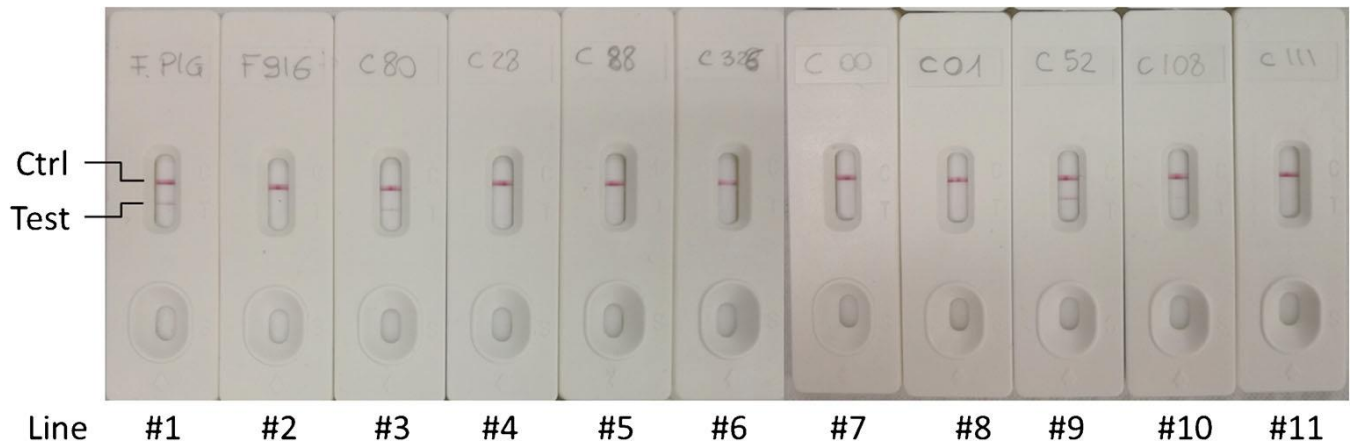


**Figure 3.2.5.** LFIA results obtained by analysing sera from two foxes (lines #1-2) and nine cats (lines #3-11). A clearly visible Test line indicated positivity for three samples (lines #1, #3 and #9). One sample (line #10) was weakly positive.

### 3.2.4 Conclusions

Performance of rapid tests available on the Brazilian market for the rapid diagnosis of CVL has been reviewed by W. Pinto et al. [38]. Although validation studies were heterogeneous in sample size and regarding the reference methods used to classify samples (IFAT, ELISA, PCR) some conclusions can be drawn. Not considering the Rapidtest assay, which validation precedes the others by about ten years, the diagnostic specificity of existing point-of-care-test for CVL varied between 90.6% provided by the SNAP Leishmania test [60] to 100% shown by the Kalazar Detect assay [44]. Noticeably, sensitivity ranged between 32.6% (Kalazar Detect) to 98% (Dual-path platform, dpp<sup>®</sup>), with a strong variability associated to the phase of the disease. Asymptomatic dogs were hardly recognized as sick by most of the rapid tests reviewed (sensitivity: 32.6-94.7%) while symptomatic animals were more easily identified as infected (sensitivity: 77-98%). The highest sensitivity value was provided by the dpp<sup>®</sup> test (98%). Another LFIA kit for CVL diagnosis, the Speed leish K [61], has been validated in a study by Ferroglio et al. [53]. The sensitivity and specificity were 96.3% and 100%, respectively, when calculated for canine sera with high IFAT titres (>1/160), which likely correspond to animals showing clinical signs of infection or in advanced stage of disease [53]. Otranto et al. validated a LFIA for CVL based on a recombinant K39 antigen that provided 97.06% and 100% sensitivity and specificity, respectively [55]. The LFIA for detecting canine anti-leishmanial antibodies developed in this study has higher sensitivity (98.4%) compared to other LFIAs, and the validation also included subjects with low IFAT titre. Therefore, it can candidate as a reliable tool for the accurate early detection of CVL. Specificity is comparable to the mean of LFIA kits available on the market for Leishmaniasis diagnosis. The LFIA device is also robust, as the visual output demonstrated to be stable over time and not influenced by the occasional increase of the temperature. It shows long-term stability (up to six months), without requiring refrigeration. In conclusion, it is suitable for on field applications by non- trained personnel and in low-resources settings. Furthermore, the design of the assay allows for its facile adaptation to diagnosing VL in other companion animals and wild carnivores that have been confirmed to have a role in the spreading of VL transmission. This versatility represents a further benefit for keeping the broadening of infection transmission under control in a timely and efficient way. The LFIA provides a qualitative yes/no response that may be used as a first screening test. In case of a positive result, a quantitative serology (ELISA or IFAT) should be performed to better discriminate the stage of infection and direct treatments.

### Compliance with Ethical Standards

Disclosure of potential conflicts of interest: The author Chiara Nogarol works at In3diagnostic company (L.go P. Braccini 2, Grugliasco (TO), Italy) which may commercialize the device. However, this does not alter the authors' adherence to the principles of good scientific practice and to relevant policies on sharing data and materials. The authors declare no other competing interest.

## Research involving Animal Participants

Informed consent: Blood samples were obtained during routine activities at the Veterinary Teaching Hospital of the Department of Veterinary Science or performed by veterinary practitioners. The study encompassed dogs from a private kennel/small animal veterinary clinics and informed consent was obtained from the owner. The consent was provided in oral form. No additional permission was required. All procedures were conducted in accordance with EU Directive 2010/63/EU for animal experiments, as well as subject to informed owner consent.

## References

- [1] "Rapid Tropical Parasitic Tests - Malaria Pf/Pan Ag Rapid Test CE Wholesale Trader from Hyderabad." <https://www.biochromescientific.com/rapid-tropical-parasitic-tests.html> (accessed Feb. 03, 2021).
- [2] C. C. Lin *et al.*, "Diagnostic value of immunoglobulin g (igg) and igm anti-hepatitis e virus (hev) tests based on hev rna in an area where hepatitis e is not endemic," *J. Clin. Microbiol.*, vol. 38, no. 11, pp. 3915–3918, 2000, doi: 10.1128/jcm.38.11.3915-3918.2000.
- [3] X. Wang *et al.*, "Efficacy of a combination of HBV RNA and HBeAg in predicting HBeAg seroconversion in patients treated with entecavir for 144 weeks," *Int. J. Infect. Dis.*, vol. 99, pp. 171–178, Oct. 2020, doi: 10.1016/j.ijid.2020.07.031.
- [4] G. Matusali *et al.*, "Performance of rapid tests in the management of dengue fever imported cases in Lazio, Italy 2014–2019," *Int. J. Infect. Dis.*, vol. 99, pp. 193–198, Oct. 2020, doi: 10.1016/j.ijid.2020.07.008.
- [5] W. Choe, T. A. Durgannavar, and S. J. Chung, "Fc-binding ligands of immunoglobulin G: An overview of high affinity proteins and peptides," *Materials*, vol. 9, no. 12. MDPI AG, 2016, doi: 10.3390/ma9120994.
- [6] A. Srisrattakarn *et al.*, "Development of a prototype lateral flow immunoassay for rapid detection of staphylococcal protein a in positive blood culture samples," *Diagnostics*, vol. 10, no. 10, 2020, doi: 10.3390/diagnostics10100794.
- [7] Z. Huang *et al.*, "Characteristics and roles of severe acute respiratory syndrome coronavirus 2-specific antibodies in patients with different severities of coronavirus 19," *Clin. Exp. Immunol.*, vol. 202, no. 2, pp. 210–219, Nov. 2020, doi: 10.1111/cei.13500.
- [8] M. Infantino *et al.*, "Closing the serological gap in the diagnostic testing for COVID-19: The value of anti-SARS-CoV-2 IgA antibodies," *J. Med. Virol.*, Mar. 2020, doi: 10.1002/jmv.26422.
- [9] G. Bauer, "The variability of the serological response to SARS-corona virus-2: Potential resolution of ambiguity through determination of avidity (functional affinity)," *Journal of Medical Virology*, vol. 93, no. 1. John Wiley and Sons Inc, pp. 311–322, Jan. 01, 2021, doi: 10.1002/jmv.26262.
- [10] N. M. A. Okba *et al.*, "Severe Acute Respiratory Syndrome Coronavirus 2-Specific Antibody Responses in Coronavirus Disease Patients," *Emerg. Infect. Dis.*, vol. 26, no. 7, pp. 1478–1488, Jul. 2020, doi: 10.3201/eid2607.200841.
- [11] G. Lippi *et al.*, "Assessment of immune response to SARS-CoV-2 with fully automated MAGLUMI 2019-nCoV IgG and IgM chemiluminescence immunoassays," *Clinical Chemistry and Laboratory Medicine*, vol. 58, no. 7. De Gruyter, pp. 1156–1159, Jul. 01, 2020, doi: 10.1515/cclm-2020-0473.
- [12] Y. Shi *et al.*, "Diagnosis of Severe Acute Respiratory Syndrome (SARS) by Detection of SARS Coronavirus Nucleocapsid Antibodies in An Antigen-Capturing Enzyme-Linked Immunosorbent Assay," *J. Clin. Microbiol.*, vol. 41, no. 12, pp. 5781–5782, Dec. 2003, doi: 10.1128/JCM.41.12.5781-5782.2003.
- [13] Y. J. Tan *et al.*, "Profiles of Antibody Responses against Severe Acute Respiratory Syndrome Coronavirus Recombinant Proteins and Their Potential Use as Diagnostic Markers," *Clin. Diagn. Lab. Immunol.*, vol. 11, no. 2, pp. 362–371, Mar. 2004, doi: 10.1128/CDLI.11.2.362-371.2004.
- [14] W. Zeng *et al.*, "Biochemical characterization of SARS-CoV-2 nucleocapsid protein," *Biochem. Biophys. Res. Commun.*, vol. 527, no. 3, pp. 618–623, Jun. 2020, doi: 10.1016/j.bbrc.2020.04.136.

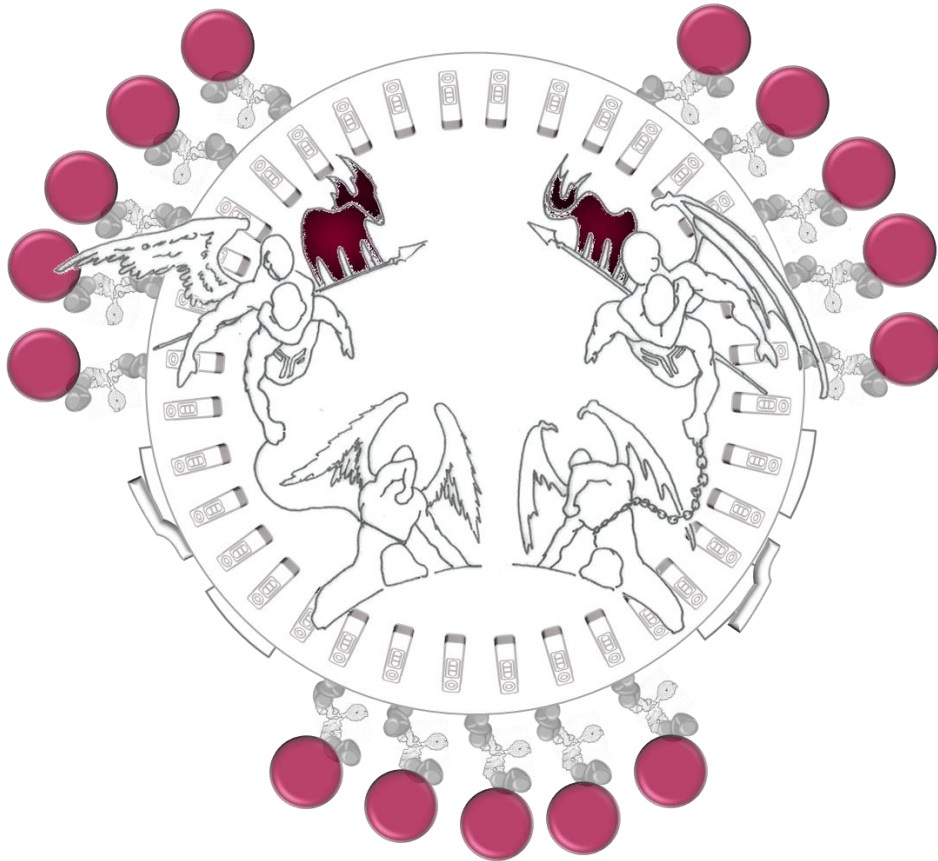
- [15] Q. X. Long *et al.*, “Antibody responses to SARS-CoV-2 in patients with COVID-19,” *Nat. Med.*, vol. 26, no. 6, pp. 845–848, Jun. 2020, doi: 10.1038/s41591-020-0897-1.
- [16] “ERADIKIT™ COVID19-IgG | In3Diagnostic.” <http://www.in3diagnostic.com/en/eradikit-covid19-igg-2/> (accessed Feb. 03, 2021).
- [17] S. Rosati *et al.*, “Development of recombinant capsid antigen/transmembrane epitope fusion proteins for serological diagnosis of animal lentivirus infections,” *J. Virol. Methods*, vol. 121, no. 1, pp. 73–78, Oct. 2004, doi: 10.1016/j.jviromet.2004.06.001.
- [18] J. Turkevich, P. C. Stevenson, and J. Hillier, “A study of the nucleation and growth processes in the synthesis of colloidal gold,” *Discussions of the Faraday Society*, vol. 11, pp. 55–75, 1951, doi: 10.1039/DF9511100055.
- [19] Z. Chen *et al.*, “Rapid and Sensitive Detection of anti-SARS-CoV-2 IgG, Using Lanthanide-Doped Nanoparticles-Based Lateral Flow Immunoassay,” *Anal. Chem.*, vol. 92, no. 10, pp. 7226–7231, May 2020, doi: 10.1021/acs.analchem.0c00784.
- [20] “SARS-CoV-2 (Covid-19): Diagnosis by IgG/IgM Rapid Test Clinisciences.” <https://www.clinisciences.com/it/read/newsletter-26/sars-cov-2-covid-19-diagnosis-by-2264.html> (accessed Feb. 03, 2021).
- [21] “COVID-19 Rapid POC CE-IVD Test (25 tests) - Assay Genie.” <https://www.assaygenie.com/covid-19-rapid-poc-ce-ivd-test-25-tests/> (accessed Feb. 03, 2021).
- [22] “COVID-19 IgM/IgG Rapid Test – BioMedomics Inc.” <https://www.biomedomics.com/products/infectious-disease/covid-19-rt/> (accessed Feb. 03, 2021).
- [23] “COVID-19 IgG/IgM Rapid Test | Prima Home Test.” [https://primahometest.com/it/covid-19\\_test\\_sierologico](https://primahometest.com/it/covid-19_test_sierologico) (accessed Feb. 03, 2021).
- [24] “Rapid test Covid-19 - 2019-nCov - Sars-CoV-2 - Screen Italia.” <https://www.screenitalia.it/coronavirus-covid-19-rapid-test/> (accessed Feb. 03, 2021).
- [25] “COVID-19 — English.” <https://www.technogenetics.it/en/products-1/covid-19> (accessed Feb. 03, 2021).
- [26] Z. Li *et al.*, “Development and clinical application of a rapid IgM-IgG combined antibody test for SARS-CoV-2 infection diagnosis,” *J. Med. Virol.*, vol. 92, no. 9, pp. 1518–1524, Sep. 2020, doi: 10.1002/jmv.25727.
- [27] H. Q. Yu *et al.*, “Distinct features of SARS-CoV-2-specific IgA response in COVID-19 patients,” *European Respiratory Journal*, vol. 56, no. 2, European Respiratory Society, Aug. 01, 2020, doi: 10.1183/13993003.01526-2020.
- [28] L. Guo *et al.*, “Profiling early humoral response to diagnose novel coronavirus disease (COVID-19),” *Clin. Infect. Dis.*, vol. 71, no. 15, pp. 778–785, Aug. 2020, doi: 10.1093/cid/cia310.
- [29] S. Rosati *et al.*, “Prokaryotic Expression and Antigenic Characterization of Three Recombinant Leishmania Antigens for Serological Diagnosis of Canine Leishmaniasis,” *Clin. Diagn. Lab. Immunol.*, vol. 10, no. 6, pp. 1153–1156, Nov. 2003, doi: 10.1128/CDLI.10.6.1153-1156.2003.
- [30] A. Boarino *et al.*, “Development of recombinant chimeric antigen expressing immunodominant B epitopes of Leishmania infantum for serodiagnosis of visceral leishmaniasis,” *Clin. Diagn. Lab. Immunol.*, vol. 12, no. 5, pp. 647–653, May 2005, doi: 10.1128/CDLI.12.5.647-653.2005.
- [31] B. H. Al-Adhami and A. A. Gajadhar, “A new multi-host species indirect ELISA using protein A/G conjugate for detection of anti-Toxoplasma gondii IgG antibodies with comparison to ELISA-IgG, agglutination assay and Western blot,” *Vet. Parasitol.*, vol. 200, no. 1–2, pp. 66–73, Feb. 2014, doi: 10.1016/j.vetpar.2013.11.004.

- [32] K. Stöbel, A. Schönberg, and C. Staak, "A new non-species dependent ELISA for detection of antibodies to *Borrelia burgdorferi* s. l. in zoo animals," *Int. J. Med. Microbiol.*, vol. 291, pp. 88–99, Jun. 2002, doi: 10.1016/S1438-4221(02)80018-2.
- [33] F. Daprà *et al.*, "Validation of a recombinant based antibody ELISA for diagnosis of human and canine leishmaniasis," *J. Immunoass. Immunochem.*, vol. 29, no. 3, pp. 244–256, Jul. 2008, doi: 10.1080/15321810802116006.
- [34] A. Intaramat *et al.*, "Protein A/G-Based immunochromatographic test for serodiagnosis of pythiosis in human and animal subjects from Asia and Americas," *Med. Mycol.*, vol. 54, no. 6, pp. 641–647, Aug. 2016, doi: 10.1093/mmy/myw018.
- [35] S. Omachi, Y. Matsumoto, and Y. Goto, "Immunoglobulins in the pathophysiology of visceral leishmaniasis," in *Kala Azar in South Asia: Current Status and Sustainable Challenges, Second Edition*, Springer International Publishing, 2017, pp. 187–195.
- [36] A. Adel, D. Berkvens, E. Abatih, A. Soukehal, J. Bianchini, and C. Saegerman, *No Title*, vol. 11, no. 8. Public Library of Science, 2016, p. e0161051.
- [37] S. Paltrinieri, L. Gradoni, X. Roura, A. Zatelli, and E. Zini, "Laboratory tests for diagnosing and monitoring canine leishmaniasis," *Veterinary Clinical Pathology*, vol. 45, no. 4. American Society for Veterinary Clinical Pathology, pp. 552–578, Dec. 01, 2016, doi: 10.1111/vcp.12413.
- [38] W. Pinto, A. J. Ribeiro, and V. M. Tafuri, "The Immunochromatography Use in Canine Visceral Leishmaniasis in Brazil: A 'Quick Solution' of a Complex Diagnostic? Rapid Test in Dogs with Leishmaniasis," 2016.
- [39] E. Ferroglio, S. Zanet, W. Mignone, M. Poggi, A. Trisciuglio, and P. Bianciardi, "Evaluation of a rapid device for serological diagnosis of leishmania infantum infection in dogs as an alternative to immunofluorescence assay and western blotting," *Clin. Vaccine Immunol.*, vol. 20, no. 5, pp. 657–659, May 2013, doi: 10.1128/CVI.00719-12.
- [40] V. M. T. Lattanzio, N. Guarducci, S. Powers, B. Ciasca, M. Pascale, and C. Von Holst, "Validation of a lateral flow immunoassay for the rapid determination of aflatoxins in maize by solvent free extraction," *Anal. Methods*, vol. 10, no. 1, pp. 123–130, Jan. 2018, doi: 10.1039/c7ay02249b.
- [41] V. M. T. Lattanzio, C. Von Holst, and A. Visconti, "Experimental design for in-house validation of a screening immunoassay kit. the case of a multiplex dipstick for *Fusarium* mycotoxins in cereals," *Anal. Bioanal. Chem.*, vol. 405, no. 24, pp. 7773–7782, Sep. 2013, doi: 10.1007/s00216-013-6922-1.
- [42] F. Di Nardo *et al.*, "Validation of a qualitative immunochromatographic test for the noninvasive assessment of stress in dogs," *J. Chromatogr. B Anal. Technol. Biomed. Life Sci.*, vol. 1028, pp. 192–198, Aug. 2016, doi: 10.1016/j.jchromb.2016.06.019.
- [43] P. A. Kaplan LA, *Clinical chemistry. Theory, analysis, correlation*, 5th ed. Maryland Heights, MO, 2010.
- [44] G. Matlashewski *et al.*, "Diagnosis of Visceral Leishmaniasis in Bihar India: Comparison of the rK39 Rapid Diagnostic Test on Whole Blood Versus Serum," *PLoS Negl. Trop. Dis.*, vol. 7, no. 5, 2013, doi: 10.1371/journal.pntd.0002233.
- [45] E. S. da Silva, W. F. van der Meide, G. J. Schoone, C. M. F. Gontijo, H. D. F. H. Schallig, and R. P. Brazil, "Diagnosis of canine leishmaniasis in the endemic area of Belo Horizonte, Minas Gerais, Brazil by parasite, antibody and DNA detection assays," *Vet. Res. Commun.*, vol. 30, no. 6, pp. 637–643, Jul. 2006, doi: 10.1007/s11259-006-3324-2.
- [46] P. Chun, "Colloidal gold and other labels for lateral flow immunoassays." Humana Press, pp. 75–93, 2009.
- [47] N. A. Byzova, I. V. Safenkova, E. S. Slutskaya, A. V. Zherdev, and B. B. Dzantiev, "Less is More: A Comparison of Antibody-Gold Nanoparticle Conjugates of Different Ratios,"



- Bioconjug. Chem.*, vol. 28, no. 11, pp. 2737–2746, Nov. 2017, doi: 10.1021/acs.bioconjchem.7b00489.
- [48] L. Anfossi, M. Calderara, C. Baggiani, C. Giovannoli, E. Arletti, and G. Giraudi, “Development and application of a quantitative lateral flow immunoassay for fumonisins in maize,” *Anal. Chim. Acta*, vol. 682, no. 1–2, pp. 104–109, Dec. 2010, doi: 10.1016/j.aca.2010.09.045.
- [49] M. D. S. Solcà *et al.*, “No Title,” *PLoS One*, vol. 9, no. 7, p. e103635, Jul. 2014, doi: 10.1371/journal.pone.0103635.
- [50] L. Solano-Gallego, S. Villanueva-Saz, M. Carbonell, M. Trotta, T. Furlanello, and A. Natale, “Serological diagnosis of canine leishmaniosis: Comparison of three commercial ELISA tests (Leiscan®, ID Screen® and Leishmania 96®), a rapid test (Speed Leish K®) and an in-house IFAT,” *Parasites and Vectors*, vol. 7, no. 1, Mar. 2014, doi: 10.1186/1756-3305-7-111.
- [51] O. C. Moreira, Z. E. Yadon, and E. Cupolillo, “The applicability of real-time PCR in the diagnostic of cutaneous leishmaniasis and parasite quantification for clinical management: Current status and perspectives,” *Acta Tropica*, vol. 184. Elsevier B.V., pp. 29–37, Aug. 01, 2018, doi: 10.1016/j.actatropica.2017.09.020.
- [52] C. Pomares *et al.*, “Western blot analysis as an aid for the diagnosis of cutaneous leishmaniasis due to *Leishmania major*,” *Trans. R. Soc. Trop. Med. Hyg.*, vol. 106, no. 7, pp. 452–454, Jul. 2012, doi: 10.1016/j.trstmh.2012.03.001.
- [53] E. Ferroglio, E. Centaro, W. Mignone, and A. Trisciuglio, “Evaluation of an ELISA rapid device for the serological diagnosis of *Leishmania infantum* infection in dog as compared with immunofluorescence assay and Western blot,” *Vet. Parasitol.*, vol. 144, no. 1–2, pp. 162–166, Mar. 2007, doi: 10.1016/j.vetpar.2006.09.017.
- [54] C. Adams E, Hasker E, “Diagnostics evaluation series No. 4: Visceral Leishmaniasis Rapid Diagnostic Test Performance,” no. 4, 2011.
- [55] D. Otranto *et al.*, “Recombinant K39 dipstick immunochromatographic test: A new tool for the serodiagnosis of canine leishmaniasis,” *J. Vet. Diagnostic Investig.*, vol. 17, no. 1, pp. 32–37, 2005, doi: 10.1177/104063870501700107.
- [56] R. M. Cardoso *et al.*, “Expanding the knowledge about *Leishmania* species in wild mammals and dogs in the Brazilian savannah,” *Parasites and Vectors*, vol. 8, no. 1, Mar. 2015, doi: 10.1186/s13071-015-0780-y.
- [57] C. H. Gao, J. Y. Wang, S. Zhang, Y. T. Yang, and Y. Wang, “Survey of wild and domestic mammals for infection with *leishmania infantum* following an outbreak of desert zoonotic visceral leishmaniasis in Jiashi, People’s Republic of China,” *PLoS One*, vol. 10, no. 7, Jul. 2015, doi: 10.1371/journal.pone.0132493.
- [58] M. G. Pennisi, “Leishmaniosis of companion animals in Europe: An update,” *Vet. Parasitol.*, vol. 208, no. 1–2, pp. 35–47, Feb. 2015, doi: 10.1016/j.vetpar.2014.12.023.
- [59] J. Millán, E. Ferroglio, and L. Solano-Gallego, “Role of wildlife in the epidemiology of *Leishmania infantum* infection in Europe,” *Parasitology Research*, vol. 113, no. 6. Springer Verlag, pp. 2005–2014, 2014, doi: 10.1007/s00436-014-3929-2.
- [60] “SNAP *Leishmania* - IDEXX UK.” <https://www.idexx.co.uk/en-gb/veterinary/snap-tests/snap-leishmania/> (accessed Feb. 03, 2021).
- [61] “Virbac BVT - Speed Leish K.” <https://bvt.virbac.com/en/home/diagnostic-solutions/pour-le-veterinaire-praticien/vector-borne-and-parasitic-disea/main/produits/speed-leish-k.html> (accessed Feb. 03, 2021).

## Chapter 4



---

### The class-specific antibody LFIA

---

## Introduction

As reported in the chapter 3.1 the most common target for antibody testing is the IgG class. Detecting a single class of antibodies is a standard and, generally, comfortable, practise. In those situations where the clinical intervention differs according to the stage of the infection, it could be important to discriminate between classes IgG and IgM [1]–[4]. Some classes are peculiar to biological specimens, such as IgA, and furnish complementary information to those carried by serum IgG [5]–[8]. The different roles and behaviour of the antibody classes can have many implications, from the vaccine administration routes to the monitoring of their efficiency, from the discrimination between an early infection to a complete seroconversion[9].

As discussed in the previous chapter, LFIAs for antibody testing generally target the IgG class or apply the ‘untargeted’ approach, indiscriminately addressing the sum of Ig or the sole class detectable within the system. Ig class differentiation is generally accomplished by laboratory tests. However, recently, some LFIAs aimed at detecting separately IgG and IgM have been reported [10]–[12], profiting of the simplicity of testing multiple targets in a single strip.

This section enlightens the importance of two rarely exploited, characteristics of the LFIA: the multiplexing ability and the specificity in the isolation of the target in non-conventional matrices.

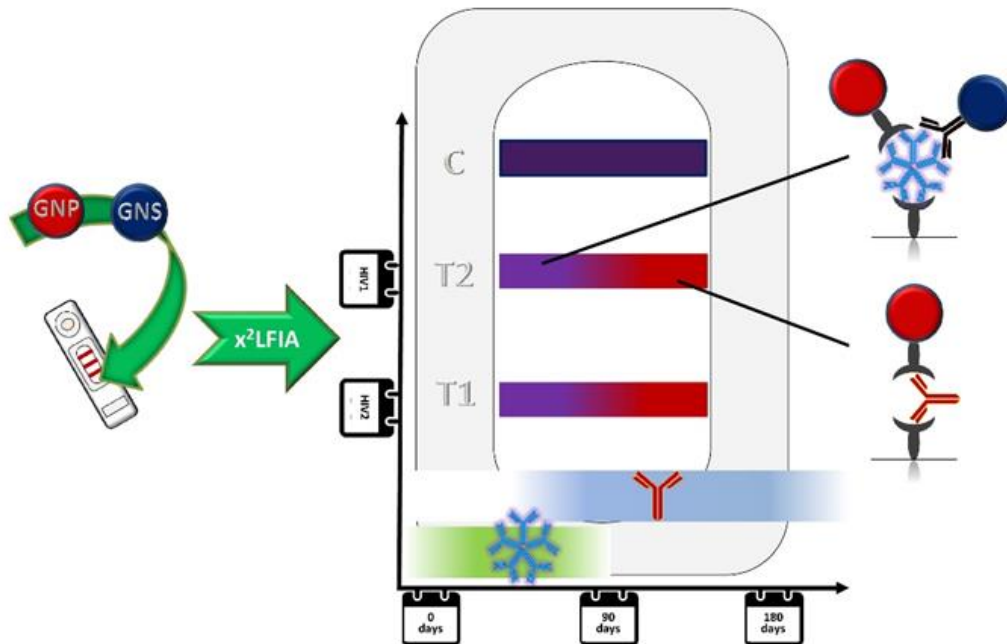
Hereafter are reported two examples of the strategies exploited for improving these aspects. The first example deals with the enhancement of the number of information achieved in a single test by upgrading the standard multiplexing into a multimodal format following three different strategies. Comparing their results using the same samples allowed, furthermore, for understanding the importance of the roles of the immunoreagents.

The second was on the development of a LFIA strip to target a single, strategic, class of antibodies in a non-conventional matrix, the saliva, easier to be sampled and with less interfering non-specific antibodies, by using a dual detection system.

## 4.1



### Multimodal $x^2$ LFIA for HIV



Based on

S. Cavallera, F. Di Nardo, L. Forte, F. Marinoni, M. Chiarello, C. Baggiani, L. Anfossi, **Switching from Multiplex to Multimodal Colorimetric Lateral Flow Immunosensor**, *Sensors (Basel)*, 20, 2020, 6609. <https://doi.org/10.3390/s20226609>.

#### Abstract

*Multiplex lateral flow immunoassay (LFIA) is largely used for point-of-care testing to detect different pathogens or biomarkers in a single device. The increasing demand for multitargeting diagnostics requires multi-informative single tests. In this study, we demonstrated three strategies to upgrade standard multiplex LFIA to multimodal capacity. As a proof-of-concept, we applied the strategies to the differential diagnosis of Human Immunodeficiency Virus (HIV) infection, a widespread pathogen, for which conventional multiplex LFIA testing is well-established. In the new two-parameter LFIA ( $x^2$ LFIA), we exploited colour encoding, in which the binding of multiple targets occurs in one reactive band and the colour of the probe reveals which one is present in the sample. By combining the sequential alignment of several reactive zones along the membrane of the LFIA strip and gold nanoparticles and gold nanostars for the differential visualization, in this demonstration, the  $x^2$ LFIA can furnish information on HIV serotype and stage of infection in a single device. Three immunosensors were designed. The use of bioreagents as the capturing ligand anchored onto*

*the membrane or as the detection ligand labelled with gold nanomaterials affected the performance of the  $x^2$ LFIA. Higher detectability was achieved by the format involving the HIV-specific antigens as capturing agent and labelled secondary bioligands (anti-human immunoglobulins M and protein G) as the probes.*

#### **4.1.1 Design of the prototypes**

Here, we propose a two-parameter multiplexing LFIA strategy ( $x^2$ LFIA), which combines multiple lines and the colour-encoded approach to expand the number of information achievable within a single strip test. The work aims at demonstrating the feasibility and the potentiality of the  $x^2$ LFIA approach to get a tetravalent information in a two-line and two-colour assay. As a proof-of-concept of the multimodal approach, we used a set of immunoreagents for the diagnosis of the Human Immunodeficiency Virus (HIV) infection. HIV is one of the main fields of application of point-of-care testing since it still has a severe impact on society [13] and especially in low-resource settings. POCT diagnostics involving conventional and multiplex LFIA for HIV are well-established [14]. HIV testing rely typically on the detection of the serological response to the infection. Antibody-screening LFIAs discriminate between HIV1 and HIV2 serotypes by exploiting the specificity of the recognition between the type-dependent viral proteins and the human anti-HIV antibodies [15]. Recombinant envelope glycoproteins gp41 and gp36 are generally used as the antigens to specifically recognize HIV1 and HIV2 antibodies, respectively [16], [17]. The spatial resolution is the most common strategy to multi-targeting the single assay [18]–[24]. For instance, in a typical HIV serotyping test, the discrimination is made by coating the specific antigens in two spatially confined bands (test lines) (Figure 4.1.1 a) and anti-HIV antibodies are indiscriminately revealed by labelled secondary antibodies as the signal reporters. The anti-HIV antibodies form immunocomplexes with the labelled secondary antibodies and are captured by the antigens at the test lines. This results in the accumulation of the signal reporters with the formation of coloured lines. On the other hand, the double antigen approach has been reported also. In this case, the probe is represented by the labelled antigen and the sandwich-type complex comprises the anti-HIV antibody bridging two antigens, one anchored to the support (capture) and the second one labelled (detection). In microplate-based ELISA this approach was shown to increase specificity and sensitivity and some LFIA formats adopted this strategy [25], [26]. The serological response to infection involves the production of different classes of immunoglobulins, which follows a typical temporal pattern, in which IgM are produced first, followed by IgG [9], [27]. Then, the IgM/IgG ratio is exploited for identifying the stage of the infection [28], [29]. HIV testing embedding both serotyping capability and infection stage discrimination are not available currently. The two discrimination levels in a single test as the illustration of the potential of the multimodal approach were combined. Various combinations of specific bioreagents as capturing agents coated onto the nitrocellulose and signal reporters conjugated to GNP and GNS two xLFIA and three  $x^2$ LFIA immunosensors were designed and their performance investigated. For the studying  $x^2$ LFIA immunosensors and comparing their performance, we used gp41 and gp36 to bind specifically the two HIV serotypes and protein G and anti-human immunoglobulins M (anti-hIgM) secondary antibody to bind IgG and IgM, respectively.

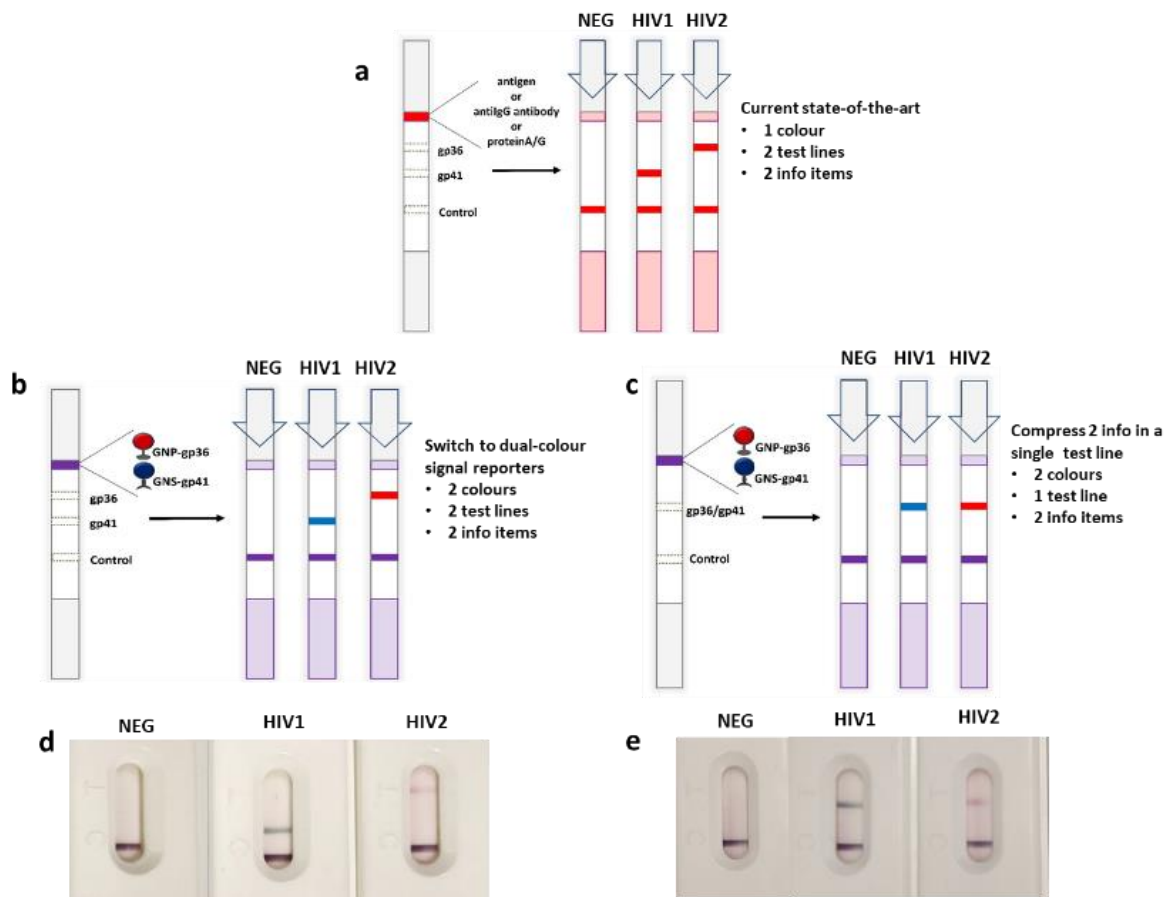


**Figure 4.1.1.** Conceptual framework of the new generation multiplexing LFIA with the addition of a dual colour probe: state-of-the-art in multiplexing (a) schematic of the possible use of red- and blue-coloured gold nanomaterials to discriminate HIV1 and HIV2 (b) and to merge the two information items in a single test line (c). Results from a known negative, a HIV1 positive, and a HIV2 positive serum samples, respectively are also shown to confirm the feasibility of the xLFIA (d) and x<sup>2</sup>LFIA (e).

The three immunosensors differed each other by the role and position that immunoreagents played in the assay. Immunosensor 1 used secondary bioligands (e.g., protein G and anti-hlgM) as the capturing agents and the GNP/GNS -labelled HIV antigens as the probes. Immunosensor 2 was the exact reverse. The two HIV antigens were coated on the test lines and acted as the capturing agents while secondary bioligands were labelled with two distinct signal reporters. Immunosensor 3 relied on the double antigen strategy, where HIV antigens were used both for capture and for signal reporting, both linked to the red GNP. The blue-labelled anti-hlgM was added to add the information on infection stage. Generally, the double antigen approaches are reported as more sensitive than other formats, precisely because of its selectivity [30]. The three immunosensors were tested using a panel of control sera for investigating the ability to combine the spatial and colour resolution to provide multiple response and for elucidating the effect of the role played by the immunoreagents on the immunosensors performance. The importance of multiplexing is growing day by day, parallel to the comprehension of the relevance of intersecting information on several biomarkers at one time [31]–[34]. This study discloses the possibility to expand the multiplexing capability of the LFIA platform for multi-target screening tests without requiring expensive instrumentation for miniaturized spots reading.

## 4.1.2 Materials and Methods

### Immunoreagents, chemicals and materials

Gold (III) chloride trihydrate (ACS reagent), hydroquinone, streptococcal protein G, sodium caseinate, anti-human IgM ( $\mu$  chain specific) antibody produced in goat, and bovine serum albumin (BSA) were purchased from Sigma–Aldrich (St. Louis, MO, USA). Tween20 and other chemicals were of analytical grade and were obtained from VWR International (Milan, Italy). HIV-antigens gp36 and gp41 were purchased from Arista Biologicals Inc. (Allentown, PA, USA). Casein-biotin for conjugation to GNPs was obtained from In3diagnostics (Torino, Italy). Nitrocellulose membranes with cellulose adsorbent pad (CNPC-SS12-L3-P25) and sample pads (FR-1) were purchased from MDI membrane technologies (Ambala, India), while conjugate pads (GF) were obtained from Merck Millipore (Billerica, MA, USA).

### Synthesis of Gold Nanoparticles and Gold Nanostars

Spherical gold nanoparticles (GNP) were synthesized as reported in Chapter 3.1.2. GNS were synthesized through a seeding growth approach using a stepwise reduction of Au (III) to Au (I) by citrate and Au (I) to Au (0) by hydroquinone. The protocol followed one previously reported [20] and involved the synthesis of GNP seeds with a localized plasmon resonance (LSPR) band centred at 517 nm. These were obtained as described above, except for the volumes used, which were 0.6 mL of 1% w/v sodium citrate added to 30 mL of 0.01% tetrachloroauric acid. For GNS preparation,  $1.9 \times 10^{-8}$  mol of tetrachloroauric acid was mixed with  $9.3 \times 10^{-13}$  mol of GNP seeds and  $7.5 \times 10^{-9}$  mol of sodium citrate. The mixture was stirred for 2 min at room temperature. Then,  $3.0 \times 10^{-5}$  mol of hydroquinone was rapidly under vigorous stirring. The solution was kept under stirring at room temperature for further 20 min.

### Preliminary study for GNP and GNS conjugates preparation.

Generally, previously described flocculation test is a common preliminary phase to estimate the minimum stabilizing concentration of protein to functionalize the GNP and GNS. However, antigens are not always suitable for such studies, being less robust than antibodies and less able to protect the GNP from aggregation. In fact, no info was made available from the flocculation tests about the adsorption of the gp36 antigen onto the red GNP and of the gp41 onto the GNS. For biotin and gp36 adsorption on the GNP and for the anti-M antibody adsorption on the GNS 4 to 10  $\mu\text{g}$  of protein per ml\*OD of GNP resulted widely sufficient to passivate the gold surface. Protein G showed protection from aggregation at as low amount as 2  $\mu\text{g}/\text{ml}*\text{OD}$ . For this work we decided to normalize to 10  $\mu\text{g}/\text{ml}*\text{OD}$  all the conjugates (with exception for multivalent protein G, 2  $\mu\text{g}/\text{ml}*\text{OD}$ ).

## Labelling Immunoreagents with GNPs and GNSs

The red-coloured GNP-gp36 conjugate was prepared by adsorbing the gp36 antigen onto the GNP surface. In detail, 10 mL of GNP (optical density ca. 1) was basified with carbonate buffer (50 mM pH 9.6) to pH 8 and added dropwise with 100  $\mu$ g of gp36 antigen under gentle stirring at room temperature for 40 min. Next, 1 mL of casein (5% in borate buffer) was added and reacted for 10 min to saturate the free GNP surface. GNP-gp36 was recovered by centrifugation (8000 $\times$  g 10 min) and washed with borate buffer supplemented with 0.5% casein. Finally, the GNP-gp36 was re-suspended in the CAS-storage buffer (borate buffer with 0.5% casein, 0.25% Tween 20, 2% sucrose and 0.02% sodium azide) and stored at 4 °C until use. The red GNP-gp41 and GNP-biotin conjugates were obtained by the same procedure. For the GNP-protein G conjugate, 10 mL of GNP was brought to pH 6 with carbonate buffer and added with 20  $\mu$ g of protein G under gentle stirring at room temperature for 40 min. Next, 1 mL of BSA (10% in borate buffer) was added and reacted for 10 min to saturate the free GNP surface. GNP-protein G was recovered by centrifugation (8000 $\times$  g, 10 min) and washed with borate buffer supplemented with 1% BSA. Finally, the GNP-protein G was re-suspended in BSA-storage buffer (borate buffer with 1% BSA, 0.25% Tween 20, 2% sucrose and 0.02% sodium azide). Successful conjugation of proteins to gold nanomaterials was confirmed by UV-vis spectroscopy (Figure 4.1.2 e-f). The blue-coloured GNS-gp41 and GNS-anti IgM conjugates were prepared likewise, except that GNS with optical density ca 0.6 were used and reacted with 10  $\mu$ g of protein. Nevertheless, labelling with antigens with GNS was less easy on respect to GNP counterparts, as we will see in the following paragraph.

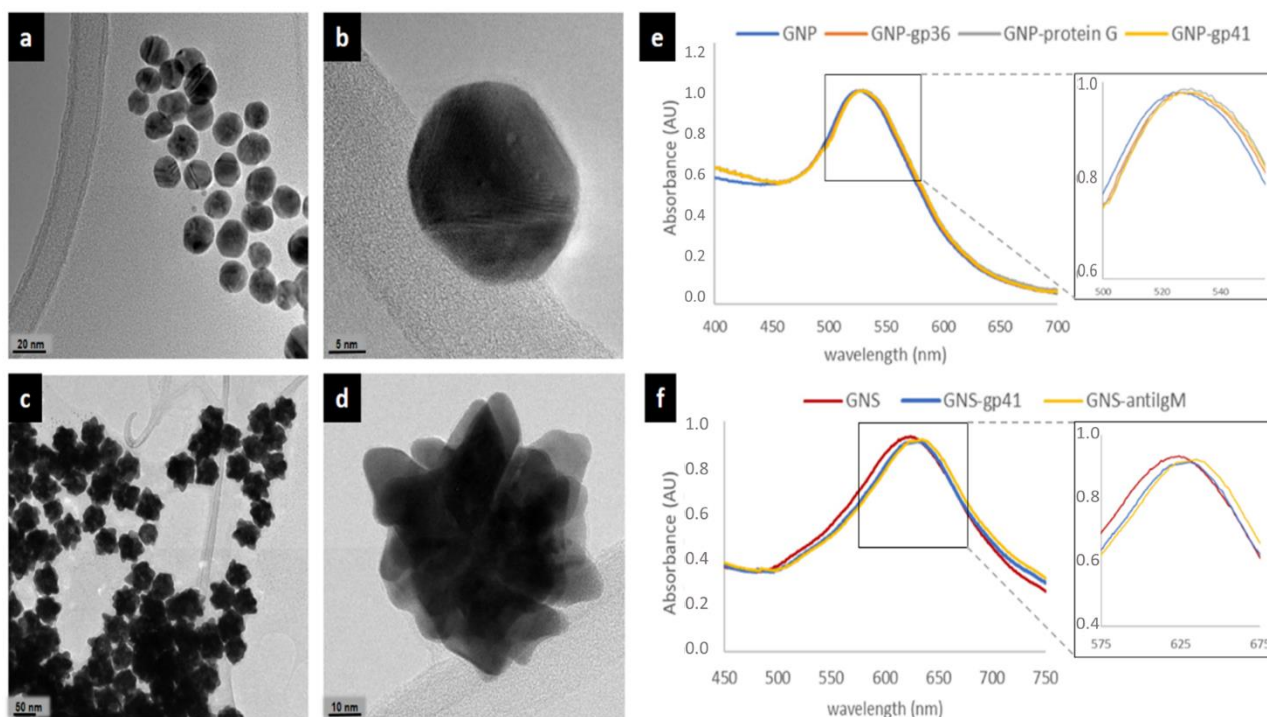


**Figure 4.1.2.** Spectroscopic characterization of gold nanomaterials: images obtained by high-resolution transmission electron microscopy of the GNP (a,b) and GNS (c,d), and visible spectra of bare GNP (e) and GNS (f) and of the conjugates to bioreagents. Insets show a magnification of the LSPR band region. Blue shifts witness increased dimensions due to the absorption of both the antigen and the saturation protein.



## Preparation and stabilization of GNS-gp41 conjugate

Studies aimed at reaching stable and functional GNS-gp41 conjugate were conducted by varying the additive used to saturate the free GNP surface and the pre-saturation of the conjugate pad onto which the conjugate was dispensed (Table 4.1.1). Optimal conditions were established on a pass-no pass approach based upon i) avoiding GNP agglomeration during and after the conjugation process, ii) providing no signal for negative samples, and iii) showing intense colouring with positive samples. For the experiments, 3 serum samples #5 (HIV2+), #8 (HIV1+) and #10 (negative) from Zeptomatrix panel were tested. The evaluation was made by naked eye observation between 5 and 10 minutes from sample application. Symbols represent: (-) absent, (-/+) weak, (+) moderate, and (++) strong red-colour developed at the test lines. The performance of the GNS-gp41 was considered acceptable if the agglomeration tendency was negligible (pass), the signal for negative sample was absent/weak (pass) and the signal of positive samples from moderate to strong (pass). GNS-gp41 adsorption was carried at room temperature under gentle stirring. Stable GNS-gp41 conjugates were obtained by using 10 µg/ml\*OD of gp41 to GNP at pH 8 with casein in the overcoating, washing and storage buffers. Typically, the colour of the solution turned dark brown during the conjugation step, due to the hydroquinone shift in basic medium. After washing, hydroquinone was eliminated, and the colour returned blue and remained stable hereafter. The GNS-gp41 conjugate did not show any aggregation phenomena, which should be expected for unstable antigen gold-conjugates. Results on the preliminary LFIA are shown in Table 4.1.1.

**Table 4.1.1.** Experimental conditions tested for the adsorption of the recombinant antigen onto GNS. Selected conditions for the preparation of GNS-gp41 conjugate are shown in bold. The saturation agents were dissolved in borate buffer. The same buffer was used in the saturation, washing and resuspension steps of the conjugation. Unsuitable conditions were no further investigated (nd means that previous check was not passed)

Saturation			Pre-adsorbent agent		Signal for negative sample (NEG)	Signal for positive sample (HIV1+)
agent	Concentration (w/v% final)	Agglomeration tendency	agent	Concentration (w/v% final)		
BSA	0.1	moderate	nd	nd	nd	nd
BSA	1	weak	nd	nd	nd	nd
Casein	0.5	no	none	nd	-	++
Casein	0.5	no	BSA	1	+/-	nd
Casein	0.5	no	casein	0.5	-	+

## LFIA Strip Preparation

The configurations of the preliminary LFIA immunosensors and of the three formats of x<sup>2</sup>LFIA are shown in Figures 4.1.1 and 4.1.3. All strips were prepared by dispensing the immunoreagents on nitrocellulose membranes (CNPC-SS12-L3-P25) employing an XYZ3050 platform (Biodot, Irvine, CA, USA). Immunoreagents were diluted in phosphate buffer (20 mM, pH 7.4) to a concentration of 0.5 mg/mL and were dispensed at a flow rate of 1  $\mu$ L/cm, keeping 4 mm between the lines. The concentration of 0.5 mg/mL was chosen as the best compromise between signal intensity and non-specific interaction with the GNP and GNS conjugates. After coating, membranes were dried at 37 °C for 60 min under vacuum. The conjugate pads were previously saturated with borate buffer supplemented with 0.25% Tween 20, 2% sucrose and 0.02% sodium azide, dipped into the proper probe solution at optimal optical density (2–3) and dried for 3 h at room temperature, protecting from light and dust. Strips were composed by layering the NC membrane with the sample and the conjugate pads and cutting (4 mm width) by CM4000 guillotine (Biodot, Irvine, CA, USA). Strips were finally included into plastic cassettes (Kinbio, Shangai, China) to obtain stand-alone LFIA devices.

## Serum Samples

Control sera used in the study are listed in Table 4.1.2. Negative, HIV1 and HIV2 positive samples (#10, #8 and #5 respectively) and HIV1 seroconverting positive samples were from Zeptometrix International FDA approved HIV- panels. Samples X (9081-03), Y (9089-06) and Z (9019-03) were taken after 27, 26 and 38 days from infection, respectively.

**Table 4.1.2.** The human serum samples from panels used in the study: one negative (#10), two fully seroconverted samples (#8 and #5) and 3 early-infected HIV1 positive samples.

ID (#)	serotype	Type elapsed from infection (days)	seroconversion
NEG (#10)	negative	-	-
HIV1 (#8)	HIV1	>?	complete
HIV2 (#5)	HIV2	>?	complete
X (9081-03)	HIV1	27	In progress
Y (9089-06)	HIV1	26	In progress
Z (9019-03)	HIV1	38	In progress

## The LFIA Test Procedure

Serum samples of the HIV panels were diluted 1/10 in the dilution buffer (phosphate 20 mM buffer, pH 7.4 with 1% BSA, 1% Tween20); 80  $\mu$ L of the mixture was applied to LFD device

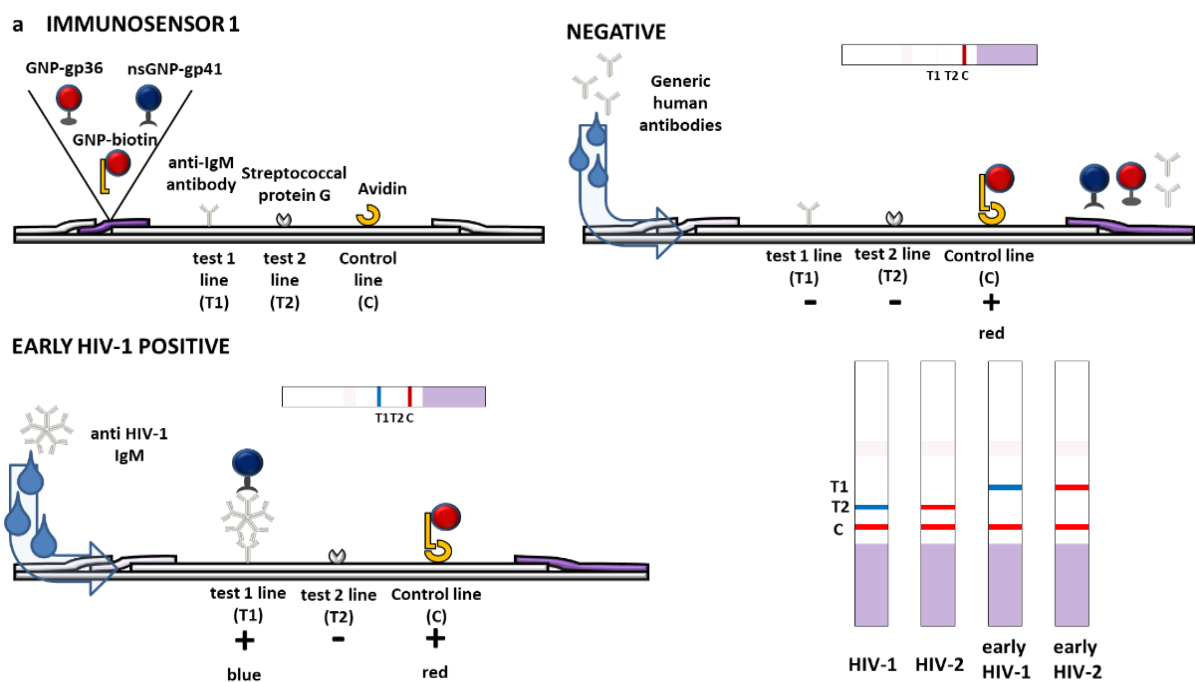
and the results were visually inspected after 10 min. The immunosensors were designed as qualitative ones, and the results were interpreted visually by comparing the colour of the test lines with the one of the control lines to judge on the red/blue balance. However, to confirm visual judgements, we estimated red and blue colour contribution to mixed lines by a RGB analysis, as detailed in F. Di Nardo et al. [35]. Briefly, the blue and red colour channels were plotted as histograms and a threshold approach was applied to count the number of pixels for each channel. The R and B colours measured at the test line were normalized by the corresponding one measured at the control line.

## 4.1.3 Results and Discussion

### Design of Multimodal LFIA Immunosensors

Preliminary, we investigated the applicability of the signal resolution obtained through labelling the specific recognition elements with dual colour gold nanomaterials (e.g., gold nanospheres, GNP and gold nanostars, GNS). Gold nanomaterials were prepared as previously reported [18,20] and were characterized through transmission electron microscopy and UV-vis absorption. GNP were almost spherical, mono-dispersed and with a mean diameter of ca. 30 nm (Figure 4.1.2a-b) The UV-vis spectrum showed a localized surface plasmon resonance (LSPR) band centred at 525 nm (Figure 4.1.2e), which corresponded to the perception of a ruby red colour. GNS exhibited a blue colour that was confirmed by the position of the LSPR band centred at ca. 620 nm (Figure 4.1.2f). Transmission electron microscopy images showed nanomaterials characterized by larger diameters (ca. 70 nm) and a star-like structure (Figure 4.1.2c-d). We employed them in a conventional two-line serotyping strip based on the double antigen approach and labelled the HIV1 specific antigen (gp41) with GNS (blue) and the HIV2 specific antigen (gp36) with GNP (red), respectively (Figure 4.1.2e-f) to verify the functionality of the in-house prepared LFIA strips and of probes. The model LFIA was a rapid test for HIV1/2 antibodies detection developed by Primalab SA and under evaluation of the performance according to EC directive 2009/886 [36]. In the traditional format, the antigens were both labelled by GNP and deposited to form two test lines (Figure 4.1.1a). Selectivity and affinity of the labelled antigens towards HIV1/2 antibodies and their specificity towards other serum components (e.g., other proteins) were then assumed based on the performance of the traditional test. To this aim, a protocol to prepare stable gold nanomaterials-antigen probes was established. In particular, the use of high amounts of casein (5%) in the saturation step stabilized GNP and GNS antigen conjugates and protected from non-specific interactions. However, the use of casein to protect gold nanoprobe from aggregation, led to the partial inhibition of the specific interactions, as well. Finding a compromise in the use of casein was needed to equilibrate the S/N ratio. The amount of capture bioreagents and probes was adjusted to reach clearly perceivable colouring at test lines. The blue GNS-gp41 and the red GNP-gp36 probes were mixed and included in the conventional xLFIA for HIV serotyping. An additional (red) GNP-biotin probe was added to form the signal at the control line, which comprised avidin. In fact, the setup of the double antigen approach includes an independent system to create the control line, not influenced by the specific probes, which can be regarded as a limitation of the strategy. There was no mutual interference between the different signal reporters; no false positive signals were observed by applying the control negative sample, while HIV1 and HIV2 positive samples were correctly assigned based on the position of the line and on the colour of the probe (Figure 4.1.1b). The mix of probes was then applied to a device with a single test line formed by a mix of the two antigens to compress the two information items in a single line (Figure 4.1.1c) and to achieve the signal resolution that we also have called “colour-encoding” strategy [35]. If the stability and the absence of mutual interference was maintained no colour change on respect to the two-line system was expected, since HIV-antibodies to gp36 and gp41 are known to do not cross-react with each other [37]. The absence of any false positive results due to non-specific binding and the correct assignment of the serotype based on the “colour code” was verified in these conditions. The colour code

was defined as follows: a red colouring of the test line was interpreted as positivity associated to HIV2 serotype while the blue colour indicated positivity again but due to HIV1 serotype, finally no colouring of the test line meant absence of any serological response and thus negativity (Figure 4.1.1c). Based on the results from these preliminary studies, three different  $x^2$ LFA immunosensors were designed to disclose the potential of the multimodal strategy to combined multiple information in a single device. In this illustration, the prototypes allowed four information items to be obtained from two lines and two probes for the discrimination of the serotype (HIV1/HIV2) and of the class of immunoglobulins IgG/IgM present in the patient' serum. Therefore, we introduced two additional bioligands specific to IgM (anti-human IgM) and IgG (protein G), respectively. Two out of the three immunosensors varied for the role played by immunoreagents (capture or detection) in the typical serological immunometric assay and the third was designed to apply with the double antigen approach. The format of immunosensor 1 included secondary ligands (anti-human IgM and protein G) separately coated on two test lines to capture anti-HIV antibodies. Therefore, the spatial resolution allowed for discriminating the immunoglobulin class. The differentiation of the serotype was realized on each line by employing the two signal reporters, namely GNS-gp41 to reveal HIV1 and GNP-gp36 to reveal HIV2, respectively. The GNP-biotin probe was added to form the control line (Figure 4.1.3a, Immunosensor 1). In the second immunosensor, the role of capturing and detection reagents was inverted. Hence, the first gp36-coated test line captured anti-HIV2 antibodies and the second gp41-coated test line captures anti-HIV1 ones. By using (blue) GNS-anti-IgM antibody and (red) GNP-protein G as the signal reporters, we expected a blue response for very early infection and a progressive red shift proportional to seroconversion rate on each test line. (Figure 4.1.3b, immunosensor 2).



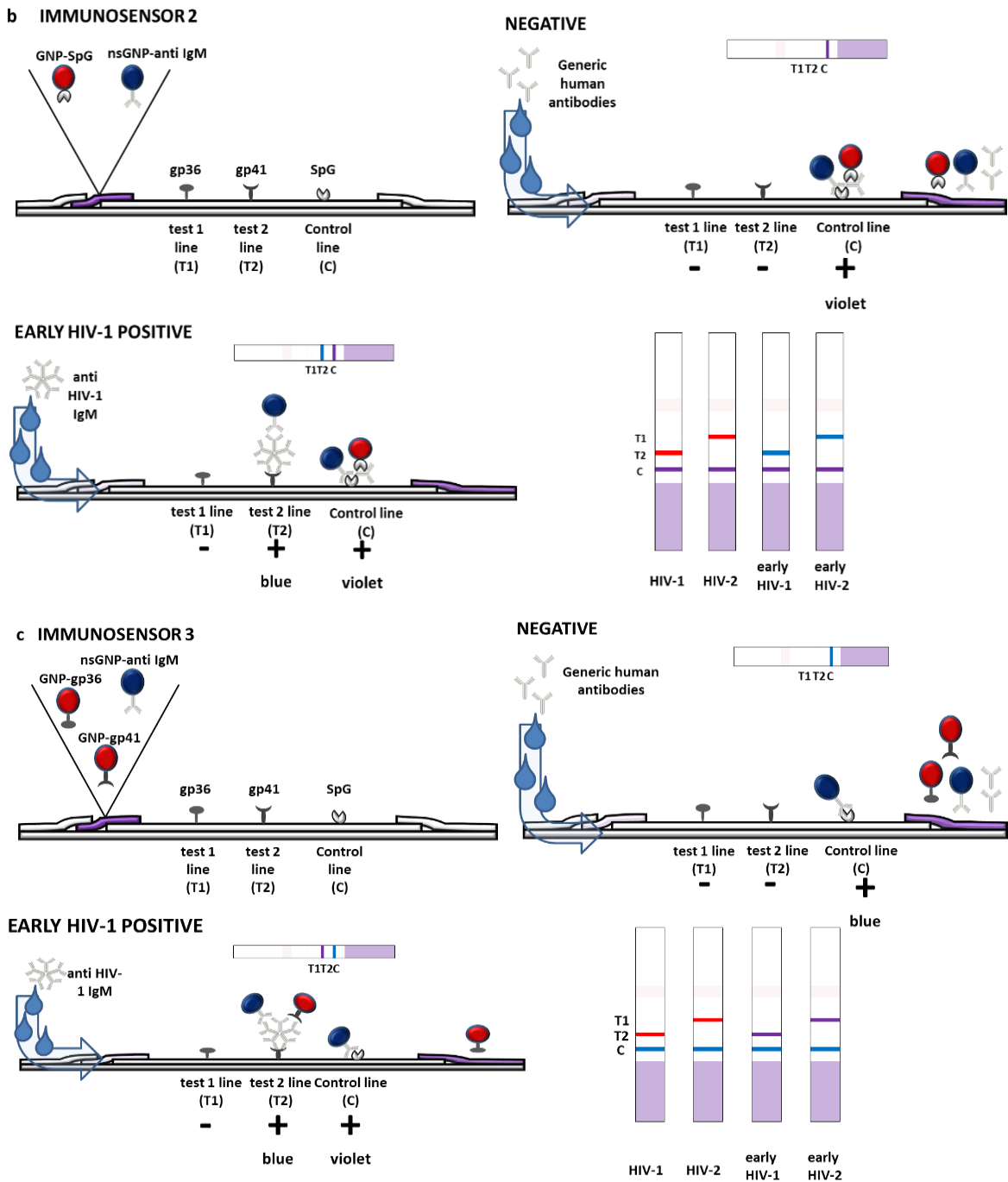


**Figure 4.1.3.** Scheme of the three immunosensors of  $x^2$ LFIA unlocked by the combining spatial resolution with dual colour gold nanomaterials. The binding and coloured results expected for a negative and a HIV1 positive sample containing both IgG and IgM (early infected) is depicted. The three formats varied for the role played by immunoreagents as follows: (a) HIV-specific antigens were labelled and reacted with anti-HIV antibodies in the sample, which were then captured by anti-IgM and protein G coated to form test lines (immunosensor 1); (b) HIV-specific antigens were coated and captured anti-HIV antibodies, which were revealed by labelled anti-IgM and protein G (immunosensor 2); and (c) HIV-specific antigens were both coated and labelled and reacted with anti-HIV antibodies to form a double antigen sandwich. The addition of the blue-labelled anti-IgM to the red-labelled antigen provided the additional information on the infection stage (immunosensor 3).

In this second format, the control line comprised protein G, which was able to capture both probes and then directly reflected their stability. The set-up of coated antigens described for immunosensor 2 was maintained for designing immunosensor 3. Instead, the mix of signal reporters included the two antigens both labelled with GNP (red) and the anti-human IgM

labelled with blue GNS. The total antibody response was red coloured such as in a conventional double-antigen assay based on the two-line set-up. However, the presence of specific IgM turned the colour of the line to violet, due to accumulation of the blue GNS-anti-human IgM probes. (Figure 4.1.3c, Immunosensor 3).

### Performance of the x<sup>2</sup>LFIA Immunosensors for HIV Serotyping and Discrimination of the Infection Stage

To investigate the multiplexing capability of the three multimodal approaches and to compare their performance, the x<sup>2</sup>LFIA formats were tested by control human sera (Table 4.1.2). Results were visually observed and captured by common smartphone cameras. The images were processed and compared as relative intensities of the red and blue components of the colorimetric signal. The comparative study on immunosensors 1 and 2, which differed for the role played by immunoreagents, and with immunosensor 3, which differed for the assay format, were investigated in terms of detectability and specificity in correlation to what is expected by the control samples. Details on the immunosensors format and on interpretation of the results are reported in Table 4.1.3. The three x<sup>2</sup>LFIA formats were tested with control human sera and with samples from seroconversion panels, which were supposed to contain anti-HIV1 IgM. The outcomes considerably differed among the immunosensor formats, both in the colour encoding response and in terms of detectability (Figure 4.1.4). All x<sup>2</sup>LFIA immunosensors correctly assigned the fully seroconverted positive samples and did not show non-specific binding with the negative sample. Immunosensor 1 provided a single test line at the T1 (IgM) or at the T2 (IgG) position, blue coloured for HIV1 positive and red coloured for HIV2 positive sera, respectively.

**Table 4.1.3.** Schematic of the xLFIA and x<sup>2</sup>LFIA formats used in this study.

Format	Reporter				Capture			
	adsorbed on GNP		adsorbed on GNS	optical density (ratio) <sup>b</sup>	Test line 1 (T1)	Test line 2 (T2)	Control line (C)	
xLFIA	A	gp36	biotin <sup>a</sup>	gp41	2.5 (1+0.5+1)	gp36	gp41	avidin
	B	gp36	biotin <sup>a</sup>	gp41	2.5 (1+0.5+1)	gp36/gp41	-	avidin
x <sup>2</sup> LFIA	1	gp36	biotin <sup>a</sup>	gp41	2.5 (1+0.5+1)	anti-IgM	protein G	avidin
	2	protein G		anti-IgM	3 (1.5+1.5)	gp36	gp41	protein G
	3	gp36	gp41	anti-IgM	3 (1+1+1)	gp36	gp41	protein G

<sup>a</sup> to form the control line

<sup>b</sup> the probes were mixed to reach the optical density in variable ratio

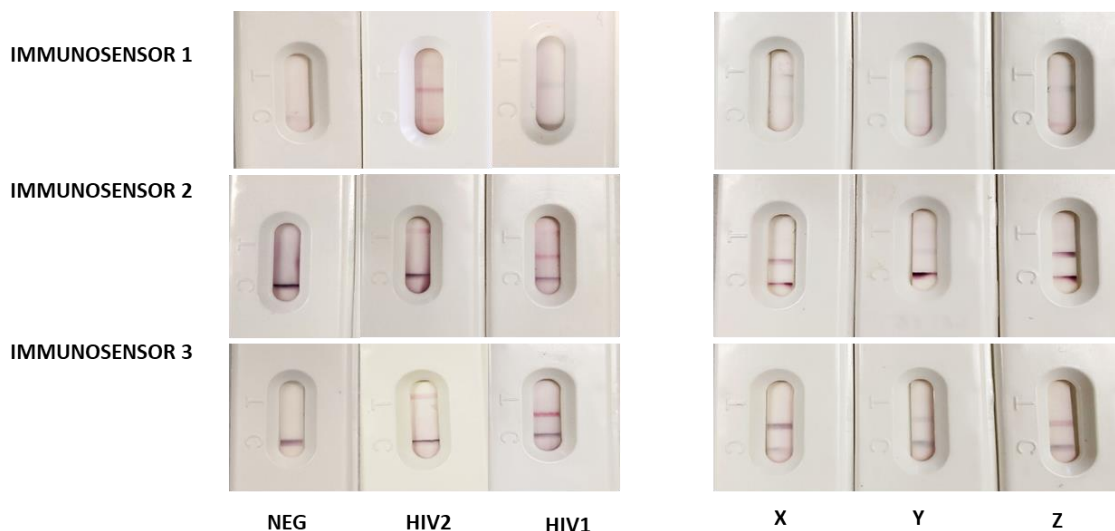


**Figure 4.1.4.** Multiple information obtained from the  $x^2$ LFIA immunosensors on the negative (NEG), two fully seroconverted (HIV1 and HIV2) and the three early infected (X, Y and Z) serum samples from Zeptomatrix panels.

The seroconverting samples resulted in two blue-coloured test lines, where the variable IgM/IgG ratio reflected in the relative intensities of the two lines (Figure 4.1.4, immunosensor 1 and 4.1.5a). Samples X and Y showed colouring at both lines, with a slight disproportion in favour of T1 (IgM) for sample X. On the contrary, sample Z showed an evident preponderance of IgG. In general, largely lower intensities were obtained from immunosensor 1 on respect to other two  $x^2$ LFIA formats. Immunosensor 2 provided a red coloured test line at T2 position for HIV1 positive, and at T1 position for HIV2 positive sera, respectively. The three seroconverting samples resulted in a single violet test line at the T2 (HIV1) position, which intensity varied (Figure 4.1.4, immunosensor 2). Serum X provided a signal at the test with a larger contribute of the blue probe compared to the control line indicating the prevalence of blue-labelled anti-hIgM, while serum Z showed a red-purple colour at the test line, witnessing the prevalence of the red GNP-protein G reporter (Figure 4.1.5b). Compared to immunosensor 1, using anti-hIgM antibody and protein G for signal reporting and the antigens as capturing agents instead of the opposite increased the detectability (Figure 4.1.4). We argued that the difference on the fact that probes disposed of longer time to bind to their targets (because they are mixed with the sample and reacts during flowing), while capturing reagents should be particularly efficient as the time of contact with the target was limited. Alternatively, we guessed that the different flow rate of the HIV-specific antibodies compared to non-specific immunoglobulins present in the serum samples determined the observed behaviour. In immunosensor 1, anti-HIV antibodies bound to the GNP-labelled antigen and were slower than unbound non-specific antibodies. Probably, the faster unbound immunoglobulins reached the lines of capturing reagents first so inhibiting the following binding of the specific ones linked to GNPs. In immunosensor 2 all immunoglobulins bound to GNP probes and moved with the same velocity, while immunosensor 3 eliminated the competing binding of non-specific immunoglobulins, as it included only HIV-specific bioreagents. Immunosensor 1 and 2 furnished spatially separated outcomes, as a “two-line x two-colour” response. Immunosensor 3 showed a single red coloured test line, at the T2 position for HIV1 positive and at the T1 position for HIV2 positive sera, respectively.



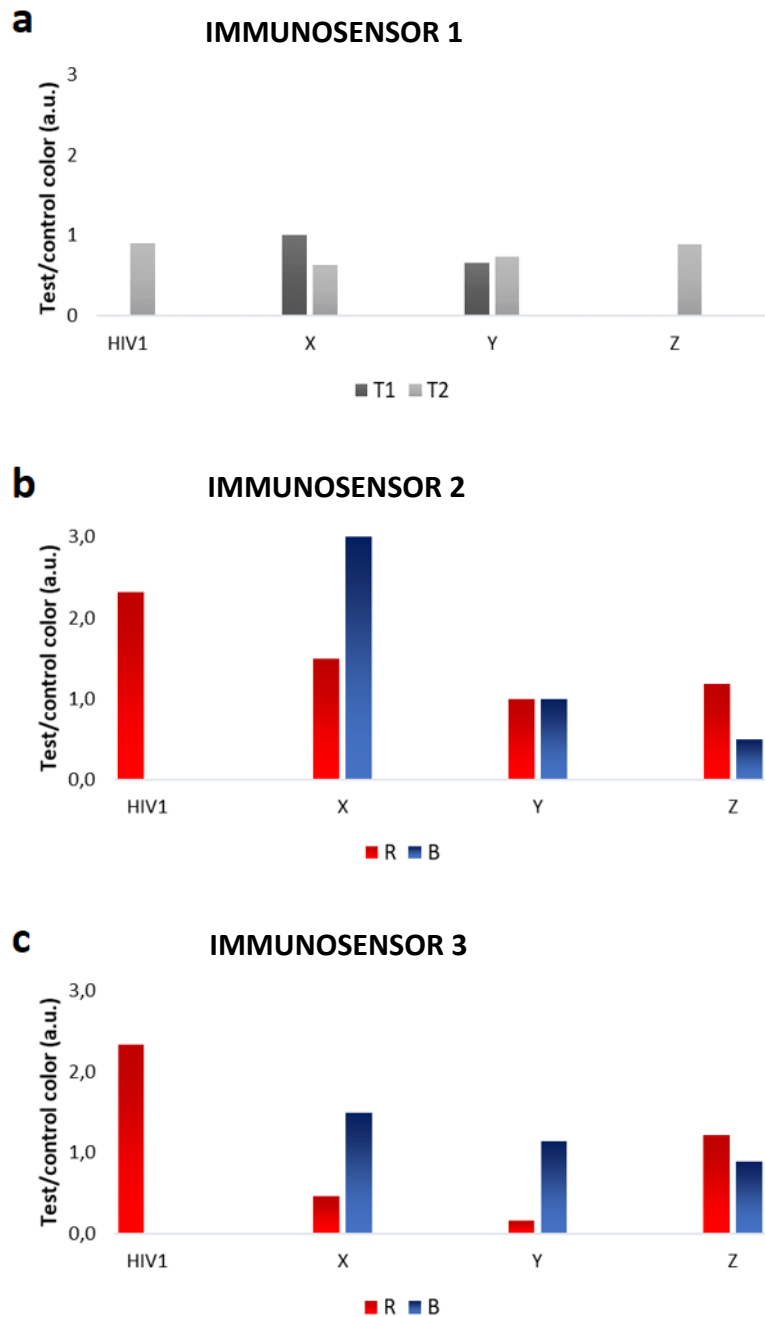


**Figure 4.1.5.** Colour intensities for test and control lines were measured as the total number of pixels for Format 1 and reported as a function of line positioning (a). Red (R) and blue (B) components were extracted and measured for Formats 2 and 3 as reported in F. Di Nardo et al. [18] (b-c). Colour at test lines was normalized for the corresponding one measured at the control line.

In the absence of anti-HIV IgM, the results from the immunosensor 3 overlapped the ones from immunosensor 2. Serum belonging to individuals with late infections (HIV1 and HIV2) provided a response indicating the sole presence of immunoglobulins G (Figure 4.1.4, immunosensor 3). Compared to immunosensor 2, the signal intensity was almost unaffected by the change of the probes. The sensitivity was supposed to be boosted by the double antigen approach; however, we did not observe relevant improvements, except on serum Y. The presence of the blue GNS-anti-hlgM antibody provoked a violet-shift in the presence of anti-HIV IgM, because of the additive effect of red and blue probes. The three seroconverting

samples resulted in a single intense violet test line at the T2 (HIV1) position. Patient Z resulted in an almost red line, suggesting the prevalence of IgG, while sample X and Y provided a blue-shifted line, which indicates the presence of IgM, besides IgG (Figure 4.1.5c). The classification of the three seroconverting sera (X, Y, and Z) was coherent within the immunosensor formats. Anti-HIV1 IgM significantly contributed to the serological response for patients X and Y indicating very early infection, while patient Z was assigned as having predominantly IgG, though some IgM were also revealed. The outputs of  $x^2$ LFIA agreed with the time of blood collection from infection, as well. Serum Z (9019-03) was a sample taken 38 days from infection, while the other two were from earlier sampling (27, 26 days). The colour evaluation, though susceptible of subjective interpretation was facilitated by the comparison to the control line, which acted as a sort of internal reference, besides confirming the validity of the assay, as usual. Immunosensor 3 appeared to be more sensitive to IgM variation in a narrow interval compared to others. Noticeably, immunosensor 3 added the discrimination ability by simply including an additional probe with differentiable signal to the standard double antigen set-up. Multiplexing LFIsA based on differentiable colour probes are conventionally based on using latex microparticles embedding dyes with different adsorption peaks [38], [39] and noble metal nanoparticles showing localized plasmon resonance bands at variable wavelengths according to their size and shapes [40]–[42]. However, these approaches involves aligning several lines along the strip to differentiate the target to be detected and the colour of the probe is simply exploited to help simplifying the visual reading of the result. Here, we designed a two-parameter strategy, in which the colour and space resolution were combined to expand the number of analytes simultaneously detected by a single device. As a proof-of-concept, dual colour probes (i.e., red and blue gold nanomaterials) were combined with a two-line arrangement of capturing ligands to reach a  $2 \times 2$  analytical platform ( $x^2$ LFIA). Theoretically, the strategy could be implemented by including more than two different probes and by aligning more than two test line. In this regard, the use of latex microspheres embedding dyes will increase further the number of information that could be furnished by a single device.

## 4.1.4 Conclusions

The use of LFIA devices for HIV diagnosis is well-established and largely diffuse, as such we use it as the model as a proof-of-concept to verify the feasibility of the multimodal approach combining the spatial resolution with colour encoding to expand the multiplexing capability of the LFIA platform. Taking advantage of the unique spectroscopic properties of gold nanomaterials and the simplicity of their conjugation with proteins (antigens and antibodies) by passive adsorption, three  $x^2$ LFIA immunosensors were designed. Immunosensors were explored in this work, to investigate the ability of differentiating serum samples belonging to individuals with different serological conditions. We investigated, also, the impact of changing the role of immunoreagents, in the  $x^2$ LFIA set-up, showing that it strongly affected the detectability of the assay. Moreover, we designed a strategy enabling the discrimination of the antibody class that can be embedded in the conventional double antigen strategy. In conclusion, we introduced a general route to enlarge the number of information achievable within one LFIA strip as the product of the number of probes for the number of lines, conserving the one-step and equipment-free operability.

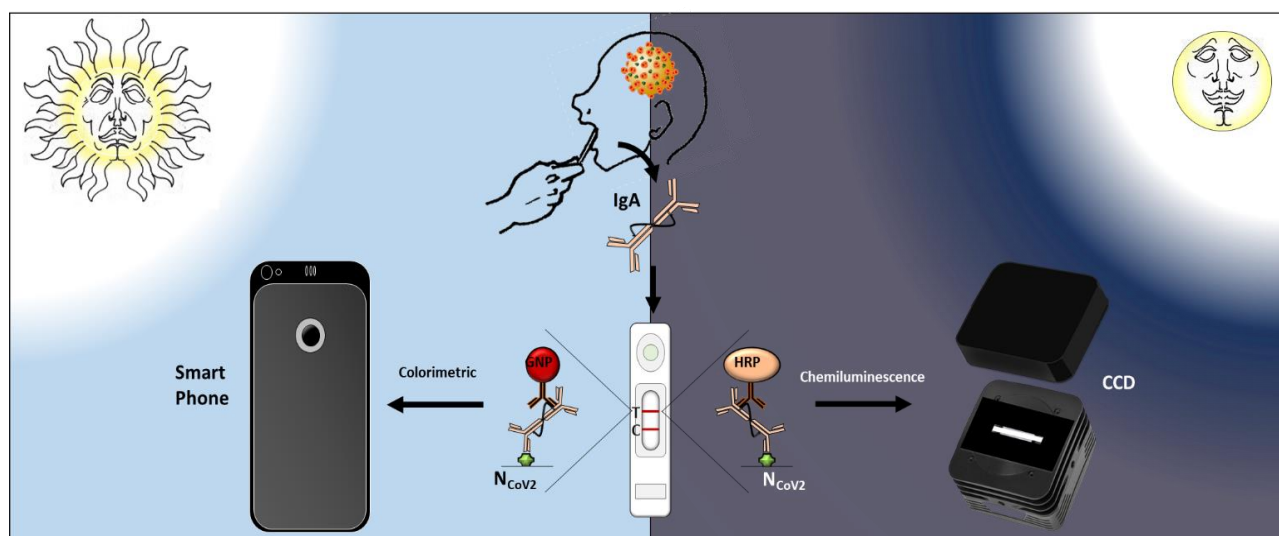
### Acknowledgments

The authors acknowledge the Ministry of University and Research of Italy (PRIN: 2017Y2PAB8) for financial support.

## 4.2



### Dual approach detecting IgA to SARS CoV-2



Based on

A. Roda, S. Cavallera, F. Di Nardo, D. Calabria, S. Rosati, P. Simoni, B. Colitti, C. Baggiani, M. Roda, L. Anfossi, **Dual lateral flow optical/chemiluminescence immunosensors for the rapid detection of salivary and serum IgA in patients with COVID-19 disease**, *Biosensors and Bioelectronics*, 172, 2021, 112765, ISSN 0956-5663, <https://doi.org/10.1016/j.bios.2020.112765>.

### Abstract

*To accurately diagnose COVID-19 infection and its time-dependent progression, the rapid, sensitive, and non-invasive determination of immunoglobulins A specific to SARS CoV-2 in saliva and serum is needed to complement tests that detect immunoglobulins G and M. We have developed a dual optical/chemiluminescence format of a lateral flow immunoassay (LFIA) immunosensor for IgA in serum and saliva. A recombinant nucleocapsid antigen specifically captures SARS CoV-2 antibodies in patient specimens. A labelled anti-human IgA reveals the bound IgA fraction. A dual colorimetric and chemiluminescence detection enables the affordable and ultrasensitive determination of IgA to SARS CoV-2. Specifically, a simple smartphone-camera-based device measures the colour signal provided by nanogold-labelled anti-human IgA. For the ultrasensitive chemiluminescence transduction, we used a contact imaging portable device based on cooled CCD, and measured the light signal resulting from the reaction of the HRP-labelled anti-human IgA with a H<sub>2</sub>O<sub>2</sub>/luminol/enhancers substrate. A total of 25 serum and 9 saliva samples from infected and/or recovered individuals were analysed by the colorimetric LFIA, which was sensitive and reproducible enough for the semi-quantification of IgA in subjects with a strong serological response and in the early stage of COVID-19 infection. Switching to CL detection, the same immunosensor exhibited higher detection capability, revealing the presence of salivary IgA in infected individuals. For the*

*patients included in the study (n = 4), the level of salivary IgA correlated with the time elapsed from diagnosis and with the severity of the disease. This IgA-LFIA immunosensor could be useful for noninvasively monitoring early immune responses to COVID-19 and for investigating the diagnostic/prognostic utility of salivary IgA in the context of large-scale screening to assess the efficacy of SARS CoV-2 vaccines.*

#### **4.2.1 Architecture of the test**

For IgA analysis, we developed an LFIA based on a SARS CoV-2- specific antigen (the nucleocapsid protein N), which is used as the capturing reagent and anchored onto the detection membrane. The N protein was selected among antigenic targets of the SARS coronavirus structure in a previous work of the group because it is highly immunogenic and abundantly expressed [43] and according to its reactivity to human sera from COVID-19 patients [44]. The optical immunosensor includes an anti-human IgA (anti-IgA) labelled with gold nanoparticles (GNP) to reveal the IgA bound to the N antigen. The anti-SARS CoV-2 IgA in the serum/saliva sample is captured by the N antigen and stained by the GNP-labelled anti-IgA, forming a coloured band at the test line. For signal transduction and quantification of the GNP-based LFIA, we imaged the coloured strip using a smartphone camera. We reported the results in RGB scale under optimized reading conditions using the smartphone flash, as previously reported [45]. To achieve higher detectability compared to the coloured GNP probe, we used the same LFIA format, but with chemiluminescence (CL) detection mediated by a horseradish peroxidase (HRP) labelled anti-IgA and an enhanced CL luminol/H<sub>2</sub>O<sub>2</sub>/enhancer substrate [46]. The CL signal to noise was improved compared to the previous system by adding the CL substrate solution directly to the control and test line area after the LFIA run, thus minimizing the nonspecific light signal. The CL emitted light is measured by an ultrasensitive cooled CCD in contact imaging mode, with the data reported in relative light units. Both immunosensor platforms allow data recording and can be used for comparative evaluation within the same patient to monitor the presence of IgA in saliva and/or serum and connect this data to disease progression and a possible decrease in viral load. The non-invasive collection of saliva is a further strength of this test. This work describes the first dual LFIA platform for the rapid detection of salivary and serum IgA and illustrates its application for SARS CoV-2 infection.

## 4.2.2 Materials and methods

### Immunoreagents, chemicals and materials

Gold (III) chloride trihydrate (ACS reagent), mouse antihuman immunoglobulin A monoclonal antibody A ( $\alpha$ -chain specific), protein A from *Staphylococcus aureus* (SpA), sucrose, and bovine serum albumin (BSA) were obtained from Merck group (Darmstadt, Germany). Tween 20 and other chemicals were purchased from VWR International (Milan, Italy). Nitrocellulose membranes with cellulose adsorbent pad, blood separator, and saliva-specific sample pads were purchased from MDI Membrane Technologies (Ambala, India). Glass fibre conjugate pads were obtained from Merck Millipore (Billerica, MA, USA). HRP-labelled mouse antihuman IgA were obtained from Invitrogen, Thermo Fisher Scientific (Rockford, IL). The Supersignal ELISA Femto CL substrate for HRP was purchased from Thermo Fisher Scientific Inc. (Rockford, IL).

### The IgA-LFIA strip

The LFIA strip for the colorimetric IgA-LFIA biosensor is schematized in Figure 4.2.1a. The nucleocapsid (N) antigen (1 mg/ml in phosphate buffer 20 mM pH 7.4) and staphylococcal protein A (SpA, 0.5 mg/ml in phosphate buffer) were spotted at 1  $\mu$ l/cm by means of a XYZ3050 platform (Biodot, Irvine, CA, USA) to form the test (TL) and control (CL) lines, respectively. The preparation of the recombinant nucleocapsid protein was previously described in [44] and is described in Chapter 3.1.2. For the optical IgA-LFIA, gold nanoparticles (GNP) of ca. 30 nm diameter and SPR band centred at 525 nm were synthesised as reported in Chapter 3.1.2 and conjugated to a murine anti-human IgA by passive adsorption, as previously reported [47]. Briefly, the anti-IgA was added to a pH-adjusted GNP solution (pH 8.5), in the proportion 10  $\mu$ g per ml of GNP (optical density, OD 1). The uncovered GNP surface was saturated with BSA and the GNP-anti IgA were concentrated and recovered by centrifugation. GNP-labelled anti-IgA were pre-adsorbed in the conjugate pad (0.1 ml/cm). Sample pad, conjugate pad, the membrane, and adsorbent pad were overlapped, and strips were cut (4 mm-width). The strips were inserted into plastic cassettes. For the chemiluminescence detection, strips were prepared as described above, except for the detection reagent (anti-human IgA-HRP, from Sigma-Aldrich), which was pre-adsorbed onto the conjugate pad as diluted 1/1000 with phosphate buffer. In addition, the membrane was saturated with 1% BSA after line deposition. In this case, the cassette was not used to maximise the contact between the strip and the CL reader.

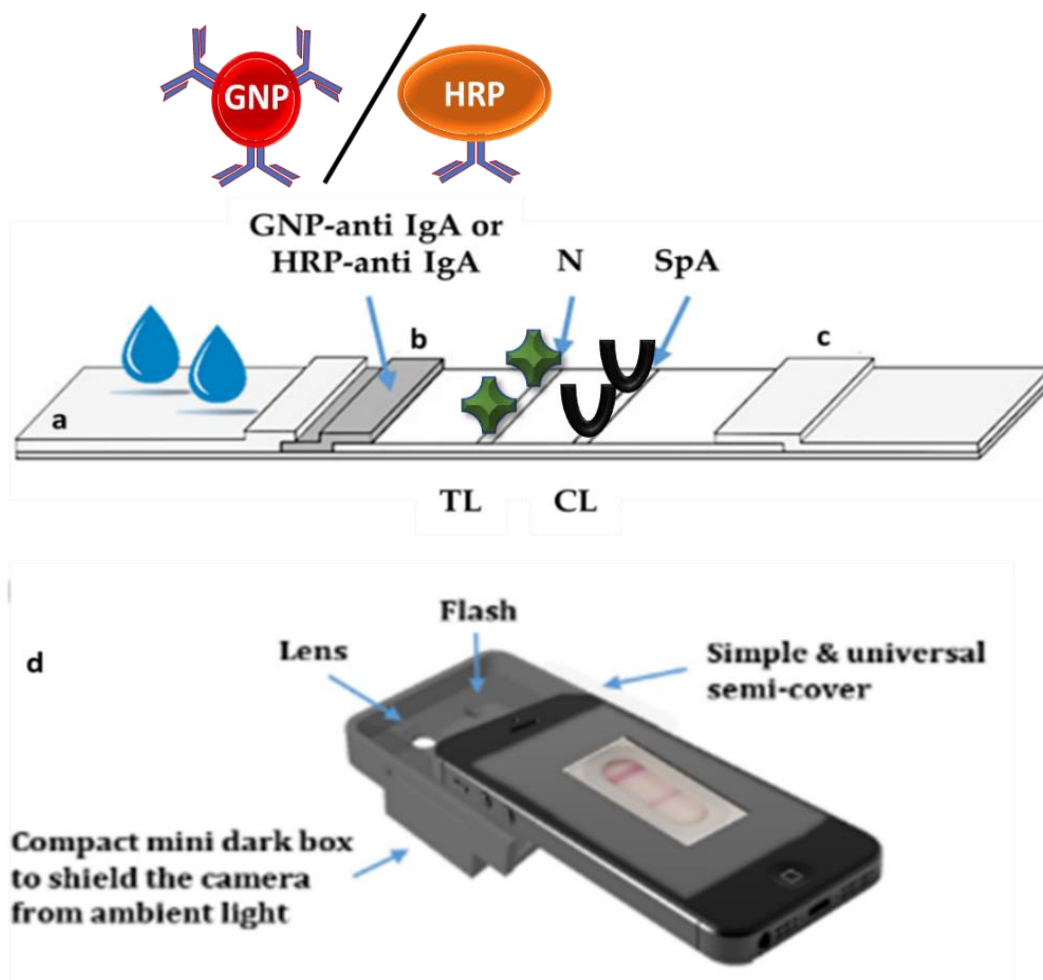


**Figure 4.2.1.** Scheme of: (a) the LFIA strip to detect anti- SARS CoV-2 IgA. The serum or salivary sample is applied to the sample pad and flows longitudinally by capillarity, (b) resuspends the probe (GNP or HRP-labelled anti human IgA), and the mix flows through the detection membrane where it encounters the nucleocapsid protein (N) on the test line (TL) and the staphylococcal protein A (SpA) on the control line (CL). (c) The adsorbent pad provides the capillary force and collect the liquid excess. Anti-SARS CoV-2 IgA in the sample are selectively captured at the TL and stained by the probe. The CL captures the probe, regardless of the presence of the target immunoglobulins in the sample. (d) the smartphone reader used for the optical immunosensor.

### Optical LFIA to detect IgA specific to SARS CoV-2

Serum and saliva were diluted by 1:10 and 1:5 v/v with Tris-glycine buffer 0.1 M (pH 8, with 0.2% casein and 1% Tween 20 added), respectively. 80  $\mu$ l of diluted specimen were used and LFIA results were visually inspected at 15 min from sample application. For the (semi)-quantitative evaluation of TL colour, the LFIA strip was placed in front of the back-illuminated CMOS based camera, inside the mini dark box to exclude ambient light, and an additional lens was used to focus the T and C line image and standardize the reading using the smartphone flash illumination. A semi-cover and a mini dark box adaptable to any smartphones were made with 3D printing (Figure 4.2.1d). Images were then digitally processed using an RGB scale to quantify the colour.

## Smartphone colour reader

Any smartphone with a back-illuminated CMOS (e.g., iPhone X) can be used. A 3D-printed semi-cover frame allows it to be fixed to the reader. The target area corresponding to the test and control line of the LFIA membrane strip was uniformly illuminated by adding a PDMS light diffuser in the dark box (40 × 40 × 60 mm) placed in front of the smartphone flash. The focal distance of the smartphone camera has been reduced to ~ 10 mm by adding a 0.4X wide-angle two-lenses optical element with a 140° viewing angle. The dark box avoids interference from ambient light. The smartphone holder can be ad-hoc designed according to the smartphone model to ensure correct positioning of the smartphone camera and flash. The dark box is then connected to the lab-case and the smartphone is inserted in the holder. 15 minutes upon delivering the sample on the LFIA strip, the image is acquired with the dedicated app Camera FV-5 Lite using the following acquisition parameters: ISO 800, time exposure 0.1 s, flash on. The image is saved in TIFF format and then quantitative image analysis is performed using the freeware software ImageJ v.1.46. For each image, a region of interest (ROI) corresponding to the sample chamber containing the test and control lines of the LFIA membrane was selected, then the RGB values were computed and converted to HSV. The Saturation (S) value of HSV colour space obtained from the image acquired in a different area of the membrane (background signal) was then subtracted from the S value obtained 60 s after sample application, to obtain a corrected S value.

## CL-LFIA to detect IgA anti SARS CoV-2

For the chemiluminescence detection, we developed a simple device based on a cooled CCD camera with the LFIA strip in contact with the sensor using a fibre optic faceplate. The scheme of the device is reported in Figure 4.2.2a and further detailed in the following paragraph. The assay was carried out in a similar way to the colorimetric assay. At 15 min from sample application, the activity of the HRP labelled antibody was measured by overlaying a transparent glass fibre pad on the detection membrane (Figure 4.2.2b).

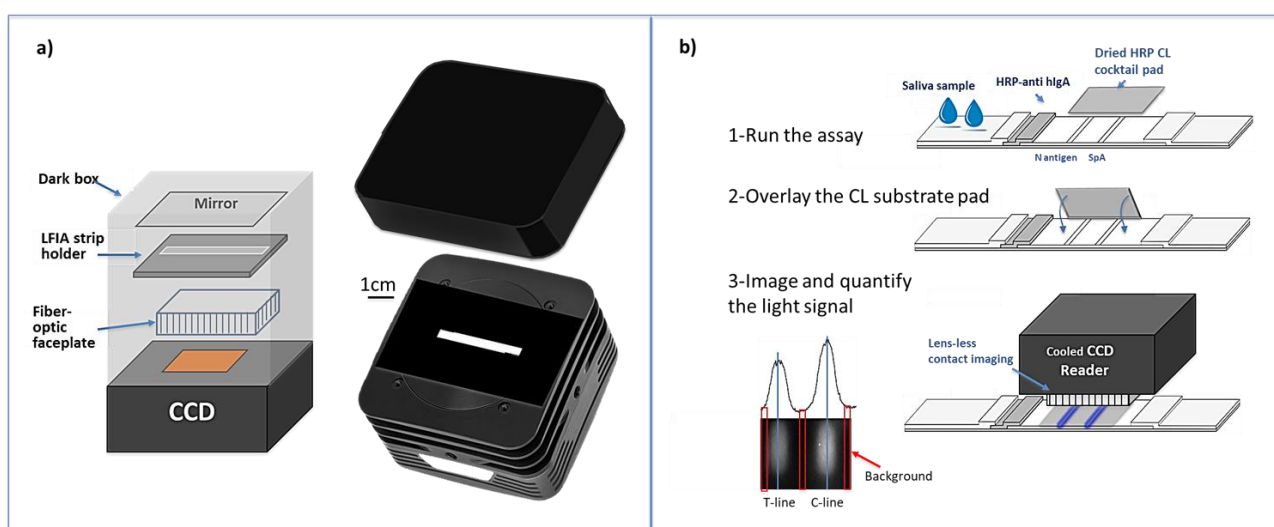




**Figure 4.2.2.** a) Scheme of the CCD camera, and b) protocol for the ultra-high sensitivity CL detection of salivary IgA by the developed immunosensor. After completion of the IgA-LFIA (1), a transparent glass fibre pad (which was pre-impregnated with the CL cocktail substrate) is placed onto the membrane at the test and control line (2). 20 µl of water is added to assist the re-suspension of the CL substrate; finally, the strip is placed in the holder of the cooled CCD camera for lens-free imaging detection (3). The pad contained freeze-dried sodium perborate, luminol, and p-iodophenol [48]. Once in contact with the LFIA strip and following the addition of 20 µl of water, this delivered the CL substrate with production of light [49]. The cooled CCD reader and device were placed in contact with the strip, imaged, and the CL analytical signal was quantified and expressed in relative light units (RLU).

## CCD device for CL imaging

A commercially available CCD camera (ATIK 11000, ATIK Cameras, New Road, Norwich) equipped with a large format, high resolution monochrome CCD sensor (Kodak KAI 11002, sensor size 37.25 × 25.70 mm) cooled by a two-stage Peltier element to reduce thermal noise was used as CL signal reader. The CCD camera was modified by replacing its upper part (i.e., the CCD sensor compartment and the optical glass window) with an aluminium cartridge housing assembly, which ensures the correct alignment of the CCD sensor with the LFIA strip during the measurement and avoids interference from ambient light. The cartridge housing assembly is composed by the strip holder and a lower fixing plate. The inner cavity of the strip holder fits the dimensions of the LFIA cartridge and ensures the close contact between the LFIA cartridge and the fibre optic faceplate. The fibre optic faceplate (size 26 × 26 × 13 mm, Edmund Optics, Barrington, NJ) is fabricated in polymethylmethacrylate (PMMA) and conveys the CL signal from the LFIA strip to the CCD sensor. Inside the upper surface of the dark box is inserted a mirror to ensure the complete and total collection of the light, increasing the sensitivity of the measurement. The CL reader is connected to a laptop via an USB interface. The ImageJ software was used also for CL signal elaboration. The mean photon emission of the C-line and T-line of the LFIA strip was measured and corrected for the mean background signal measured in adjacent areas expressed in CL intensity in arbitrary units.

## Serum and Saliva samples

Ten negative human serum samples (collected before the SARS CoV-2 outbreak) and twenty-five positive human serum samples were collected within the SIRIT project.

Positive human sera were selected according to: i) having a positive rRT-PCR analysis on a swab sample, ii) having been assigned as positive for anti-SARS CoV-2 IgG by a validated ELISA serological kit (ERADIKIT™ COVID19-IgG)[50].

Blood samples were collected by venepuncture at variable times from the rRT-PCR diagnosis. Serum was immediately obtained from blood and stored at -20°C until analysis. Some individuals (n= 17) recovered in the meantime (according to the rRT-PCR negative). Saliva samples were collected by means of the SalivaBio Oral Swab (Salimetrics, CA, USA), immediately refrigerated, and stored for at least 24 h at 20 °C before centrifugation and analysis.

Four volunteers provided saliva samples. They were members of a COVID-19 infected family, including father, mother, and two sons (38 and 42 years old). They provided saliva after 2 and 4 weeks from diagnosis by rt-PCR.

Subject #1, male, age 71, was affected by severe symptoms, with typical COVID-19 clinical manifestation and chest radiology. He was hospitalized in an intensive care unit for 10 days, and then clinically recovered after 4 weeks.

Subject #2, female, age 64, wife of #1, was affected by moderate/mild symptoms and did not require hospitalization. After 3 weeks from diagnosis fully recovered.

Subjects #3, age 35 male, and Subject #4, age 43 male, brothers, and sons of #1 and #2 were asymptomatic or with only slight fatigue and caught manifestation.

Subjects 1-4 were also tested by a serological assay for the content of IgM and IgG in serum, at two weeks from diagnosis (Table 4.2.1).

The saliva of an additional subject, called 'unknown', male, age 30, was available in the lab, as it was collected on February 2019, before COVID-19 outbreak, for another study. The subject had shown clinical manifestation attributable to the SARS CoV-2 infection but recovered before the outbreak and was not submitted to rt-PCR testing.

All donors provided informed consent to the use of their specimens. Donors of specimen collected before the outbreak were contacted and were requested to provide informed consensus for this study.

## 4.2.3 Results and discussion

### IgA-LFIA to detect IgA specific to SARS CoV-2 in serum

We made an optical LFIA prototype to selectively detect anti-SARS CoV-2 IgA and verified its ability to detect the target immunoglobulins in the serum of COVID-19-infected individuals. The immunosensor included the recombinant nucleocapsid protein from SARS CoV-2 to capture antibodies specific to the virus, and an anti-IgA labelled with GNP as the probe (Figure 4.2.1a). The test line (TL) was coloured in the presence of anti-SARS CoV-2 IgA in the specimen because these interacted with the immobilized N antigen and were stained by the GNP probe. SpA, which captured the excess of the labelled anti-IgA used as the control line (CL) to confirm the validity of the assay. The diagnostic specificity of the IgA-LFIA was checked by analysing ten serum samples that did not contain any SARS CoV-2-specific antibodies, as they were collected before the COVID-19 outbreak. No false positive results were recorded (false positive rate = 0/10). Regarding positive samples, we analysed 25 human sera from infected individuals as confirmed by rt- PCR. Blood samples were collected at variable times from the diagnosis, and some individuals ( $n = 17$ ) recovered in the meantime. Of the 25 serum samples analysed by the IgA-LFIA, 15 showed colouring of the TL and were then assigned as IgA positive. Compared to the rt-PCR method, the false negative rate was calculated as 40.0% (10/25). Interestingly, plotting the number of IgA positive samples on the timeframe from infection diagnosis and recovery showed two clear patterns (Figure 4.2.3a).

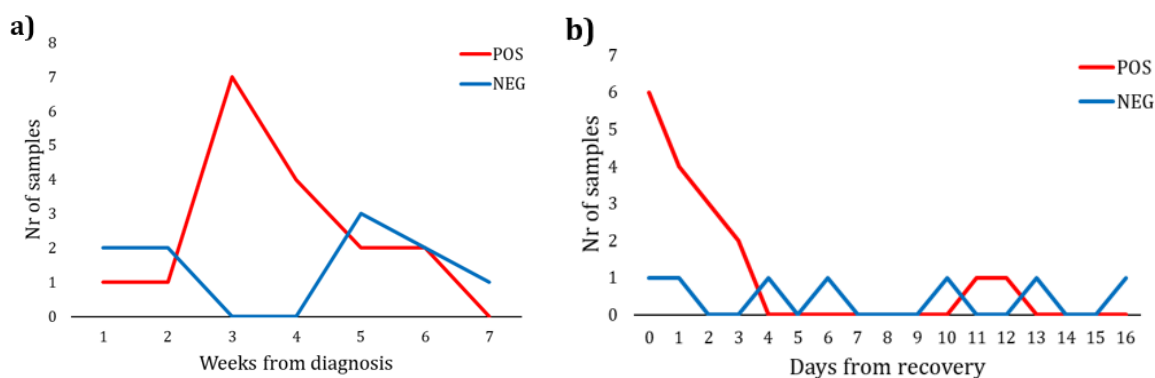


**Figure 4.2.3.** Results obtained from the optical immunosensor for the serum IgA specific to SARS-CoV-2 as a function of time from infection (a) and recovery (b) diagnosis.

Although the number of analysed samples is not sufficient to draw conclusions, we speculate that IgA increased during the second week of infection, peaked at the fourth week, and then declined. This trend is congruent with that reported by [51]. We also observed that the IgA level in serum dramatically dropped a few days after recovery (Figure 4.2.3b). Repeatability of the IgA-LFIA was studied by analysing, in duplicate, three serum samples classified as positive and three as negative, then calculating the mean relative standard deviation (RSD%). Stability was investigated by analysing one positive and one negative serum sample at 0, 7,

and 28 days from IgA-LFIA device construction. The quantification of TL colour of positive results by the smartphone camera showed that the colorimetric IgA-LFIA provided sufficiently repeatable and stable results (RSD% for duplicate analysis of three positive samples were below 15%, and the TL intensity varied within 10% over four weeks from IgA-LFIA construction).

### IgA-LFIA to detect anti-SARS CoV-2 IgA in saliva

The prototype IgA-LFIA for serum was then adapted and optimized for use with saliva specimens. To this end, the blood separator sample pad included in the original device was replaced by a new sample pad recommended by the manufacturer for application to saliva and oral fluid specimens. In previous studies, we demonstrated that replacing the optical detection of GNP with chemiluminescence detection of HRP as a label increased the detectability of LFIA assays by a factor of ten [49]. We also showed that detectability could be further increased by using a more sensitive CL reader based on cooled CCD instead of the smartphone camera [45]. Therefore, we modified the IgA-LFIA to enable CL detection. Although increasing the sensitivity, the CL detection required an additional step to add the CL substrate. The flow of the CL substrate across the strip produced a strong background light, which affected the signal-to-noise ratio and largely increased the analysis time. To overcome these limitations, we designed a semi-integrated system in which the dried CL substrate was embedded in a glass fibre pad. The pad was layered onto the detection zone of the strip, after completion of sample run, so that the CL substrate was quickly dissolved by the wet LFIA. To help the CL substrate resuspension, we also added a drop of water. This innovative and effective strategy was adapted from J. Deng et al. [48], who set up a self-contained system, by which CL reagents were stored in dried form and were delivered directly on the detection zone by a microfluidic system aimed at revealing the enzymatic amplification of nucleic acids. Here, the addition of the CL in a very confined zone showed clear advantages over the traditional flow strategy as the CL substrate was background light was strongly reduced thus increasing the signal-to-noise ratio. In addition, by avoiding running the CL substrate by capillarity, the assay was accelerated, completing in 15 min instead of in over 30 min. The IgA-LFIA prototypes were applied to analyse nine salivary samples. Eight were from four COVID-19 infected individuals and were collected at two and four weeks from rt-PCR diagnosis (Table 4.2.1). One sample was collected in February for another study from a donor who, in that period, showed symptoms compatible with COVID-19 (cough, fever, fatigue, difficulty breathing), but without confirmation of COVID-19. The detectability of both colorimetric and CL IgA-LFIA was sufficient to reveal salivary IgA in three out of the five subjects with good agreement between the detection methods (Figure 4.2.4a and b). In particular, the IgA-LFIA with both colour and CL detection revealed very high salivary IgA levels in subject #1, who was known to have a severe disease. Salivary IgA to SARS CoV-2 were present at 2 and 4 weeks from diagnosis and confirmed the tendency for levels to decrease over the time from infection observed for serum samples.

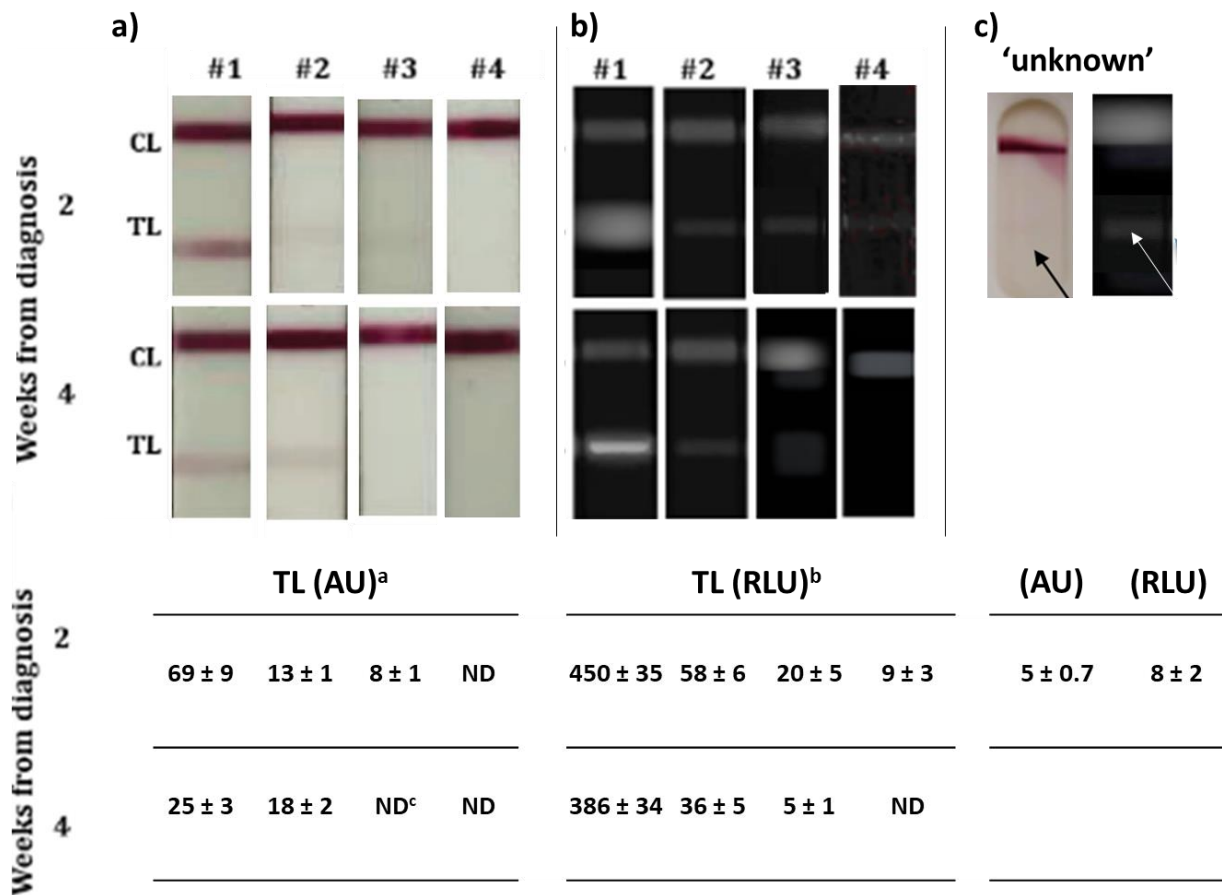
**Table 4.2.1.** Salivary anti-SARS CoV-2 IgA measured by the colorimetric and chemiluminescence IgA-LFIA immunosensor in four subjects affected by Covid-19 infection after 2 and 4 weeks from the diagnosis. Salivary

IgA data were compared with serum anti-SARS CoV-2 IgG and IgM as evaluated by a commercial colorimetric rapid test (KHB Covid-19 antibody from Techno Genetics).

Subject	Weeks from diagnosis	Salivary IgA (RLU) <sup>a</sup>	Salivary IgA (AU) <sup>b</sup>	Serum IgG	Serum IgM
#1	2	450 ± 35	69 ± 9	POS ++	POS +
	4	386 ± 34	25 ± 3	POS +++	POS ++
#2	2	58 ± 6	13 ± 1	POS +++	POS ++
	4	36 ± 5	18 ± 2	POS +++	POS +
#3	2	20 ± 5	8 ± 1	NA <sup>c</sup>	NA
	4	5 ± 1	ND	POS +++	NEG
#4	2	9 ± 3	ND	NA	NA
	4	ND <sup>d</sup>	ND	POS++	NEG

<sup>a</sup> RLU: relative light units; <sup>b</sup> AU arbitrary units; <sup>c</sup> NA: not available; <sup>d</sup> ND: below detectability (threshold: mean background signal + 2 standard deviation)

Subject #2, who reported moderate symptoms, showed IgA levels lower than #1. However, they were still detectable, especially by the ultrasensitive CL immunosensor. For subject #2, the intensity of the colour signal increased with time, while the CL detection confirmed the trend of IgA levels decreasing over time. Subjects #3 and #4 provided results that were undetectable by colorimetric detection (a slight signal, close to the limit of detection, was shown for subject #3 only after 2 weeks from infection). In contrast, the CL detection highlighted the presence of salivary IgA in these subjects, at least in the early stage of the disease (week 2). The improved detectability of the CL immunosensor was confirmed by the “unknown” sample. The results were at the limit of detection for colorimetric IgA-LFIA but were clearly positive with CL detection (Figure 4.2.4c). For the subjects with a known clinical condition, the results obtained by the IgA-LFIA correlate with severity of symptoms and with serum IgG and IgM levels, as measured by a reference assay (Table 4.2.1). Moreover, the new IgA-LFIA suggested that the ‘unknown’ sample belonged to a subject that was presumably infected in an early phase of the pandemic. These few data suggest that salivary IgA can be quantified using both detection strategies.



<sup>a</sup> arbitrary units as measured by the smartphone reader, <sup>b</sup> relative lights units as measured by CCD camera, <sup>c</sup> not detectable (threshold: mean background signal + 2 standard deviation)

**Figure 4.2.4.** IgA-Anti-SARS CoV-2 detection in saliva from four donors as detected by the colorimetric (a) and chemiluminescent (b) IgA-LFIA sensor. A salivary sample collected in Italy before the outbreak of the pandemic from an individual with symptoms compatible with those of COVID-19 was shown to contain apparent anti-SARS CoV-2 IgA by the IgA-LFIA (c). Data are shown as the mean ± std dev of two replicate measurements.

## 4.2.4 Conclusions

The colorimetric immunosensor coupled with the smartphone reading enabled the one-step affordable determination of IgA levels in saliva. The introduction of a simple and portable tool to quantify the colour at the test line, which is related to amount of IgA, can help providing information on the severity and/or stage of the infection. The CL detection using the portable cooled back illuminated CCD camera provided higher sensitivity and more accurate quantification compared to the smartphone BI-CMOS allowing to detect positivity in subjects with low serological response. Moreover, compared to previously reported CL-LFIA, we improved the signal-to-noise ratio by adding the CL substrate directly on the detection zone instead of flowing it across the LFIA strip. This modification of the protocol strongly reduced the light background and increasing detectability. The new protocol also halved the time required to complete the assay (15 min instead of 30 min), which is a major improvement for point-of-care testing. The combination with an optical/chemiluminescence transduction device also provides the option of connectivity for promptly communicating the patient's infection and/or recovery status. Although IgG and IgM specific to SARS CoV-2 have been reported to be present in saliva, as well as IgA, and can then be considered as possible markers for the non-invasive detection of the serological response to the infection [52], [53], to the best of our knowledge, this is the only immunosensor for detecting salivary IgA reported to date. This is because almost all the rapid serology tests focus on serum IgM, IgG, and total immunoglobulins. However, the lack of information regarding the clinical meaning of salivary IgA measurements and the intrinsic variability of the composition of the oral fluids, which can affect the result especially in quantitative analysis, are current limitation of the method and needs further investigation. The validation of the developed IgA-LFIA by considering a larger number of samples is ongoing. Hopefully, results will be also double-checked by lab-scale tests to measure IgA (though methods for salivary IgA are still unavailable). The availability of this rapid test may enable additional largescale studies on the significance of IgA as biomarkers of immune response to COVID-19 and the non-invasive screening to assess the efficacy of new vaccines. In the context of precision medicine, it could also support a personalized therapeutic intervention.

### Acknowledgments

Authors thank Dr. Domenico Cosseddu from A.O. Ordine Mauriziano, Ospedale Umberto I di Torino (Turin, Italy) and Dr. Franca Fagioli from Department of Public Health and Pediatrics, Regina Margherita Children's Hospital, University of Turin (Turin, Italy) for providing serum samples and their characterization by rRT-PCR. and Grace Fox for the English style editing.

## References

- [1] "Rapid Tropical Parasitic Tests - Malaria Pf/Pan Ag Rapid Test CE Wholesale Trader from Hyderabad." <https://www.biochromescientific.com/rapid-tropical-parasitic-tests.html> (accessed Feb. 03, 2021).
- [2] G. Matusali *et al.*, "Performance of rapid tests in the management of dengue fever imported cases in Lazio, Italy 2014-2019," *Int. J. Infect. Dis.*, vol. 99, pp. 193–198, Oct. 2020, doi: 10.1016/j.ijid.2020.07.008.
- [3] C. C. Lin *et al.*, "Diagnostic value of immunoglobulin g (igg) and igm anti-hepatitis e virus (hev) tests based on hev rna in an area where hepatitis e is not endemic," *J. Clin. Microbiol.*, vol. 38, no. 11, pp. 3915–3918, 2000, doi: 10.1128/jcm.38.11.3915-3918.2000.
- [4] X. Wang *et al.*, "Efficacy of a combination of HBV RNA and HBeAg in predicting HBeAg seroconversion in patients treated with entecavir for 144 weeks," *Int. J. Infect. Dis.*, vol. 99, pp. 171–178, Oct. 2020, doi: 10.1016/j.ijid.2020.07.031.
- [5] H. Gaines *et al.*, "Detection of immunoglobulin M antibody in primary human immunodeficiency virus infection," *AIDS*, vol. 2, no. 1, pp. 11–15, 1988, doi: 10.1097/00002030-198802000-00002.
- [6] R. Dhakal, K. Gajurel, C. Pomares, J. Talucod, C. J. Press, and J. G. Montoya, "Significance of a positive toxoplasma immunoglobulin M test result in the United States," *J. Clin. Microbiol.*, vol. 53, no. 11, pp. 3601–3605, Nov. 2015, doi: 10.1128/JCM.01663-15.
- [7] M. L. Landry, "Immunoglobulin M for acute infection: True or false?," *Clin. Vaccine Immunol.*, vol. 23, no. 7, pp. 540–545, Jul. 2016, doi: 10.1128/CVI.00211-16.
- [8] F. Javed, Z. Akram, M. S. Binshabaib, S. S. ALHarthi, S. V. Kellesarian, and F. Vohra, "Is salivary IgA level a potential biomarker for immunosuppression in HIV-positive children? A systematic review and meta-analysis," *Reviews in Medical Virology*, vol. 27, no. 4. John Wiley and Sons Ltd, Jul. 01, 2017, doi: 10.1002/rmv.1933.
- [9] G. D. Tomaras and B. F. Haynes, "HIV-1-specific antibody responses during acute and chronic HIV-1 infection," *Current Opinion in HIV and AIDS*, vol. 4, no. 5. NIH Public Access, pp. 373–379, Sep. 2009, doi: 10.1097/COH.0b013e32832f00c0.
- [10] "COVID-19 IgG/IgM Rapid Test | Prima Home Test." [https://primahometest.com/it/covid-19\\_test\\_sierologico](https://primahometest.com/it/covid-19_test_sierologico) (accessed Feb. 03, 2021).
- [11] "COVID-19 IgM/IgG Rapid Test – BioMedomics Inc." <https://www.biomedomics.com/products/infectious-disease/covid-19-rt/> (accessed Feb. 03, 2021).
- [12] "SARS-CoV-2 (Covid-19): Diagnosis by IgG/IgM Rapid Test Clinisciences." <https://www.clinisciences.com/it/read/newsletter-26/sars-cov-2-covid-19-diagnosis-by-2264.html> (accessed Feb. 03, 2021).
- [13] "UNAIDS data 2020 | UNAIDS." <https://www.unaids.org/en/resources/documents/2020/unaid-data> (accessed Oct. 01, 2020).
- [14] A. Sands, "Diagnostics for HIV diagnosis," 2015, Accessed: Oct. 01, 2020. [Online]. Available: <https://www.ncbi.nlm.nih.gov/books/NBK316033/>.
- [15] T. C. Granade, S. Workman, S. K. Wells, A. N. Holder, S. M. Owen, and C. P. Pau, "Rapid detection and differentiation of antibodies to HIV-1 and HIV-2 using multivalent antigens and magnetic immunochromatography testing," *Clin. Vaccine Immunol.*, vol. 17, no. 6, pp.



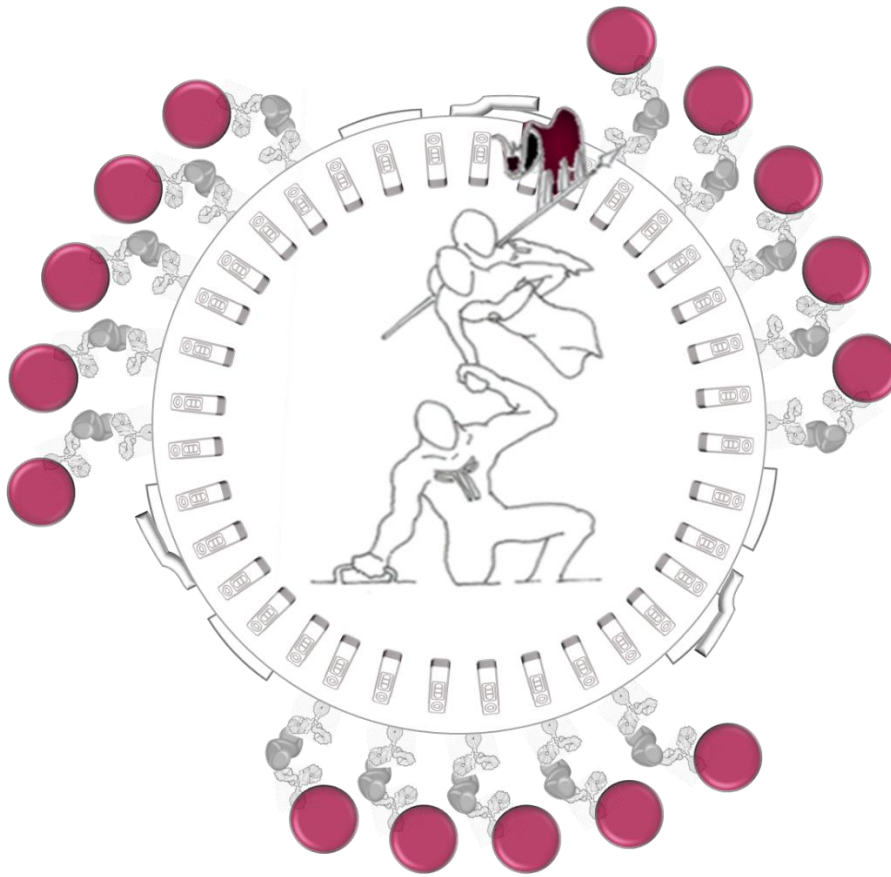
1034–1039, Jun. 2010, doi: 10.1128/CVI.00029-10.

- [16] B. Bottiger *et al.*, “Envelope Cross-Reactivity between Human Immunodeficiency Virus Types 1 and 2 Detected by Different Serological Methods : Correlation between Cross-Neutralization and Reactivity against the Main Neutralizing Site,” vol. 64, no. 7, pp. 3492–3499, 1990.
- [17] N. Meda *et al.*, “Serological diagnosis of human immunodeficiency virus in Burkina Faso: Reliable, practical strategies using less expensive commercial test kits,” *Bull. World Health Organ.*, vol. 77, no. 9, pp. 731–739, 1999.
- [18] J. Peng, Y. Wang, L. Liu, H. Kuang, A. Li, and C. Xu, “Multiplex lateral flow immunoassay for five antibiotics detection based on gold nanoparticle aggregations,” *RSC Adv.*, vol. 6, no. 10, pp. 7798–7805, 2016, doi: 10.1039/C5RA22583C.
- [19] N. A. Taranova, A. N. Berlina, A. V Zherdev, and B. B. Dzantiev, “Traffic light immunochromatographic test based on multicolor quantum dots for the simultaneous detection of several antibiotics in milk,” *Biosens. Bioelectron.*, vol. 63, pp. 255–261, 2015, doi: <https://doi.org/10.1016/j.bios.2014.07.049>.
- [20] S. Song *et al.*, “Multiplex Lateral Flow Immunoassay for Mycotoxin Determination,” *Anal. Chem.*, vol. 86, no. 10, pp. 4995–5001, May 2014, doi: 10.1021/ac500540z.
- [21] B. Liu *et al.*, “A gold immunochromatographic assay for simultaneous detection of parathion and triazophos in agricultural products,” *Anal. Methods*, vol. 10, no. 4, pp. 422–428, 2018, doi: 10.1039/C7AY02481A.
- [22] Y. Sun *et al.*, “Development of an immunochromatographic lateral flow strip for the simultaneous detection of aminoglycoside residues in milk,” *RSC Adv.*, vol. 8, no. 17, pp. 9580–9586, Feb. 2018, doi: 10.1039/c8ra01116h.
- [23] Q. Wang, Y. Liu, M. Wang, Y. Chen, and W. Jiang, “A multiplex immunochromatographic test using gold nanoparticles for the rapid and simultaneous detection of four nitrofurantol metabolites in fish samples,” *Anal. Bioanal. Chem.*, vol. 410, no. 1, pp. 223–233, Jan. 2018, doi: 10.1007/s00216-017-0714-y.
- [24] M. Z. Zhang *et al.*, “Development of a colloidal gold-based lateral-flow immunoassay for the rapid simultaneous detection of clenbuterol and ractopamine in swine urine,” *Anal. Bioanal. Chem.*, vol. 395, no. 8, pp. 2591–2599, Dec. 2009, doi: 10.1007/s00216-009-3181-2.
- [25] Y. Qin, R. Sha, Y. Feng, and Y. Huang, “Comparison of double antigen sandwich and indirect enzyme-linked immunosorbent assay for the diagnosis of hepatitis C virus antibodies,” *J. Clin. Lab. Anal.*, vol. 34, no. 11, p. e23481, Nov. 2020, doi: 10.1002/jcla.23481.
- [26] T. Xiang *et al.*, “A novel double antibody sandwich-lateral flow immunoassay for the rapid and simple detection of hepatitis C virus,” *Int. J. Mol. Med.*, vol. 30, no. 5, pp. 1041–1047, Nov. 2012, doi: 10.3892/ijmm.2012.1121.
- [27] L. Stamatatos, L. Morris, D. R. Burton, and J. R. Mascola, “Neutralizing antibodies generated during natural HIV-1 infection: good news for an HIV-1 vaccine?,” *Nat. Med.*, vol. 15, no. 8, pp. 866–870, Aug. 2009, doi: 10.1038/nm.1949.
- [28] H. E. Prince, C. Yeh, and M. Lapé-Nixon, “Utility of IgM/IgG ratio and igg avidity for distinguishing primary and secondary dengue virus infections using sera collected more than 30 days after disease onset,” *Clin. Vaccine Immunol.*, vol. 18, no. 11, pp. 1951–1956, Nov. 2011, doi: 10.1128/CVI.05278-11.
- [29] Cucunawangsih, N. P. H. Lugito, and A. Kurniawan, “Immunoglobulin G (IgG) to IgM ratio in secondary adult dengue infection using samples from early days of symptoms onset,” *BMC Infect. Dis.*, vol. 15, no. 1, p. 276, Jul. 2015, doi: 10.1186/s12879-015-1022-9.

- [30] D. Daskalakis, "HIV diagnostic testing: Evolving technology and testing strategies," *Top. Antivir. Med.*, vol. 19, no. 1, pp. 18–22, 2011.
- [31] D. Zhang *et al.*, "Quantitative and ultrasensitive detection of multiplex cardiac biomarkers in lateral flow assay with core-shell SERS nanotags," *Biosens. Bioelectron.*, vol. 106, pp. 204–211, May 2018, doi: 10.1016/j.bios.2018.01.062.
- [32] M. Calderón-Santiago *et al.*, "Human sweat metabolomics for lung cancer screening," *Anal. Bioanal. Chem.*, vol. 407, no. 18, pp. 5381–5392, 2015, doi: 10.1007/s00216-015-8700-8.
- [33] T. Bansal, A. Pandey, D. Deepa, and A. K. Asthana, "C-reactive protein (CRP) and its association with periodontal disease: A brief review," *J. Clin. Diagnostic Res.*, vol. 8, no. 7, pp. 21–24, 2014, doi: 10.7860/JCDR/2014/8355.4646.
- [34] T.-T. Tsai, T.-H. Huang, N. Y.-J. Ho, Y.-P. Chen, C.-A. Chen, and C.-F. Chen, "Development of a multiplex and sensitive lateral flow immunoassay for the diagnosis of periprosthetic joint infection," *Sci. Rep.*, vol. 9, no. 1, p. 15679, 2019, doi: 10.1038/s41598-019-52051-6.
- [35] F. Di Nardo *et al.*, "Colour-encoded lateral flow immunoassay for the simultaneous detection of aflatoxin B1 and type-B fumonisins in a single Test line," *Talanta*, vol. 192, no. July 2018, pp. 288–294, 2019, doi: 10.1016/j.talanta.2018.09.037.
- [36] European Commission, "COMMISSION DECISION of 27 November 2009 amending Decision 2002/364/EC on common technical specifications for in vitro diagnostic medical devices," *Off. J. Eur. Union*, no. 3, 2009.
- [37] S. Y. Shin, M. K. Lee, S. Y. Kim, S. Y. Jang, and K.-S. Hahm, "The use of multiple antigenic peptide (MAP) in the immunodiagnosis of human immunodeficiency virus infection," *IUBMB Life*, vol. 43, no. 4, pp. 713–721, Nov. 1997, doi: 10.1080/15216549700204521.
- [38] M. Zhu, Y. Jia, L. Peng, J. Ma, X. Li, and F. Shi, "A highly sensitive dual-color lateral flow immunoassay for brucellosis using one-step synthesized latex microspheres," *Anal. Methods*, vol. 11, no. 22, pp. 2937–2942, Jun. 2019, doi: 10.1039/c9ay00944b.
- [39] J. Fitzgerald, P. Leonard, M. Danaher, and R. O'Kennedy, "Rapid Simultaneous Detection of Anti-Protozoan Drugs Using a Lateral-Flow Immunoassay Format," *Appl. Biochem. Biotechnol.*, vol. 176, no. 2, pp. 387–398, May 2015, doi: 10.1007/s12010-015-1582-6.
- [40] F. Di Nardo, C. Baggiani, C. Giovannoli, G. Spano, and L. Anfossi, "Multicolor immunochromatographic strip test based on gold nanoparticles for the determination of aflatoxin B1 and fumonisins," *Microchim. Acta*, vol. 184, no. 5, pp. 1295–1304, 2017, doi: 10.1007/s00604-017-2121-7.
- [41] C. W. Yen *et al.*, "Multicolored silver nanoparticles for multiplexed disease diagnostics: Distinguishing dengue, yellow fever, and Ebola viruses," *Lab Chip*, vol. 15, no. 7, pp. 1638–1641, Apr. 2015, doi: 10.1039/c5lc00055f.
- [42] J. Kim, X. E. Cao, J. L. Finkelstein, W. B. Cárdenas, D. Erickson, and S. Mehta, "A two-colour multiplexed lateral flow immunoassay system to differentially detect human malaria species on a single test line," *Malar. J.*, vol. 18, no. 1, p. 313, 2019, doi: 10.1186/s12936-019-2957-x.
- [43] W. Zeng *et al.*, "Biochemical characterization of SARS-CoV-2 nucleocapsid protein," *Biochem. Biophys. Res. Commun.*, vol. 527, no. 3, pp. 618–623, Jun. 2020, doi: 10.1016/j.bbrc.2020.04.136.
- [44] S. Cavalera *et al.*, "A multi-target lateral flow immunoassay enabling the specific and sensitive detection of total antibodies to SARS COV-2," *Talanta*, vol. 223, no. Pt 1, Feb. 2021, doi: 10.1016/j.talanta.2020.121737.
- [45] D. Calabria, C. Caliceti, M. Zangheri, M. Mirasoli, P. Simoni, and A. Roda, "Smartphone-based enzymatic biosensor for oral fluid L-lactate detection in one minute using confined

- multilayer paper reflectometry," *Biosens. Bioelectron.*, vol. 94, pp. 124–130, Aug. 2017, doi: 10.1016/j.bios.2017.02.053.
- [46] F. Di Nardo *et al.*, "A fluorescent immunochromatographic strip test using Quantum Dots for fumonisins detection," *Talanta*, vol. 150, pp. 463–468, Apr. 2016, doi: 10.1016/j.talanta.2015.12.072.
- [47] F. Di Nardo, C. Baggiani, C. Giovannoli, G. Spano, and L. Anfossi, "Multicolor immunochromatographic strip test based on gold nanoparticles for the determination of aflatoxin B1 and fumonisins," *Microchim. Acta*, vol. 184, no. 5, pp. 1295–1304, May 2017, doi: 10.1007/s00604-017-2121-7.
- [48] J. Deng, M. Yang, J. Wu, W. Zhang, and X. Jiang, "A Self-Contained Chemiluminescent Lateral Flow Assay for Point-of-Care Testing," *Anal. Chem.*, vol. 90, no. 15, pp. 9132–9137, Aug. 2018, doi: 10.1021/acs.analchem.8b01543.
- [49] M. Zangheri *et al.*, "A simple and compact smartphone accessory for quantitative chemiluminescence-based lateral flow immunoassay for salivary cortisol detection," *Biosens. Bioelectron.*, vol. 64, pp. 63–68, Feb. 2015, doi: 10.1016/j.bios.2014.08.048.
- [50] "ERADIKIT™ COVID19-IgG | In3Diagnostic." <http://www.in3diagnostic.com/en/eradikit-covid19-igg-2/> (accessed Feb. 03, 2021).
- [51] A. Padoan *et al.*, "IgA-Ab response to spike glycoprotein of SARS-CoV-2 in patients with COVID-19: A longitudinal study," *Clin. Chim. Acta*, vol. 507, pp. 164–166, Aug. 2020, doi: 10.1016/j.cca.2020.04.026.
- [52] N. Pisanic *et al.*, "COVID-19 serology at population scale: SARS-CoV-2-specific antibody responses in saliva," *J. Clin. Microbiol.*, vol. 59, no. 1, Jan. 2021, doi: 10.1128/JCM.02204-20.
- [53] B. Isho *et al.*, "Persistence of serum and saliva antibody responses to SARS-CoV-2 spike antigens in COVID-19 patients," *Sci. Immunol.*, vol. 5, no. 52, Oct. 2020, doi: 10.1126/sciimmunol.abe5511.

# Chapter 5



---

## Direct Antigen LFIA

---

## Introduction

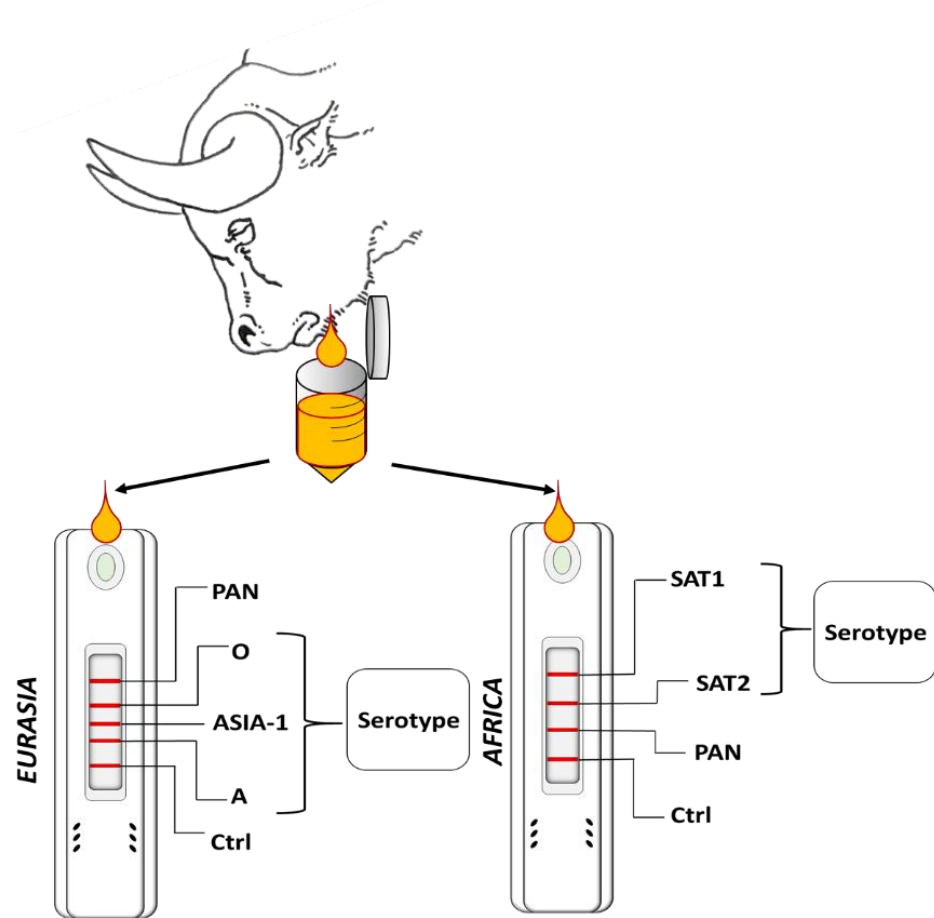
As a general rule for infectious diseases, the antigen detection allows for earlier diagnosis on respect to any antibody tests [1]. As explained in the chapter 1.4.2 the nature of the epitopes directly influences the possibility to set homologous or heterologous sandwich immunoassay, i.e., using the same or a pair of different antibodies. Examples of challenging upgrades of the antigenic tests are the fourth-generation tests for the early diagnosis of HIV [2]. Though working with selected antibodies should assure high sensitivity, the amount of antigen in biologic fluids can be remarkably low and this aspect renders the antigenic tests not always available in practice. In principle, as for some antibody tests (chapter 4.1), there is also the possibility to add serotyping information by using serotype specific antibodies [3]–[5]. This can be made by using multitarget LFIA devices to gather information about diagnosis and serotype of infection in the same device.

In the next chapter, the development of two multitarget devices applied to animal healthcare is reported. Important aspects, such as the phenomena occurring in the case of homologous and heterologous sandwiches, have been explored and reported for the first time. The positioning of the test lines along the strip (i.e., the distance of the reactive zone from the sample application point) was observed to heavily impact sensitivity and specificity of the devices. In addition, the tests are addressed to non-conventional matrices, such as vesicular fluids and extract from epithelium homogenates.

## 5.1



### Direct and Serotyping LFIA for FMDV



Based on

S. Cavallera, A. Russo, B. Colitti, S. Rosati, C. Nogarol, S. Grazioli, E. Brocchi, F. Di Nardo, M. Chiarello, C. Baggiani, L. Anfossi, **Design of multiplexing lateral flow immunoassay based on combining type-specific and pan-specific monoclonal antibodies to the foot-and-mouth disease virus: evidence of a new type of the hook effect.** (*imminent submission*)

#### Abstract

*Multiplex serotyping rapid tests are useful for the characterization of the spread of viral infection pandemics and crucial for differential vaccination. The LFIA is a widely used technique for the screening of foot-and-mouth-disease virus (FMDV), considering the extremely high contagiousness and economic losses entailed by the outbreaks, as it optimally fulfils the requirements of broad screening capacity, quick detection, and prompt intervention. In this work is reported the development of a dual multiplex LFIA for detection and serotyping of FMDV from two macro areas (Eurasia and Africa). The discrimination between the five on the remaining six known serotypes (A,*

*O, Asia-1, SAT-1 and SAT-2) could ensure the almost complete control of the infection spread worldwide.*

### **5.1.1 Architecture of the test**

Here, a multiplexing lateral flow immunoassay for the diagnosis of FMD and the simultaneous identification of major circulating serotypes of the FMD virus was established based on a sandwich-type colorimetric immunoassay. We combined pairs of monoclonal antibodies (mAb) specific to the various FMDV serotypes and a PAN-FMDV mAb, which was employed as the detector and to form a broad-specific PAN-FMDV test line. MAbs used here were selected in previous works and were validated for the use in direct ELISA (enzyme-linked immunosorbent assay) for FMDV diagnosis and serotyping [6]. LFIAs based on some of these mAbs have been also reported previously [3], [7]. In particular, the PAN-FMDV was exploited to set up a general LFIA, which was shown to be able to detect seven FMDV serotypes (O, A, Asia 1, C, SAT 1, and SAT 2) with excellent concordance with the ELISA based on the same antibody [7]. A second device with improved detection capability towards the SAT 2 type was then established, using a pair of type-specific mAbs [8]. With the aim of establishing an ultimate LFIA device capable of detecting and differentiating all circulating FMDV serotypes, we used five mAbs combinations specific for O, A, Asia 1, SAT 1 and SAT 2 serotypes. In addition, the PAN-FMDV was selected to detect C and possibly new, or mutated FMDV types. Therefore, two lateral flow devices (LFIA) were designed following the geographical distribution of FMDV serotypes [9]. One LFIA was aimed at detecting and identifying O, A, Asia-1 strains and was named “Eurasia” according to the endemic area of these types. Serotype C, formerly circulating in the Eurasian countries, was considered as eradicated [10] and was not included in the LFIA. The second device, named “Africa”, enabled the SAT 1 and SAT 2 serotypes detection and differentiation. Both devices also included the PAN-FMDV line reporting on infection from FMDV, regardless the strain involved (including eventually the C-type). Accordingly, five reactive zones were arranged in the LFIA-Eurasia (three serotype-specific, one PAN-specific and a control line to ensure correct operation of the device) and four for the LFIA-Africa (two serotype-specific, one PAN-specific and the control line) to achieve a total of six simultaneous analyses. The PAN-FMDV was used as the detector in the Eurasia LFIA, while an anti-SAT 1 and anti-SAT 2 mAbs labelled with gold nanoparticles were employed to reveal African FMDV types. In our peculiar design, we expressly combined cross-reacting mAbs in each device; in fact, the broad-specific antibody coated to form the PAN-FMDV test line competed with type-specific mAbs for capturing the viral antigens. Moreover, we used both heterologous mAb pairs (i.e., including two different antibodies, one for capturing and the other for detecting the viral antigen) such as in the case of type-specific test lines, and a homologous mAb sandwich for the PAN-FMDV detection of the Eurasia LFIA (Figure 5.1.2a). Also, the Africa LFIA included one heterologous and two homologous combinations of mAbs (Figure 5.1.2c). The rationale was the use of these mAb combinations in the reference ELISAs, which exploited antibody binding to epitopes repeated in the virus. However, we showed for the first time that an “uncommon” hook effect occurring when homologous sandwich assays are realized in the lateral flow immunoassay platform. We investigated the unusual hook effect and proposed a model

for interpreting it. According to the model, we also suggested a general route for designing multiplexing LFIA in which antibodies interconnected each other (because of the cross-reactivity or because the same bioligand is used for capturing and detection).

The two LFIA prototypes, including optimal amounts of each mAb for reaching high sensitivity and specificity, were finally validated by testing epithelium tissue samples collected in Tanzania during 2014-2018 sampling campaigns.



## 5.1.2 Materials and Methods

### Immunoreagents, chemicals and materials

Gold (III) chloride trihydrate (ACS reagent), anti-mouse immunoglobulin G antibody produced in goat (secondary antibody), casein sodium salt from milk, sucrose, and bovine serum albumin (BSA) were obtained from Sigma–Aldrich (St. Louis, MO, USA). Tween20 and other chemicals were purchased from VWR International (Milan, Italy). Nitrocellulose membranes (CNPC-SS12) with cellulose adsorbent pad and glass fibre BR4 sample pads were purchased by MDI membrane technologies (Ambala, India). Glass fibre conjugate pads were obtained from Merck Millipore (Billerica, MA, USA). Statistical calculations were carried out with SigmaPlot 11.0 software. The anti-FMDV mAbs (1F10, HD7, 2H6, 3D8, 3B11, 2A10, 5F6, and 4D12) used for gold nanoparticles conjugates and to form the test lines were available at the Istituto Zooprofilattico Sperimentale della Lombardia e dell'Emilia Romagna “Bruno Ubertyni”. Details on the mAb, including specificity are displayed in Table 5.1.1.

**Table 5.1.1.** Monoclonal antibodies used to develop the ultimate LFIA for FMDV diagnosis and serotyping ([4], [8], [11]).

#mAb	specificity	use in ELISA
1F10	PAN- O, A, Asia1, C, and SAT1	capture and detection
3D8	FMDV-ASIA1	capture
3B11	FMDV-O	capture
2A10	FMDV-O	capture
5F6	FMDV-A	capture
4D12	FMDV-A	capture
2H6	FMDV-SAT1	capture and detection
HD7	FMDV-SAT2	capture and detection

### Preparation of the colorimetric probes: labelling anti-FMDV mAbs with GNP

GNPs with a localized surface plasmon resonance (LSPR) band centered at 525 nm and mean diameter of ca. 30 nm were prepared as reported in Chapter 3.1.2. Signal reporters used in the LFIA devices were prepared by adsorbing the 1F10, 2H6 and HD7 mAbs onto GNPs, respectively. The optimal antibody/GNP ratio for conjugation was determined by the flocculation stress test [12], [13].

Briefly, concentrated sodium chloride is added as the aggregation promoter, to GNP-antibody conjugates obtained from variable GNP/Ab ratios. When the GNP-antibody conjugate is saturated by the mAb, no salt-induced aggregation occurred. According to the stress test, the optimal amount for conjugating 1F10, HD7, and 2H6 mAbs to GNPs were found as 4  $\mu\text{g}$ , 6  $\mu\text{g}$  and 6  $\mu\text{g}$  of the mAb per 1 ml of GNP at optical density (OD) equal to 1 GNP, respectively (details on the flocculation stress test are reported in the following section).

For conjugate preparation, the appropriate amount of the mAb was added to 10 mL buffered GNP (pH 8.5). The solution was gently stirred for 30 min at 37°C. Then, 1mL of 1% (w/v) BSA solution in borate buffer (20 mM, pH 8) was added and the mixture was incubated for 10 min at 37°C. Finally, the GNP–mAb conjugate was recovered by centrifugation (10 min at 7100 $\times$ g), washed once with borate buffer supplemented with 0.1% BSA, and reconstituted in the same buffer supplemented with 2% (w/v) sucrose and 0.25% (v/v) Tween 20. GNP-mAb probes were stored at 4 °C until use.

### Flocculation stress test

The GNP solution obtained from the synthesis was buffered at pH 8.0 with carbonate buffer (50 mM, pH 9,6) and adjusted to OD1. 250  $\mu\text{l}$  was inserted in wells of a microtiter plate and incubated for 30 min with increasing volumes (0-25  $\mu\text{l}$ ) of the various mAbs (0.1 mg/ml in PB). Then, 10  $\mu\text{l}$  of aqueous NaCl (10% v/v) was added and reacted for 10 min to promote aggregation of unstable GNP. The absorbance was read at 540 and 620 nm by a microplate reader (Multiskan™ FC Microplate Photometer, Thermo Fisher Scientific, Waltham, MA USA). The 540 nm absorbance was related to the non-aggregated fraction of GNP, while the absorbance at 620 nm was proportional to aggregation, as the shift of the LSPR band towards higher wavelengths is due to aggregation. The ratio of absorption (540/620) was calculated and plotted as a function of mAb amount added. The optimal amount of the antibody able to stabilize GNP and then to enable preparing a stable mAb-GNP conjugate was defined as the one providing the higher absorbance ratio, i.e., the major proportion of non-aggregated GNP.

The curves obtained for the three mAbs to be labelled with GNP are shown in Figure 5.1.1. The 1F10 mAb showed the typical increase of the stabilization effect over the amount of mAb added: 1  $\mu\text{g}$  of 1F10 (corresponding to 4  $\mu\text{g}$  per 1 ml of GNP) were sufficient to produce a stable probe and were selected for its preparation. Instead, 2H6 and HD7 mAbs showed a bimodal behaviour, with an initial stabilization effect of the increasing amount of the mAb, which peaked at around 1.5  $\mu\text{g}$  (corresponding to 6  $\mu\text{g}$  per 1 ml of GNP) and then decreased. The peak amount was then chosen to prepare the probes.

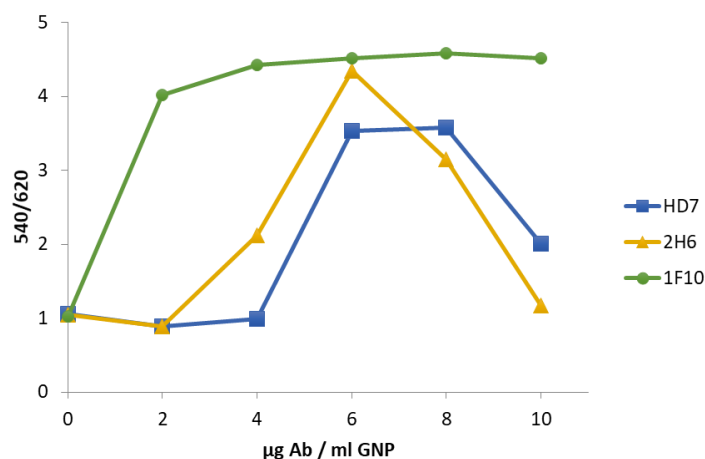


**Figure 5.1.1.** Flocculation stress test conducted for defining the optimal amounts of the 1F10 (green rounds), 2H6 (yellow triangles), and HD7 (blue squares) mAbs to be adsorbed onto GNP for LFIA probes preparation. The absorbance at 540 nm and 620 nm was measured and the ratio plotted versus the amount of mAbs added to 0,25 ml of GNP (OD=1).

## Development of the Eurasia and Africa LFIA devices

Parameters studied for the development of the Eurasia device included: (i) the concentration of the coated mAbs; (ii) the amount of the probe; (iii) the composition of the diluent buffer; and (iv) the material of the sample pad. MAbs were coated at 0,5 and 1 mg/ml. Based on the affinity and cross-reactivity defined by previous studies ref, the capture of type O and type A FMDV required a combination of two mAbs. The same ratios optimized for the ELISA method were employed for the LFIA, namely 1+1 (3B11+2A10) for O-type and 0.75+1 (5F6 + 4D12) for A-type were maintained. In these cases, the concentration of the coated reagent was considered as the individual mAb concentration (i.e., 1 mg/ml 3b11 + 1 mg/ml 2A10 were mixed to form the “1 mg/ml” line). The amount of the probe included in the LFIA was modified by diluting the GNP-1F10 conjugate to OD 0.5, 1 or 2. Definition of the diluent composition was made by considering pH (7.4 vs 8), buffer salt (phosphate vs carbonate) and protein additive (BSA vs casein). Criteria used to judge the results were: no signal appearing at test lines for the negative virus strain (and for non-specific FMDV types) and the highest colour observed at each line for the specific FMDV type. To compare colour intensity, images of the strips were acquired as reported for Chapters 3.1 and 3.2.

The *Africa* LFIA was developed starting from some conditions defined for *Eurasia* LFIA, such as the diluent buffer and the sample pad material. Concentration of coated mAbs (#2H6 and #HD7) and amount of the probe were studied as described for the Eurasia device. In addition, since the detection of SAT types of the virus was made by a combination of three mAbs (#1F10, #2H6, and #HD7), the antibodies were separately adsorbed onto GNP and then mixed in variable ratios. The two anti-SAT mAbs were mixed 1+2; 1+1; 2+1. Once defined their proportion, the #1F10-GNP was added.

## Investigation of the new 'hook effect'

To shed light on the empirical observation that the sensitivity of the PAN-FMDV test line in the Eurasia LFIA depended on its positioning with respect to the sample application point, we used ICS of O- A- and Asia 1-FMDVs and measured the colour of the PAN- and type- specific test lines as a function of the amount of the detector (anti-PAN-FMDV antibody labelled with GNP), the amount of the antigen, and distance from sample application point.

Similarly, the investigation was repeated for the *Africa* LFIA, using SAT 1 and SAT 2 ICS and measuring colour of the test line as a function of the amount of the detector (#2H6-GNP or #HD7-GNP, respectively) and the amount of the antigen. Images were acquired by a scanner, converted in greyscale, and processed by ImageJ software.

## Production of the Eurasia and Africa LFIA devices

The various capture antibodies used for drawing test and control lines of the LFIA devices were diluted in phosphate buffer (20 mM pH 7.4) and applied at 1  $\mu$ L/cm onto the nitrocellulose membrane by means of a XYZ3050 platform (Biodot, Irvine, CA, USA), equipped with BioJetQuanti™ 3000 Line Dispenser for non-contact dispensing. The order of the test lines allowing for optimal analytical performances is depicted in Figure 1. The LFIA *Eurasia* device included 5 lines, as follows: the PAN-reactive mAb (#1F10); a 1:1 mixture of two O-type reactive mAbs (#3B11 and #2A10); the Asia 1-reactive mAb (#3D8); a mixture of two A-type reactive mAbs (#5F6 and #4D12) in the ratio 4:3 and the secondary antibody as the control line. Lines were drawn at 3 mm distance each other. The probe comprised #1F10-GNP (OD =2). The *Africa* device was designed as a 4-lines LFIA strip where the first line contained the SAT 1-reactive mAb (#HD7) and the second the SAT 2-reactive mAb (#2H6). The third line contained the PAN-reactive mAb (#1F10). As the signal reporter, we used a mixture of #1F10-GNP, #HD7-GNP, and #2H6 in the ratio 1:2:2 (total OD =5).

MAB concentrations were 1mg/ml. The gold probes were diluted to optimal OD with GNP dilution buffer (borate buffer with 0.25% Tween 20, 2% sucrose and 0.02% sodium azide), adsorbed onto a pre-saturated glass fibre conjugate pad and dried for 4 hours at room temperature. Strips were composed as follows: sample pad, conjugate pad, membrane, and adsorbent pad and were cut in 4.2 mm- width) by means of a CM4000 guillotine (Biodot, Irvine, CA, USA). Finally, strips were inserted into plastic cassettes (Eximio Biotec Co., China) to fabricate the ready-to-use LFIA device. Cassettes were stored in the dark in plastic bags containing silica at room temperature until use.

## Detection and serotyping of FMD virus by the LFIA devices

The development of the LFIA devices was conducted by using inactivated culture suspensions (ICS) of FMDV of the serotypes included in the study; the virus strains used are listed in Table 5.1.1. An inactivated suspension of swine vesicular disease virus (SVDV) was used as a negative antigen. For matrix effect experiments, the tongue epithelium of healthy cattle was collected at slaughterhouse during regular slaughter procedures. Extraction was made according with the protocol of the manufacturer in compliance with OIE diagnostic Manual (Manual of Diagnostic tests and vaccines for terrestrial animals 2019, Ch 3.1.8.[14]). An amount of ca 200 mg of epithelium was cut and added with 1 ml of the diluent buffer. After an extensive grinding of the mixture, the solid residue was decanted, and three drops of the supernatant were dispensed in the sample well of the device. The supernatant of virus culture and epithelium homogenates were diluted 1+1 with the diluent buffer and applied to the sample well of the cassette. The extracts from cattle tongue epithelium were directly added to the LFIA (three drops corresponding to approximately 75 µl). The result was visually inspected after 10 minutes from sample application and judged by three independent operators.

## Analytical evaluation of the Eurasia and Africa LFIAs

Selectivity of the devices was evaluated by considering reciprocal cross-reactivity of the various FMDV types on other test lines. Also, ICS samples of types O, A, and Asia1 FMDV were applied to *Africa* LFIA, and SAT 1 and SAT 2 ICS were applied to the *Eurasia* LFIA.

Matrix effect was studied by analysing tongue extracts from healthy cattle before and after spiking with FMDV of the various serotypes.

The analytical sensitivity was studied by serially diluting the epithelium homogenate sample positive for one strain of each serotype with the diluent buffer and analysing diluted samples by the LFD. The limit of detection was defined as the sample dilution that showed a perceivable colour at the test line, as judged coherently by three operators. The sample dilutions were measured in parallel by means of the reference ELISAs.

### 5.1.3 Results and Discussion

#### Development of the Eurasia and Africa LFIA devices

Monoclonal antibodies towards FMDV, fully characterized as far as their selectivity towards the various variant of the virus, were available from [6]–[8], [11]. A summary of the mAb used in this work and of their features is shown in Table 5.1.1. The Eurasia LFIA was developed first and was designed to allow for the indistinct detection of four FMDVs (including O, A, Asia 1, and C types) by means of a PAN-FMDV mAb, and the simultaneous serotyping of the circulating types (O, A, Asia 1). Therefore, four test lines were drawn, namely the PAN- and the three type-specific lines (Figure 5.1.2a). The detection sites were formed by coating the 1F10 mAb, a 1:1 mix of the two O-specific mAbs (2B11+2A10), the Asia 1-specific mAb (3D8), and a 1:0.75 mix of the two A-specific mAbs (4D12 and 5B6) to form the PAN-FMDV and the three type-specific lines, respectively.

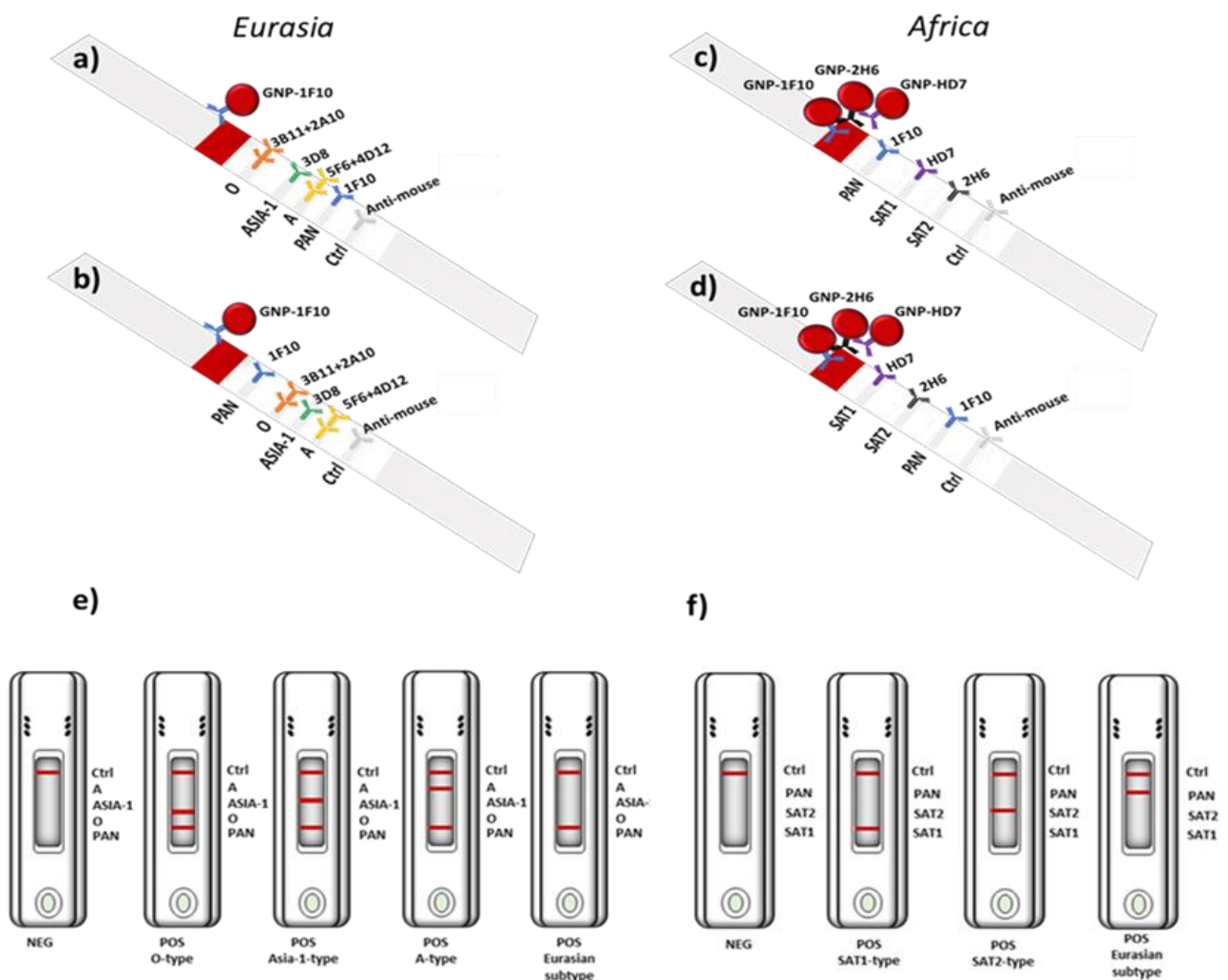


**Figure 5.1.2.** Scheme of the LFIA devices, including three type specific and the PAN-FMDV test lines (Eurasia LFIA) and two type specific and the PAN-FMDV test lines (Africa LFIA). The optimal arrangement of reactive sites for the Eurasia and Africa LFIA is depicted in b) and d), while the arrangements in a) (Eurasia) and c) showed a significantly lower

detection capability. Results were visually read and assigned as shown in e) and f) for Eurasia and Africa LFIAs, respectively.

The proportion of mixed mAbs for the O- and A- were defined according to their reactivity measured by the ELISA. Preliminary experiments allowed us to conclude that 1 mg/ml of each antibody was sufficient to assure intense colouring of the type-specific lines in the presence of the FMDV samples (inactivated supernatant from cell culture, icc, Table 5.1.2) diluted 1/10 in PBS. Lower amounts decrease the signal, while higher amounts did not produce an appreciable increase of the colour at the lines (data not shown). Similarly, increasing the optical density of the 1F10-GNP probe from 1 to 2 was shown to increase the colour at the type-specific test lines, while a further increase resulted in a higher background without significantly improving the detectability.

As far as the PAN-FMDV line, we initially opted for positioning it as the farthest from sample application, so that type-specific interactions were favoured (Figure 5.1.2a). However, the sensitivity of the PAN-FMDV was very poor, whatever FMDV type was used as the sample (Figure 5.1.3a). The hypothesis was made that the capture of the antigens by the type-specific lines prevented them to reaching the PAN-FMDV line. Differently from ELISA, where each mAb-antigen interaction occurs separately, in the LFIA platform, the cross-reactivity may cause false positive results and, also, false negative results, when the cross-reacting antibody captures the antigen and prevents the binding to the specific one. Then, the PAN-FMDV line was placed as the first reactive zone encountered by the sample during the flow (Figure 5.1.2b and 5.1.3b). This configuration enabled recovering the sensitivity of the PAN-FMDV without interfering significantly with the detection capability of the type-specific lines.

The Africa LFIA included two specific test lines formed by the anti-SAT 1 and anti-SAT 2 mAbs. The same mAbs were also labelled with GNP and the two probes were mixed to allow revealing SAT 1 and SAT 2 FMDV types. The optimal proportion and the absolute amount of each probes were investigated by maximizing colouring of both lines while limiting background signal.

According to the quantitative analysis of images the following conditions were established: mixing the probes in equal proportion and reaching a final concentration of each GNP-mAb corresponding to OD2. Although the PAN-FMDV was not reactive to all SAT strains, it was shown to be able to recognize most SAT 1 FMDV [ref] and, considering that O, A, and Asia 1 strains may be found also in African countries[10], a PAN-FMDV test line was included in the Africa device, as well. Based on the previous observations, this line was positioned near to the sample well, followed by the SAT 1 and SAT 2 specific lines, respectively (Figure 5.1.2c). However, the insertion of the PAN-FMDV line and the consequent distancing of the two specific lines, caused a dramatic loss of sensitivity, mainly for the SAT 1 detection. Coherently with the reactivity of the PAN-FMDV mAb, which cross-reacted with SAT 1 strains, most of the SAT 1 antigen apparently was subtracted by the PAN-FMDV line and was not able to reach the specific line so causing the lowering of the detection ability of this serotype. The ultimate arrangement of reactive sites was established for the Africa LFIA as: SAT 1, SAT 2, and PAN-FMDV test lines, followed by the control line (Figure 5.1.2d). The probe was formed by a mixture of three mAb-GNP (i.e.: 1F10-, HD7- and 2H6-GNP in the optimal proportion of 1:2:2).

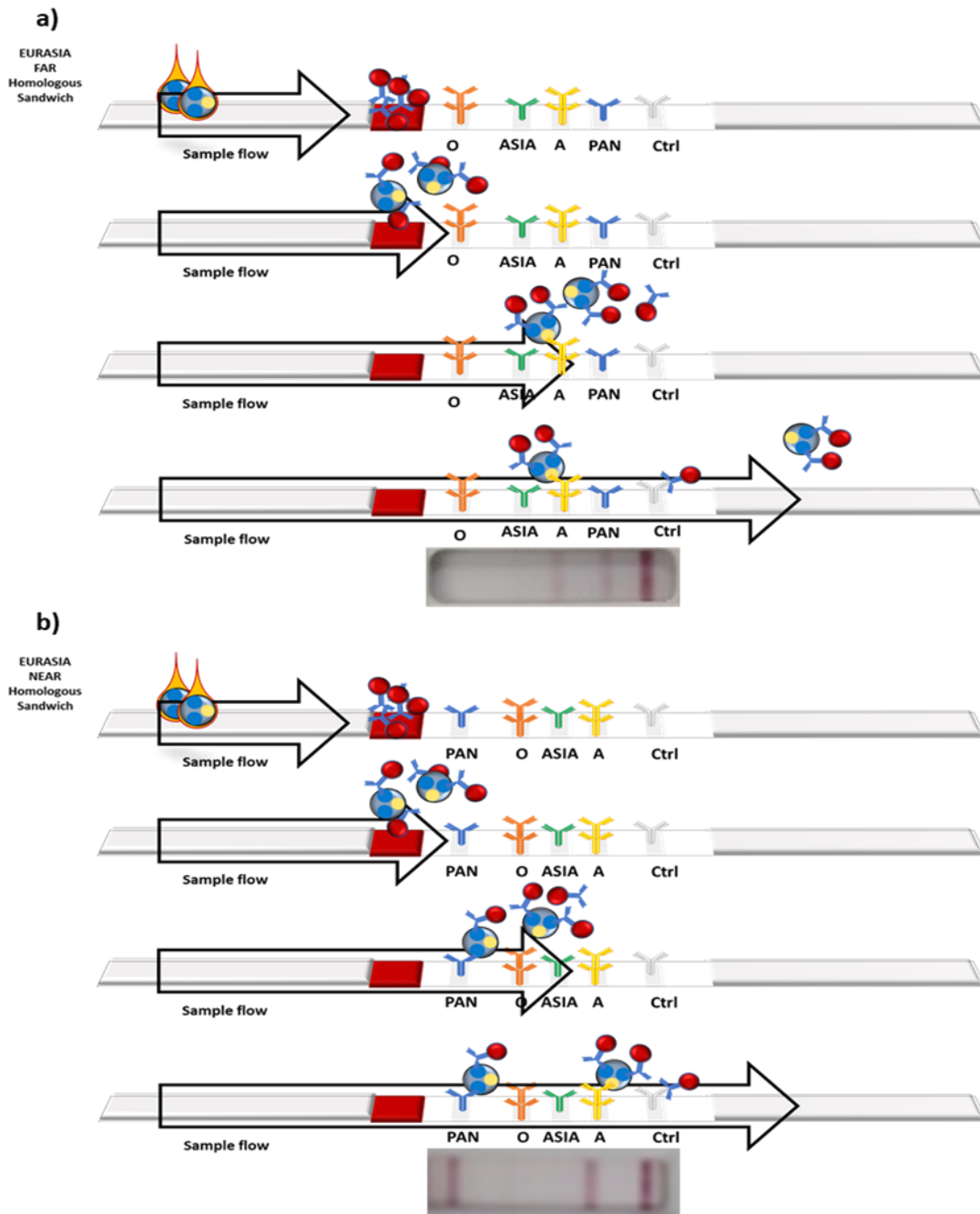


**Figure 5.1.3.** The difference between the behaviour of homologous and heterologous sandwiches testing the same sample on different position of test line including the homologous sandwich: a) far from sample application point, b) near to sample application point.

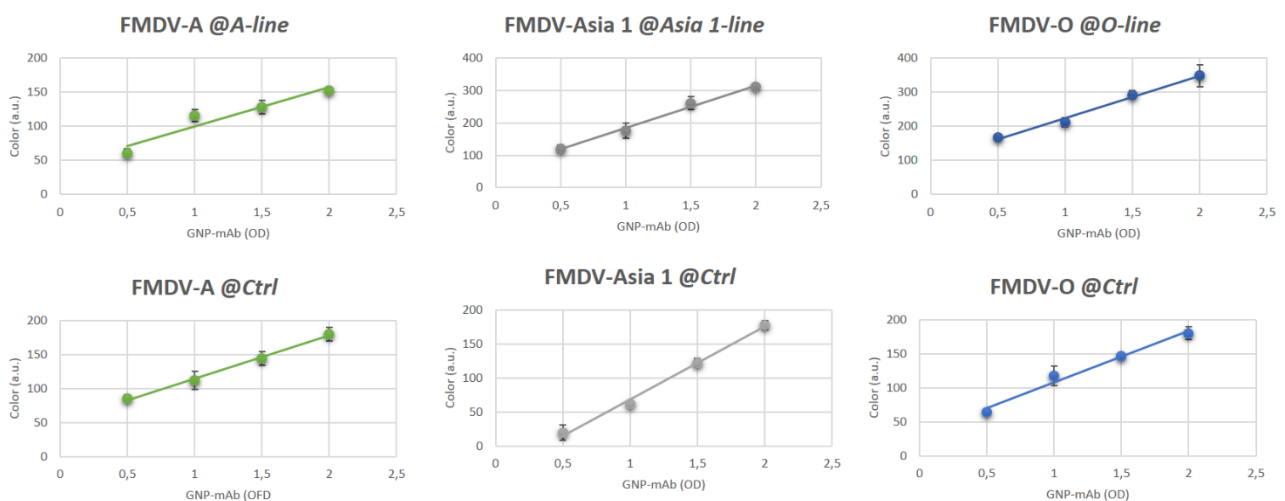
### Evidence of an inverted “Hook effect”

The empirical observation on the significant effect due to the apparent cross-reactions among antibodies and the consequent importance of the intelligent arrangement of reactive zones was further investigated. In fact, the two devices had opposite optimal configurations: the alignment of capture mAbs included the PAN-FMDV as the last and as the first bioligand in the *Eurasia* and *Africa*



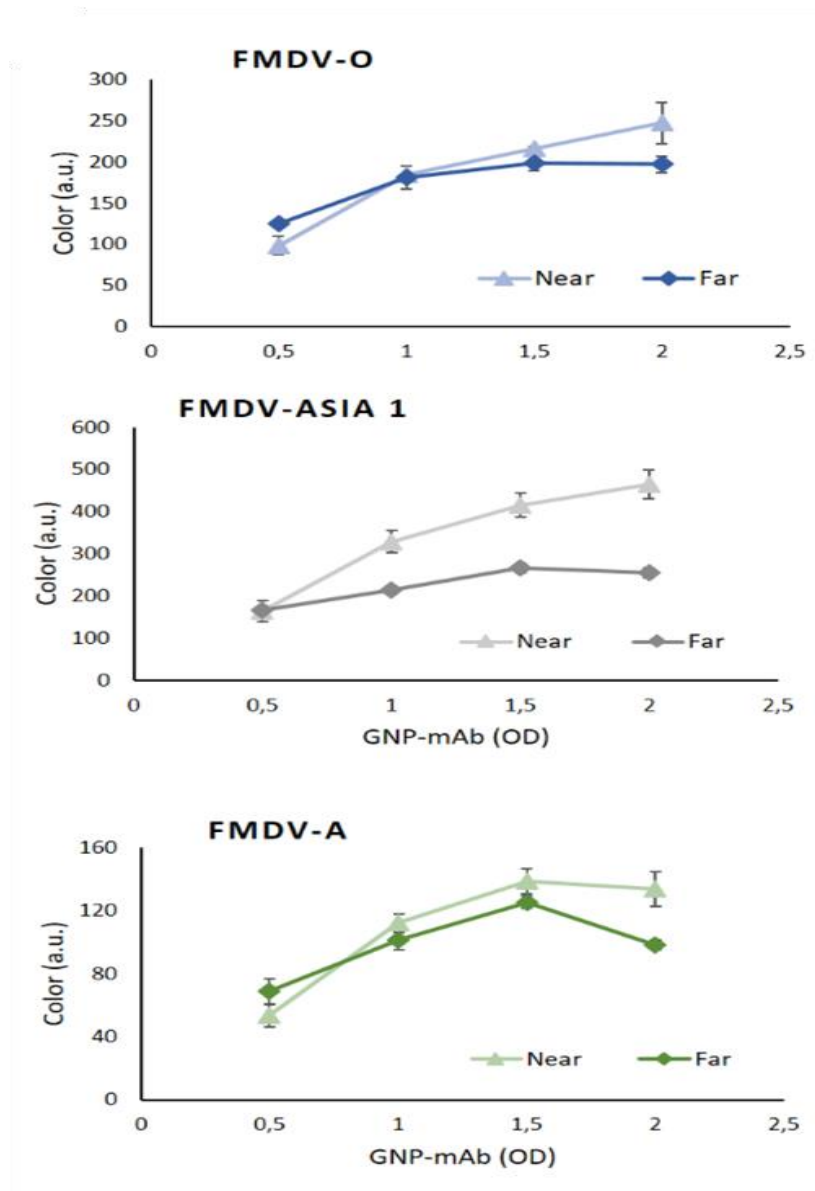
LFIAs, respectively. Of course, the different relative affinities of the various mAbs may explain the observed behaviour. Nevertheless, we noticed also that when O-, Asia 1-, and A-FMDV were applied to the *Africa* LFIA (which included only one reactive site for these serotypes, i.e., the PAN-FMDV site), the signal was significantly lower compared to the one provided by the same samples when applied to the *Eurasia* LFIA, despite the capturing mAb and the detector were the same in the two configurations. The net effect of distancing a reactive site from the sample well is the increase of the contact time between the sample and the detector before they reach the capture site. We supposed that the interaction between the viral antigens and the detector antibody, which occur in solution during their flowing across the membrane, could lead to the saturation of the antigen epitopes and to preventing the subsequent binding to the capture antibody. The suggested effect should impact more on homologous sandwich assays, which are based on the simultaneous binding of two molecules of the same antibody to two equivalent epitopes on one viral particle. We exactly observed that the positioning of the homologous sandwich assay was the most critical, as for the PAN-FMDV and SAT-specific antibody pairs for the *Eurasia* and *Africa* LFIAs, respectively. To shed light into these findings, we measured the colour formed at the several test lines as a function of the quantity of the detector and of the antigen.

Starting from the *Eurasia* system, we found an almost linear relationship between the colouring of lines (including the control line) and the amount of the probe (Figure 5.1.4), apart from the PAN-FMDV line (Figure 5.1.5). The behaviour was qualitatively similar whatever FMDV serotype was used as the sample. In the case of the homologous sandwich, initially the increase of the probe amount provoked a parallel increase of the signal, followed by a saturation or a decrease of the signal, which is typical of the so-called “hook effect” [15]. However, the hook effect has been correlated to an excess of the antigen compared to the two antibodies used for its detection.



**Figure 5.1.4.** Colour measured at the test line including a mAb diverse from the one used as the detector. The signal was plotted versus the GNP-mAb amount (as the optical density of the conjugate at the maximum of LSPR band). Samples containing inactivated FMDV of O, Asia 1 and A types were analysed by the *Eurasia* LFIA, while samples of the SAT 1 and SAT 2 types were checked by the *Africa* LFIA. Samples were diluted 1:5 with the diluent and directly submitted to the LFIAs.

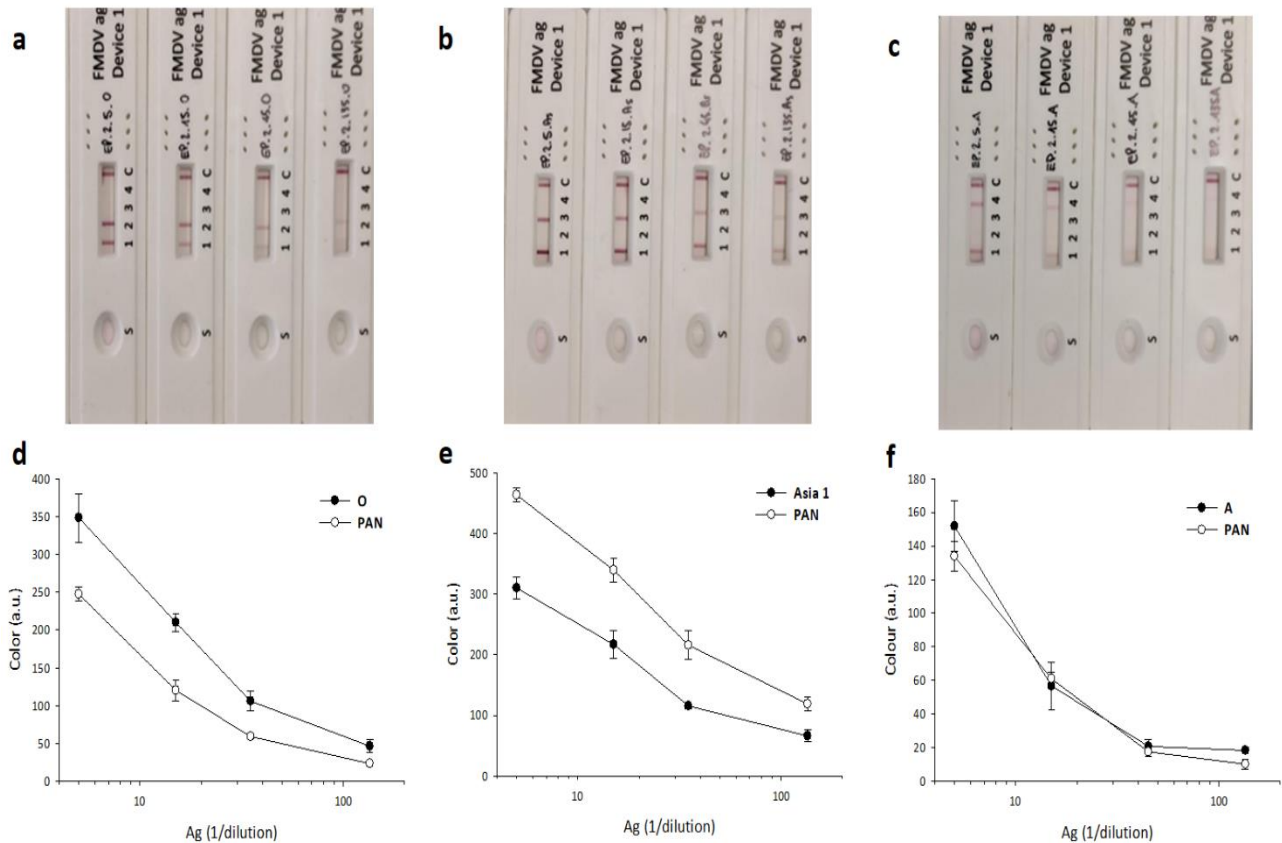
In the classic hook effect, when the quantity of the antigen increases over the linearity range, the probability of the simultaneous binding of the capture and detector antibodies to the same antigen decreases, and the detector is subtracted by the excess of the antigen (Figure 5.1.3a) ultimately leading to a decrease of the observed signal. In the present work, we observed a different saturation effect, due conversely to the excess of the probe that subtracts the antigen and prevents its binding to the capturing antibody (Figure 5.1.3b).



**Figure 5.1.5** Colour developed at the ‘PAN-FMDV’ test line upon application of samples containing FMDV types O, Asia 1 and A. The test line was positioned near to the sample well (ca. 1 cm, ‘near’) and at higher distance (ca. 2 cm, ‘far’). The amount of the GNP-PAN antibody was varied from OD 0.5 to OD 2.

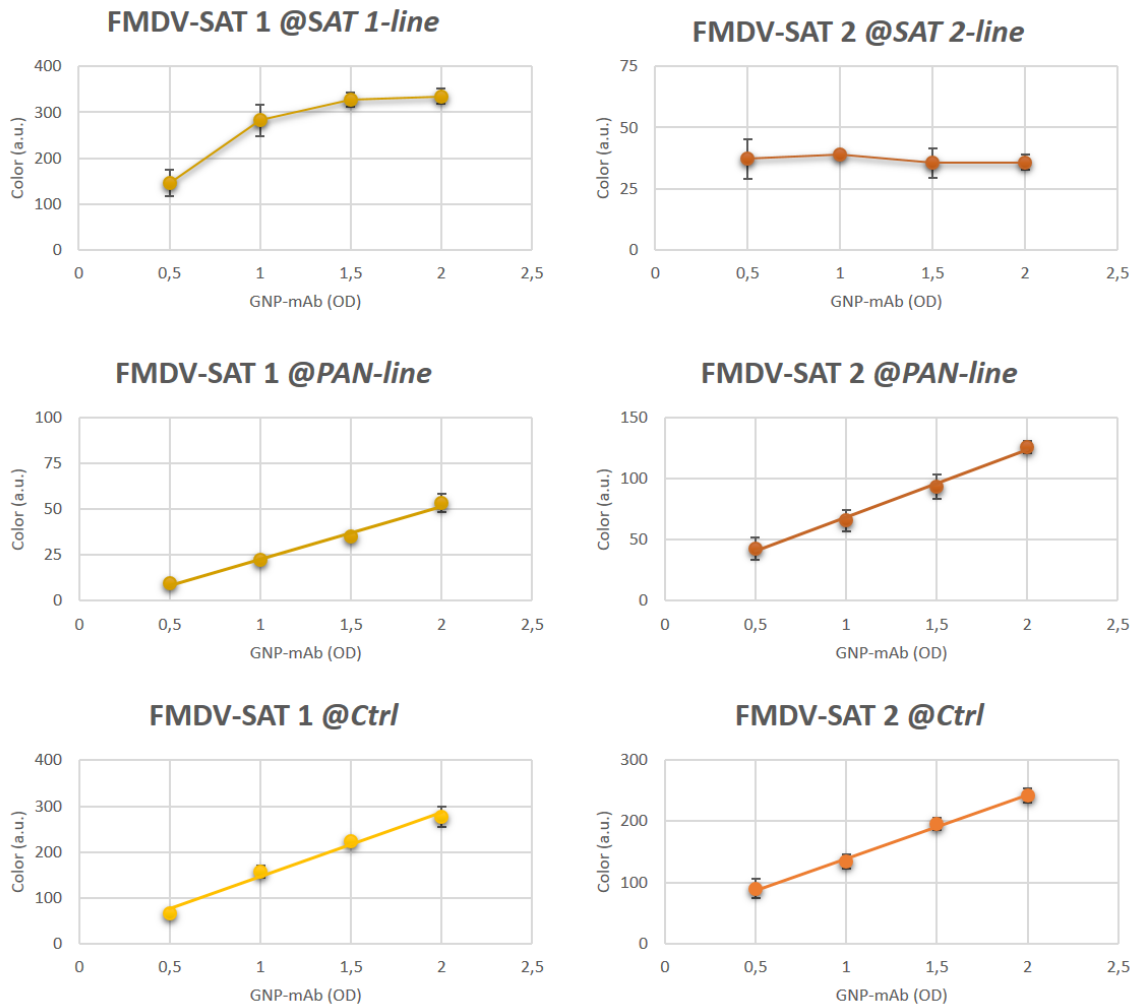
The different order of the interactions occurring in flow compared to those realized in stationary state explained the observation. To support our hypothesis, we carried out two further experiments: in one case, we varied the amount of the antigen and in a second one we repeated the same study as above described but shifting the test line comprising the homologous antibody so that the contact time between the antigen and the probe before reaching the test line was increased. As shown in

Figure 5.1.6, a linear relationship between the antigen quantity and the signal measured was found independently on the sample tested. On the contrary, again a typical hook effect pattern was obtained when the amount of the probe was varied (Figure 5.1.5). Coherently with the hypothesis made, the shift of the line farthestmost resulted in the exasperation of the effect, which caused a general loss of sensitivity compared to the system with the PAN-FMDV line near to the sample well, more pronounced for the case of high concentration probe (Figure 5.1.5).



**Figure 5.1.6:** Signal dependence on antigen concentration: ICS of the FMDV-O (a), -Asia 1 (b) and A-type (c) were serially diluted by the extraction buffer and applied to the *Eurasia* LFIA. The colour formed at the type-specific and PAN lines were recorded and plotted towards ICS dilution for the three samples (d, e, f).

The conclusions drawn by the study were confirmed and reinforced by considering the *Africa* device. In this assembly, the two type-specific reactions were based on homologous sandwich assays whereas the PAN-FMDV was involved in a heterologous sandwich with the anti-SAT 1 and anti-SAT 2 detection reagents. Again, considering the two homologous sandwich assays, we observed the atypical hook effect, i.e., the bimodal dependency of the signal on the amount of the probe used (Figure 5.1.7). Therefore, we concluded that the behaviour could be generalized. Although, other authors have evidenced that the amount of the probe should be optimized [16], [17] and that an excess of the probe may lead to decrease the sensitivity of the LFIA, we shown that the position of the capturing reagent is the key-point to maximize the sensitivity, while the maximum signal achievable by a “distant” reactive zone remained lower than the one provided by test lines near to the sample well. These findings also implied that the antigen-probe interaction was extremely rapid. Indeed, the few seconds elapsed between probe resuspension by the sample and reaching the “near” reactive zone was enough to form the complex.



**Figure 5.1.7.** Colour measured at the test and control line. The signal was plotted versus the GNP-mAb amount (measured as the optical density of the conjugate at the maximum of LSPR band). ICS samples containing inactivated SAT 1 and SAT 2 types were analysed by the *Africa* LFIA.

### Preliminary evaluation of the LFIA's performance

By employing inactivated culture supernatants of FMDV serotypes O, Asia 1, A, SAT 1 and SAT 2, we checked the cross-reactions of each type on the other non-specific lines. No interference was observed in any cases (Figure 5.1.8). A non-FMDV antigen (SVDV) was also analysed as a negative control. No colouring of test lines was observed for the negative control by the two LFIA's.

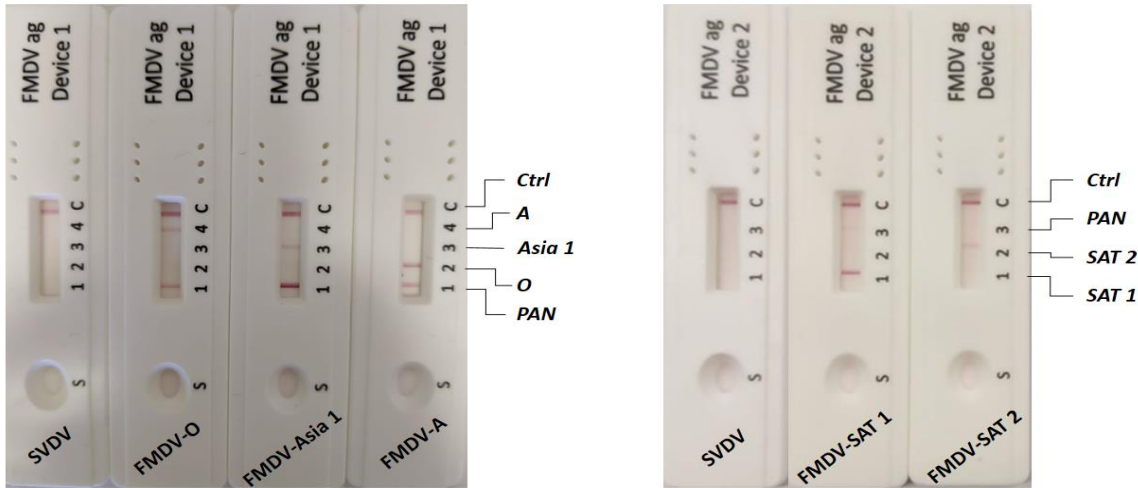


**Figure 5.1.8:** Results obtained by the two LFIA upon application of inactivated supernatants of various FMDV serotypes Device 1 was the *Eurasia* FLD, device 2 was *Africa* LFIA. An inactivated supernatant of the SVD virus was used as the negative control. Test lines indicating positivity and the specific type of the virus are clearly visible, while cross-reactions were not shown.

Type-specific and PAN-FMDV lines were revealed coherently with the strain analysed. To evaluate the matrix effect (ME), tongue epithelium from healthy cattle, collected during regular slaughter procedures, was used. The epithelium was weighted, roughly minced, and then extracted according to the protocol of the tissue viral extraction kit (In3diagnostic, Grugliasco, Italy)]. The extraction was repeated on three samples and the extracts were directly analysed by the LFIA. No signal was observed for any test lines, while the control line confirmed the validity of the assay (Figure 5.1.9). Then, extracts were fortified by adding separately a small volume of the O-, A-, and Asia 1- type ICS. The fortified extracts were analysed again and the type-specific and PAN-FMDV positivity were revealed (Figure 5.1.9), thus confirming that the Extraction protocol allowed for the FMDV detection by the *Eurasia* LFIA. For each serotype, the analytical sensitivity was evaluated on reference viruses in parallel with the reference ELISA. The strains were correctly classified with analytical sensitivity like that shown by the ELISA and absence of cross-reactivity between serotypes. The pan-FMDV test line was clearly visible, irrespective the serotype analysed (Table 5.1.3)

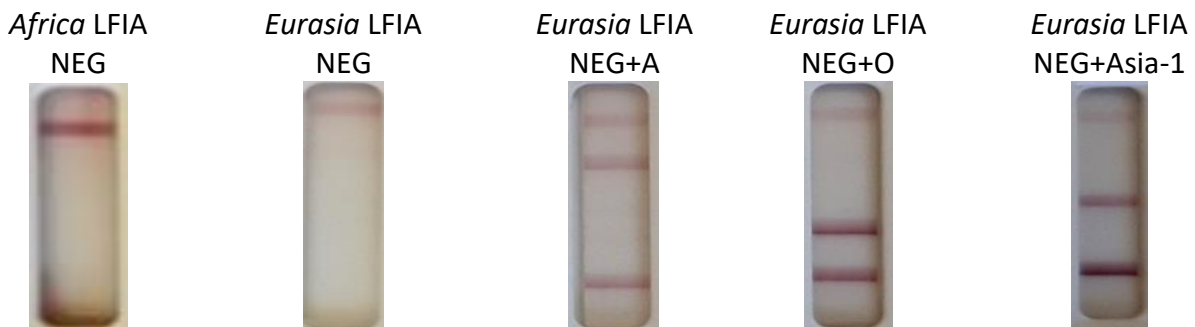


**Figure 5.1.9:** results on negative and fortified epithelia. Magnification of the reading window for highlighting the results and lack of cross reactivity.

**Table 5.1.3** Analytical sensitivity of the LFIA devices

LFID	FMDV type	Sample origin	Limit of detection (TCID50)
<i>Eurasia</i>	O	O Manisa - O Panasia 2	$6,3 \times 10^2 - 10^3$
	A	A22 Iraq - A G-VII	$3,2 \times 10^2 - 1,5 \times 10^3$
	Asia1	Shamir - Sind-08	$4,3 \times 10^3 - 3,2 \times 10^4$
<i>Africa</i>	SAT 1	SAT1	$5,1 \times 10^2 - 10^3$
	SAT 2	SAT2	$2,4 \times 10^2 - 1,5 \times 10^3$

### FMDV detection and serotype differentiation in epithelium homogenate from cattle

The two LFIAs, as above described, were preliminary checked by their capability of specifically detecting the various FMDV serotypes by using epithelium homogenates (EH) collected in Tanzania during the period 2011-2018. The samples were analysed by ELISA (both type-specific and PAN-FMDV) and by rPCR (pan and topotype-specific) and were assigned according to the ELISA score as positive/negative for the various FMDV. Samples confirmed as O- and A-FMDV were analysed by the Eurasia LFIA, while those recognized as containing SAT 1 and SAT 2 virus were analysed by the Africa LFIA. Instead, the inactivated culture suspension of all serotypes and of the negative antigen (SVDV) were analysed by both LFIAs. Therefore, 18 samples were submitted to the Eurasia LFIA detection, including 15 samples which were positive for O, A or Asia 1 FMDV according to the rPCR, and 3 negative samples (SAT 1 and SAT 2 ICS, beside the negative antigen). Instead, 15 samples were submitted to the Africa LFIA detection, among which 11 were positive for the presence of SATs FMDV and 4 were negative (Table 5.1.2).

**Table 5.1.2.** Preliminary assessment of the LFIAs for the detection of major circulating FMDV serotypes.

Sample id #	Type-specific		PAN-FMDV	
	ELISA score <sup>a</sup>	LFIA	ELISA score <sup>a</sup>	LFIA
O/ICS	+++	+++	+++	+++
O/TANZ Ring'wani18	+	+	+++	+
O/TANZ Mbilikili/2014	-	+/- <sup>b</sup>	-	+/- <sup>b</sup>
O TANZ Miseke/2014	++	+++	+++	+++
O/TANZ Miseke/2014	++	+++	++	+++
O/TANZ Kemgesi/2018	+	+++	+++	+++
A/ICS	++	+	+++	++
A/TANZ Motuker/2015	+++	++	+++	++
A TANZ Kyabakari/2012	+	+/-	+	-

A/TANZ Natambiso/2015	+++	+++	+++	+++
A/TANZ Park Nyigoti/2012	++	+++	+++	+++
A/TANZ Nyichoka/2015	+	+++	+	+
A/TANZ Robanda/2015	+	+++	+	+
A/TANZ Robanda/2016	++	+++	++	+++
Asia 1/ICS	+++	+++	++++	+++
SAT1/ICS	++	+++	++	+/--
SAT1/TANZ Motukeri/2013	+++	+++	+	++
SAT1/TANZ Motukeri/2014	++	+++	++	+++
SAT1/TANZ Bonchugu/2014	++	+	+	+
SAT2/ICS	+	+	++	++
SAT2/TANZ Nyichoka/2012	+++	++	+	++
SAT2/TANZ Tamau/2012	+++	+	-	+/--
SAT2/TANZ Burunga/2018	+++	+	-	+
SAT2/TANZ Nyichoka/2018	+++	++	-	++
SAT2/TANZ Kyabakari/2012	++	+	+	+/-
SAT2/TANZ Rwamchanga/2012	+	+/-	+	+/--

<sup>a</sup> Samples were classified according to OD measured by the ELISA: >2.5 (+++), 1-2.5 (++), 0.06-1 (+), <0.06 (-)

<sup>b</sup> Weak signal (+/-) or very very weak (+/--)

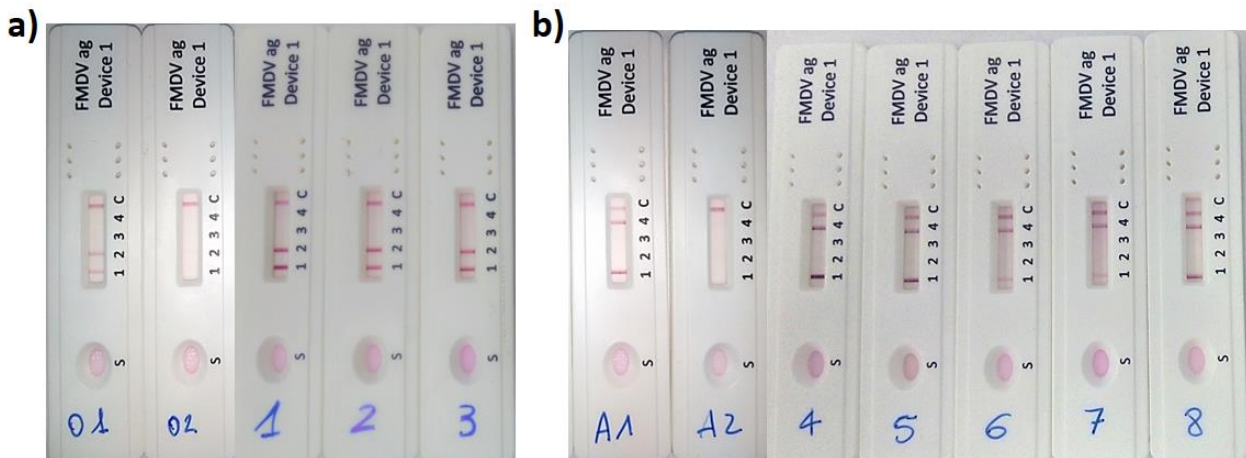


**Figure 5.1.10.** Results on the Eurasia LFIA with on-field positive and negative epithelia.

Results of the assessment and the comparison with ELISA using the same mAbs are summarized in Table 5.1.2 and Figure 5.1.10. Regarding the *Eurasia* LFIA, 14/15 samples were correctly assigned as positive by the ELISA according to the type-specific and the PAN-specific assays, respectively. Thirteen samples were assigned as positive by both assays, while one O-type strain and one A-strain



were false negative according to the type-specific and the PAN-FMDV assay, respectively. The LFIA assigned as positive 15/15 samples based on the colour of the type-specific line and 14/15 based on the PAN-FMDV line. The two false negative results of the ELISA were not confirmed by the LFIA, which instead correctly classified these samples. No cross-reaction was observed, which attested the high specificity of the LFIA. Indeed, the fifteen samples positive for one FMDV-type were contemporary tested also by the other two type-specific lines and were correctly qualified as negative. The three negative samples were also correctly classified, as they did not provide any colouring at any test lines. Considering results from 18 samples x 4 tests condensed in the single LFIA device, the overall accuracy was calculated as 98.6% (92.5-99.9%, C.I.95%). The performance of the *Africa* LFIA was studied by applying SAT 1- and SAT 2- positive homogenates. All samples were correctly classified according to results observed at the type-specific test line (Table 5.1.2 and Figure 5.1.11).

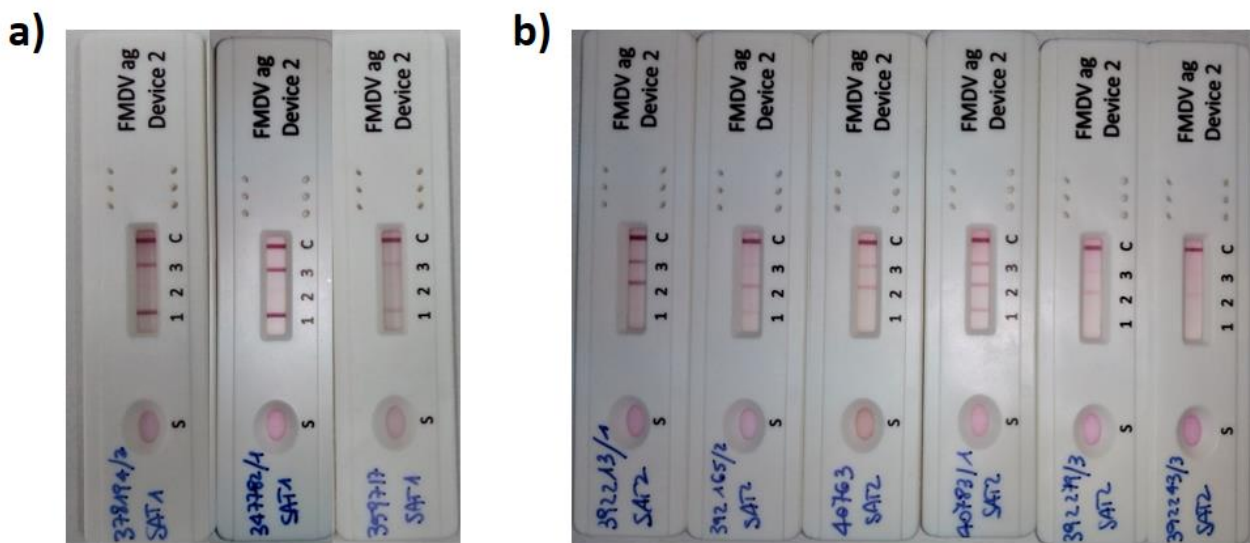


**Figure 5.1.11.** Results on the Africa LFIA with on-field positive and negative epithelia.

According to the ELISA, 3/7 SAT 2-positive samples were not recognized by the PAN-specific assay. On the contrary the PAN-FMDV test line confirmed the positivity of all homogenates. Two samples (SAT2/TANZ Nyichoka/2018 and SAT2/TANZ Tamau/2012) showed cross-reactivity at the SAT 1-specific line. However, the latter provided a very faint colouring, while the first was shown to react with anti-SAT 2 mAbs also by the ELISA. No other false positive results were shown by applying other FMDV types at the three test lines. In summary, the false negative rate was 0% (n= 22), the false positive rate was 5,9% (n=24) and the accuracy was 96.4% (87.7% - 99.6%).



## 5.1.4 Conclusions

The two devices reached promising analytical performances, comparing to the ones from the existing devices reported in Table 5.1.4. The accuracy of the Eurasia device [98.6% (92.5-99.9%)] and Africa device [96.4% (87.7% - 99.6%)] on respect to ELISA reference methods ensures us the high versatility given by the all-encompassing serotyping capability was not reached at the expense of the sensitivity.

**Table 5.1.4.** Literature survey on LFIAs for the direct antigen detection of FMDV.

LFIA	Antibodies	serotype detected	Serotype differentiated	Performance	ref.
Single line	PAN-reactive	O, A, Asia 1, C, SAT1, SAT2	No	Vs rPCR: Se=84%, Sp=85%; vs ELISA: Se=99% Sp=99.9%	[7]
Single line	SAT2	SAT2	-	Vs PCR: Se=88%, Sp=100%	[11]
Single line	PAN-reactive	O, A, Asia 1, C	No	Vs ELISA: Se=87% Sp=88%	[18]
Three strips with single test line	O, A, Asia 1	O, A, Asia 1	O, A, Asia 1	Comparable to double antibody sandwich ELISA	[8]
Multiplex	O, A, Asia 1	O, A, Asia 1	O, A, Asia 1	Comparable to double antibody sandwich ELISA	[4]
Multiplex	PAN-reactive, O, A, Asia 1, C	O, A, Asia 1, C, SAT1, SAT2	O, A, Asia 1, C	not specified	[3]
Single	SAT2	SAT2	-	not specified	[6]
Two strips with single test line	SAT1, SAT3	SAT1, SAT3	-		[19]
Three strips with single test line	O, A, Asia 1	O, A, Asia 1	O, A, Asia 1	Vs rPCR: Se=88% Sp=97%	[20]

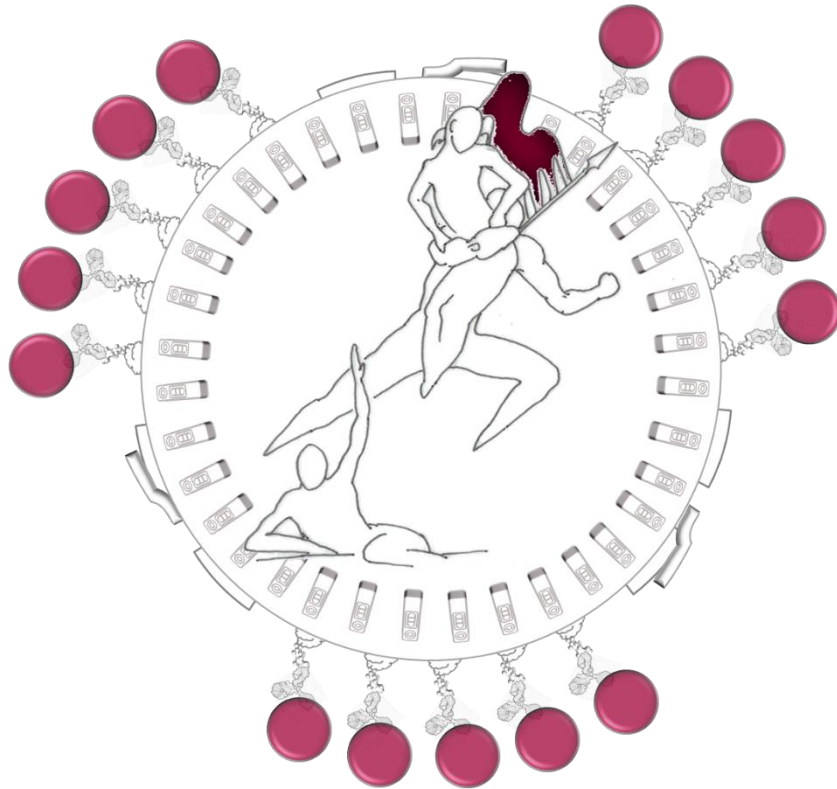
In addition, the study on the positioning of the reactive lines and on the proper optical density of the gold conjugates to include in the devices, disclosed interesting phenomena, such as the evidence of an 'inverted' hook effect. It seemed not to follow the general rules of managing the hook effect by means of diluting the sample but affects mostly the amount of probe and saturation effected occurring within the run of the assay. The different behaviour of the homologous and heterologous sandwiches is consistent to a specific pre-saturation of the probe that worsen with the distance from the start of the run, or contingently, with the run-time. These observations can be useful for the development of any kind of multiplexed antigen test involving heterologous and homologous sandwiches.

## References

- [1] J. C. Patton, A. H. Coovadia, T. M. Meyers, and G. G. Sherman, "Evaluation of the ultrasensitive human immunodeficiency virus type 1 (HIV-1) p24 antigen assay performed on dried blood spots for diagnosis of HIV-1 infection in infants," *Clin. Vaccine Immunol.*, vol. 15, no. 2, pp. 388–391, Feb. 2008, doi: 10.1128/CVI.00265-07.
- [2] I. Nakagiri et al., "Screening for human immunodeficiency virus using a newly developed fourth generation lateral flow immunochromatography assay," *J. Virol. Methods*, vol. 274, p. 113746, Dec. 2019, doi: 10.1016/j.jviromet.2019.113746.
- [3] K. Morioka et al., "Development and Evaluation of a Rapid Antigen Detection and Serotyping Lateral Flow Antigen Detection System for Foot-and-Mouth Disease Virus," *PLoS One*, vol. 10, no. 8, pp. 1–10, Aug. 2015, doi: 10.1371/journal.pone.0134931.
- [4] M. Yang, N. R. Caterer, W. Xu, and M. Goolia, "Development of a multiplex lateral flow strip test for foot-and-mouth disease virus detection using monoclonal antibodies.," *J. Virol. Methods*, vol. 221, pp. 119–126, Sep. 2015, doi: 10.1016/j.jviromet.2015.05.001.
- [5] T. R. Kozel and A. R. Burnham-Marusch, "Point-of-care testing for infectious diseases: Past, present, and future," *Journal of Clinical Microbiology*, vol. 55, no. 8. American Society for Microbiology, pp. 2313–2320, Aug. 01, 2017, doi: 10.1128/JCM.00476-17.
- [6] M. Yang, B. Mudabuka, K. Quizon, and C. Nfon, "Generation of monoclonal antibodies against foot-and-mouth disease virus SAT 2 and the development of a lateral flow strip test for virus detection," *Transbound. Emerg. Dis.*, vol. 66, no. 3, pp. 1158–1166, May 2019, doi: 10.1111/tbed.13076.
- [7] N. P. Ferris et al., "Development and laboratory validation of a lateral flow device for the detection of foot-and-mouth disease virus in clinical samples," *J. Virol. Methods*, vol. 155, no. 1, pp. 10–17, 2009, doi: <https://doi.org/10.1016/j.jviromet.2008.09.009>.
- [8] M. Yang, M. Goolia, W. Xu, H. Bittner, and A. Clavijo, "Development of a quick and simple detection methodology for foot-and-mouth disease virus serotypes O, A and Asia 1 using a generic RapidAssay Device," *Virol. J.*, vol. 10, no. 1, p. 125, 2013, doi: 10.1186/1743-422X-10-125.
- [9] K. Poonsuk, L. Giménez-Lirola, and J. J. Zimmerman, "A review of foot-and-mouth disease virus (fmdv) testing in livestock with an emphasis on the use of alternative diagnostic specimens," *Anim. Heal. Res. Rev.*, vol. 19, no. 2, pp. 100–112, 2018, doi: 10.1017/S1466252318000063.
- [10] B. Pattnaik et al., "Foot-and-mouth Disease: Global Status and Future Road Map for Control and Prevention in India," *Agricultural Research*, vol. 1, no. 2. Springer India, pp. 132–147, Jun. 01, 2012, doi: 10.1007/s40003-012-0012-z.
- [11] N. P. Ferris et al., "Development and laboratory validation of a lateral flow device for the detection of serotype SAT 2 foot-and-mouth disease viruses in clinical samples," *J. Virol. Methods*, vol. 163, no. 2, pp. 474–476, 2010, doi: <https://doi.org/10.1016/j.jviromet.2009.09.022>.
- [12] F. Di Nardo, C. Baggiani, C. Giovannoli, G. Spano, and L. Anfossi, "Multicolor immunochromatographic strip test based on gold nanoparticles for the determination of aflatoxin B1 and fumonisins," *Microchim. Acta*, vol. 184, no. 5, pp. 1295–1304, 2017, doi: 10.1007/s00604-017-2121-7.
- [13] Y.-R. Guo, S.-Y. Liu, W.-J. Gui, and G.-N. Zhu, "Gold immunochromatographic assay for simultaneous detection of carbofuran and triazophos in water samples," *Anal. Biochem.*, vol. 389, no. 1, p. 32–39, 2009, doi: 10.1016/j.ab.2009.03.020.

- [14] "Manual of Diagnostic tests and vaccines for terrestrial animals 2019."  
[https://www.oie.int/fileadmin/Home/esp/Health\\_standards/tahm/3.01.08\\_Fiebre\\_aftosa.pdf](https://www.oie.int/fileadmin/Home/esp/Health_standards/tahm/3.01.08_Fiebre_aftosa.pdf) (accessed Feb. 04, 2021).
- [15] J. Tate and G. Ward, "Interferences in immunoassay," *Clin. Biochem. Rev.*, vol. 25, no. May, pp. 105–120, 2004, Accessed: Feb. 04, 2021. [Online]. Available:  
[https://scholar.google.com/scholar\\_lookup?author=JTate&author=GWard&title=Interferences+in+immunoassay&pages=105-120&volume=25&publication\\_year=2004](https://scholar.google.com/scholar_lookup?author=JTate&author=GWard&title=Interferences+in+immunoassay&pages=105-120&volume=25&publication_year=2004).
- [16] P. Manta et al., "Optical Density Optimization of Malaria Pan Rapid Diagnostic Test Strips for Improved Test Zone Band Intensity.," *Diagnostics (Basel, Switzerland)*, vol. 10, no. 11, p. 880, Oct. 2020, doi: 10.3390/diagnostics10110880.
- [17] N. A. Byzova, I. V. Safenkova, E. S. Slutskaya, A. V. Zherdev, and B. B. Dzantiev, "Less is More: A Comparison of Antibody-Gold Nanoparticle Conjugates of Different Ratios," *Bioconjug. Chem.*, vol. 28, no. 11, pp. 2737–2746, Nov. 2017, doi: 10.1021/acs.bioconjchem.7b00489.
- [18] J. K. Oem, N. P. Ferris, K.-N. Lee, Y.-S. Joo, B.-H. Hyun, and J.-H. Park, "Simple and Rapid Lateral-Flow Assay for the Detection of Foot-and-Mouth Disease Virus," *Clin. Vaccine Immunol.*, vol. 16, no. 11, pp. 1660 LP – 1664, Nov. 2009, doi: 10.1128/CVI.00213-09.
- [19] M. Yang et al., "Development of two rapid lateral flow test strips for detection of foot-and-mouth disease virus SAT 1 and SAT 3," *J. Virol. Methods*, p. 113967, Sep. 2020, doi: 10.1016/j.jviromet.2020.113967.
- [20] T. Jiang et al., "A simple and rapid colloidal gold-based immunochromatographic strip test for detection of FMDV serotype A," *Virol. Sin.*, vol. 26, no. 1, pp. 30–39, 2011, doi: 10.1007/s12250-011-3166-5.

# Chapter 6



---

## Therapeutic drug monitoring LFIA

---

## Introduction

The therapeutic drug monitoring (TDM) is a transdisciplinary approach involving any kind of control system to assure the correct dosage and compliance of a drug regimen [1]–[5]. One of the branches of the TDM is the control of the compliance to the therapy. It intervenes to identify the source of some of the therapeutic failures as caused by the low adherence from the patient, excluding eventual ineffectiveness of the regimen [6], [7]. The point-of-care knowledge of the lack of compliance allows for a rapid intervention and avoids counterproductive re-arrangements of the therapy. Some analytical methods and diagnostic tools, including LFIA, are used for the rapid and on-site assessment of the adherence to the therapy by the patients [7], [8].

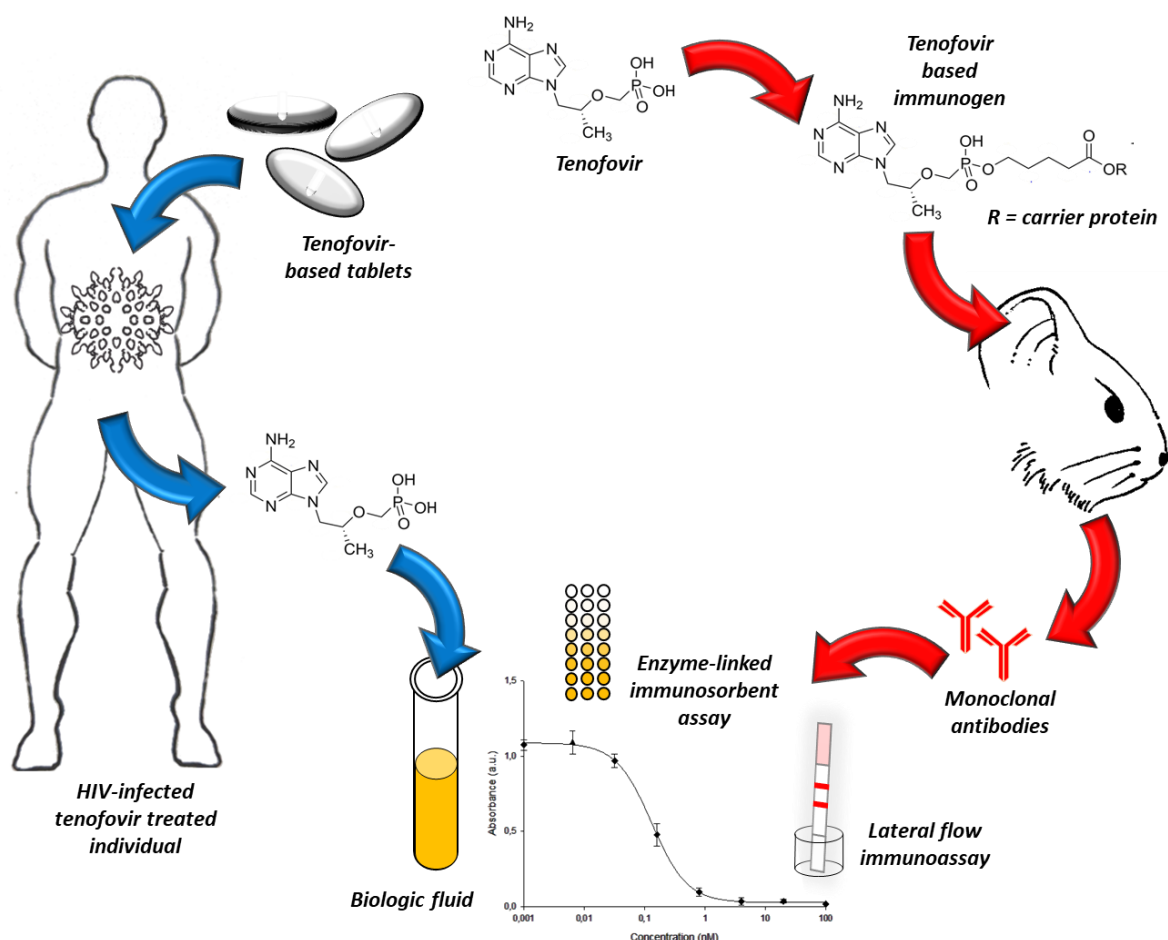
According to the principles of immunoassay, the detection of small molecules, as many drugs, forces to use competitive formats. The competitive assays are theoretically less sensitive than non-competitive ones and need a lot of work to find the optimal conditions for operating. Moreover, especially for point of care testing, they are quite counterintuitive, while the “user friendliness” figure of merit includes the easy understanding of the results. In fact, LFIA in competitive formats should be intended as “positive” when the test line is absent. Nevertheless, for the use in therapeutic drug monitoring, the interpretation is reversed. The normal case, or “no-alarm” situation, is the presence of the analyte in the specimen, which is given by a no-test line outcome. On the contrary, the diagnosis of “alarm” situation is given by the absence of the analyte, producing a signal at the test line. For this reason, for therapeutic drug monitoring, control of compliance to the therapy, or any other assessment of correct excretion of the drug, the competitive format is much more straightforward than for other applications.

In the following chapter, the application of this aspect to the therapeutic drug monitoring of an antiretroviral drug is reported. The project started at the very beginning of the assay development, from the synthesis of a suitable hapten derived from the drug and its conjugation to proteins to prepare antigens for the assay and for antibody production. The protein-hapten conjugate was inoculated into mice to generate antibodies through the hybridoma technology. The strategic element lied in the selection of the hybridomas expressing monoclonal antibodies through a checkerboard testing including the competition feature as part of the screening. The selected antibodies were tested for their sensitivity in buffer and in a simulated matrix (urine) by ELISA. Finally, the best performing mAb was employed to set POCT prototypes aimed at detecting the drug in urine, where the target compound is excreted and then is expected to reach high concentrations, and in saliva, a less invasive and easy to collect matrix. The LFIA device and an in-house validated ELISA devoted to drug detection in saliva were established and showed sufficient sensitivity for the application, although the expected levels of the drug were dramatically lower in this matrix [9]–[13]

## 6.1



### Compliance monitoring LFIA for Tenofovir



Based on

S. Cavalera, C. Agulló, J. V. Mercader, F. Di Nardo, M. Chiarello, L. Anfossi, C. Baggiani, A. D'Avolio, A. Abad-Somovilla and A. Abad-Fuentes, **Monoclonal antibodies with sub-nanomolar affinity to tenofovir for monitoring adherence to antiretroviral therapies: from hapten synthesis to prototype development**, *Journal of Materials Chemistry B*, 2020, 8, 10439, <https://doi.org/10.1039/D0TB01791D>.

And on further implementations

### Abstract

Approximately 32 million people have died of HIV infection since the beginning of the outbreak, and 38 million are currently infected. Among strategies adopted by the Joint United Nations Programme on HIV/AIDS to end the AIDS global epidemic, the treatment, diagnosis, and viral suppression of the infected subjects are considered crucial for HIV prevention and transmission. Although several antiretroviral (ARV) drugs are successfully used to manage HIV infection, their efficacy strictly relies on perfect adherence to the therapy, which is seldom achieved. Patient supervision, especially in HIV-endemic, low-resource settings, requires

*rapid, easy-to-use, and affordable analytical tools, such as the ELISA and especially the LFIA. In this work, high-affinity monoclonal antibodies were generated to develop ELISA and LFIA prototypes for monitoring tenofovir (TFV), an ARV drug present in several HIV treatments. TFV was functionalized by inserting a carboxylated C5-linker at the phosphonic group of the molecule, and the synthetic derivative was conjugated to proteins for mice immunization. Through a rigorous screening strategy of hybridoma supernatants, a panel of monoclonal antibodies strongly binding to TFV was obtained. Following antibody characterization for affinity and selectivity by competitive ELISA, a LFIA prototype was developed and tentatively applied to determine TFV in simulated urine and in salivary matrix. The point-of-care test showed ultra-high detectability (the visual limit of detection was 2.5 nM, 1.4 ng/mL), excellent selectivity, and limited proneness to matrix interference, thus potentially making this rapid method a valuable tool for the on-site assessment of patient adherence to ARV therapy.*

### **6.1.1 From the cradle to the architecture of the test**

As recommended by the WHO the best strategy for assessing therapy adherence is the Point of Care Testing and a prominent role could be played by the LFIAs. The development of LFIA for the determination of TFV has gained great attention in the last two years. To this aim, specific recognition elements (i.e., anti-TFV antibodies) have been generated. TFV is a small molecule, non-immunogenic by itself, so it requires to be functionalized and covalently attached to a macromolecular carrier to trigger the immune response and generate specific antibodies. However, TFV is an amphiphilic molecule, which complicates the introduction of functional groups for linking it to a carrier. Moreover, some endogenous compounds structurally related to TFV are present in biological samples at very high concentrations, like adenine and its derivatives, adenosine, ADP and ATP. In 2018, G. Pratt et al. [14] reported the production of rabbit polyclonal antibodies to TFV and their implementation in a LFIA test for measuring the drug in urine. However, the developed prototype showed some major limitations for practical application, more likely derived from the complex structure of the spacer arm linking TFV to the carrier protein, which eventually resulted in antibodies of moderate affinity to TFV. Almost simultaneously, Gandhi et al. published a paper describing the development of an ELISA to TFV and its application to the determination of this ARV drug in urine [12]. This work was followed by several others wherein the same research group reported comprehensive clinical studies using this immunoassay to follow patient adherence to the TFV based HAART, and more recently on the development of a LFIA enabling the determination of clinically relevant TFV levels in urine [9], [15], [16]. While these studies provided compelling evidence of the suitability of immunoanalytical approaches for monitoring the compliance to the ARV therapy, the developed tests showed limited adaptability to more challenging analytical demands, like the analysis of TFV in plasma and saliva samples, or following adherence in patients administered with TAF, which is replacing TDF in ARV coformulations because it shows equivalent efficacy at lower dosage. Moreover, none of these studies discloses the structure of the hapten that was used for the generation of the polyclonal antibodies, nor their binding properties (affinity and specificity) to the analyte. In TDM by rapid assays, it is commonly acknowledged that monoclonal antibodies are better suited than polyclonal antibodies if a commercial POC test is intended. In this respect, while we were writing this paper, D. Sevenler et al. reported on the generation of



monoclonal antibodies to TFV [17]. In order to reach this goal, these authors employed a novel hapten containing a carboxylate functional group that was coupled to proteins by carbodiimide-mediated chemistry, so no bulky groups were introduced in the linker. Unexpectedly, these antibodies showed only moderate affinity to TFV, as previously developed antisera. Moreover, the assay exhibited strong interferences by components present in plasma samples, thus precluding the assay of being sensitive enough for its intended use. These results suggest that a good hapten design, although essential, is not sufficient for generating high-affinity antibodies for a particular target. TFV is highly concentrated in urine on respect to other matrices and the dose-adherence correlation was widely investigated. Nevertheless, it could be easily counterfeited because its sampling does not allow the presence of the physician and is mildly invasive. Another possible matrix where Tenofovir can be measured is the saliva. Nevertheless, TFV is 5 orders of magnitude less concentrated in saliva than in urine, rendering the sensitivity requirements extremely challenging. The aim of this work was the generation of monoclonal antibodies with superior binding properties to TFV over those developed so far and the incorporation of these biomaterials into prototypes of POC tests, like ELISA and LFIA, for rapid and on-site diagnostics of TFV in common biological samples (urine, blood, plasma, and saliva) at clinically relevant concentrations.

To achieve this goal, a hapten was synthesized, which turned out to be very similar to that used by D. Sevenler et al. [17], and it was coupled to carrier proteins and a reporter enzyme. More importantly, an optimized protocol for the screening of hybridoma supernatants was implemented at very early steps of the antibody selection process. The strategy, consisting of a two-step evaluation procedure that includes a differential and a checkerboard competitive ELISA, has previously demonstrated its efficacy with other analytes for selecting high-affinity and specific binders among a population of clones secreting antibodies with a variety of binding properties. The rationale behind this approach is simple; testing cell cultures for the recognition of free TFV in solution at the very beginning of the hybridoma selection process allows those cell lines that preferentially bind the coating antigen to be ruled out (competing bioconjugate). Accordingly, only monoclonal antibodies with a proven ability of adequately performing in competitive assays are chosen for further cloning, expansion, and in vitro production. The main goal of this part of the work was addressing the lack of a commercial, reliable point-of-care drug monitoring system for TFV through the generation of high-performance immunoreagents.

Once obtained these high, we developed and in-house validated an enzyme-linked immunosorbent assay (ELISA) for the dosage of Tenofovir in fortified saliva samples. In addition, we use this approach to develop and in-house validate a sensitive LFIA for the potential assessment of the adherence in salivary matrix. In the absence of an appropriate salivary cut-off level for TDF and TAF administered patients we identify adherence-relevant concentration ranges and evaluated the potentialities of the newly developed immunoassays [13]. The scheme is reported in Figure 6.1.

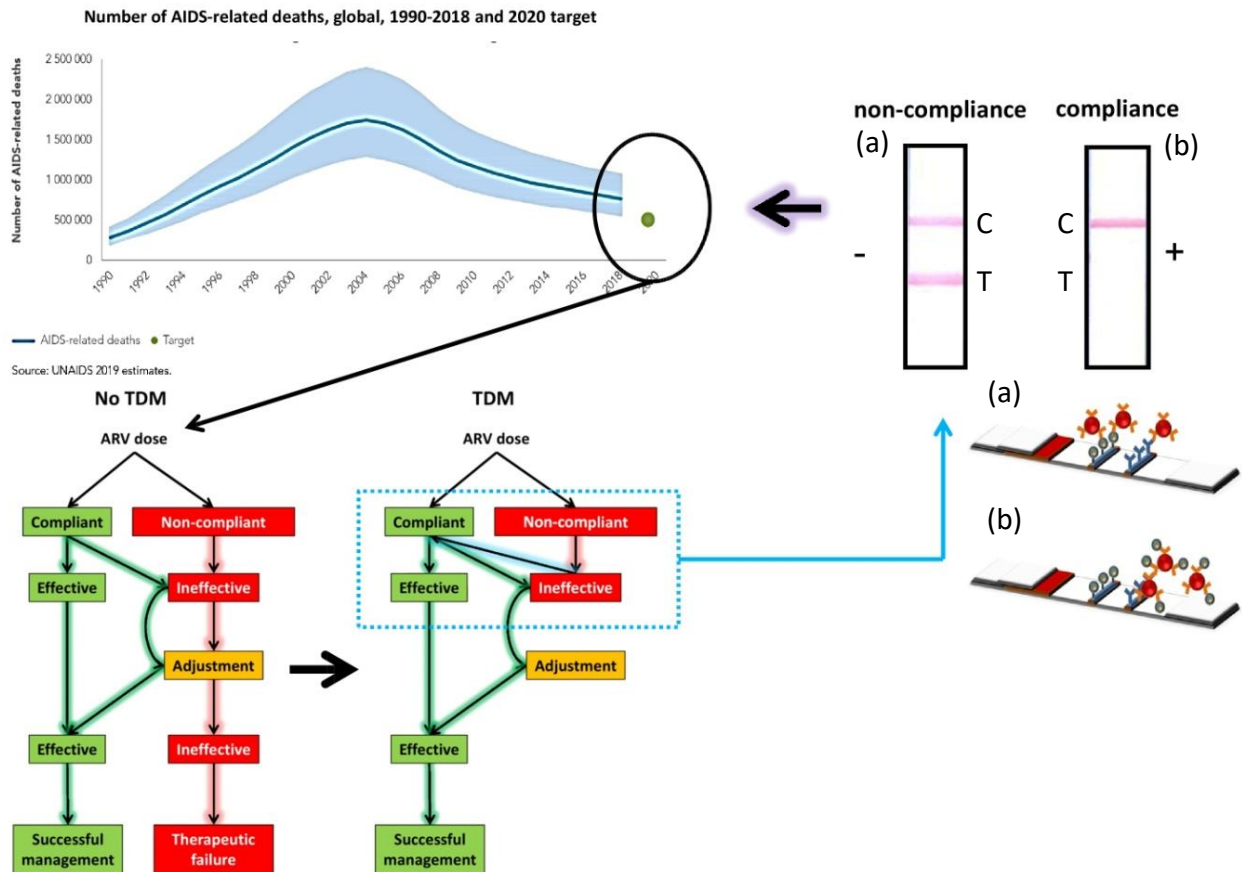


**Figure 6.1:** The graph of the yearly HIV-related deaths evidences the gap between the trend and the WHO target. The reason must be found in the lack of compliance: the diagram explains the critical step in which the intervention of the TDM can be inserted. The embodiment of this intervention is the POCT and its features, including the easy interpretation to boost the efficacy of the treatments to low the gap. Scheme of the functioning of the LFIA for detecting Tenofovir. The anti-TFV antibody labelled with gold nanoparticles (GNP-mAb) is pre-adsorbed on the conjugate reservoir. The antigen (TFV-OVA) and a goat anti-mouse antibody (GAM) are spotted to form the test and the control lines, respectively. The application of the sample re-suspends the labelled antibody and drives it along the membrane. In the absence of the target drug, the GNP-mAb bind to the TFV-OVA and to the GAM and accumulate both at the test and control lines resulting in the appearance of two visible red lines (a). In the presence of the drug (TFV), the binding to the TFV-OVA at the test line is inhibited, thus only the control line becomes visible (b).

## 6.1.2 Materials and Methods

### Immunoreagents, chemicals and materials

Tenofovir monohydrate was acquired from Tokyo Chemical Industry UK Ltd. Tenofovir Disoproxil Fumarate (TDF), Tenofovir Disoproxil Alafenamide (TAF), Tenofovir Diphosphate (TDP), were purchased by Selleck Chemicals (Houston, TX, USA). Elvitegravir was provided by Advanced ChemBlocks Inc (Burlingame, CA, USA), Dolutegravir by Ark Pharm (Arlington Heights, IL, USA), Adenosine triphosphate (ATP) by BDH Biochemical (Basel, CH). The rest of the reagents and solvents were acquired from Merck (Darmstadt, Germany) and utilized without purification. Bovine serum albumin (BSA) fraction V was obtained from Roche Applied Science (Mannheim, Germany). Horseradish peroxidase (HRP), ovalbumin (OVA), fetal bovine serum, hybridoma fusion and cloning supplement, and Freund's adjuvants were obtained from Merck (Darmstadt, Germany). HiTrap Sephadex G-25 desalting columns for conjugate purification and HiTrap protein G HP columns for mouse IgG purification were procured from GE Healthcare (Uppsala, Sweden). Immunoassays were carried out with Costars 96-well flat-bottom high-binding polystyrene ELISA plates obtained from Corning (Corning, NY, USA). Goat anti-mouse immunoglobulin polyclonal antibody (GAM) was obtained from Jackson ImmunoResearch Laboratories (West Grove, PA, USA). Peroxidase labelled rabbit anti-mouse immunoglobulin polyclonal antibody (RAM-HRP) was obtained from Dako (Glostrup, Denmark). o-Phenylenediamine was obtained from Merck (Darmstadt, Germany). Hapten density of protein conjugates was determined using a 5800 matrix-assisted laser desorption ionization time-of-flight (MALDI-TOF/TOF) mass spectrometry instrument from AB Sciex (Framingham, MA, USA). An ELx405 washer and a PowerWave HT microplate reader from BioTek Instruments (Winooski, VT, USA) were employed for microplate washing and immunoassay absorbance reading, respectively.

For the dipstick prototype, colloidal gold (20 nm, OD 1) solution was purchased from BBI Solutions (CrumLin, UK). Backed high-binding nitrocellulose membranes (25 mm wide and 15 µm pore size) obtained from MDI Advanced Microdevices PVT Ltd (Ambala Cantt, India), cellulose sample pads (17 mm wide) obtained from Millipore Corporation (Billerica, MA, USA), cellulose absorbent pads obtained (43 mm wide) from Ahlstrom-Munksjo" (Helsinki, Finland), and 8 x 30 cm backing cards obtained from Kenosha (Amstelveen, The Netherlands) were used to build the strips for the dipstick LFIA prototype for urine.

To develop the standalone lateral flow for saliva were used the following materials. Gold (III) chloride trihydrate (ACS reagent), sucrose, bovine serum albumin (BSA), obtained from Sigma–Aldrich (St. Louis, MO, USA). Tween20 and other chemicals were purchased from VWR International (Milan, Italy). Nitrocellulose membranes with cellulose adsorbent pad and glass fibre BR4 sample pads were purchased by MDI membrane technologies (Ambala, India) and glass fibre conjugate pads were obtained from Merck Millipore (Billerica, MA, USA). Colour measurements and processing was made by using ImageJ software and statistical calculations were carried out with SigmaPlot 11.0 software.

### Hapten synthesis

The strategy that was followed to synthesize the carboxylated hapten of TFV is schematically summarized in Figure 6.2. The following are the specific details used to prepare this hapten and intermediates of its synthesis.

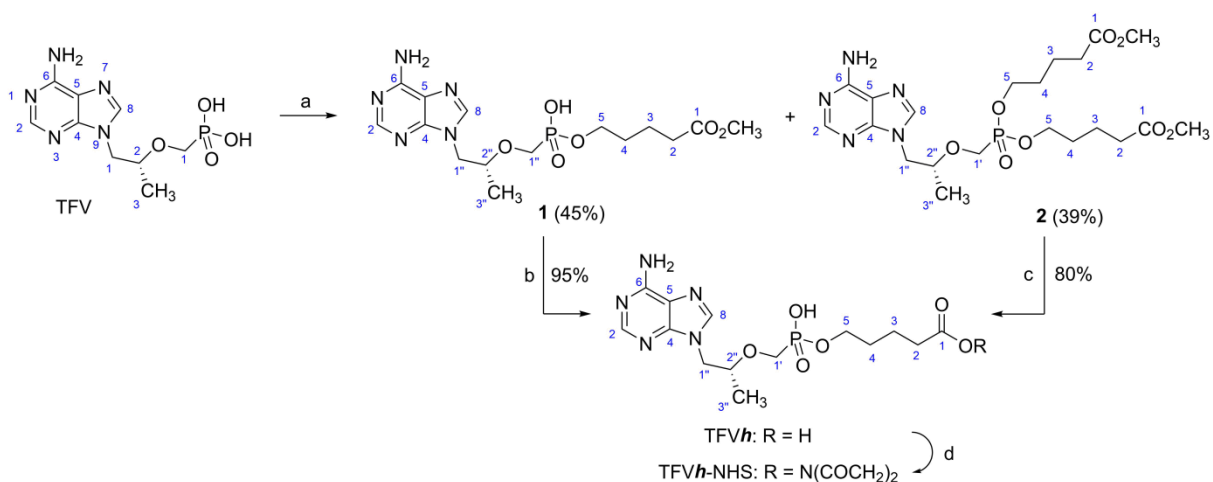


**Figure 6.2** Synthesis of TFVh and its N-hydroxysuccinimidyl ester (TFVh-NHS). Reagents and conditions: (a) Et<sub>3</sub>N, Br(CH<sub>2</sub>)<sub>4</sub>CO<sub>2</sub>CH<sub>3</sub>, DMF, 85 °C, 24 h; (b) 1 M NaOH, CH<sub>3</sub>OH, rt, 16 h; (c) 1 M NaOH, CH<sub>3</sub>OH, 90 °C, mw, 2 h; (d) DSC, Et<sub>3</sub>N, DMF, rt, 24 h.

Synthesis of methyl 5-((((R)-1-(6-amino-9H-purin-9-yl)propan-2-yl)oxy)methyl)(hydroxy)phosphoryl)oxy)pentanoate (**1**) and dimethyl 5,50-((((1-(6-amino-9H-purin-9-yl)propan-2-yl)oxy)methyl) phosphoryl) bis(oxy))(R)-dipentanoate (**2**).

Et<sub>3</sub>N (200 mL, 1.435 mmol, 4.4 equiv.) was dropwise added to a stirred suspension of tenofovir monohydrate (100 mg, 0.328 mmol) in 2 mL of anhydrous N,N'-dimethylformamide (DMF). After stirring for a few minutes under nitrogen at rt, a clear solution was obtained, which later transformed into a white suspension. Then, methyl 5-bromopentanoate (135.5mg, 99.4 mL, 0.695 mmol, 2.1 equiv.) was added and the reaction mixture was heated at 85 °C. Upon reaching this temperature, the initial suspension changed into a slightly brownish solution and then the formation of an abundant white precipitate (NEt<sub>3</sub>\_HBr) was observed. After stirring for 24 h, the reaction mixture was cooled down to rt, water (10 mL) was added, and the mixture was concentrated at reduced pressure. 10 mL of water was added, and the mixture was again concentrated to dryness. The residue was dissolved in the minimum amount of acetone and adsorbed onto a small amount of silica. The solvent was removed under reduced pressure and the resulting solid was charged onto a silica gel chromatography column and eluted using CHCl<sub>3</sub>. The eluate, a solution of diester **2** and some NEt<sub>3</sub>\_HBr in CHCl<sub>3</sub>, was transferred to a separatory funnel and washed with water and brine, dried over anhydrous MgSO<sub>4</sub>, and concentrated under reduced pressure to give pure diester **2** (66 mg, 39%) as a viscous oil. Further elution of the silica column with MeOH afforded monoester **1** (59 mg, 45%) as a white foam, which crystallized from EtOAc–MeOH as white crystals (m.p. 126.5–128.2 °C). The spectroscopic characterization data of methyl ester **1** (Figure 6.3 and 6.4) and diester **2** (Figure 6.5 and 6.6) were made as follows. <sup>1</sup>H and <sup>13</sup>C NMR spectra were recorded on a Bruker Avance DRX-300 MHz, in the solvent indicated, at 300 MHz and 75 MHz, respectively. <sup>31</sup>P-NMR spectra were recorded under high-power proton decoupling conditions. The abbreviation used for NMR data are as follows: s = singlet, d = doublet, t = triplet, dd = double doublet, br = broad, m = multiplet, Pur = purine ring.



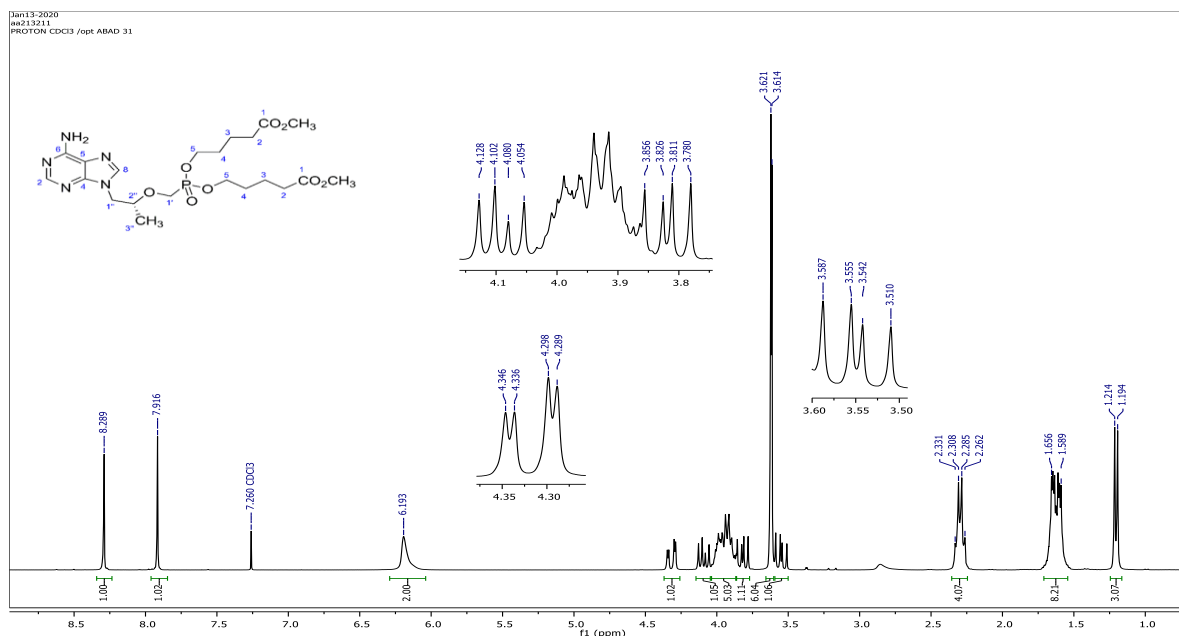


**Figure 6.5:**  $^1\text{H}$  NMR (300 MHz,  $\text{CDCl}_3$ )  $\delta$  8.29 (1H, s, H-2 Pur), 7.92 (1H, s, H-8 Pur), 6.19 (2H, br s,  $\text{NH}_2$ ), 4.32 (1H, dd,  $J = 14.4, 3.0$  Hz,  $\text{H}_a-1''$ ), 4.09 (1H, dd,  $J = 14.4, 7.8$  Hz,  $\text{H}_b-1''$ ), 4.03-3.87 (5H, m,  $2\text{H}_2-5, \text{H}-2''$ ), 3.82 (1H, dd,  $J = 13.6, 9.1$  Hz,  $\text{H}_a-1'$ ), 3.62 and 3.61 (3H each, each s,  $2 \times \text{OCH}_3$ ), 3.55 (1H, dd,  $J = 13.6, 9.7$  Hz,  $\text{H}_b-1'$ ), 2.31 and 2.28 (2H each, each t,  $J = 6.9$  Hz,  $2 \times \text{H}_2-2$ ), 1.70-1.55 (8H, m,  $2 \times \text{H}_2-3, 2 \times \text{H}_2-4$ ), 1.20 (3H, d,  $J = 6.2$  Hz,  $\text{H}_3-3''$ )

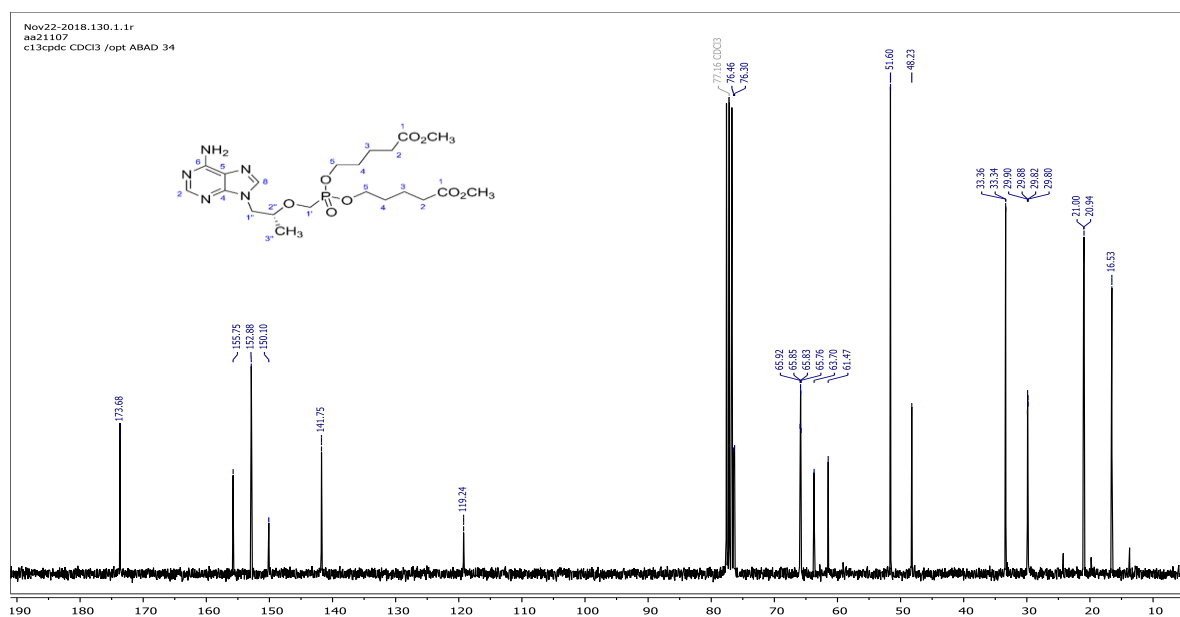


**Figure 6.6:**  $^{13}\text{C}$  NMR (75 MHz,  $\text{CDCl}_3$ )  $\delta$  173.7 (C-1), 155.7 (C-6 Pur), 152.9 (C-2 Pur), 150.1 (C-4 Pur), 141.8 (C-8 Pur), 119.2 (C-5 Pur), 76.4 (d,  $J = 12.3$  Hz, C-2''), 65.9 and 65.8 (two d,  $J = 5.3$  Hz,  $2 \times \text{C}-5$ ), 62.6 (d,  $J = 168.4$  Hz, C-1'), 51.6 ( $2 \times \text{OCH}_3$ ), 48.2 (C-1''), 33.4 and 33.3 ( $2 \times \text{C}-2$ ), 29.9 and 29.8 (two d,  $J = 5.9$  Hz,  $2 \times \text{C}-4$ ), 21.0 and 20.9 ( $2 \times \text{C}-3$ ), 16.5 (C-3'');

$^{31}\text{P}$  NMR (121 MHz,  $\text{CDCl}_3$ )  $\delta$  21.02; HRMS calcd for  $\text{C}_{21}\text{H}_{35}\text{N}_5\text{O}_8\text{P}$   $[\text{M}+\text{H}]^+$  516.2218, found 516.2209.

*Synthesis of 5-((((R)-1-(6-amino-9H-purin-9-yl)propan-2-yl)oxy)-methyl)(hydroxy)phosphoryl)oxy) pentanoic acid (TFVh).*

(a) From ester 1. A 1 M NaOH (0.2mL, 0.197mmol, 4 equiv.) solution was dropwise added to a solution of ester 1 (19.7 mg, 0.049 mmol) in  $\text{CH}_3\text{OH}$  (0.8 mL) at rt, and the resulting solution

was stirred overnight. Then, the reaction mixture was treated with 1 M HCl (0.2 mL, 4.0 equiv.) to give a clear solution of pH 6–7 that was concentrated at reduced pressure to dryness. The white solid residue obtained (32 mg) was resuspended in CH<sub>3</sub>OH (1 mL) and the suspension was stirred for 5 min, then filtered with a 0.2mm syringe filter to remove NaCl, and the filtrate was concentrated under vacuum to give TVFh (18 mg, 95%) as an amorphous solid.

(b) From diester 2. A 1 M aqueous solution of NaOH (530 mL, 0.530 mmol, 5.6 equiv.) and diester 2 (49 mg, 0.095 mmol) in CH<sub>3</sub>OH (2 mL), prepared in a septum-sealed microwave tube, was irradiated with microwaves (Discover System, CEM Corporation) at 90 °C (300 W) for 2 h. The mixture was let cool down to rt, treated with 1 M aqueous HCl, and concentrated at reduced pressure. The white solid residue obtained (78 mg) was washed gently with CHCl<sub>3</sub> to remove the generated 5-hydroxyvaleric acid, then resuspended in CH<sub>3</sub>OH (2 mL) and processed as described above for the hydrolysis of 1 to give TVFh as the hydrochloride salt (32.1 mg, 80%).

The progress of reactions was followed by thin-layer chromatography (TLC), using aluminium plates coated with silica gel (60F245 Merck). TLC plates were visualized by exposure to short wave ultraviolet light (254 nm) and irreversibly stained by treatment with an aqueous solution of ceric ammonium molybdate followed by heating. Purification of the synthesized compounds was achieved with a Merck silica gel 60 flash chromatography column (230-400 mesh), using the mobile phase solvent mixture indicated. The spectroscopic characterization was made as previously described Figures 6.7-9.

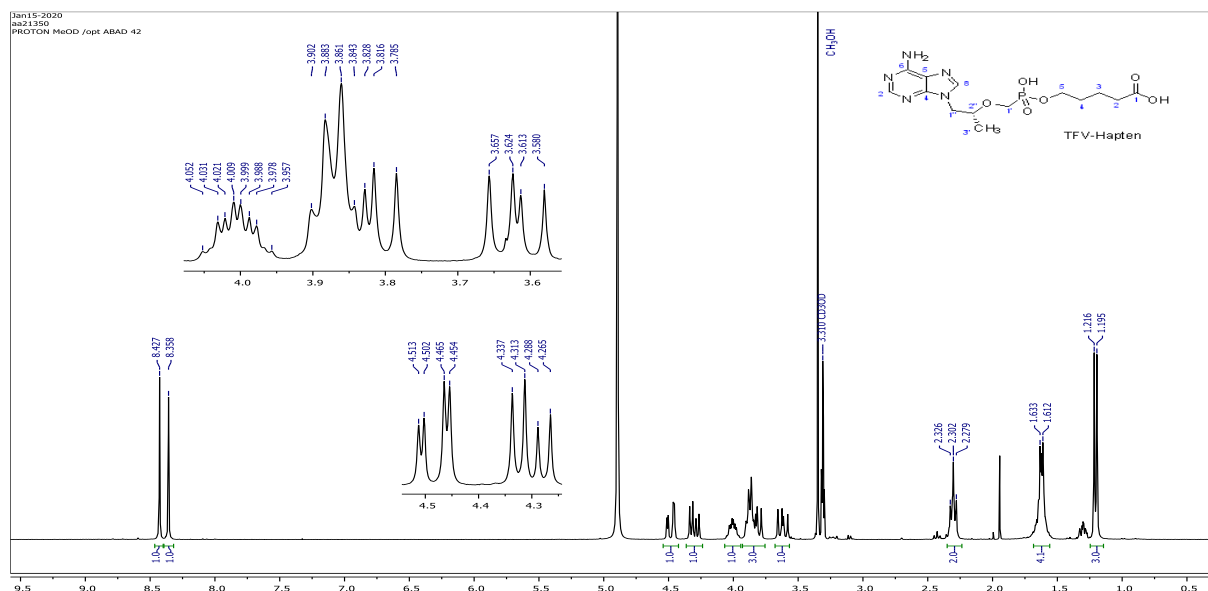
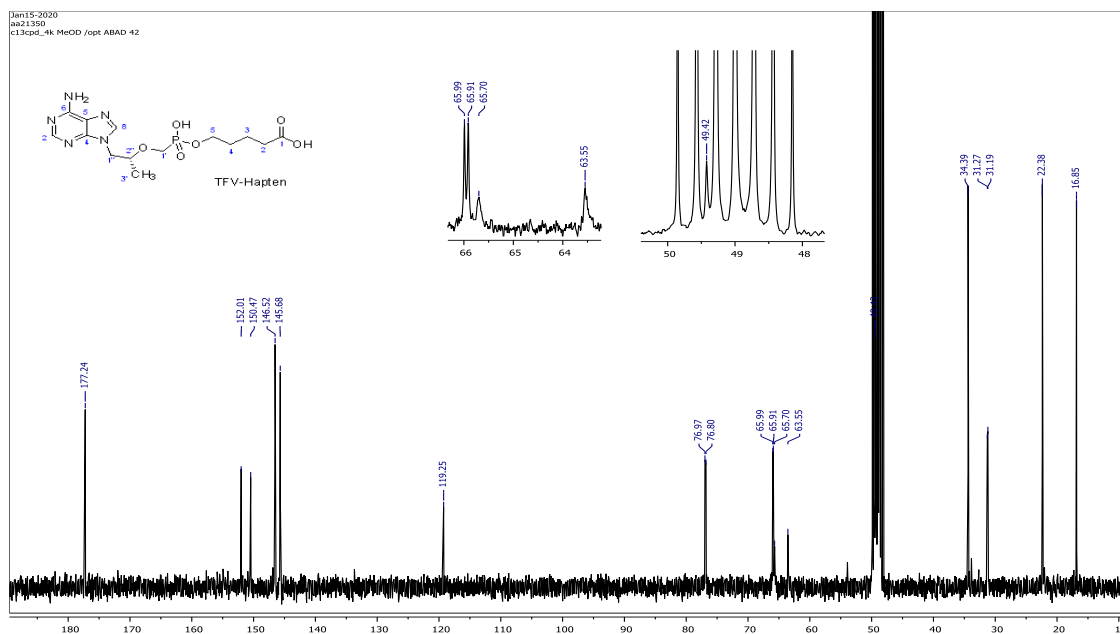


**Figure 6.7:** <sup>1</sup>H NMR (300 MHz, CD<sub>3</sub>OD) δ 8.43 (1H, s, H-2 Pur), 8.36 (1H, s, H-8 Pur), 4.48 (1H, dd, *J* = 14.4, 3.1, H<sub>a</sub>-1''), 4.30 (1H, dd, *J* = 14.4, 7.0 Hz, H<sub>b</sub>-1''), 4.00 (1H, dt, *J* = 6.6, 3.0 Hz, H-2''), 3.87 (2H, dt, 5.6, 5.6 Hz H<sub>2</sub>-5), 3.82 (1H, *J* = 13.1, 9.3 Hz, H<sub>a</sub>-1'), 3.62 (1H, dd, *J* = 13.1, 9.8 Hz, H<sub>b</sub>-1'), 2.30 (2H, t, *J* = 7.1 Hz, H<sub>2</sub>-2), 1.68-1.56 (4H, m, H<sub>2</sub>-3, H<sub>2</sub>-4), 1.21 (3H, d, *J* = 6.2 Hz, H<sub>3</sub>-3'')



Figures 6.8:  $^{13}\text{C}$  NMR (75 MHz,  $\text{CD}_3\text{OD}$ )  $\delta$  177.2 (C-1), 152.0 (C-6 Pur), 150.5 (C-4 Pur), 146.5 (C-2 Pur), 145.7 (C-8 Pur), 119.2 (C-5 Pur), 76.9 (d,  $J = 12.6$  Hz, C-2''), 66.0 (d,  $J = 5.9$  Hz, C-5), 64.6 (d,  $J = 162.1$  Hz, C-1'), 49.4 (C-1''), 34.4 (C-2), 31.2 (d,  $J = 6.2$  Hz, C-4), 22.4 (C-3), 16.9 (C-3'');  $^{31}\text{P}$  NMR (121 MHz,  $\text{CD}_3\text{OD}$ )  $\delta$  17.51; HRMS calcd for  $\text{C}_{14}\text{H}_{23}\text{N}_5\text{O}_6\text{P}$   $[\text{M}+\text{H}]^+$  388.1380, found 388.1371

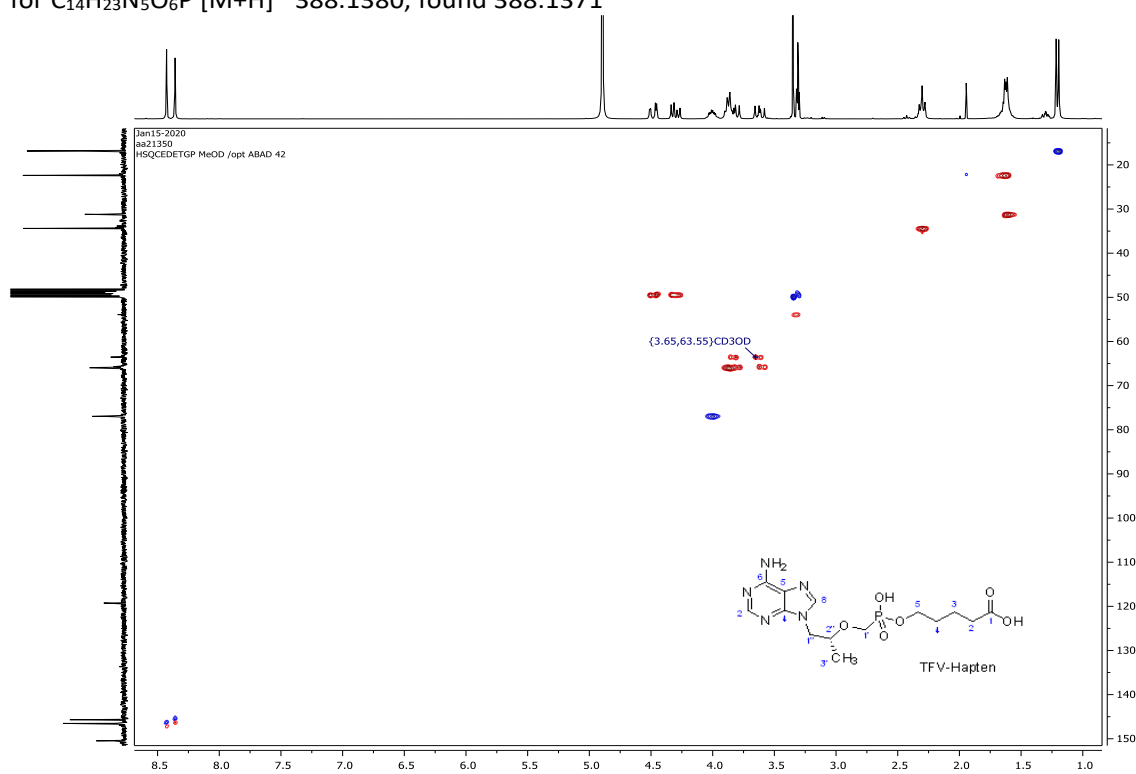


Figure 6.9: Edited HSQC NMR spectrum of TFVh (75 MHz,  $\text{CD}_3\text{OD}$ ).

## Hapten conjugation to proteins

TFVh was coupled to three carrier proteins. First, the carboxylic functional group of the hapten was activated via formation of the corresponding N-hydroxysuccinimidyl ester (Figure



6.2), which facilitates its subsequent conjugation to the lysine residues of the proteins through formation of an amide bond.

(a) Hapten activation: preparation of the N-hydroxysuccinimidyl ester of TFVh (TFVh-NHS). Anhydrous Et<sub>3</sub>N (10 mL, 0.072 mmol, 2.3 equiv.) was added to a solution of TFVh (13 mg, 0.031 mmol) in anhydrous DMF (310 mL) at rt under nitrogen. Then, a solution of N,N'-disuccinimidyl carbonate (10 mg, 0.039 mmol, 1.3 equiv.) in DMF (150 mL) was added, and the mixture was stirred for 24 h. The resulting reaction mixture, containing the formed TFVh-NHS ester, was used directly for the preparation of the protein-hapten conjugates, as described below. Confirmation of the formation of the active ester of TFVh was obtained from the NMR spectra of the reaction crude obtained by evaporation under reduced pressure of an aliquot of the above-mentioned reaction mixture.

<sup>1</sup>H NMR (300 MHz, DMSO-d<sub>6</sub>) signals corresponding only to the N-hydroxysuccinimidyl ester of TFVh are given: δ 8.16 and 8.14 (1H each, each s, H-8 and H-2 Pur), 7.25 (2H, s, NH<sub>2</sub>), 4.25 (1H, dd, J = 14.4, 3.5, Ha-100), 4.15 (1H, dd, J = 14.4, 6.0 Hz, Hb-100), 3.88 (1H, m, H-200), 3.75–3.40 (4H, m, H2-5, H2-10), 2.80 (4H, s, COCH<sub>2</sub>CH<sub>2</sub>CO), 2.66 (2H, t, J = 7.1 Hz, H2-2), 1.65–1.40 (4H, m, H2-3, H2-4), 1.02 (3H, d, J = 6.1 Hz, H3-300); <sup>31</sup>P NMR (121 MHz, DMSO-d<sub>6</sub>) δ 15.18.

(b) Preparation of hapten-protein conjugates. A 50 mM solution of TFVh-NHS in DMF was added dropwise to a protein solution in PB (100 mM phosphate buffer, pH 7.4) under gentle stirring in amber glass vials. The coupling reactions were carried out for 16 h at rt, and the DMF concentration in the final mixture never exceeded 20% (v/v). As carrier proteins, bovine serum albumin (BSA) was used for immunogen preparation, and ovalbumin (OVA) and horseradish peroxidase (HRP) were employed for coating antigen and enzyme tracer preparation, respectively. The initial hapten-to-protein molar ratios were 40 for BSA, 20 for OVA, and 10 for HRP. Bioconjugates (BSA-TFVh, OVA-TFVh and HRP-TFVh) were purified by gel filtration chromatography using a Sephadex G-25 HiTrap Desalting Column using PB as an eluent at 5 mL/min. The BSA-TFVh conjugate solution was filter sterilized, brought to 1 mg/mL with sterile PB, and stored frozen at -20 °C. The OVA-TFVh conjugate solution was diluted with PB with 0.01% (w/v) thimerosal and stored at -20 °C. The HRP-TFVh tracer solution was 1:1 (v/v) diluted with PBS containing 1% (w/v) BSA and 0.02% (w/v) thimerosal and stored at 4 °C. The obtained hapten-to-protein molar ratio (MR) of each conjugate was determined by Matrix-Assisted Laser Desorption Ionization Time-of-Flight Mass Spectrometry (MALDI-TOF-MS) using water-dialyzed samples of the purified bioconjugates (Figure 6.10).

## MALDI Mass Spectrometry Analysis of Bioconjugates

High resolution mass spectra (HRMS) were obtained by electrospray ionization (ESI) mode in a TripleTOF™ 5600 LC/MS/MS System (ABSciex, Framingham, MA, USA) mass spectrometer equipped with an electrospray source (Waters, Manchester, United Kingdom). The obtained data are expressed as mass/charge ratio (*m/z*).

### *Sample preparation*

A 100 μL aliquot of protein conjugates purified by size-exclusion chromatography was dialyzed against Milli-Q water for 24 h. One microliter of every sample solution, containing about 1 μg/μL of protein conjugate, was spotted onto the MALDI plate, after the droplets

were air-dried at room temperature, 1  $\mu\text{L}$  of matrix [10 mg/mL sinapinic acid (Bruker) in 70%  $\text{CH}_3\text{CN}$ , 0.1%  $\text{CF}_3\text{CO}_2\text{H}$ ] was added and allowed to air-dry at room temperature.

### Mass spectrometry analysis

The resulting mixtures were analysed in a 5800 MALDI TOF/TOF (ABSciex) in positive linear mode. Previously, the plate and the acquisition method were calibrated with 1  $\mu\text{L}$  of the TOF-TOF calibration mixture (ABSciex), in 13 positions. Every sample was calibrated by 'close external calibration' method with a BSA, OVA or HRP spectrum acquired in a close position.

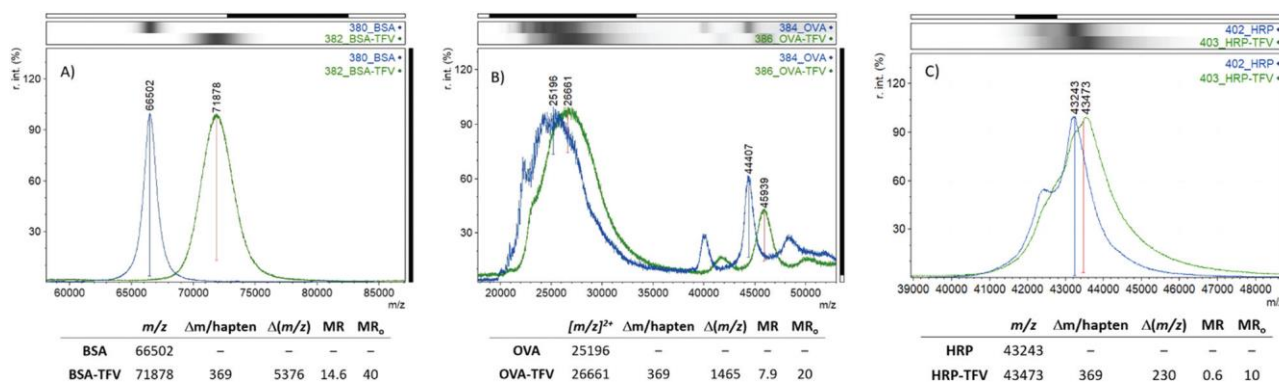


**Figure 6.10:** MALDI-TOF-MS spectra of protein-TFVh bioconjugates (green). Unmodified proteins (blue) were also analysed for the calculation of the hapten densities, and their spectra were also included in the graphs for visual comparison. MR<sub>0</sub>: initial hapten-to-protein molar ratio; MR: hapten-to-protein molar ratio in the final conjugate. The hapten-to-protein molar ratio of the OVA conjugate is based on doubly charged protein and conjugate molecular ions.

### Monoclonal antibody generation

The experimental design was approved by the Bioethics Committee of the University of Valencia. Animal manipulation was performed in compliance with the European Directive 2010/63/EU and the Spanish laws and guidelines (RD1201/2005 and 32/2007) concerning the protection of animals used for scientific purposes. A set of six mice was immunized with the BSA-TFVh conjugate by intraperitoneal injections, at 21-day intervals, using complete Freund's adjuvant for the first injection and incomplete Freund's adjuvant for the two subsequent injections. Each animal received 100 mg of conjugate in each boost. Four days before cell fusion, a final injection was administered with the same amount of bioconjugate in sterile PBS. Hybridoma cells were obtained from three independent cell fusions by employing, in each experiment, the spleen cells from two immunized mice. PEG1500 was used as the fusing agent to generate hybridoma cells and they were cultivated following standard protocols.[18] Hybridoma culture supernatants were assayed twelve days after the cell fusion using a double screening procedure consisting of a differential competitive ELISA (parallel assays were carried out with and without TFV) followed by a checkerboard competitive ELISA using the OVA-TFVh conjugate as the coating antigen. The differential test was carried out in microplates coated with 100  $\mu\text{L}$  per well of OVA-TFVh solution at 0.1 mg/mL in coating buffer (50 mM carbonate–bicarbonate buffer, pH 9.6). Each culture supernatant (40  $\mu\text{L}$ ) was added to two contiguous wells containing 50  $\mu\text{L}$  of PBS (11.9 mM phosphate, pH 7.4, containing 137 mM NaCl and 2.7 mM KCl) or 100 nM TFV solution in PBS. Those supernatants scored as positive (high signal provided by antibody binding to the

coating antigen) and competitive (signal inhibition was higher than 50% with TFV) were re-evaluated by checkerboard competitive ELISA using microplates coated with 0.01 mg/mL and 0.1 mg/mL solutions of the OVA-TFVh antigen. Supernatants four-fold serially diluted in PBS and TFV solutions (10 and 100 nM) were prepared in PBS. The competitive step was carried out by adding 50  $\mu$ L per well of supernatant dilution in PBS and 50  $\mu$ L per well of TFV solution in PBS or blank PBS solution. Those hybridomas that produced high-affinity mAbs were cloned by limiting dilution using HT medium (hypoxanthine-thymidine solution containing 1% (v/v) hybridoma fusion and cloning supplement and 20% (v/v) foetal bovine serum). Stable cell clones were expanded in vitro and cryopreserved in liquid nitrogen. Immunoglobulins were purified from late stationary-phase culture supernatants by double ammonium sulphate precipitation and affinity chromatography with protein G. Purified mAbs were stored as ammonium sulphate precipitates at 4 °C.

### Direct competitive ELISA (dcELISA)

This cELISA format was performed with the immobilized antibody and direct detection using a tracer conjugate.[19] Microwells were coated by overnight incubation at 4 °C with 100  $\mu$ L per well of GAM solution at 1 mg mL<sup>-1</sup> in coating buffer. Plates were washed four times with washing solution after each incubation step. Then, 100  $\mu$ L per well of anti-TFV antibody solution in PBS-T was added and incubated for 1 h at rt. After washing the plates, the competitive reaction was carried out by mixing 50  $\mu$ L per well of TFV solution prepared in PBS and 50  $\mu$ L per well of HRP-TFVh solution prepared in PBS-T. The plates were incubated at rt for 1 h, washed, and the signal was generated as described before for the icELISA. ELISA data analysis Calibration curves of TFV were prepared using five-fold serial dilutions in PBS (from 0.0064 to 100 nM) and a blank was also included. Absorbance values were fitted to a four-parameter logistic equation for standard curves using the SigmaPlot software (Chicago, IL, USA). Amax is the absorbance of the blank, and the TFV concentration affording a 50% reduction of Amax (IC<sub>50</sub>) was considered as an estimation of the apparent affinity constant of the antibody.

### Indirect competitive ELISA (icELISA)

This cELISA format was carried out with the immobilized conjugate and indirect antibody detection.[19] Microplate wells were coated with 100  $\mu$ L per well of OVA-TFVh solution in coating buffer by overnight incubation at rt. Plates were washed four times with washing solution (140 mM NaCl with 0.05% (v/v) Tween 20) after each incubation step. The competitive immunochemical reaction was performed by mixing 50  $\mu$ L per well of TFV solution in PBS with 50  $\mu$ L per well of the anti-TFV mAb solution in PBS-T (PBS containing 0.05% (v/v) Tween 20). The mixture was incubated for 1 h at rt and the plates were washed. The fraction of bound mAb was detected by adding 100  $\mu$ L per well of a 1/2000 dilution in PBS-T of peroxidase labelled rabbit anti-mouse immunoglobulin polyclonal antibody (RAM-HRP). The plates were incubated at rt for 1 h, and after washing as before, the signal was generated by adding 100  $\mu$ L per well of 2 mg/mL o-phenylenediamine solution in enzyme buffer (25 mM citrate and 62 mM sodium phosphate buffer, pH 5.4, containing 0.012% (v/v) H<sub>2</sub>O<sub>2</sub>). The enzymatic reaction was stopped after 10 min at rt by adding 100  $\mu$ L per well of 1 M H<sub>2</sub>SO<sub>4</sub>. The absorbance was immediately read at 492 nm with a reference wavelength of 650 nm.

## Analytical validation of the indirect competitive ELISA (icELISA) in saliva

Once selected the best antibody, the ELISA protocol was further implemented until the obtainment of an effective method for the detection of TFV in saliva. For this purpose, the buffer used to dilute the mAb and the sample, the antigen and antibody amounts, and the dilution factor of the sample were re-defined. In details, a checkerboard titration using the OVA-TFV<sub>h</sub> in concentration 40, 100, 400 ng/mL and mAb concentration 40, 100, 400 ng/mL was made. The matrix effect minimization was addressed by changing sample dilution (1/2, 1/4, 1/8, 1/16, 1/25), buffer pH (6.4, 7.4) additives (casein: 0, 0.5, 1%; NaCl: 0.15, 0.3, 0.6, 1 M), number of washings (3, 5). The optimal standard curve of TFV was made by dissolving TFV in a predilution buffer (20 mM phosphate buffer, pH 7, 630 mM NaCl, 0.05% Tween20, 1% w/v casein). The test involves a 1:25 dilution of salivary samples by the working buffer (PBS-T). The rest of the assay was carried as described in the previous section. The in-house validation of the method included estimating precision, accuracy, recovery, and dynamic range. The imprecision was estimated by measuring between and within-assay reproducibility and was calculated by analysing each calibrator level in four replicates in the same days and on three days (for a total of 12 replicates). The overall imprecision at each level was calculated as the mean CV% values. The recovery test was made by using a pool of saliva samples spiked at three levels corresponding to the threshold assuring perfect compliance, 2x threshold and 0,5x threshold. Recovery estimated TFV concentration / fortification concentration x 100.

## Monoclonal antibody labelling with gold nanoparticles

Conjugation of anti-TFV mAb to gold nanoparticles was conducted by passive adsorption in basic medium, as previously described.[20] Briefly, 1 mL of GNP suspension was centrifuged for 10 min at 7100  $\times$  g, and the supernatant was removed and replaced with the same volume of 20 mM HEPES, pH 8.5. Two microlitres of mAb solution (1 mg/mL in HEPES buffer) was added to the buffered GNP. The solution was gently stirred and left reacting for 45 min at rt. Then, 50 mL of 5% (w/v) BSA solution in HEPES was added and the mixture was incubated for 30 min at rt. Finally, the GNP–mAb conjugate was recovered by centrifugation (10 min at 7100  $\times$  g), washed once with 10 mM Tris–HCl buffer, pH 8.5, and reconstituted in the same buffer supplemented with 0.05% (v/v) Tween 20. GNPs labelled with the antibodies were stored at 4 °C until use. For the prototypes used for urine dipstick format commercial GNPs from BBI were used. The standalone device home-made GNPs were synthesized as reported in Chapter 3.1.2.

## Lateral flow immunoassay

LFIA strips in the competitive format[20] were prepared by using BSA-TFV<sub>h</sub> and GAM to form the test and control lines, respectively. A 300-mm long nitrocellulose membrane was dispensed with immunoreagents using a XZ1010 Dispense Platform (BioDot, Irvine, CA, USA) dispenser at 0.5  $\mu$ L/cm. The test line comprised TFV<sub>h</sub> conjugate (1 mg/mL), whereas the control line was drawn by dispensing GAM solution (1 mg/mL). Both reagents were diluted in PBS for dispensing. The membrane was dried at rt before assembling. The LFIA strips were

assembled by sequentially pasting the dry nitrocellulose membrane, the sample pad, and the adsorbent pad on a backing support. Then, the membrane was cut into 4-mm width strips using a CM5000 Guillotine Cutter (BioDot, Irvine, CA, USA) and stored sealed in dry tubes at 4 °C. Signal from lateral flow assays was read using an EPSON Perfection V39 ultra-compact colour image scanner from Seiko Epson Corp. (Suwa, Japan).

#### *LFIA for TFV in synthetic urine*

TFV standard solutions were prepared by five-fold serial dilution from a 25 nM solution in the synthetic urine diluted in the running buffer (Tris–HCl 10 mM, pH 7.4, 0.25% (v/v) Tween 20) from which 75 µL was added to a well of a microtiter plate. The wells were supplemented with 25 µL of GNP–mAb suspension and incubated for 5 min at rt. The strips were then dipped into the well. After 10 min, the strips were removed and gently cool-air dried. At this time, strips were scanned, and images were digitally processed to quantify the colour intensities of the lines. The signal from lateral flow assays was read using an EPSON Perfection V39 ultra-compact colour image scanner from Seiko Epson Corp. (Suwa, Japan). The intensity that was measured at the test line (T) was divided by that of the control line (C) and the T/C intensity ratio was plotted versus the TFV concentration. Synthetic urine as a surrogate of human urine was prepared as reported in the literature.[20] Fortified urine samples were generated by adding TFV to the synthetic urine to a final concentration of 0.04, 0.2, 1, 5, and 25 nM. Samples were subjected to LFIA as described above, except that 37.5 mL of fortified urine was diluted with 37.5 mL of running buffer and then mixed with 25 mL of GNP–mAb suspension.

#### *LFIA for TFV in saliva*

Saliva samples were collected at 1 pm by using the Salivette Swab (Sarstedt AG&Co, Nümbrecht, Germany) and following supplier's instructions. In details, each subject was requested to rinse the mouth with water, wait for 10 minutes and then put the swab under the tongue for 3 minutes. The swab was placed in the upper part of the collector, immediately refrigerated at -20°C for at least 24 hours. After thawing, saliva was recovered by centrifugation of the swab (15 min at 2000 x g) and immediately analysed.

The LFIA for TFV was carried out at room temperature. 90 µL of fortified saliva sample was dispensed on the sample pad through the sample well to start the capillary flowing of the solution towards the adsorbent pad. After 10 min, the results were visually estimated, as shown in Figure 6.1. The signals generated at the test and control lines, due to GNP-Ab binding to immobilized antigens and secondary antibodies, were measured by acquiring the images of the LFD by a portable scanner (OpticSlim 550 scanner, Plustek Technology GmbH, Norderstedt, Germany) and quantifying the intensity of the colour on each line with QuantiScan 3.0 software (Biosoft, Cambridge, U.K.). The performance was compared according to the following points: (1) intensity of colouring of the test (and control) lines, and (2) sensitivity of the LFIA for measuring TFV and (3) cross reactivity towards interfering molecules. Accordingly, TFV standard solutions (0, 0.05, 0.25, 0.5, 1 and 1.5 ng/ml) were prepared directly in collected saliva. The signals produced at the test (T) and control (C) lines were singularly quantified, converted in T/C ratios as a normalization normalized for the signal of the blank and then plotted toward TFV concentration to estimate the IC<sub>50</sub> and LOD.

### 6.1.3 Results and Discussion.

#### Hapten synthesis and bioconjugate preparation

Since TFV is a non-immunogenic substance, it needs to be linked to a macromolecular carrier (typically a protein) to elicit the immune response. Accordingly, functionalization is required to introduce an activatable chemical group for the subsequent covalent coupling to the protein. Moreover, it is advisable to include a spacer arm to keep the target molecule distant from the protein surface, thus promoting the production of antibody binding sites directed towards the analyte rather than to epitopes from the carrier. With this aim, a TFV hapten was synthesized by inserting a five-carbon aliphatic linker at the phosphonic acid moiety of the drug structure. The designed route is quite straightforward and followed a two-step pathway (Figure 6.2). The first one involved an O-alkylation reaction of the phosphonic acid group of TFV with methyl 5-bromovalerate. This alkylation reaction led to a mixture of the mono- and dialkylated products, 1 and 2, respectively, which were easily separated by conventional column chromatography.

The conversion of each compound into the designed hapten, TVFh, was carried out by hydrolysis in basic medium. With the methoxycarbonyl group of 1, the hydrolytic reaction leading to the corresponding carboxylic acid took place under very mild temperature conditions, providing TFVh with a very high yield (95%). However, the transformation of 2, which required the hydrolysis of both the carboxylate and the phosphonate groups, needed much more drastic conditions. After testing different reaction procedures, it was found that hydrolysis could be performed quite efficiently and in a relatively short time using microwaves as the heating source. After acidification, an equimolecular mixture of the hapten and 5-hydroxyvaleric acid was obtained, which were separated with relative ease by taking advantage of the much greater solubility of the latter in  $\text{CHCl}_3$ .

In summary, TFVh was obtained from TFV with an excellent overall yield of 74%. It is worth mentioning that the hapten (TFV-PO) employed by D. Sevenler et al. [20] for the generation of anti-TFV mAbs only differs from TFVh in the linker length, even though the synthetic details and full characterization data of a carboxylated derivative of TFV are herein reported for the first time. The terminal carboxylic group of TFVh was converted into the corresponding active NHS ester and covalently linked, by the formation of an amide bond, to three different proteins, BSA, OVA, and HRP. The synthesis of TFVh-NHS was carried out using N,N'-disuccinimidyl carbonate and Et<sub>3</sub>N in anhydrous DMF (Figure 6.2). The advantage of using DSC over other NHS-based activating agents is that it does not need dehydration agents and urea derivatives are not produced. The so-formed active ester was used directly without prior purification for the preparation of the protein conjugates. Following the purification of the bioconjugates by size exclusion chromatography, the hapten-to-protein molar ratios were determined by MALDI-TOF-MS. Hapten densities of ca. 14.6, 5.8, and 0.6 for BSA-TFVh, OVA-TFVh, and HRP-TFVh conjugates, respectively, were obtained (Figure 6.10).

#### Generation of monoclonal antibodies for TFV conjugation

Three independent cell fusion experiments with B lymphocytes from 6 BSA-TFVh immunized BALB/c mice were carried out. In total, 36 96-well cell culture plates were seeded with the nascent hybridoma cell lines. The mean fusion efficiency (percentage of wells with cell

growth 11 days after fusion) was 92%, with an average of 2.3 clones per well. The hybridoma screening strategy first consisted of a differential competitive ELISA in which each culture supernatant was assayed in two contiguous OVA-TFVh coated microwells (0.1 mg/mL) with (100 nM) or without TFV in solution. The number of positive wells, i.e., wells showing a clear binding (signal higher than 1.0) to the coating antigen, was 73 (2.1%), and 27 of those were also able to strongly recognize free TFV. On the next day, 66 wells were selected for a more comprehensive characterization by checkerboard competitive ELISA. In that assay, supernatants were serially diluted by 1/8, 1/32, 1/128, and 1/516 with PBS-T and tested on microplates coated with the OVA-TFVh bioconjugate at 0.01 and 0.1 mg/mL, whereas TFV was employed at 10 and 100 nM plus a blank. This strategy allowed us to easily rank hybridomas according to the antibody binding properties with the free drug, thus avoiding wasting resources and time on hybridomas that produce antibodies that recognize the protein–hapten bioconjugate but poorly bind the target analyte (Figure 6.11).

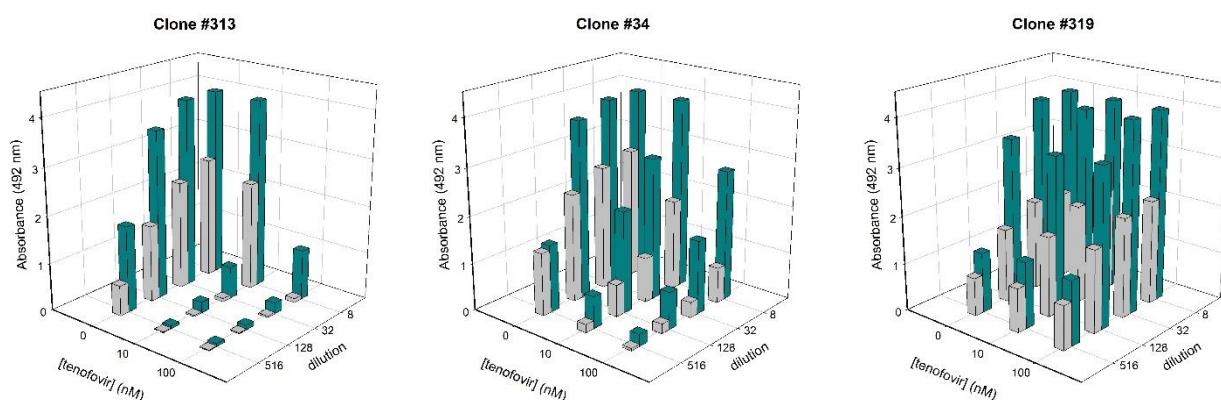


**Figure 6.11** Checkerboard competitive ELISA of post-fusion hybridoma supernatants tested on microwells coated with the conjugate OVA-TFVh at 0.01 mg/mL (grey bars) and at 0.1 mg/mL (cyan bars). Each graph represents a different hybridoma producing a monoclonal antibody capable of binding the coating conjugate and showing high affinity to TFV (clone #313), medium affinity to TFV (clone #34), and no binding to TFV (clone #319). These three hybridomas would afford similar results in a conventional non-competitive screening strategy. In contrast, in our double screening procedure, the identification of good and poor TFV binders is straightforward, so clones #34 and #319 would not be cloned.

## Characterization of monoclonal antibodies by competitive ELISA

The output of the implemented double screening process was a collection of 7 hybridoma cell lines, which were cloned by limiting dilution, expanded, and cryopreserved. Following purification by protein G affinity chromatography from late stationary phase cell cultures, the corresponding mAbs were comprehensively characterized by icELISA using several concentrations of the coating conjugate (10, 30, 100, and 300 ng/mL) and of every antibody (30, 100, and 300 ng/mL). For each immunoreagent combination, a 7-point standard curve of TFV plus a blank was assayed. Table 6.1 lists a summary of the obtained results for the 7 mAbs with the optimum immunoreagent combinations, that is, those providing the lowest IC50 value together with an Amax value higher than 0.5. Remarkably, all the mAbs exhibited outstanding affinities to TFV, with IC50 values lower than 1 nM. It is worth mentioning that several antibodies showed apparent affinity constants even lower than 0.3 nM, which means IC50 values 1000 times lower than those exhibited by the previously reported anti-TFV antibodies. These outstanding results are particularly relevant because, as we mentioned

before, the hapten that we used for the generation of the mAbs only differs from the one employed by D. Sevenler et al. in the spacer arm length.[20]

**Table 6.1** Checkerboard titration of anti-TFV monoclonal antibodies by icELISA<sup>a</sup>

mAb	[mAb] (ng/mL)	[OVA-TFVh] (ng/mL)	A <sub>max</sub>	Slope	IC50(nM)
#13	300	100	1.34±0.22	1.51±0.30	0.98±0.57
#117	300	30	1.13±0.13	1.55±0.32	0.57±0.28
#120	300	30	0.66±0.20	1.51±0.33	0.41±0.05
#216	100	30	1.16±0.20	1.42±0.07	0.43±0.06
#313	100	100	0.96±0.13	1.65±0.32	0.23±0.03
#321	100	100	1.16±0.06	1.44±0.04	0.23±0.02
#322	100	30	1.52±0.21	1.42±0.21	0.36±0.07

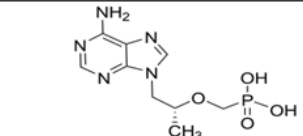
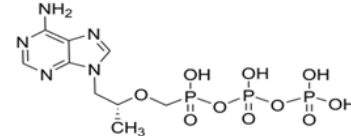
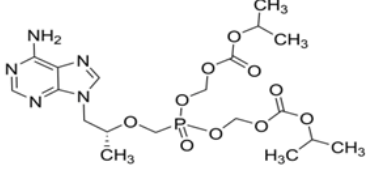
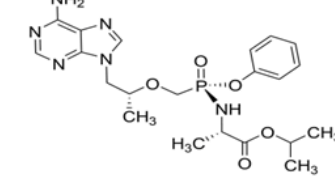
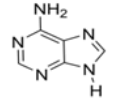
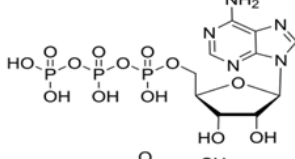
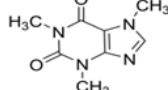
<sup>a</sup> Different concentration of each mAb were tested in plates coated with the OVA-TFVh conjugate at several concentrations. The results shown in this table correspond to the particular combination, for each antibody, resulting in the lowest IC50 value, provided that a A<sub>max</sub> value higher than 0.5 was obtained.

The lowest IC50 value reported by those authors for TFV was 480 nM. While we do not have a definite explanation for the reason why our antibodies exhibited higher affinity values, the longer immunization protocol (90 days vs. 19 days), which could have allowed for an effective maturation of the immune response, in combination with an optimal screening strategy, is likely to be at the heart of those results. The performance of the antibody collection was also assessed in the dcELISA format. In this case, the antibody was anchored to the solid support through a capture antibody, and the HRP-TFVh conjugate was used as the tracer for signal generation. While insufficient signals were obtained with most antibodies, mAb #321 performed particularly well.

Following affinity characterization of the antibody collection, the specificity of the mAbs providing the lowest IC50 values (mAb #313, #321, and #322) was determined by testing the recognition towards compounds with similar chemical structures and components of biological fluids that may potentially interfere. Cross-reactivity was measured toward the two TFV prodrugs (TDF and TAF), three analogue compounds eventually found in biological samples (adenine, caffeine, and adenosine triphosphate, ATP), and towards the TFV main metabolite (tenofovir diphosphate, TDP) (Table 6.2). The antibodies showed high specificity towards TFV, except for a very limited recognition of the metabolite TDP. Tenofovir is metabolized to TDP (the active form of the drug) in HIV target cells and inhibits the activity of HIV reverse transcriptase. Because TFV is excreted unchanged in urine, TDP is not expected to be found in this biological fluid while it is present in the blood cells.[10], [21] Remarkably, mAb #321, which showed the highest affinity towards TFV (Figure 6.12), was also highly specific, whereas mAbs #313 and #322 showed a very low but not negligible binding to TDP (CR was around 3%).

**Table 6.2** Cross-reactivity values (%) obtained by icELISA for the three selected monoclonal antibodies in buffer.



Compound	mAb		
	#313	#321	#322
A 	100	100	100
B 	3.3	0.4	3.5
C 	0.04	0.09	0.01
D 	0.02	<0.01	<0.01
E 	<0.01	<0.01	<0.01
F 	<0.01	0.02	0.02
G 	<0.01	<0.01	<0.01

A, tenofovir; B, tenofovir diphosphate; C, tenofovir diisopropyl; D, tenofovir alafenamide; E, adenine; F, adenosine triphosphate; G, caffeine.

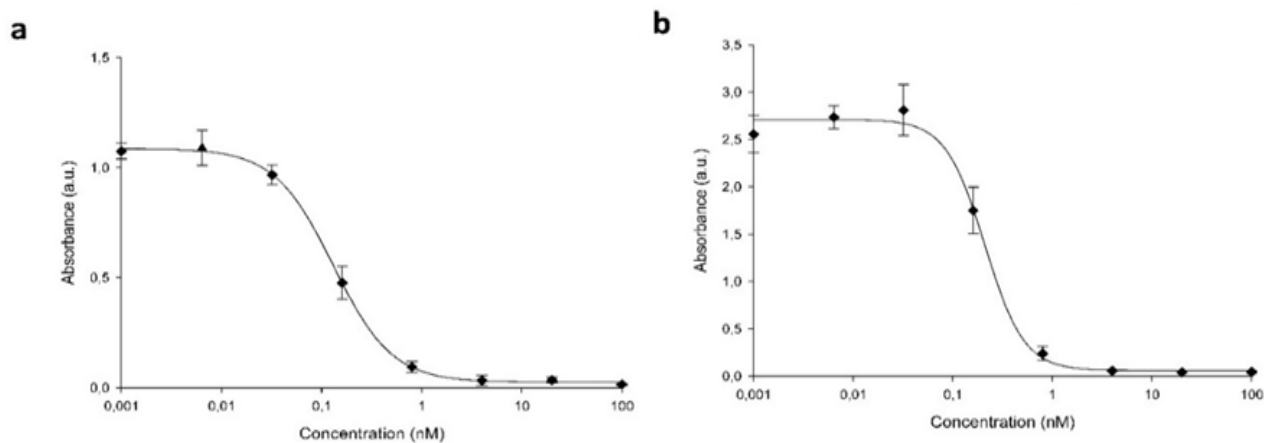
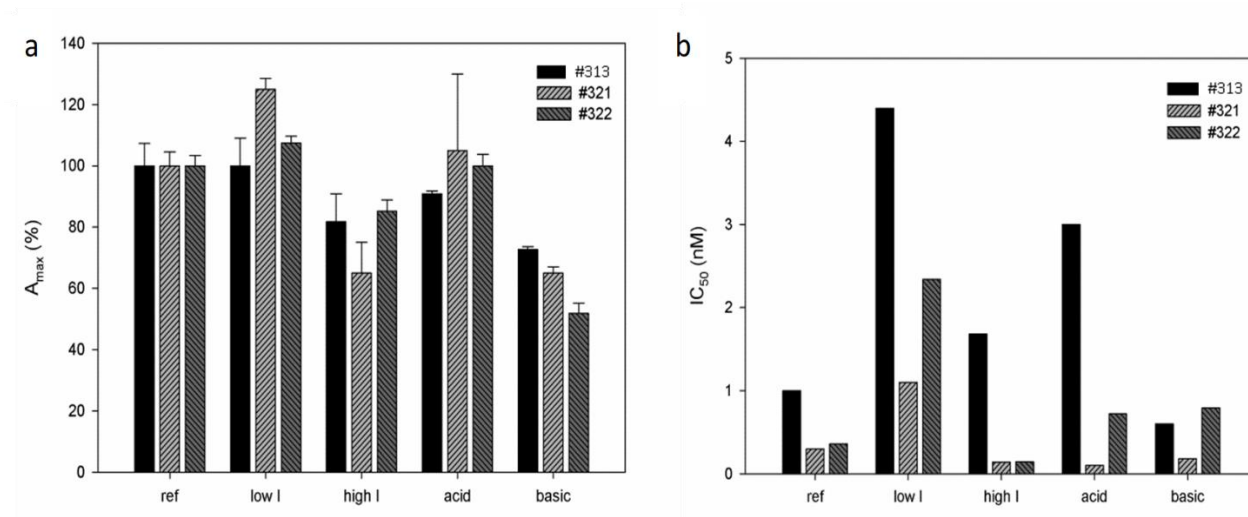


Figure 6.12. icELISA (a) and dcELISA (b) calibration curves for mAb #321 with TFV diluted in buffer.

## Robustness to pH and ionic strength

The robustness of the three mAbs towards ionic strength and pH was studied by carrying out calibration in the icELISA format in different media. The amount of salt and the pH were lowered and increased compared to the reference phosphate buffer (20 mM, pH 7.4 supplemented with 130 mM NaCl) used in this work. The amount of salt added was 0 and 230 mM, and the pH was lowered to 6.5 and increased to 8.5. The binding to the antigen, and the sensitivity of the mAbs, as measured by the  $A_{max}$  and  $IC_{50}$  values, respectively, were affected differently by the medium (Figure 6.13).



**Figure 6.13:** Effect of salt amount (low I and high I represent 0 and 230 mM of NaCl added to the phosphate buffer) and pH (acid and basic correspond to 6.5 and 8.5, respectively) on the binding to the antigen and on the assay sensitivity, as measured by  $A_{max}$  variation (a) and  $IC_{50}$  value (b). The reference buffer was composed as follows: 20 mM phosphate, pH 7.4, with 130 mM of NaCl added.

In general, increasing the salt amount and pH value lowered the binding to the antigen (Figure 6.13a) while acidic medium had a limited impact. The effect on sensitivity was largely different for the three antibodies (Figure 6.13b): mAbs #313 and 322 were largely affected by both pH and salt modification, although in different ways, while mAb #321 was confirmed to be more robust.

## Proneness to urinary and salivary matrix effect

Proneness to matrix interference was evaluated by plotting TFV standard curves with variable proportions of a simulated urine formulation[22] and fortified blank saliva samples. Inhibition curves were plotted and their  $A_{max}$  and  $IC_{50}$  values were compared with those obtained with the calibration curve run in buffer. As reported in Figure 6.14 for mAb #321, the main parameters of the fitted standard curves remained stable over the studied range of urine concentrations.

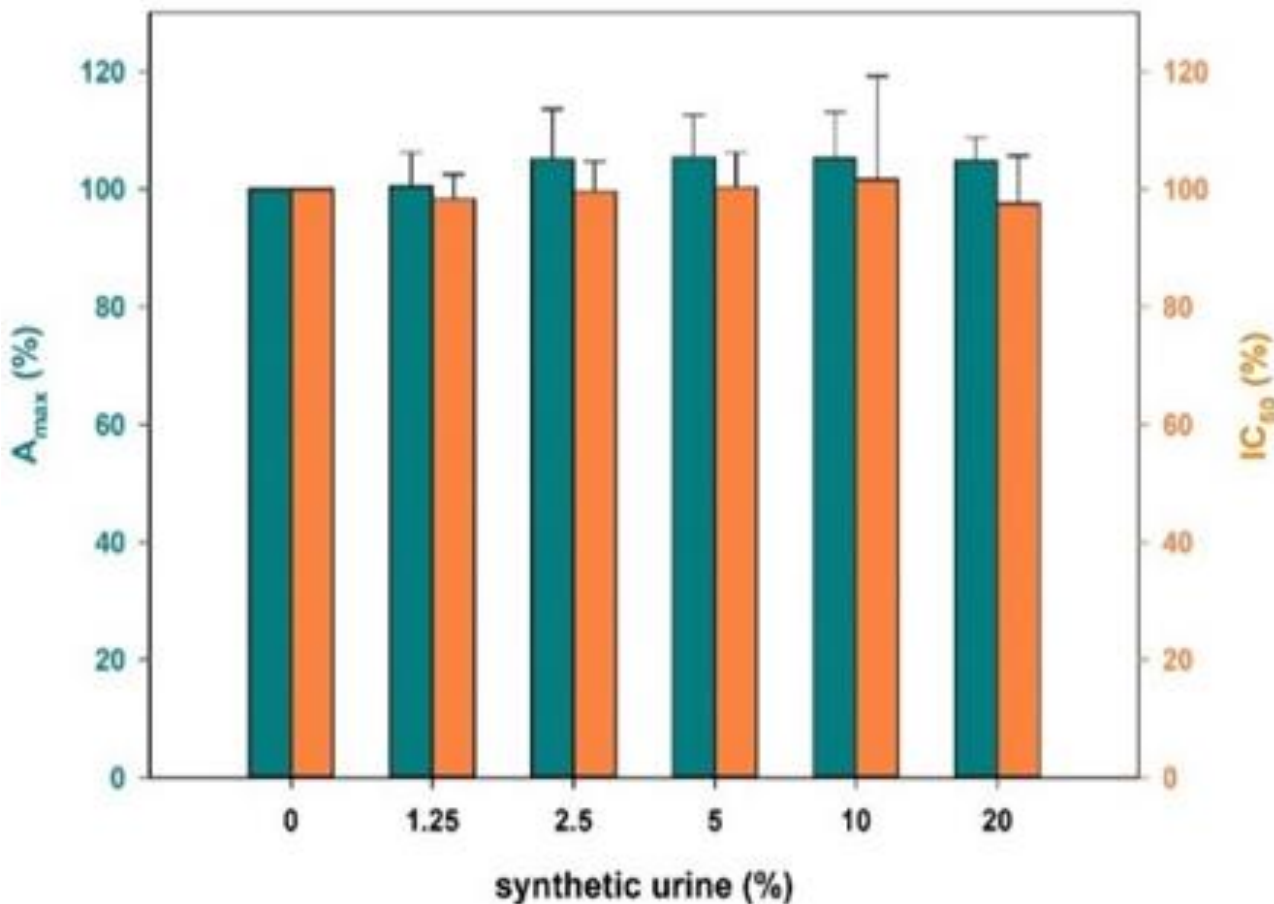


**Figure 6.14.** Interference of different proportions of a simulated urine formulation over the  $A_{max}$  and  $IC_{50}$  values of the icELISA standard curve based on mAb #321. Each value represents the mean of three determinations carried out on different days.

Accordingly, a simple 1/5 dilution of the sample in buffer may suffice for minimizing matrix effects, thus proving the ability of the assay to measure TFV at extremely low concentrations. Considering the required 5-fold dilution factor, the ELISA based on mAb #321 would allow urine samples containing concentrations as low as 0.2 nM TFV, i.e., 0.06 ng/mL, to be analysed. TFV urinary levels have been measured by Drain et al. for TDF regimens and correspond to 4000–14 000 ng/mL for perfect adherence, 2000–5000 ng/mL for medium adherence, and 200–600 ng/mL for low adherence.[23] Therefore, the detectability of the developed ELISA exceeds by far the lowest TFV levels found in low adherence situations. In fact, it would allow monitoring of the therapy in patients following TAF regimens, wherein the TFV dose is 10 times lower than in TDF regimens[24]–[26]. Concerning the salivary matrix, the dilution is expected to be lower, so, exploring higher amount of matrix was necessary (Figure 6.15)

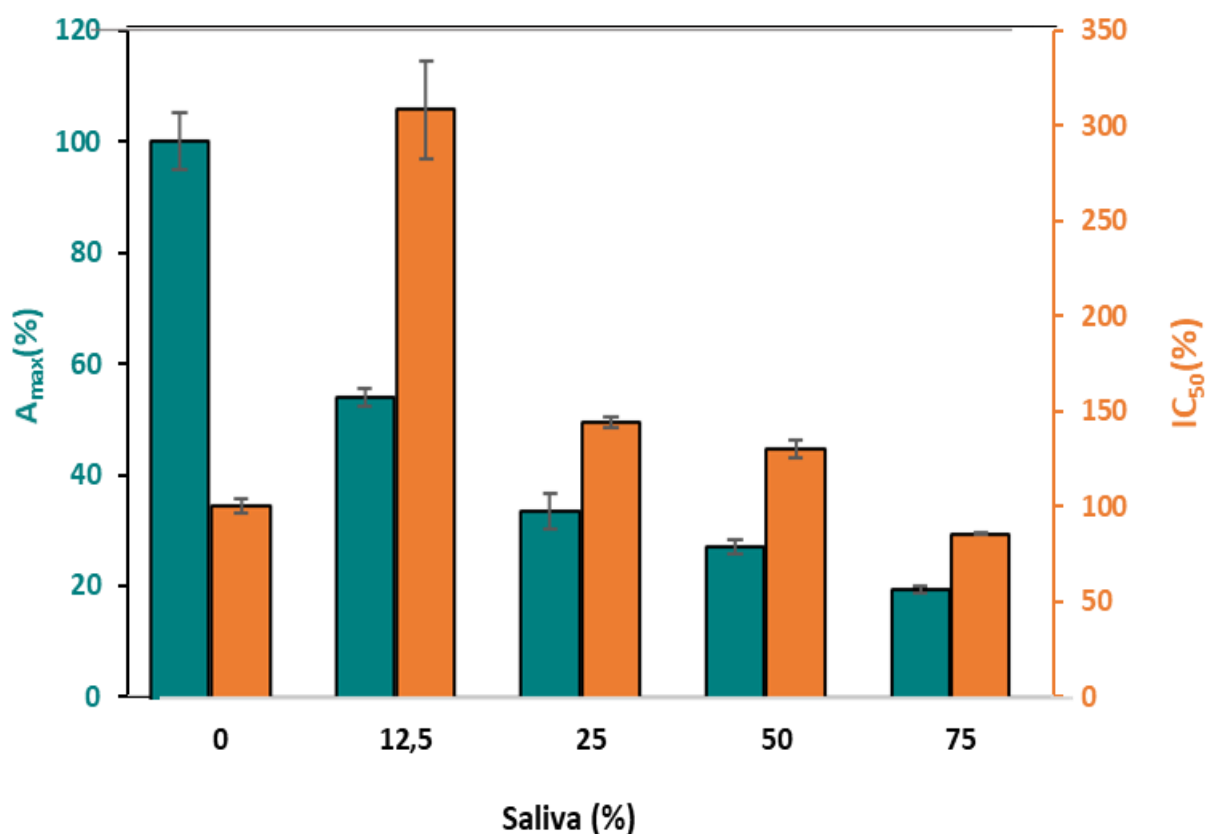
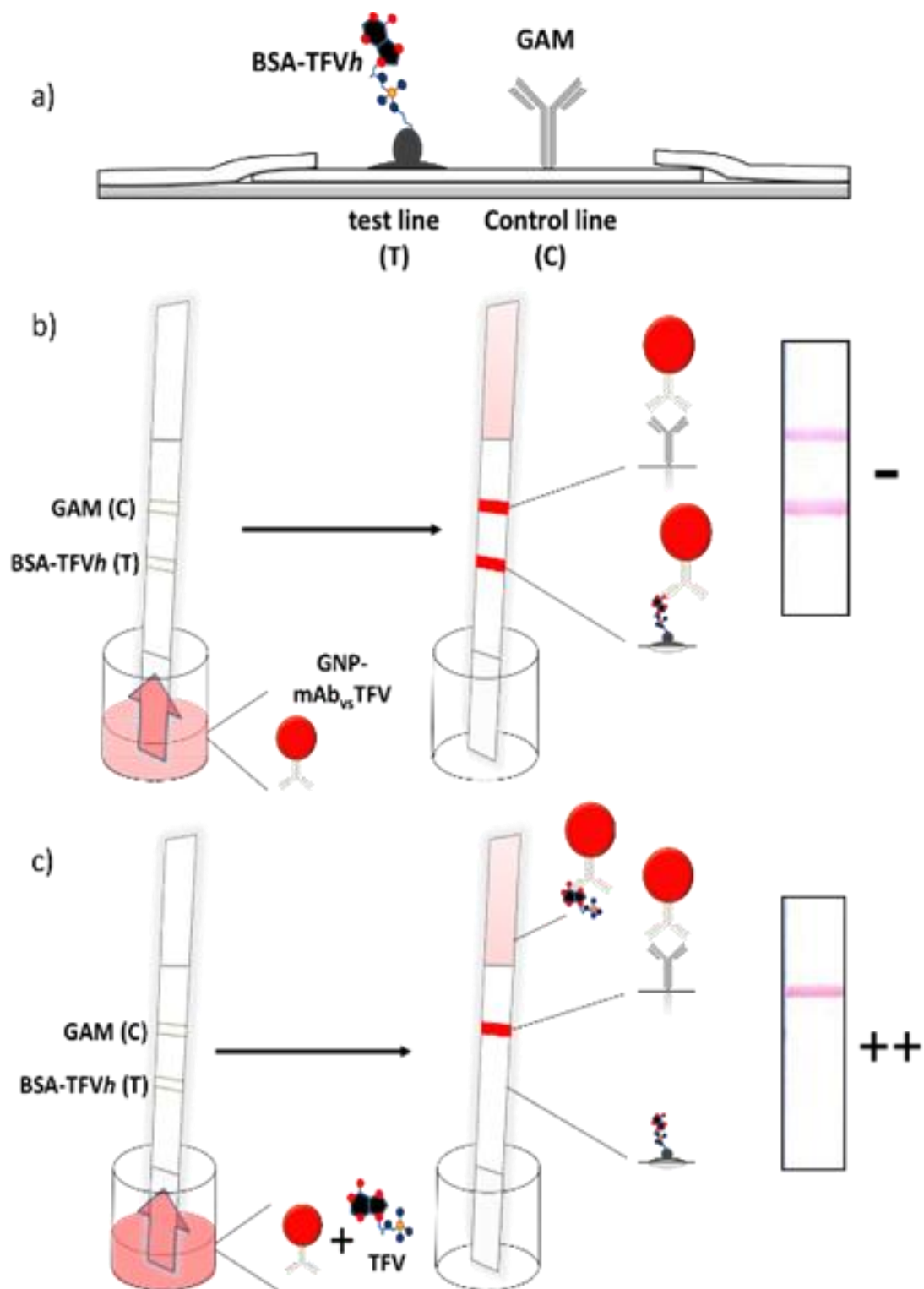


Figure 6.15: Interference of different proportions of a simulated urine formulation over the  $A_{max}$  and  $IC_{50}$  values of the icELISA standard curve based on mAb #321. Each value represents the mean of three determinations carried out on different days.

### Development of a LFIA exploiting high affinity mAbs for TFV in urine

As a proof-of-concept to illustrate the potential for point-of-care testing of the herein reported immunoreagents, the three mAbs displaying the highest affinity to TFV were selected as candidates for inclusion in a lateral flow immunoassay. A schematic representation of the LFIA, using GNPs as the colorimetric probe, is shown in Figure 6.16. Briefly, in the absence of TFV, the GNP-labelled antibodies bind to the test line, resulting in the accumulation of GNPs and the formation of a red line. Instead, the presence of increasing amounts of TFV in the sample progressively inhibits the binding of GNP-labelled antibodies to the test line. Correspondingly, the colour of the test line fades until disappearance. The three mAbs under investigation (#313, #321, and #322) were labelled with GNPs by passive adsorption [27]. Previously, the appropriate amount of each mAb to be adsorbed onto the GNPs was established by a flocculation test [28], [29]. The amounts of antigen required to form the test line and that of GNP labelled antibodies were established for each mAb by a checkerboard approach, as those assuring a clearly visible colouring of the test line in the absence of TFV. The strips were tested by applying solutions with TFV serially diluted in the running buffer and in diluted synthetic urine. The urine matrix prevented the gold conjugate from flowing through the membrane; however, a 1 + 1 dilution with the buffer sufficed to re-establish a rapid and uniform flow. To investigate the matrix effect, synthetic urine was spiked with 2x concentrated TFV standard solution and diluted 1 + 1 with the buffer to reach the same nominal concentration of the calibrators prepared in buffer (Figure 6.17). The LFIA results were observed by the naked eye and



**Figure 6.16.** Scheme of the LFIAs for TFV detection. (a) The antigen (BSA–TFVh) and GAM were spotted onto the capillary membrane to form the test and the control lines, respectively. (b) Strips were dipped in a microplate well containing the anti-TFV antibody labelled with gold nanoparticles (GNP–mAb) and the sample. In the absence of the target drug, the GNP–mAb bound to BSA–TFVh and to GAM, so it accumulated both at the test and control lines resulting in the appearance of two visible red lines. (c) In the presence of the drug (TFV), the binding to the BSA–TFVh at the test line was inhibited, thus only the control line was made visible.

images were photographically captured for quantitative analysis. Colour intensities of the test (T) and control (C) lines were measured, and the T/C ratio was plotted versus the TFV concentration to calculate the IC<sub>50</sub> parameter. As the LFIA was intended for point-of-care testing application, we also estimated the visual limit of detection (vLOD), which was defined as the TFV concentration that completely inhibited the colouring of the test line. The control line largely varied and increased as a function of the increasing TFV amount. This can be explained by the displacement of GNP–mAb from the test line, which resulted in its accumulation at the control line. This phenomenon was observed when TFV was dissolved in the running buffer; however, it seemed more pronounced in the presence of the synthetic urine matrix. The net effect of the increasing colouring of the control line parallel to the decrease of the colour at the test line was that the variation of the signal (T/C ratio) versus TFV concentration was magnified and contributed to the high sensitivity of the LFIA. Therefore, in this case, the control line not only reduced strip-to-strip variability, as previously observed,[30] but also increased the sensitivity. As reported in Table 6.3, the three mAbs showed high sensitivities with IC<sub>50</sub> values below 1 nM, both in buffer and in urine. mAb #322 showed the best performance in terms of IC<sub>50</sub>, while mAb #321 provided the lowest vLOD, causing the complete disappearance of the test line colour at as low as 2.5 nM TFV when dissolved in buffer. In general, a slight decrease of sensitivity, measured by the IC<sub>50</sub> and vLOD parameters, was observed for the three systems. Particularly, the signal of the control line was more influenced by the studied matrix, especially for mAb #322.

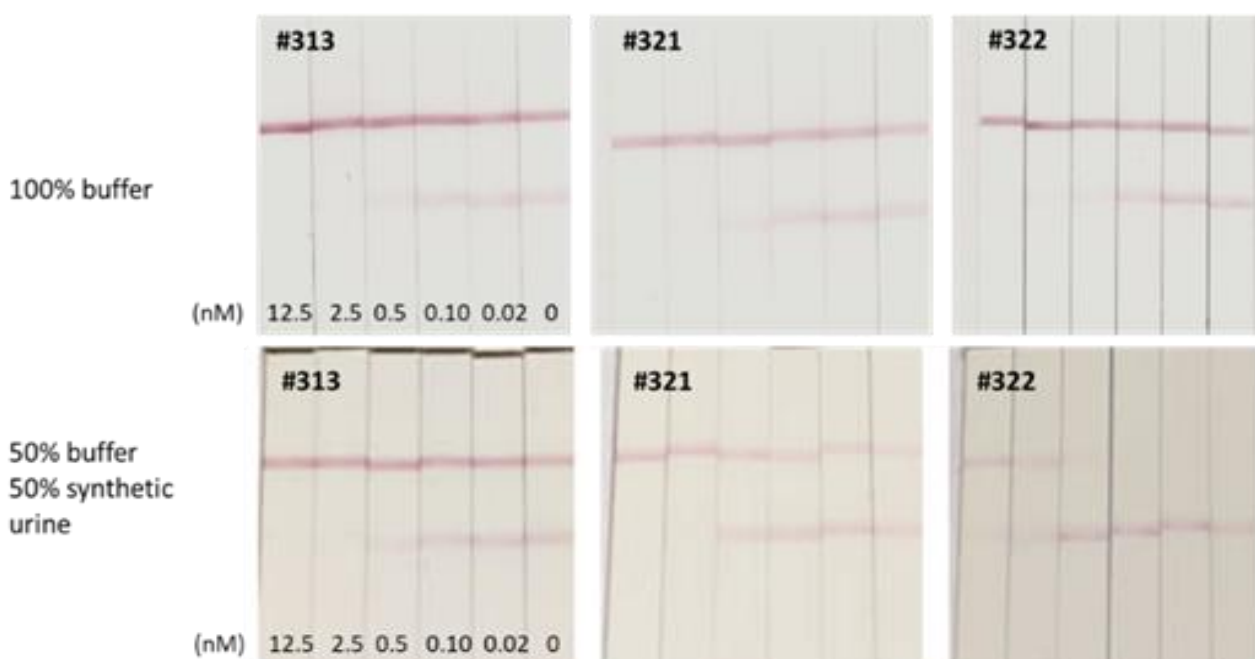


**Figure 6.17** LFIA calibration carried out for TFV (from left to right: 12.5, 2.5, 0.5, 0.1, 0.02, and 0 nM). The curves were plotted using synthetic urine, which was 2x concentrated and subsequently diluted 1 + 1 with the running buffer to reach the same nominal concentration of TFV as that used for the curve in the running buffer. Actual urinary TFV levels were obtained by multiplying by two the values in the figure.

**Table 6.3.** Detectability of TFV by the LFIAs including the selected mAbs. The analytical performance of the LFIAs were checked by diluting TFV in the running buffer and in 1+1 diluted synthetic urine.

mAb	IC <sub>50</sub> (nM)		vLOD <sup>a</sup> (nM)	
	Running buffer	Synthetic urine	Running buffer	Synthetic urine
#313	0.4	0.7	2.5	12.5
#321	0.5	0.7	2.5	2.5
#322	0.3	_ <sup>b</sup>	12.5	>12.5

<sup>a</sup>The vLOD was defined as the TFV concentration that caused the complete disappearance of the colour at the test line. <sup>b</sup> Not determined, since the T/C ratio could not be calculated for the blank sample.

The vLODs achieved in urine, capitalizing on the high-affinity mAbs reported herein, were in the 2.5–25 nM range, which corresponds to TFV concentrations between 1.4 and 7.2 ng/mL in the urine sample. In the work by M. Gandhi et al.[15], a discrete cut-off value for urinary TFV (1500 ng/mL) was proposed to correctly classify the adherence to therapy in 98% of the individuals administered with TDF. The LFI prototype described herein showed a 1000-fold lower vLOD than required, and 600 times lower than those previously reported. Although exceeding current requirements, the low vLOD that was reached fits with the incoming needs of increasing TFV detectability, due to the introduction of the TAF prodrug. In fact, TAF penetrates the blood and hepatic cells better than TDF, and it is administered usually in 10-fold lower amounts compared to TDF [24]. Therefore, the point-of-care test intended for checking adherence to regimens including TAF is required to show proportionally reduced limits of detection.

### Analytical validation of the ELISA method for TFV in saliva using mAb #321

The saliva is an extremely variable matrix and, without any correction, strongly affects the ELISA performances (Figure 6.15). Adjustments on the standard and working buffers were made to simulate the inhibitory effect of the matrix, changing pH, ionic strength, dilution factor, additives, etc... To simulate real sample condition a pool of blank saliva was fortified with TFV and used as the template for the standard curve. The determination of the best conditions was considered for the maximal similarity between the standard curve and the curve made by fortifying the pool of blank saliva samples. The standards of TFV were dissolved in a predilution buffer (20 mM phosphate buffer, pH 7, 630 mM NaCl, 0.05% Tween20, 1% w/v casein) mimicking the saliva. The test involves a 1:25 dilution of salivary samples by the working buffer. The overlap between the two curves is shown in the Figure 6.18. Once adjusted these conditions, the validation was made by evaluating the recovery, inter- and intra-assay variability and the quantification range (lower limit of detection, LLOD-upper limit of detection, ULOD). For testing the recovery, three levels of fortification were used, one above, one near and one below the cut-off reference level for assessing adherence relevant presence of TFV in the sample (1.3, 2.7 and 5.4 ng/ml). The CV% values have been estimated below the threshold value of 15% and the recovery ranged between 73.4±0.6 and 133.6±11.1 (Table 6.4). The precision was measured on the whole levels used in the calibration curve by repeating the curve in three days in quadruplicate to evaluate inter- and intra-assay variability (Table 6.5). Considering the LOD as the lowest concentration reached by an error lower than 25% [31]–[38] the method shows a LOD value of 5 nM or 2 nM, respectively. The accuracy ranged between 85.8% and 145.6% (Table 6.5). The variability

caused by the salivary matrix within the method seems to be more randomizable by testing in different days than testing replicates in the single assay.

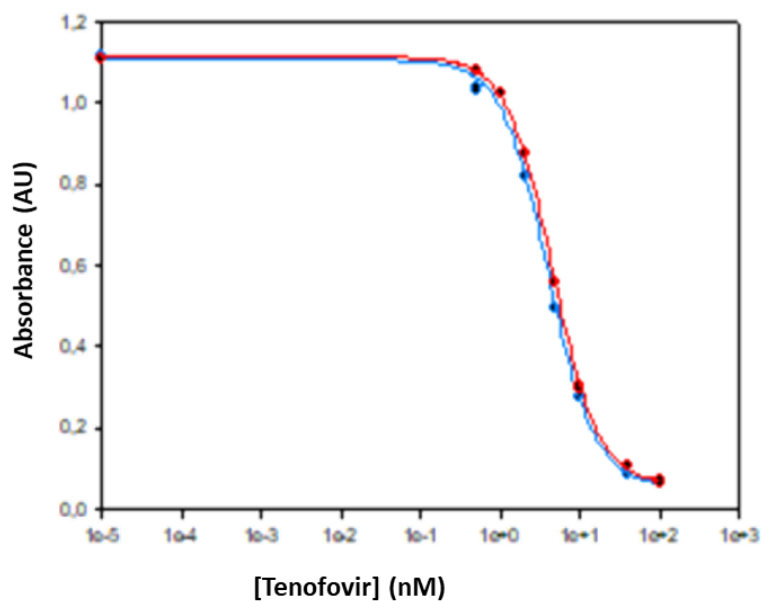


**Figure 6.18:** Curves made in predilution ultimate buffer (blue) and fortifying the blank saliva pool (red).

**Table 6.4:** recovery and coefficients of variation for three fortification levels of TFV in the salivary matrix

Spiking level (ng/ml)	Mean concentration $\pm$ SD (ng/ml)	Mean recovery $\pm$ SD (%)	CV (%)
1.3	0.95 $\pm$ 0.079	73.4 $\pm$ 0.6	8.2
2.7	2.88 $\pm$ 0.320	106.8 $\pm$ 11.9	11.1
5.4	7.21 $\pm$ 0.596	133.6 $\pm$ 11.1	8.3

**Table 6.5:** Repeatability and reproducibility of TFV quantification in salivary matrix

Fortification level	Intra-assay (%)	Inter-assay (%)	Accuracy (mean n=3x3)
100	9,5	9,5	85,8
40	9,6	4,2	120,3
10	13,4	3,5	99,0
5	24,0	3,1	96,7
2	49,6	11,6	106,4
1	63,4	28,2	111,2
0.5	75,5	17,0	145,6



## Development of a LFIA exploiting mAb #321 for TFV in saliva

The TFV-fortified salivary standard curve was made as reported in the previous section for the ELISA analytical validation. The 4-parameters logistic equation was chosen as the model for calibration and its equation was extracted. The visual LOD (vLOD) was assessed between 0.5 and 1 ng/ml for the complete disappearance of the signal, as show in Figure 6.19.

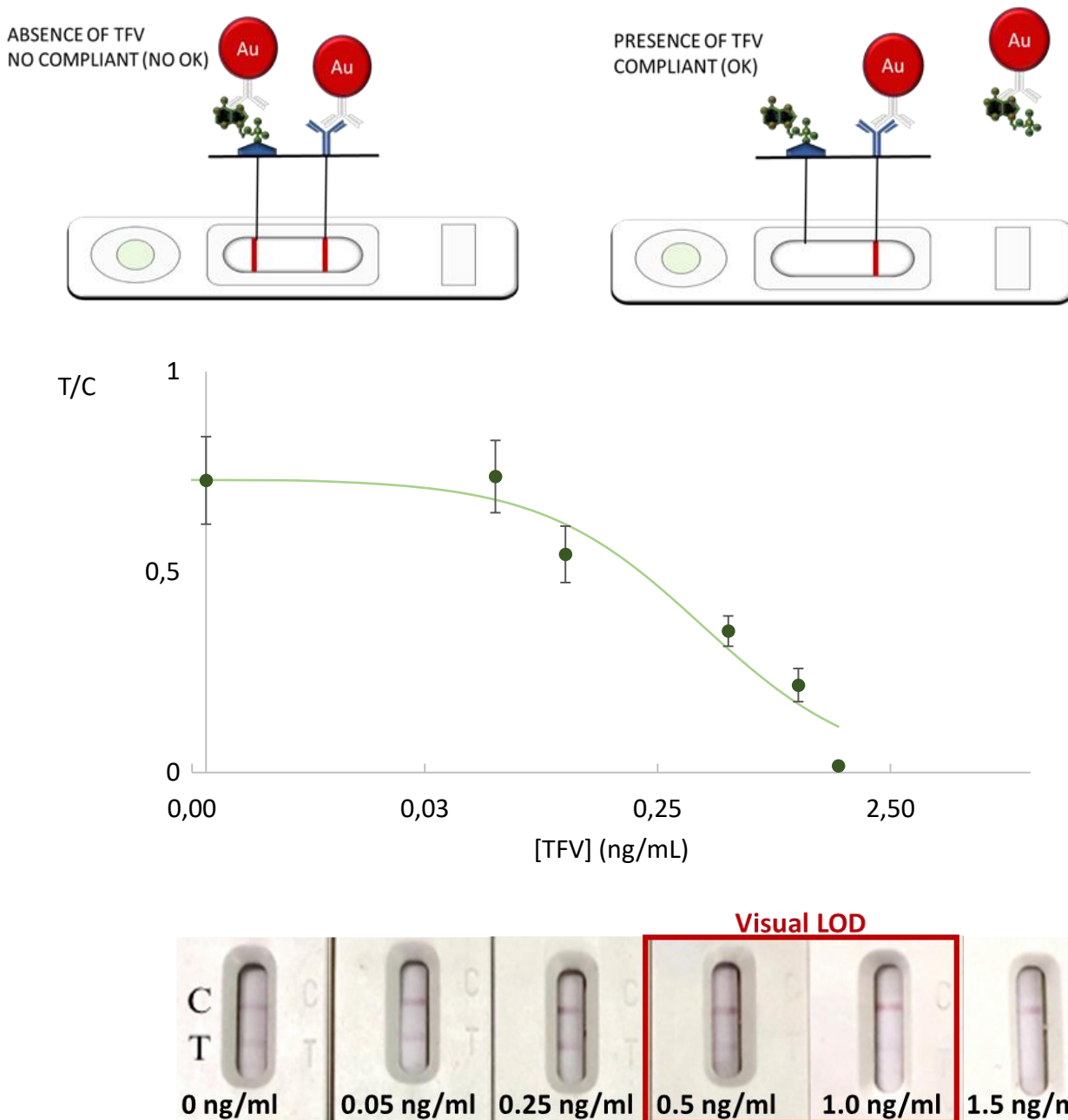


**Figure 6.19.** Standard TFV-fortified saliva curve (0-0.05-0.25-0.1-0.5-1.5 ng/ml). The values are normalized for the blank as T/C signal ratios. On the bottom left of the graph the analytical figures of merit of the competition capacity

This value is lower than reference level measured by V. de Lastours et al.[13] (0.4-25ng/ml, average 2.75ng/ml) for perfect adherence to TDF administered patients. This is not a guarantee for a correct classification, but rather a *condictio sine qua non*. Being a diagnostic tool prototype, where the

*diagnosis* is the *non-compliant behaviour*, it is important to have not any signal above 2.75 ng/ml avoiding false positive classification. On the other hand, to avoid false negatives is important to avoid signal in sub-optimal adherent concentration. Nevertheless, simply putting the cut-off at the maximum of sensitivity (in order to classify all adherent as true-negative) would be imprudent. The TFV concentration distribution of the non-adherent population could partially overlap the perfect adherent one. In this occurrence the cut-off should be strategically optimized to compromise the number of false negative and false positives. The vLOD can be adjusted to optimize classification, by changing amounts of reagents. Another aspect is the TAF administration (25mg/day) that, theoretically, should deliver 10-fold lower concentration of TFV in saliva (coarsely calculated around 0.04-2.50 ng/ml, mean 0.28ng/ml). These concentrations are below the vLOD, giving a high risk of false positives among the adherent patients. Anyway, these speculations should be compared to real measurements of TFV in saliva for TAF administered patients.

### Selectivity of the LFIA in saliva

Selectivity towards the target was again checked and determined in saliva by means of single point measurement directly on the standalone LFIA test, by both visual evaluation, and signal quantification. As the interfering molecules the two TFV-based pro-drug (TDF and TAF), two antiretrovirals (Dolutegravir, DTG and Elvitegravir, EVG) that are currently not co-formulated with TFV and three common molecular analogues that can be found in saliva (Adenosine triphosphate ATP and Adenine as endogenous, Caffeine as an exogenous) were chosen[39]–[41]. The visual results are shown in Table 6.6 and Table 6.7. Among the possible interfering substances, only TDF and TAF showed measurable CR%. Even though these cross-reactivity values are extremely low but, in case of counterfeit, the amount of pro-drug in the saliva is unpredictable (e.g., “chewing” 300mg of TDF right before the check by the physician).

**Table 6.6:** (from left to right) LFIA visual results with negative saliva, 1000 nM of TDF (1), TAF (2), DTG (3), EVG (4) and 100 nM of ATP (5), adenine (6) and caffeine (7) fortified saliva samples.

	negative	1	2	3	4	5	6	7
C								
T								

**Table 6.7:** The CR% calculated for the 7 interfering molecules as a result of substitution in the TFV 4-parameter logistic competition curve.

<i>Interfering molecule (nM)</i>	<i>CR%</i>
1) <i>TDF (1000)</i>	<i>0,8%</i>
2) <i>TAF (1000)</i>	<i>0,1%</i>
3) <i>DTG (1000)</i>	<i>&lt;0,003%</i>
4) <i>EVG (1000)</i>	<i>&lt;0,003%</i>
5) <i>ATP (100)</i>	<i>&lt;0,03%</i>
6) <i>Adenine (100)</i>	<i>&lt;0,03%</i>
7) <i>Caffeine (100)</i>	<i>&lt;0,03%</i>

## 6.1.4 Conclusions

In this work, we designed, synthesized, and characterized a new hapten of TFV and generated seven mAbs with ultra-high affinity towards this ARV drug. Compared to other antibodies suggested for TFV, our selection strategy provided bioligands with higher affinity and selectivity properties.[17] The mAbs were characterized by icELISA and were explored for their implementation in a LFIA-based point-of-care test for TFV detection in urine. The sensitivity showed exploiting the novel mAbs, was largely above the requirement for assessing adherence to anti-retroviral therapy in urine, even considering new co-formulations including the TAF prodrug.[24] This high detectability, which largely exceeds that of the previous rapid analytical tests, allows for the detection of TFV in other important matrices, such as saliva, where the levels of TFV are much lower. Thanks to this, we in-house validated an icELISA method and developed a rapid LFIA for the detection of TFV in saliva. The developed ELISA method is the first represented for this kind of assessment in saliva and is the most sensitive for the detection of TFV, to the best of our knowledge. As a further application of the first part of the project, we developed a LFIA for the on-field detection of TFV in the salivary matrix. The selectivity in terms of CR%, that was measured and assessed as very low (0.08% for TDF as the highest) for 7 potentially interfering molecules. These performances appear as suitable for TDF adherence assessment whereas there could be more work to do about TAF administration for which the salivary level could fall by 10-fold decrease. Further measurements should be done to determine the correct reference ranges for adherence classes to establish an appropriate decision cut-off by means of which adjust the LFIA to obtain a stand-alone test. This can be very helpful for several reasons. Firstly, there are still no devices for this kind of assessment. In addition, it must be said that competitive immunoassays are generally counterintuitive. Especially for inexperienced users, in rural or non-laboratory settings, the disappearance of the signal is hard to be correlated to an intervention-requiring situation. This is true when the diagnosis is correlated to the presence of the small target molecule. In this case the issue is the lack of the small target molecule. Therefore, the appearance of the analytical signal must be correlated to an intervention-requiring situation. This aspect renders the LFIA approach much more straightforward. Hence the importance to promote the evolution of this work for future easy interpretable point-of-care therapeutic drug monitoring for on-field applications.

### Conflicts of interest

There are no conflicts to declare.

### Acknowledgements

This work was supported by the Spanish Ministerio de Economía y Competitividad (AGL2015-64488 and RTI2018-096121) and co-financed by European Regional Development Funds. The work was also supported by Università degli Studi di Torino, Ricerca Locale grant. Samples of the immunoreagents for TFV reported herein are available upon request from A. Abad-Fuentes.

## References

- [1] D. Cattaneo, S. Baldelli, V. Cozzi, E. Clementi, D. J. E. Marriott, and C. Gervasoni, "Impact of Therapeutic Drug Monitoring of Antiretroviral Drugs in Routine Clinical Management of People Living With HIV: A Narrative Review," *Ther. Drug Monit.*, vol. 42, no. 1, pp. 64–74, Feb. 2020, doi: 10.1097/FTD.0000000000000684.
- [2] B. Punyawudho *et al.*, "Therapeutic drug monitoring of antiretroviral drugs in HIV-infected patients," *Expert Review of Clinical Pharmacology*, vol. 9, no. 12. Taylor and Francis Ltd, pp. 1583–1595, Dec. 01, 2016, doi: 10.1080/17512433.2016.1235972.
- [3] A. Paci *et al.*, "Review of therapeutic drug monitoring of anticancer drugs part 1 - Cytotoxics," *European Journal of Cancer*, vol. 50, no. 12. Elsevier Ltd, pp. 2010–2019, 2014, doi: 10.1016/j.ejca.2014.04.014.
- [4] N. Mohammadpour, S. Elyasi, N. Vahdati, A. H. Mohammadpour, and J. Shamsara, "A review on therapeutic drug monitoring of immunosuppressant drugs.," *Iran. J. Basic Med. Sci.*, vol. 14, no. 6, pp. 485–498, Nov. 2011.
- [5] N. La Maida, A. Di Trana, R. Giorgetti, A. Tagliabracchi, F. P. Busardò, and M. A. Huestis, "A Review of Synthetic Cathinone–Related Fatalities From 2017 to 2020," *Ther. Drug Monit.*, vol. 43, no. 1, pp. 52–68, Feb. 2021, doi: 10.1097/FTD.0000000000000808.
- [6] A. Cushing and R. Metcalfe, "Optimizing medicines management: From compliance to concordance," *Therapeutics and Clinical Risk Management*, vol. 3, no. 6. Dove Press, pp. 1047–1058, 2007, Accessed: Feb. 04, 2021. [Online]. Available: [/pmc/articles/PMC2387303/?report=abstract](#).
- [7] J. Lin, G. E. Sklar, V. M. Sen Oh, and S. C. Li, "Factors affecting therapeutic compliance: A review from the patient's perspective," *Therapeutics and Clinical Risk Management*, vol. 4, no. 1. Dove Press, pp. 269–286, 2008, doi: 10.2147/tcrm.s1458.
- [8] B. Sanavio and S. Krol, "On the slow diffusion of point-of-care systems in therapeutic drug monitoring," *Frontiers in Bioengineering and Biotechnology*, vol. 3, no. FEB. Frontiers Media S.A., 2015, doi: 10.3389/fbioe.2015.00020.
- [9] M. A. Spinelli *et al.*, "Low tenofovir level in urine by a novel immunoassay is associated with seroconversion in a preexposure prophylaxis demonstration project," *AIDS*, vol. 33, no. 5, pp. 867–872, Apr. 2019, doi: 10.1097/QAD.0000000000002135.
- [10] B. P. Kearney, J. F. Flaherty, and J. Shah, "Tenofovir disoproxil fumarate: Clinical pharmacology and pharmacokinetics," *Clinical Pharmacokinetics*, vol. 43, no. 9. pp. 595–612, 2004, doi: 10.2165/00003088-200443090-00003.
- [11] B. Fernandez-Fernandez *et al.*, "Tenofovir nephrotoxicity: 2011 update," *AIDS Research and Treatment*, vol. 2011. 2011, doi: 10.1155/2011/354908.
- [12] M. Gandhi *et al.*, "Development and Validation of an Immunoassay for Tenofovir in Urine as a Real-Time Metric of Antiretroviral Adherence," *EclinicalMedicine*, vol. 2–3, pp. 22–28, Aug. 2018, doi: 10.1016/j.eclinm.2018.08.004.
- [13] V. De Lastours, J. Fonsart, R. Burlacu, B. Gourmel, and J. Molina, "Concentrations of Tenofovir and Emtricitabine in Saliva : Implications for Preexposure Prophylaxis of Oral HIV Acquisition ☐," vol. 55, no. 10, pp. 4905–4907, 2011, doi: 10.1128/AAC.00120-11.
- [14] G. W. Pratt, A. Fan, B. Melakeberhan, and C. M. Klapperich, "A competitive lateral flow assay for the detection of tenofovir," *Anal. Chim. Acta*, vol. 1017, pp. 34–40, Aug. 2018, doi: 10.1016/j.aca.2018.02.039.
- [15] M. Gandhi *et al.*, "Development and validation of the first point-of-care assay to objectively monitor adherence to HIV treatment and prevention in real-time in routine settings," *AIDS*, vol. 34, no. 2, pp. 255–260, Feb. 2020, doi: 10.1097/QAD.0000000000002395.

- [16] M. Gandhi *et al.*, “Brief Report: Validation of a Urine Tenofovir Immunoassay for Adherence Monitoring to PrEP and ART and Establishing the Cutoff for a Point-of-Care Test,” *J. Acquir. Immune Defic. Syndr.*, vol. 81, no. 1, pp. 72–77, May 2019, doi: 10.1097/QAI.0000000000001971.
- [17] D. Sevenler *et al.*, “Immunoassay for HIV Drug Metabolites Tenofovir and Tenofovir Diphosphate,” *ACS Infect. Dis.*, vol. 6, no. 7, pp. 1635–1642, Jul. 2020, doi: 10.1021/acsinfecdis.0c00010.
- [18] J. V. Mercader, C. Suárez-Pantaleón, C. Agulló, A. Abad-Somovilla, and A. Abad-Fuentes, “Production and characterization of monoclonal antibodies specific to the strobilurin pesticide pyraclostrobin,” *J. Agric. Food Chem.*, vol. 56, no. 17, pp. 7682–7690, Sep. 2008, doi: 10.1021/jf801340u.
- [19] D. Wild, “Immunoassay for Beginners,” in *The Immunoassay Handbook*, Elsevier Ltd, 2013, pp. 7–10.
- [20] M. J. Raeisossadati *et al.*, “Lateral flow based immunobiosensors for detection of food contaminants,” *Biosensors and Bioelectronics*, vol. 86. Elsevier Ltd, pp. 235–246, Dec. 15, 2016, doi: 10.1016/j.bios.2016.06.061.
- [21] M. Pyra *et al.*, “Tenofovir and tenofovir-diphosphate concentrations during pregnancy among HIV-uninfected women using oral preexposure prophylaxis,” *AIDS*, vol. 32, no. 13, pp. 1891–1898, 2018, doi: 10.1097/QAD.0000000000001922.
- [22] E. Miró-Casas *et al.*, “Capillary gas chromatography-mass spectrometry quantitative determination of hydroxytyrosol and tyrosol in human urine after olive oil intake,” *Anal. Biochem.*, vol. 294, no. 1, pp. 63–72, Jul. 2001, doi: 10.1006/abio.2001.5160.
- [23] T. R. Cressey *et al.*, “A randomized clinical pharmacokinetic trial of Tenofovir in blood, plasma and urine in adults with perfect, moderate and low PrEP adherence: The TARGET study,” *BMC Infect. Dis.*, vol. 17, no. 1, Jul. 2017, doi: 10.1186/s12879-017-2593-4.
- [24] L. Lalley-Chareczko, E. Hiserodt, G. Moorthy, A. Zuppa, K. Mounzer, and H. Koenig, “Urine Assay to Measure Tenofovir Concentrations in Patients Taking Tenofovir Alafenamide,” *Front. Pharmacol.*, vol. 11, Mar. 2020, doi: 10.3389/fphar.2020.00286.
- [25] R. Byrne, I. Carey, and K. Agarwal, “Tenofovir alafenamide in the treatment of chronic hepatitis B virus infection: rationale and clinical trial evidence,” *Therapeutic Advances in Gastroenterology*, vol. 11. SAGE Publications Ltd, Jan. 01, 2018, doi: 10.1177/1756284818786108.
- [26] S. A. Iacob, D. G. Iacob, and G. Jugulete, “Improving the adherence to antiretroviral therapy, a difficult but essential task for a successful HIV treatment-clinical points of view and practical considerations,” *Frontiers in Pharmacology*, vol. 8, no. NOV. Frontiers Media S.A., Nov. 23, 2017, doi: 10.3389/fphar.2017.00831.
- [27] L. Anfossi *et al.*, “Silver and gold nanoparticles as multi-chromatic lateral flow assay probes for the detection of food allergens,” *Anal. Bioanal. Chem.*, vol. 411, no. 9, pp. 1905–1913, Mar. 2019, doi: 10.1007/s00216-018-1451-6.
- [28] Y. R. Guo, S. Y. Liu, W. J. Gui, and G. N. Zhu, “Gold immunochromatographic assay for simultaneous detection of carbofuran and triazophos in water samples,” *Anal. Biochem.*, vol. 389, no. 1, pp. 32–39, Jun. 2009, doi: 10.1016/j.ab.2009.03.020.
- [29] F. Di Nardo, C. Baggiani, C. Giovannoli, G. Spano, and L. Anfossi, “Multicolor immunochromatographic strip test based on gold nanoparticles for the determination of aflatoxin B1 and fumonisins,” *Microchim. Acta*, vol. 184, no. 5, pp. 1295–1304, May 2017, doi: 10.1007/s00604-017-2121-7.
- [30] F. Di Nardo *et al.*, “Validation of a qualitative immunochromatographic test for the noninvasive assessment of stress in dogs,” *J. Chromatogr. B Anal. Technol. Biomed. Life Sci.*, vol. 1028, pp. 192–198, Aug. 2016, doi: 10.1016/j.jchromb.2016.06.019.

- [31] J. Dunn and D. Wild, "Calibration Curve Fitting," in *The Immunoassay Handbook*, Elsevier Ltd, 2013, pp. 323–336.
- [32] C. P. Quinn *et al.*, "Specific, sensitive, and quantitative enzyme-linked immunosorbent assay for human immunoglobulin G antibodies to anthrax toxin protective antigen," *Emerg. Infect. Dis.*, vol. 8, no. 10, pp. 1103–1110, Oct. 2002, doi: 10.3201/eid0810.020380.
- [33] Z. Zhang *et al.*, "A novel and sensitive chemiluminescence immunoassay based on AuNCs@pepsin@luminol for simultaneous detection of tetrabromobisphenol A bis(2-hydroxyethyl) ether and tetrabromobisphenol A mono(hydroxyethyl) ether," *Anal. Chim. Acta*, vol. 1035, pp. 168–174, Dec. 2018, doi: 10.1016/j.aca.2018.06.039.
- [34] A. Saeed, S. Ling, J. Yuan, and S. Wang, "The Preparation and Identification of a Monoclonal Antibody against Domoic Acid and Establishment of Detection by Indirect Competitive ELISA," *Toxins (Basel)*, vol. 9, no. 8, p. 250, Aug. 2017, doi: 10.3390/toxins9080250.
- [35] D. Sasaki and R. A. Mitchell, "How to Obtain Reproducible Quantitative ELISA Results," 1997.
- [36] G. J. Reimer, S. J. Gee, and B. D. Hammock, "Comparison of a Time-Resolved Fluorescence Immunoassay and an Enzyme-Linked Immunosorbent Assay for the Analysis of Atrazine in Water," *J. Agric. Food Chem.*, vol. 46, no. 8, pp. 3353–3358, 1998, doi: 10.1021/jf970965a.
- [37] Z. Zhang *et al.*, "An ultrasensitive competitive immunosensor using silica nanoparticles as an enzyme carrier for simultaneous impedimetric detection of tetrabromobisphenol A bis(2-hydroxyethyl) ether and tetrabromobisphenol A mono(hydroxyethyl) ether," *Biosens. Bioelectron.*, vol. 105, pp. 77–80, May 2018, doi: 10.1016/j.bios.2018.01.029.
- [38] F. Di Nardo, S. Cavalera, C. Baggiani, M. Chiarello, M. Pazzi, and L. Anfossi, "Enzyme immunoassay for measuring aflatoxin B1 in legal cannabis," *Toxins (Basel)*, vol. 12, no. 4, Apr. 2020, doi: 10.3390/toxins12040265.
- [39] B. Kočańska, R. T. Smoleński, and N. Knap, "Determination of adenine nucleotides and their metabolites in human saliva," *Acta Biochim. Pol.*, vol. 47, no. 3, pp. 877–879, 2000.
- [40] C. Bill, J. A. Danielson, and R. S. Jones, "Salivary intercellular adenosine triphosphate testing in primary caretakers: An examination of statistical significance versus diagnostic predictability," *Clin. Exp. Dent. Res.*, vol. 3, no. 6, pp. 244–250, Dec. 2017, doi: 10.1002/cre2.95.
- [41] S. P. Humphrey and R. T. Williamson, "A review of saliva: Normal composition, flow, and function," *J. Prosthet. Dent.*, vol. 85, no. 2, pp. 162–169, Feb. 2001, doi: 10.1067/mp.2001.113778.

## **Chapter 7**

---

### **Conclusions**

---



Despite the increasing demand for even more sensitive and upgraded version of the LFIA, the (literally) gold standard based on visual detection remains the most simple and user-friendly version of this technique. The long-standing quest for novel probes to permanently subvert the LFIA technique, has still not established on the market, despite of the pharaonic amount of literature claiming for the revolutionary dethronement of the gold nanoparticle-based tests. Facing up issues in low resources settings or pandemic emergencies, where the pressing need for rapid solutions is critical, the simplest choice is probably the best one. In these three years I worked on several infectious disease diagnostic problems to support human and animal healthcare, from phlebotomine to viral vectors, targeting antigens, antibodies, and anti-viral drugs. I dedicated my PhD research activity on the creation of LFIA devices, focusing on those where the strategical design used for their development could play a crucial role. The great impact of the new designs on the diagnostic performances have been studied and reported in the previous chapters. Facing several analytical challenges allowed me to explore all the LFIA formats described in chapter 1.4 apart from the indirect competitive. In chapter 3.1, after extensive studies aimed at obtaining a stable and performing antigen-GNP probe, we designed a two-test lines LFIA, employing in both cases bioligand able to capture all immunoglobulins classes present in the sample. The prototype was tested on clinical samples (85 pre-covid sera, among them 25 positives to other infectious diseases, and on 62 SARS CoV-2 positive sera). The concordance with a validated ELISA on these samples was 100% and, also on respect to rRT-PCR, the test scored good sensitivity and specificity. Targeting the total antibodies response to infection enabled achieving 100% diagnostic specificity (95.75–100, C.I. 95%, n = 85 healthy and with other infections individuals) and 94.6% sensitivity (84.9–98.9, C.I. 95%, n = 62 SARS CoV-2 infected subjects) as early as 7 days post confirmation of positivity. Moreover, the samples provided different intensity ratios on the two test lines. In the end of the study, we were able to hypothesize that the two strategies were differently sensitive to different classes of antibodies. Applying the “total antibody” approach to diagnosing Canine Visceral Leishmaniasis, in chapter 3.2, we developed a LFIA device and tested it on 167 serum samples from infected and healthy dogs and scored excellent diagnostic sensitivity (98.4%), specificity (98.9%), and agreement with serological reference methods for diagnosing canine VL (ELISA and IFAT). To complete the in-house validation also the stability over time and the robustness to temperature variation were evaluated. The long-term stability of the LFIA device was confirmed based on six months of storage at room temperature or 4 °C, and the qualitative response of the device was not affected by limited thermal stress. The developed LFIA device is currently commercialized by the In3Diagnostic that collaborated and supported the project. Furthermore, we confirmed that the use of the SpA allowed the efficacy also for testing other animal species, as cats and foxes.

In chapter 4.1, after the production of the three different multimodal  $x^2$ LFIA prototypes, they were tested on samples from official panels including 1 negative, 1 fully seroconverted HIV2 positive, 1 fully seroconverted HIV1 positive and 3 seroconverting HIV1 positive sera. The combination of spatial and color resolution enabled to embed multiple information in a single strip, such as the virus serotype and the stage of infection. This result was reached by employing two serotype-specific antigens, two immunoglobulin class-specific ligands and two differently colored gold nanomaterials. In addition to increasing the multiplexing capability, the work was also devoted to study the effect of switching the “roles” played by the immunoreagents, such as using the antigens as the capturing agents on respect to using the immunoglobulin ligands (Streptococcal protein G and anti-human IgM antibodies). Furthermore, the performance of the double antigen strategy was also compared to those of traditional serotyping approaches.

Along with the detection of total antibody to SARS CoV-2, a viable alternative, especially for using oral fluids as a convenient specimen, was explored. The salivary testing enables for an easier sampling and an earlier diagnosis, considering the nature of the respiratory illness resulting from

this infection. Results on point-of-care devices targeting the IgA class of antibodies to SARS CoV-2, seems to be a promising complementary option, as highlighted by the results in the chapter 4.2. Concerning the direct detection of antigens and their serotyping for FMD diagnosis in cattle, reported in chapter 5.1, two multiplexing devices were developed and tested on 26 epithelium homogenates (EH) from cattle and showed adequate analytical performances. The LFIA devices allowed for the facile and rapid detection and serotyping of FMDV in epithelial tissues (false negative rate: 0% (n= 22), false positive rate: 5,9% (n=24), accuracy: 96.4% (87.7% - 99.6%). In addition, the work investigated a previously unreported effect of saturation, which occurred in the homologous sandwich, as a function of the position of the test lines. Evidence of an “*inverted hook effect*” was firstly reported and discussed, which help to add a general knowledge for antigen testing. Lastly, in chapter 6.1, the checkerboard selection used in the monoclonal antibody selection, led to unprecedentedly sensitive testing for TFV in urine and saliva. The seven most promising mAbs were evaluated by direct and indirect ELISA. Among them, the three showing the highest affinity were further characterized for their proneness to pH, ionic strength, and matrix effect for the use in urine and saliva. The best performing mAb (#321) was included in a lateral flow prototype for the detection in urine, using the antigen as the capture and the mAb #321 labelled with GNPs as the detector. The sensitivity showed by the urine testing (vLOD: 1.4 - 7.2 ng/ml) was largely above the requirement, disclosing the possibility to switch to the salivary matrix, were the TFV is dramatically more diluted. The developed and in-house validated ELISA method for the semi-quantitative analysis of TFV in saliva reached outstanding analytical performances (IC50: 1.3ng/ml, Accuracy: 85.8%-145.6%, Recovery: 73.4%-133.6%), sustainable for assessing correct administration. Besides, a LFIA device for the detection of TFV in salivary matrix was produced and characterized (visual LOD 0.5-1ng/ml).

The matrix effect was explored in chapter 5 and chapter 6 since they were addressed for non-conventional matrices (saliva or epithelium homogenate). In addition, we had the possibility to use a standard “analyte” (tenofovir or culture supernatant) to fortify the buffer or different amount of matrix to study the effect. In chapter 3.1, 3.2 and 4.1, where the study was conducted directly on real samples, the lack of standard solution of representative polyclonal anti-target antibodies would have made the study less significative. In addition, the serum is well known to cover non-specific binding without interfering on the analytical signal and is generally considered as a conventional matrix. In chapter 4.2, the effect of the salivary matrix was not explored for several reasons: firstly, in the spring-summer of 2020, the provision of blank saliva samples was very difficult. As a second aspect, the lack of specific anti-N IgA resulted in the impossibility to work in buffer or fortify blank pre-covid saliva.

To conclude, all these challenges have been overcome by using the traditional LFIA materials and probes (except for a gold nanomaterial in the chapter 4.2), while engineering the structure of the assay. The overwhelming importance of a good strategy in placing the right immunoreagent in the right role was undoubtedly demonstrated. Evidence of physicochemical phenomena occurring when antigens and antibodies are found to interact in peculiar conditions and situations were observed and investigated. This work demonstrated that, after more than 60 years, there are still many aspects to be described, studied, and more deeply investigated. Surely, in the future even more challenging needs will appear and the current state-of-the-art will be not sufficient to respond to them. Then we will be ready to go further and find new expedients, enriched by knowledge accumulated by the understanding of the high potential of the “good old” standard.

# Acknowledgements

I would like to thank my supervisor Prof. Laura Anfossi, for the incommensurable support and contribution and the endless patience, determination, and motivation she dedicated to my formation, growing me up as a man and a young scientist.

I would like to thank Prof. Claudio Baggiani for sharing his knowledge with me with priceless advices. My grateful thanks to all my collaborators of the Bioanalytical Laboratory, especially to Alida, Matteo, Matteo and Thea, whose unvaluable help and support played a crucial role on many occasions, and without whom these years would have been remarkably harder.

A special thanks to Dr. Fabio Di Nardo, whose expertise, knowledge, and friendship have been a beacon of light, especially (but not only) when I was groping in the dark.

I would express my sincere gratitude to my collaborators at the Department of Veterinary Sciences, especially to Prof. Sergio Rosati for all the teachings on infectious diseases and veterinary science. Thank you for the kindness and availability demonstrated to me and to my research group in all our fortunate collaborations.

My sincere gratitude to Dr. Antonio Abad-Fuentes and to Dr. Josep Mercader-Badia for their warm welcome during my period in Valencia. Thank you for your indefatigable determination dedicated to the Tenofovir project, both when I was in Valencia and when I was in Turin.

I am grateful to Prof. Antonio Abad-Somovilla and Dr. Consuelo Agulló for their unmeasurable support and teachings on the synthesis of haptens and for the patience dedicated enriching my knowledge in organic chemistry.

I would like to thank all the PhD and 'TFMs' students at the University of Valencia and at the IATA-CSIC labs for their support, for introducing me to the everyday-life of an organic chemistry lab and for the unvaluable help in the development of the monoclonal antibodies to Tenofovir. A special thanks to Paula for the huge amount of work and dedication spent on my project and for answering my countless questions.

Thanks to Luca and Francesca from Prima Lab SA, for their energy and great help in the HIV diagnostic project.

Thanks to the collaborators of the SIRIT project for their support and availability with the sample collection during the SARS CoV-2 lockdowns.

Thanks to Prof. Aldo Roda and Dr. Donato Calabria for the tireless determination and precious contribution with chemiluminescence detection.

Thanks to all the students I looked after during these years. You taught me more about teaching, than I was supposed to teach you about science.

A very special thanks to my family and friends, for the support and love, and for enduring my inevitable rantings on immunochemistry and diagnostics during family dinners.

Last, but not least, thanks to Sara for accepting (and feeding) my rantings in her everyday life.

# Dedications

To Cristina...for everything. I will never forget you and the fact that the voice on the other end of that call, that changed my life forever, was yours.

To Prof. Gianmario Martra, whose kindness and love for science made me feel more in a big scientific family than in a doctoral school.

---

# Appendix

---

## Peer-reviewed publications

1. S. Cavalera, F. Di Nardo, L. Forte, F. Marinoni, M. Chiarello, C. Baggiani and L. Anfossi, Switching from Multiplex to Multimodal Colourimetric Lateral Flow Immunosensor, *Sensors* 2020, 20(22), 6609; <https://doi.org/10.3390/s20226609>.
2. S. Cavalera, F. Di Nardo, G. Spano, L. Anfossi, P. Manesiotis and C. Baggiani, Stoichiometric molecular imprinting using polymerisable urea and squaramide receptors for the solid phase extraction of organo-arsenic compound roxarsone, *Analytical Methods*, 2020, 12, 5729-5736, <https://doi.org/10.1039/D0AY01635G>.
3. A. Roda, S. Cavalera, F. Di Nardo, D. Calabria, S. Rosati, P. Simoni, B. Colitti, C. Baggiani, M. Roda and L. Anfossi, Dual lateral flow optical/chemiluminescence immunosensors for the rapid detection of salivary and serum IgA in patients with COVID-19 disease, *Biosensors and Bioelectronics*, Volume 172, 2021, 112765, ISSN 0956-5663, <https://doi.org/10.1016/j.bios.2020.112765>.
4. S. Cavalera, C. Agulló, J. V. Mercader, F. Di Nardo, M. Chiarello, C. Baggiani, A. D'Avolio, L. Anfossi, A. Abad-Somovilla and A. Abad-Fuentes, Monoclonal antibodies with subnanomolar affinity to tenofovir for monitoring adherence to antiretroviral therapies: from hapten synthesis to prototype development, *Journal of Materials Chemistry B*, 2020 Oct, <https://doi.org/10.1039/D0TB01791D>
5. S. Cavalera, B. Colitti, S. Rosati, G. Ferrara, L. Bertolotti, C. Nogarol, C. Guiotto, C. Cagnazzo, M. Denina, F. Fagioli, F. Di Nardo, M. Chiarello, C. Baggiani, L. Anfossi, A multi-target lateral flow immunoassay enabling the specific and sensitive detection of total antibodies to SARS COV-2, *Talanta*, 223, 1, 2021, 121737, ISSN 0039-9140, <https://doi.org/10.1016/j.talanta.2020.121737>.
6. F. Di Nardo, S. Cavalera, C. Baggiani, M. Chiarello, M. Pazzi, L. Anfossi, Enzyme Immunoassay for Measuring Aflatoxin B1 in Legal Cannabis, *Toxins*, 12, 265, 2020 <https://doi.org/10.3390/toxins12040265>.
7. L. Anfossi, C. Giovannoli, F. Di Nardo, S. Cavalera, M. Chiarello, F. Trotta, C. Baggiani, Selective enrichment of aianthone from leaves of *ailanthus altissima* by tandem reverse phase/molecularly imprinted solid phase extraction, *Microchemical Journal*, Volume 158, 2020, 105198, ISSN 0026-265X, <https://doi.org/10.1016/j.microc.2020.105198>
8. L. Anfossi, S. Cavalera, F. Di Nardo, G. Spano, C. Giovannoli, C. Baggiani, Delayed Addition of Template Molecules Enhances the Binding Properties of Diclofenac-Imprinted Polymers, 12, 1178. *Polymers* 2020, 12(5), 1178; <https://doi.org/10.3390/polym12051178>.
9. F. Di Nardo, S. Occhipinti, P. Gontero, S. Cavalera, M. Chiarello, C. Baggiani, L. Anfossi, Detection of urinary prostate specific antigen by a lateral flow biosensor predicting repeat

- prostate biopsy outcome. *Sensors Actuators, B Chem.* 325, (2020). <https://doi.org/10.1016/j.snb.2020.128812>.
10. G. Spano, S. Cavalera, F. Di Nardo, C. Giovannoli, L. Anfossi and C. Baggiani, Development of a biomimetic enzyme-linked immunosorbent assay based on a molecularly imprinted polymer for the detection of cortisol in human saliva. *Analytical Methods*, 11, 2320–2326 (2019), <https://doi.org/10.1039/C9AY00317G>.
  11. F. Di Nardo, S. Cavalera, C. Baggiani, C. Giovannoli, L. Anfossi, Direct vs Mediated Coupling of Antibodies to Gold Nanoparticles: The Case of Salivary Cortisol Detection by Lateral Flow Immunoassay. *ACS Applied Materials Interfaces*. 2019 Sep 11;11(36):32758-32768. <https://doi.org/10.1021/acsami.9b11559>. Epub 2019 Sep 3. PMID: 31381297.
  12. G. Capilli, S. Cavalera, L. Anfossi, C. Giovannoli, M. Minella, C. Baggiani and C. Minero, Amine-rich carbon nitride nanoparticles: Synthesis, covalent functionalization with proteins and application in a fluorescence quenching assay, *Nano Research*, 12, 1862–1870 (2019). <https://doi.org/10.1007/s12274-019-2449-x>.
  13. L. Anfossi, F. Di Nardo, A. Russo, S. Cavalera, C. Giovannoli, G. Spano, S. Baumgartner, K. Lauter, C. Baggiani, Silver and gold nanoparticles as multi-chromatic lateral flow assay probes for the detection of food allergens. *Analytical and Bioanalytical Chemistry*, 2019 Mar; 411(9):1905-1913. <https://doi.org/10.1007/s00216-018-1451-6>. Epub 2018 Nov 6. PMID: 30397760.
  14. F. Di Nardo, E. Alladio, C. Baggiani, S. Cavalera, C. Giovannoli, G. Spano, L. Anfossi, Colour-encoded lateral flow immunoassay for the simultaneous detection of aflatoxin B1 and type-B fumonisins in a single Test line, *Talanta*, 2019 Jan 15;192:288-294. <https://doi.org/10.1016/j.talanta.2018.09.037>. Epub 2018 Sep 18. PMID: 30348391.
  15. L. Anfossi, F. Di Nardo, M. Profiti, C. Nogarol, S. Cavalera, C. Baggiani, C. Giovannoli, G. Spano, E. Ferroglio, W. Mignone, S. Rosati, A versatile and sensitive lateral flow immunoassay for the rapid diagnosis of visceral leishmaniasis, *Analytical and Bioanalytical Chemistry*, 2018 Jul; 410(17) : 4123-4134. <https://doi.org/10.1007/s00216-018-1067-x>. Epub 2018 Apr 23. PMID: 29687248.
  16. L. Anfossi, F. Di Nardo, S. Cavalera, C. Giovannoli and C. Baggiani, Multiplex Lateral Flow Immunoassay: An Overview of Strategies towards High-throughput Point-of-Need Testing. *Biosensors (Basel)*. 2018 Dec 26;9(1):2. <https://doi.org/10.3390/bios9010002>. PMID: 30587769; PMCID: PMC6468474.
  17. L. Anfossi, F. Di Nardo, S. Cavalera, C. Giovannoli, G. Spano, E. Speranskaya, I. Goryacheva, and C. Baggiani, A lateral flow immunoassay for straightforward determination of fumonisin mycotoxins based on the quenching of the fluorescence of CdSe/ZnS quantum dots by gold and silver nanoparticles, *Microchimica Acta*, 2018, 185. <https://doi.org/10.1007/s00604-017-2642-0>.

## Oral presentations

1. Autumn Meeting for Young Chemists in Biomedical Sciences (AMYC-Biomed 2020), 13-14/10/2020 (International Webinar)  
10'+2' Oral Presentation "A Multi-Target Lateral Flow Immunoassay Enabling the Specific and Sensitive Detection of Total Antibodies to Sars-Cov-2".  
13/10/2020
2. Giornata Scientifica Bioanalitica 2019 (National Conference)  
Parma, Italy, 6/12/2019  
13'+2' Oral Presentation "A Rapid and Sensitive Lateral Flow Immunoassay for the Real Time Monitoring of the Compliance in Antiretroviral Therapies: from Hapten Synthesis to Prototype"  
6/12/2019
3. Rapid Method Europe 2018 (International Conference)  
Amsterdam, The Netherlands, 5-7/11/2018  
6' Oral Speed Presentation "A Versatile and Sensitive Point-of-care Test for the Rapid Diagnosis of Visceral Leishmaniasis"  
5/11/2018

## Poster presentations

1. XXVIII Congresso Nazionale della Divisione di Chimica Analitica 2019 (National Conference), 22-26/9/2019, Bari, Italy  
"A Sensitive ELISA Method for the Dosage of Insulin Glargine® in Rat Plasma and Serum to Support "In-Vivo" Pre-Clinical Trial Monitoring"
2. Rapid Method Europe 2018 (International Conference), 5-7/11/2018, Amsterdam, The Netherlands  
"Carbon-nitride nano-materials fluorescence quenching: application in biosensors"
3. Rapid Method Europe 2018 (International Conference), 5-7/11/2018, Amsterdam, The Netherlands  
"A versatile and sensitive point-of-care test for the rapid diagnosis of visceral leishmaniasis"
4. Giornata Scientifica Bioanalitica 2018 (National Conference), 21/10/2018, Bologna, Italy



“Synthesis and characterization of immunoreagents suitable for point-of-care devices for the HIV-1 high activity anti-retroviral treatment monitoring”

5. IX Giornate Italo-Francesi di Chimica/Journées Franco-Italiennes de Chimie, (International Conference) 2018, 16-18/4/2018, Genova, Italy  
“Inorganic Quantum Dots and Carbon-Nitride Quantum Dots fluorescence quenching: application in biosensors”

### Conferences attended

1. International (Web) Conference Autumn meeting of young chemists\_biomed 2020
2. Giornata Scientifica Bioanalitica 2019 (National Conference), 6/12/2019, Parma, Italy
3. Congresso Nazionale della Divisione di Chimica Analitica, 22-26/9/2019, Bari, Italy
4. International Conference Rapid Method Europe 2018, 5-7/11/2018, Amsterdam, The Netherlands
5. Giornata di Bioanalitica 2018, 21/10/2018, Bologna, Italy
6. International Conference Journées Franco-Italiennes de Chemie, 16-18/4/2018, Genova, Italy

### PhD courses attended

1. Drug Design 2018
2. Environmental Pollution and Health 2018
3. Advances in Nanotechnology 2018
4. Natural and Engineered Enzymes 2019
5. Advances in Pharmacology 2020
6. Advances in Pharmaceutical Technology 2020
7. Advances in Phytochemistry 2020

### Workshop and seminars attended

1. Workshop "Advances in Pharmaceutical and Biomolecular Sciences @ UniTO" 2018
2. Workshop Risorse e servizi digitali nella ricerca bibliografica
3. Seminar "Extraction processes: the viewpoint of engineers"
4. Workshop Raman Day 2018
5. Seminar NIS Colloquium 2018
6. Workshop sul trasferimento di conoscenze
7. Seminar Nanobubbles and the Future of Ultrasound: New opportunities for US molecular imaging and US-modulated cancer therapy
8. Workshop CrisDi "The Role of Crystallography in Drug Science and Biology"
9. SafeNano 2018
10. Workshop PhD Day 2 2018
11. Workshop "Advances in Pharmaceutical and Biomolecular Sciences @ UniTO", 2018
12. Seminar Cold Denaturation of Globular Proteins
13. Seminar Microbial biodeterioration of historical artifacts: biochemical aspects
14. Seminar Functionalised polymeric platforms for drug delivery: a versatile synthesis and miniaturized formulation
15. Workshop PhD Day 1 2019
16. Workshop "Advances in Pharmaceutical and Biomolecular Sciences @ UniTO", 2019
17. Workshop PhD Day 3 2019
18. Workshop PhD Day 1 2020
19. Workshop PhD Day 2 2020
20. Workshop "Advances in Pharmaceutical and Biomolecular Sciences @ UniTO", 2020